UNIVERSITY OF SOUTHAMPTON

Development and assessment of novel techniques to measure primary production in the Celtic Sea and English Channel

Katharine Woods

This thesis is submitted for
Doctor of Philosophy

Faculty of Science
School of Ocean and Earth Science

February 2003

UNIVERSITY OF SOUTHAMPTON

ABSTRACT

FACULTY OF SCIENCE
SCHOOL OF OCEAN AND EARTH SCIENCE

Doctor of Philosophy

Development and assessment of novel techniques to measure primary production in the Celtic Sea and English Channel

by Katharine Louise Woods

Marine primary production is an essential process in the global carbon cycle, controlling the flux of elements from the surface layer to the deep ocean waters. This research involved the characterisation of photosynthetic performance and primary production over different scales by three different techniques: incubations with ^{14}C, fast repetition rate fluorometry (FRRF) and satellite remote sensing. The objectives were to establish the most appropriate way to estimate primary production, to understand the limitations of techniques and to obtain seasonal estimates of production. These were addressed by a cruise in the Celtic Sea in May 2000 and a one-year time series of measurements at a coastal site in the Western English Channel in 2001.

The standard ^{14}C method gave variable results with different incubation procedures. Corrections could be made to account for different light sources used during incubations but not to compensate for incubations of different durations. However, changes in measured values often followed patterns and only the inclusion of a dark period in experiments led to significant changes in derived parameter values. The quality of the FRRF data was dependent on slow profiling and high ambient light. Under these conditions, FRRF estimates of photosynthetic parameters were comparable to those from ^{14}C incubations but showed slight day-to-day variations. Models using FRRF data always led to higher production estimates than those from the ^{14}C method. Fifty percent of the variance in ^{14}C estimates was explained by the variance in FRRF data. The FRRF offers the potential for high-resolution measurements over large horizontal scales but further research is needed to understand how these data relate to depth-integrated production.

Comparisons between SeaWiFS estimated and measured chlorophyll concentrations were limited due to cloud cover in the English Channel and clear images were obtained for only ten days when water samples were taken. SeaWiFS algorithms produced relatively poor estimates of chlorophyll. The difference between remotely sensed and measured values were greatest in the winter when the sun angle was low and the water column contained high concentrations of non-photosynthetic, optically-active substances. A complex semi-analytical production algorithm produced estimates closer to those from ^{14}C and the FRRF than simpler empirical algorithms, and explained 84% of the variance in estimates from the FRRF. Taylor Series approximation and Monte Carlo modelling showed that the error associated with the ^{14}C method and FRRF can lead to very high uncertainty on production estimates derived from models.

Estimates of annual carbon fixation at the coastal site, in the Western English Channel, ranged from 64 mg C m^{-2} to 310 mg C m^{-2} depending on the technique used. Most of the annual carbon fixation took place between April and September when between 51 mg C m^{-2} and 189 mg C m^{-2} were fixed. Primary production was consistently over-estimated by remote sensing during the winter as a result of poor chlorophyll retrieval but estimates of production during the summer compared well with measured values.

Graduate School of the
Southampton Oceanography Centre

This PhD dissertation by

Katharine Louise Woods

has been produced under the supervision of the following persons

Supervisors:

Prof. P.M. Holligan[1], Dr. I.R. Joint[2] and Mr. S.B. Groom[2]

[1]School of Ocean and Earth Science, University of Southampton
[2]Plymouth Marine Laboratory

Chair of Advisory Panel:

Prof. J.G. Shepherd

Member of Advisory Panel:

Dr. T. Tyrrell

Contents

List of Figures

List of Tables

Acknowledgements

I have received support from many people during the course of my Ph.D. Thank you to my supervisors: Ian Joint, Steve Groom and Patrick Holligan, for all their help and advice and to the remote sensing group at PML for their patience in explaining the nuances of satellite oceanography.

There are a few other people at PML to whom I am particularly grateful: Tim Smyth, for helping me realise that computers aren't all out to get me; James Fishwick and Gerald Moore for giving up their time to help me to collect and interpret data; Bob Clarke, who hasn't complained once during the numerous visits I've made to his office for advice on statistics and Jim Aiken who has unofficially supervised large chunks of the work and has always made time to help. Thanks also to Richard Geider, Dave Suggett and Mark Moore for the helpful conversations about the FRRF.

The fieldwork would not have been possible without the work of the crews of RV Squilla, RV Sepia and RRS Discovery.

Thank you also to John Shepherd and Toby Tyrrell at the University of Southampton for their advice at the panel meetings throughout the course of the PhD.
The work was funded by the EU Commision project, PROOF (CEC Contract number EVK3-CT-1999-00019) and carried out at Plymouth Marine Laboratory.

Finally, thank you to my family for all the support that helped me get this far and to Andy, who's all right!

Table of frequently used symbols

Symbol	Definition
General	
[Chl]	Chlorophyll *a* concentration (mg m^{-3})
z	Depth (m)
PP_{Daily}	Daily depth integrated primary production (mg C m^{-2} d^{-1})
$PP_{(z,t)}$	primary production at depth z and time t (mg C m^{-3} h^{-1})
P^B_S	Maximum potential light saturated photosynthetic rate under prevailing conditions, normalised to chlorophyll *a* (mg C [mg Chl]$^{-1}$ h^{-1})
P^B_{OPT}	Maximum potential light saturated photosynthetic rate in the water column over the course of a day and hence under variable irradiance, normalised to chlorophyll *a* (mg C [mg Chl]$^{-1}$ h^{-1}))
P^B_m	Specific production rate obtained at optimal light intensity, normalised to chlorophyll *a* (mg C [mg Chl]$^{-1}$ h^{-1})
α^B	Initial slope of P-E curve normalised to chlorophyll *a* (mg C [mg Chl]$^{-1}$ h^{-1} [µmol photons m^{-2} s^{-1}]$^{-1}$)
β^B	Photoinhibition parameter of P-E curve normalised to chlorophyll *a* (mg C [mg Chl]$^{-1}$ h^{-1} [µmol photons m^{-2} s^{-1}]$^{-1}$)
E_k	Light saturation index (µmol photons m^{-2} s^{-1})
K_{PUR}	A temperature dependent function to allow the effect of temperature on growth rate to be included in the production calculation in the Morel model
a^*_{max}	Maximum value of phytoplankton absorption (m^{-1})
$\phi_{\mu max}$	Quantum yield for growth (mol C mol photons absorbed^{-1})
$A^*(\lambda)$	Mean absorption cross section per unit of chlorophyll *a* (m^2 g Chl^{-1})
Fluorescence	
PSI / PSII	Photosystem I / II
F_0 / F'	Minimal fluorescence obtained when all reaction centres are open in dark adapted samples / under ambient light (arbitrary units)
F_m / F_m'	Maximum fluorescence obtained when all reaction centres are closed in dark adapted samples / under ambient light (arbitrary units)
F_v	Variable fluorescence in dark adapted samples (= $F_m - F_0$) (arbitrary units)
F_q' / F_v'	Variable fluorescence under ambient light measured in the light chamber / measured in the dark chamber (=$F_m' - F'$) (arbitrary units)
F_v/F_m	Maximum quantum efficiency of photochemistry of dark adapted samples (dimensionless)
F_q'/F_m' or F_v'/F_m'	Maximum quantum efficiency of photochemistry of samples under ambient light measured in the light chamber or dark chamber respectively (dimensionless)
σ_{PSII}	Effective absorption cross section (o^2 quanta^{-1})
NPSII	Number of PSII reaction centres per chlorophyll a (mol RCII (mol Chl)$^{-1}$)
PQ	Photosynthetic quotient (mol O_2 (mol CO_2)$^{-1}$)
ϕe	Quantum yield of electron transport (mols O_2 (mols electrons)$^{-1}$)
Light	
E	Irradiance (µmol photons m^{-2} s^{-1})
PAR	Photosynthetically active radiation (µmol photons m^{-2} s^{-1})
PUR	Photosynthetically useable radiation (µmol photons m^{-2} s^{-1})

Symbol	Definition
K_{PAR}	Attenuation coefficient for PAR (m^{-1})
$a(\lambda)$	Total absorption (m^{-1})
$b(\lambda)$	Total backscattering (m^{-1})
$\mu 0$	Average cosine for downwelling irradiance
$b_w(\lambda)$	Specific backscattering coefficient of pure seawater (m^{-1})
$a_w(\lambda)$	Specific backscattering coefficient of pure seawater (m^{-1})
$a_{Chl}(\lambda)$	Specific backscattering coefficient of chlorophyll *a* (m^{-1})
Fs	Sea surface effect on light (from Fresnel's equation)

Symbols included are those used frequently throughout the text. Those used only once in equations are defined at that point and are not shown here.

Chapter 1. Introduction

1.1 Background and overview

Human activities and natural forces have contributed to changes in the Earth's climate over the 20th century including increases in ocean and land surface temperatures, a rise in sea level and an increase in the frequency and intensity of El Nino events (Watson, 2002). The oceans contain approximately fifty times the amount of carbon that is held in the atmosphere and provide a major sink for anthropogenic carbon dioxide (Prentice, 2001). In order to understand the effect of climate change on the global carbon cycle we need to understand how it functions today and how its biological components will respond to future changes in their environment.

Primary production is an essential biogeochemical process controlling the flux of elements from the atmosphere and the surface waters to the deep ocean waters. Net primary productivity is currently estimated to be roughly 45 Pg C yr^{-1} (Balkanski *et al.*, 1999; Field *et al.*, 1998; Behrenfeld and Falkowski, 1997b; Antoine *et al.*, 1996 and Longhurst *et al.*, 1995) but specific estimates vary depending on the calculations used. The ability to accurately measure marine primary productivity on a global scale would be a major step forward in the understanding of ocean biogeochemistry in relation to climate change. Our incomplete understanding of present day controls of productivity limits our ability to predict future changes in ocean biology and its effect on atmospheric carbon dioxide levels (Pahlow and Riebesell, 2000). Accurate estimates of photosynthesis and primary production are the basis for determining the rates at which inorganic carbon is fixed and made available to higher trophic levels (Platt and Sathyendranath, 1988). In order to predict the response of marine phytoplankton to changes in climate, it is necessary to understand the main controls on their growth and at both local and global scales.

Remote sensing was identified as potential tool for measuring phytoplankton productivity over large scales over two decades ago (for example Smith, 1981). There has since been significant development of algorithms to model primary production from satellite derived data. Satellites can provide estimates of both sea surface temperature (from the Automated Very High Resolution Radiometer or AVHRR senor) and chlorophyll (from the SeaWiFS sensor). The obvious limitation of satellites is their inability to measure physiological parameters indicative of photosynthetic capacity and much work has focussed on estimating

these from alternative detectable parameters (Sathyendranath *et al.*, 1991). Satellite estimates of production have traditionally been 'tested' by comparison with production measurements from incubations with ^{14}C, the traditional method for measuring primary production on water samples. However, it is accepted that the wide range of protocols used in ^{14}C incubations can lead to a wide variety of production estimates, depending on the experimental approach used (Marra, 2002). In recent years, the fast repetition rate fluorometer (FRRF) has been used as a tool for making *in situ* measurements of primary production. This technique is used to estimate photosynthetic rates from light stimulated changes in the quantum yield of chlorophyll fluorescence (Kolber and Falkowksi, 1993). The FRRF permits rapid vertical profiling of the water column and can be towed in an undulating mode to provide measurements of primary production over large horizontal areas. As such it may offer a means to parameterise models based on satellite data to provide accurate large-scale estimates of oceanic primary production. As with estimates from remote sensing, FRRF estimates of production and photosynthetic capacity have previously been compared to estimates from the ^{14}C technique.

If production estimates from the ^{14}C technique are to be used as "benchmark" values, it is important to understand the range of estimates that can be expected from these measurements and the errors associated with these estimates. Assessments of the effects of different experimental protocols, on the outcomes of ^{14}C experiments, have been carried out in the past (and will be discussed later) but never in the context of the relationship between estimates from ^{14}C and those from other techniques. In the past, comparisons between ^{14}C and the FRRF have focussed on data from discrete cruises and/or limited timescales. Remote sensing models are often tested against data from the region and season for which they were constructed and, as expected, under such conditions they perform reasonably well. However, many of these models have been shown to perform badly when applied to other regions (Behrenfeld and Falkowski, 1997a).

This research involves the characterisation of photosynthetic performance and primary production over different scales by the three different techniques; incubations with ^{14}C, the FRRF and remote sensing. It compares estimates of production from common samples obtained by the different approaches. The overall objective of the work is to understand the limitations of the different techniques and to quantify the uncertainties associated with them. The work includes a comparison of the techniques over a year at one site to gain new understanding of the impact of seasonality on the relationships between the results from the

different techniques. These results are used to investigate the relationship between the different estimates with the changing phytoplankton population over a seasonal cycle. The comparison between FRRF measurements with remotely sensed data has not been carried out before and may show the instantaneous, optical measurements made with the FRRF to be more suitable *in situ* measures against which to compare satellite estimates of production than the ^{14}C chemical tracer approach.

1.2 The ^{14}C technique

1.2.1 Background and Introduction

The ^{14}C tracer method, introduced in 1952, is the most widely used technique for the measurement of phytoplankton productivity (Longhurst *et al.*, 1995). A known amount of ^{14}C, usually as $NaH^{14}CO_3$, is added to a contained water sample and incubated for a prescribed amount of time. After incubation, the sample is filtered, unfixed inorganic radiocarbon removed by acidification and the radioactivity incorporated into the sample is measured using a scintillation counter. Primary production is calculated from the amount of radioactive carbon incorporated into particulate (and sometimes dissolved) organic matter, and is a measure of total carbon uptake during the incubation. Incubations may be done with natural or artificial light. Incubations under natural light usually lead to estimates of production, in terms of carbon fixed per unit area per unit time, under conditions designed to be comparable to those encountered *in situ*. Such incubations may be carried out in the sea or on-deck, using filters to simulate light at the depth of collection. Alternatively, light gradient incubators may be used to study the effect of irradiance on the photosynthetic yield in order to understand the photosynthetic potential of phytoplankton populations. Data from these studies are used to generate photosynthesis-irradiance (PE) curves from which estimates of photosynthetic parameters can be derived (see below).

The ^{14}C method has been the favoured method to determine primary production because of the relative ease of measurement, sensitivity and apparent simplicity (Williams *et al.*, 1996). However, for many years, there has been lack of agreement on the interpretation of processes occurring in the samples and discussion on inconsistencies between methods used. Aside from direct problems and methodological discrepancies, the issue of how the ^{14}C uptake is described is important. Primary production can be reported either as raw values or as the derived photosynthetic parameters from photosynthesis-irradiance (PE) curves and may be

normalised to carbon, cell number or chlorophyll concentration as a measure of biomass. These different measures may give strikingly different impressions of the processes of photosynthesis (MacIntyre *et al.*, 2002).

1.2.2 Photosynthesis - irradiance curves

Photosynthesis-irradiance (PE) curves provide a convenient means of describing the response of phytoplankton to a range of irradiances and to differentiate between light limited and light saturated photosynthesis (MacIntyre *et al.*, 2002). The PE curve is accepted as a useful relationship for examining the physiology of microalgae and cyanobacteria (Henley, 1993) and the curve shape reflects the underlying metabolic processes that regulate photosynthesis (MacIntyre *et al.*, 2002). The photosynthesis-irradiance (PE) relationship is non-linear and the parameters of the PE curve contain information on the physiology of the algae and can reflect variations in environmental conditions (Macedo *et al.*, 2002). The relationship is studied by incubating a series of sub-samples in a gradient of artificial light. Resultant production values are often divided by chlorophyll concentration to give a 'normalised' rate of production.

The curve can be divided into three regions (Figure 1.1) The first region occurs at low irradiance where photosynthesis is light limited and linearly related to irradiance. This initial slope is referred to as α^B, the superscript 'B' indicating normalisation to biomass (usually chlorophyll concentration). Under these low light conditions, many reaction centres are open and the rate of electron supply from the photolysis of water controls the rate of production of reductant and subsequent carbon fixation. The value of α^B is a product of the absorption of light energy and the efficiency with which phytoplankton can convert light energy into reductant. The variable absorption of light by phytoplankton across different wavelengths means that α^B is spectrally dependent. As irradiance increases, the reaction centres close and photosynthesis becomes increasingly light saturated. When photosynthesis is fully saturated, the curve reaches a plateau and the rate of photosynthesis is independent of irradiance. The maximum rate of photosynthesis is referred to as P^B_{max} or P^B_m and is related to the number of photosystems and the time taken for electron acceptors to be re-oxidised. The latter is directly linked to the dark, enzymatically controlled, reactions of photosynthesis. At supra-optimal irradiance, the rate of photosynthesis may decline and this third portion of the curve is described by β^B, the photoinhibition parameter. Photoinhibition may occur for a number of reasons and it may reflect damage to photosystems by high light or an increase in the

proportion of photoprotective pigments to prevent damage. Whether photoinhibition occurs in nature or is purely an artefact of experimental protocols is a contentious issue. The final parameter of the PE curve is E_k, the light saturation index. E_k is the point on the irradiance axis at which α^B intersects P^B_m. It defines the irradiance level at which control of photosynthesis moves from light absorption and energy conversion to reductant utilisation (Sakshaug *et al.*, 1997). E_k is spectrally dependent and is derived by dividing P^B_m by α^B. It reflects the photoadaptive state of the population.

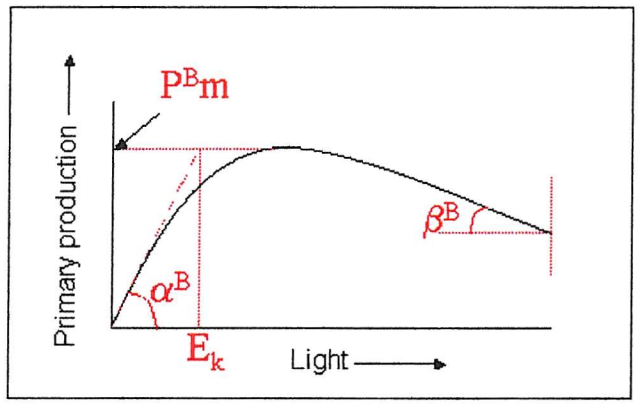

Figure 1.1. Diagram to show a typical photosynthesis-irradiance (PE) curve. Details of labelled parameters are given in the text.

The factors affecting the shape of PE curves fall into two categories: 1) those that affect the conversion of light energy to photosynthetic end products, an example of which is the light harvesting capacity and 2) those that affect the coupling between photosynthesis and cell division or growth, examples of which are respiration and the chlorophyll to carbon ratio. Variability in the parameters of the PE curve reflects the physiological state of the cells over the course of the incubation as well as their state prior to manipulation. The PE curve is a useful tool for measuring phytoplankton response to a range of irradiance levels but the relevance of the observed response to that occurring in nature depends on the sampling and incubation procedures used. For example, the irradiance received by phytoplankton during PE incubations is often different in magnitude and quality to that in nature and this can dramatically influence the shape of the PE curve.

The interpretation of PE curves depends critically on normalisation (MacIntyre *et al.*, 2002; Geider *et al.*, 1997; Henley, 1993). The amount of carbon fixed is the most important measure of photosynthesis and primary production but chlorophyll *a* concentration is widely used due to its ease of measurement and its importance in photosynthesis. However,

chlorophyll is a small and variable component of biomass accounting for between 0.1 and 5% of phytoplankton organic matter (Geider *et al.*, 1997). The chlorophyll *a* to carbon ratio varies between species and in response to irradiance, temperature and nutrients and may even exhibit diel variability (Geider *et al.*, 1997). It can also change with depth and time of year (Taylor *et al.*, 1997).

A number of equations have been used to describe the PE relationship (e.g. Platt *et al.*, 1980; Jassby and Platt, 1976) (see equations 15a and 15b in chapter 2) and although all lead to similar shaped curves, the derived parameters are often highly dependent on the model chosen (Frenette *et al.*, 1993). For ease of calculation, most production models assume constant PE parameter values over the course of the incubations (so called "steady-state" models) but some incorporate the time dependency of the parameters of the PE curve (e.g. Macedo *et al.*, 1998 and Neale and Marra, 1985). In an attempt to relate better measured values to those *in situ*, some models have included equations to approximate the effect of mixing on parameters (e.g. Neale and Marra, 1985) but such models are still based on the manipulation of initial parameters derived from steady-state values.

1.2.3 Processes that influence the interpretation of primary production experiments

Loss of fixed ^{14}C during incubations

Some ^{14}C is lost by respiration of autotrophs during the course of incubations. Respiration is the oxidation of organic carbon to provide substrates for cell growth and includes both photorespiration and dark respiration (Falkowski and Raven, 1997). The ratio of photosynthesis to respiration is critical to the calculation of production estimates (Peterson, 1980) but is variable and affected by many factors including species specific growth rate (Langdon, 1993), ambient nutrient concentrations (McAllister *et al.*, 1964 and Ryther, 1954) and respiratory substrate (Laws and Bannister, 1980 and Shuter, 1979). There is no simple parameterisation of respiration as a function of either rate of growth or of gross photosynthesis (Geider, 1992).

Photorespiration is the light dependent consumption of oxygen together with reactions that involve glycolate metabolism (Falkowski and Raven, 1997). The rate is considered to be low in aquatic plants (see Laws *et al.*, 2000) but its ecological significance is difficult to assess (Peterson, 1980). In the dark, there is a net loss of assimilated carbon. Estimates of the proportion of fixed carbon lost, due to such dark respiration, vary (see Williams, 1993a;

Harris *et al.*, 1989; Eppley and Sharp,1975 and Ryther,1954). The extent of dark respiration also varies between species and between growth substrates (Laws *et al.*, 2000; Falkowski and Raven, 1997; Langdon, 1993 and Laws and Bannister, 1980).

Fixed carbon may be lost in natural samples by processes other than phytoplankton respiration including grazing activities, heterotrophic respiration (Harris, 1986) and excretion or passive diffusion of fixed carbon as dissolved organic carbon (DOC) (Raven, 1993; Harris *et al.*, 1989 and Di Tullio and Laws, 1986). The understanding and quantification of community respiration is further complicated by the uptake of excreted organic carbon by microheterotrophs (Williams, 1993a) making it difficult to tell whether high dark losses are the result of low growth, low photosynthesis to respiration ratios and high proportional respiratory losses or rapid growth and equally rapid grazing activity (Harris *et al.*, 1989).

Due to the uncertainties about respiration rate, it is difficult to assess how ^{14}C uptake values relate to gross primary production (GPP) and net primary production (NPP). GPP is the organic carbon produced by the reduction of inorganic carbon as a result of photosynthetic processes over a specified period of time (Williams, 1993b). NPP is equal to GPP minus the loss of organic carbon due to autotrophic respiration (Williams, 1993b). It is usually assumed, when using natural samples, that short incubations measure a value close to GPP whilst 24h incubations measure a value closer to net community production, which is equivalent to NPP minus the loss due to heterotrophic respiration. As the duration of the incubation increases, the measurement moves from one of algal gross production to one of net community production as a result of cycling of carbon within the contained community.

Bottle effects

Containing water samples in bottles is a standard procedure in primary production measurements. An assumption of ^{14}C experiments is that the rate of photosynthesis of a contained population is the same during an incubation as it would be in the sea (Li and Goldman, 1981). However, the isolation of a population from external physical, chemical and biological influences is likely to cause a discrepancy between experimentally measured primary production and that taking place in the water column (Li, 1982 and Li and Goldman, 1981). Bottle effects depend greatly on the relative scales of bottle size to dispersal of organisms and the time of incubation related to grazing and remineralisation rates (Harris *et al.*, 1989). Differences between free and contained populations have been attributed to both physical and biological conditions, such as a decrease in turbulence and a change in the light

regime (Venrick *et al.*, 1977) and to biological interactions including the competitive advantage of more physically robust species (Verduin, 1960).

1.2.4 Influence of methodology on ^{14}C production estimates

Duration of incubations

Many of the processes occurring during ^{14}C incubations are non-linear over time so the duration of incubation can have an impact on the measured production; experiments of different duration may involve different processes entirely. The advantage of short-term incubations is that they reflect the physiological state of cells at the time of collection (Lizon and Lagdeuc, 1998) and they may minimize the effects of respiratory and grazing loss of labelled material (Collos *et al.*, 1993). Additionally, shorter incubations could minimise photoadaptation of the phytoplankton and yield values for photosynthetic parameters closer to those at the start of the incubation. However, short-term incubations are limited by the time lag of isotopic equilibration of carbon pools within the phytoplankton (Jackson, 1993). As time increases, the results of experiments are harder to interpret due to the increasing number of processes taking place. Longer incubation time may well yield a more representative value of community production in the water column than short-term incubations. However, longer incubations are difficult to interpret because different phytoplankton within an assemblage photosynthesise at different rates and the measurement may sum processes other than photosynthesis (Morel *et al.*, 1996).

Irradiance

The light field in experiments rarely matches that experienced by phytoplankton in nature. This is especially true when phytoplankton are exposed to artificial irradiance rather than incubations under natural daylight. Changes in daylight and vertical mixing mean that it would be unusual for a phytoplankton cell to experience a constant irradiance for time periods equivalent to incubations. The use of different light sources has been shown to influence production-irradiance curves (MacIntryre *et al.*, 2000 and Lizon and Lagdeuc, 1998). The illumination level prior to incubation can also affect experimental results (Legendre *et al.*, 1983 and Ignatiades *et al.*, 1987) and the extent of photoinhibition is affected by the length of exposure time and temperature (McAllister *et al.*, 1964 and Rodhe, 1958).

Dark bottle correction

Traditionally, the dark bottle was used to provide blank correction for possible particulate contamination of the ^{14}C ampoules, abiotic exchange and biotic uptake of CO_2 (Banse, 1993). Dark bottles were incubated for the same amount of time as light bottles and the carbon fixed subtracted from light bottle values. The basic assumption behind the correction is that processes of ^{14}C fixation taking place in the dark bottle are also taking place in the light bottle, and represent non-photosynthetic fixation of carbon. Dark uptake of ^{14}C may be due to photoautotrophs or heterotrophic bacteria.

Dark fixation of carbon by photoautotrophs is thought to be a result of β-carboxylation, the synthesis of carbomoyl acid and the synthesis of sugar phosphates (Harris *et al.*, 1989 and Ignatiades *et al.*, 1987). Heterotrophic uptake of ^{14}C may be a significant factor influencing the magnitude of dark uptake (Li and Dickie, 1991and Harris *et al.*, 1989). In tropical areas, where bacterial growth on particles is significant, light and dark values converge rapidly over time as autotrophs die (Harris *et al.*, 1989). Dark uptake is not constant over the duration of experiments or over seasons and may be affected by cell density, species composition, light history of the organisms, nutrient content of the water, temperature and whether or not samples are pre-filtered (Fernandez and Bode, 1993; Furnas, 1987; Ignatiades *et al.*, 1987 and Legendre *et al.*, 1983).

Trace metal contamination

In the early 1980's trace metal contamination was considered to be a potential problem in ^{14}C experiments. It was thought that such contamination could come from standard sampling procedures, contaminated reagents and ^{14}C solution or from the use of glass equipment (Fitzwater *et al.*, 1982). However, with modern procedures including acid washing of equipment, it is no longer considered to be a problem (IOC, 1994).

Filtration and size-fractionation

There are many variations on the basic methodology in the literature. For example some experimenters prefilter samples in an attempt to remove grazers. However, this may cause mechanical damage to phytoplankton in the water system (Furnas, 1987). Size fractionation may be used in experiments to gain an idea of different groups of plankton responsible for primary production and of their varying responses to nutrient and light availability (Frenette *et al.*, 1996 and Taguchi, 1976).

1.3 The Fast Repetition Rate Fluorometer (FRRF)

1.3.1 Background and introduction: Photosynthesis and fluorescence

Fluorescence has been used for a long time as a tool in plant physiology and increased knowledge about the molecular structure of the photosynthetic apparatus has increased our understanding of its physiological basis (Krause and Weis, 1991). Fast repetition rate fluorometry is a technique used to estimate photosynthetic rates from light stimulated changes in the quantum yield of chlorophyll fluorescence (Kolber and Falkowski, 1993). The relationship between chlorophyll fluorescence and photosynthesis is complex (Krause and Weis, 1991) and the FRRF technique is based upon the fluorescence response of phytoplankton to a range of stimulating flashes (Falkowski and Raven, 1997).

The energy to drive photosynthesis is derived from the conversion of the photochemical excitation energy to electrochemical energy in the reaction centres (Suggett *et al.*, 2001). For this to occur, the specialised chlorophyll *a* molecule in a reaction centre must undergo a charge separation to yield an oxidised chlorophyll *a* molecule and an electron. The specialised chlorophyll *a* molecules are referred to as P700 and P680 in photosystems I and II (PSI and PSII) respectively due to the wavelengths at which their maximum excitation occurs. From this stage of charge separation, the chain of reduction-oxidation reactions that make up the light dependent reactions of photosynthesis begins.

When light is absorbed by the antennae pigments in the photosynthetic apparatus, the excitation energy is transferred to the reaction centres of PSI and PSII and used to drive photosynthesis. When a photon excites a chlorophyll molecule an electron is moved from one molecular orbit to another of higher energy. Such an excited molecule is unstable and will tend to return to its original unexcited state. Photochemical reactions and fluorescence are competing pathways for the deactivation of excited chlorophyll *a* (Krause and Weis, 1991). The loss as heat or transfer to non-fluorescent pigments are alternative pathways for the dissipation of energy from the excited chlorophyll molecule. Equation 1 (after Krause and Weis, 1991) shows how the fluorescence yield is related to the contribution to energy dissipation from all the competing reactions.

$$\phi F = \frac{k_F}{(k_F + k_D + k_T + k_P)} \quad (1)$$

where ϕF, is the quantum yield of fluorescence, k_F is the deactivation of chlorophyll *a* by fluorescence, k_D is deactivation by thermal loss, k_T is transfer of the energy to non-fluorescent pigments and k_P is deactivation by photochemistry. Similarly, the quantum yield of photochemistry of PSII, ϕP, is described according to equation 2 (after Krause and Weis, 1991).

$$\phi P = \frac{k_P}{(k_F + k_D + k_T + k_P)} \quad (2)$$

Equations 1 and 2 show that there is an inverse relationship between the fluorescence yield and the yield of photochemistry.

At room temperature, most fluorescence emanates from the chlorophyll in PSII (Krause and Weis, 1991). The reason for this is that oxidised P700 in PSI is more stable than oxidised P680 in PSII and can act as a trap for excitation energy, which is then dissipated as heat (Nuijs *et al.*, 1986). As a result fluorescence techniques are based mainly on the photochemistry of PSII. In PSII, the excited electron is donated to Q_A, a quinone that is the first stable electron acceptor in the PSII electron transfer chain (ETC). The unstable positively charged chlorophyll must then receive a low energy electron from a donor to reduce it before another charge separation can occur. This low energy electron is drawn, indirectly via intermediate molecules, from the photolysis of water. Until this occurs the reaction centre is in a 'closed' state and light energy will not be used for photochemistry. The electron is transferred from Q_A to a plastoquinone, Q_B. After receiving two electrons, Q_B, previously bound to a protein, dissociates and extracts two hydrogen ions from the stromal fluid and becomes part of the plastoquinone or PQ pool. The vacant space on the protein is filled by an oxidised plastoquinone. Electrons from the PQ pool are transferred, via cytochromes to PSI.

At low light levels, this transfer occurs very efficiently and more than 85% of photons are used for photosynthesis (Bjorkman and Demmig, 1987 and Papagorgiou, 1975). As light increases, the closure of more and more reaction centres is reflected in an increased

fluorescence yield. The distribution of excitation energy between fluorescence and photochemistry is controlled by the ability of the phytoplankton to use light energy for short-term activity (Kolber, 1998). The relative fluorescence is thought to reflect the level of reduction of Q_A through its control on the charge separation of the specialised chlorophyll *a* molecule (Duysens and Sweers, 1963) and maximum fluorescence is obtained when phytoplankton are light saturated and Q_A is fully reduced. The rate of re-oxidation of Q_A depends on the rate of re-oxidation of Q_B and the plastoquinone pool which is itself dependent on electron transfer via PSI and on the use of reductant in carbon fixation and other metabolic reactions (Falkowski and Raven, 1997).

1.3.2. Active fluorescence techniques, F_v/F_m and σ_{PSII}

Active fluorescence techniques measure *in vivo* fluorescence of chlorophyll resulting from a stimulating or actinic light source (Greene *et al.*, 1994). Maximal and minimal fluorescence, F_m and F_0 respectively, are measured by using a gradient of pump flashes of increasing intensity to gradually close all reaction centres by the controlled reduction of Q_A molecules. $F_m - F_0$ gives the variable fluorescence yield, F_v. The ratio of F_v/F_m is a measure of the energy conversion efficiency of PSII (Greene *et al.*, 94). Laboratory studies suggest the maximum value for F_v/F_m is 0.65. It may be expected that under ideal conditions, the value of F_v/F_m would be 1 i.e. that fluorescence when all reaction centres are open, F_0, would be equal to zero. However, this is not the case due to inefficiencies in energy transfer and charge recombination within the reaction centres (Kolber and Falkowski, 1993). For the purpose of the FRRF work, when F_v/F_m is equal to 0.65, it is assumed that 100% of PSII reaction centres are functional and the normalisation of F_v/F_m values to 0.65 gives an indication of the fraction of PSII capable of evolving oxygen (Kolber and Falkowski, 1993). Variability in F_v/F_m is associated with the physiological state of the phytoplankton (Olaizola *et al.*, 1996). It is inversely correlated with nutrient availability in some waters (Boyd and Abraham, 2001; Olson *et al.*, 2000; Geider *et al.*, 1993; Falkowksi *et al.*, 1991and Kolber *et al.*, 1990). The low values found in nutrient limited conditions may be due to the inability to assemble reaction centres in PSII (Olaizola *et al.*, 1996). Geider *et al.* (1993) showed F_v/F_m to be correlated with hydrographic conditions; influenced by photoinhibition and subject to diel variability.

The effective absorption cross section, σ_{PSII}, is the effective size of the light absorbing target in o^2 photon^{-1} (Falkowski and Raven, 1997). It is related not only to the number of

molecules that make up the light harvesting antennae but also to the efficiency of energy transfer from these molecules to a reaction centre. The value is the 'probability that an absorbed photon will result in a photochemical event' (Falkowski and Raven, 1997). A high σ_{PSII} indicates high efficiencies at light interception and subsequent transfer of energy to produce a photochemical event and therefore faster closing of reaction centres at saturating irradiance (Suggett *et al.*, 2001). The gradual closure of all reaction centres, to measure a range of F_m and F_0 values, can also be used to calculate the value of σ_{PSII} as shown in equation 3 (after Kolber and Falkowski, 1993).

$$(F-F_0)\cdot(F_m-F_0)=1-e^{-\sigma_{PSI}I\cdot J} \qquad (3)$$

where F is the fluorescence immediately following the pump flash and J is the flash intensity in photons m^{-2}. σ_{PSII} has been shown to be sensitive to nutrient concentration with its values increasing under nitrogen starvation (Kolber *et al.*, 1998). High values are associated with low light (Vassiliev *et al.*, 1994) as phytoplankton optimise their light harvesting capability.

1.3.3 The FRRF instrument

Early techniques to measure chlorophyll fluorescence were based on the exposure of dark-adapted samples to continuous light. Such experiments caused multiple turnover (MT) excitations where saturation only occurred after reduction of the plastoquinone pool because the rate of Q_A re-oxidation was faster than the rate of excitation delivery. A variety of instruments have since been developed to measure the chlorophyll fluorescence after one or more brief flashes of light. This permits a greater understanding of the gradual saturation of photosynthesis than the early techniques based on continuous light. One such instrument is the Pulse Amplitude Modulated (PAM) fluorometer, which uses a multi-turnover (MT) actinic pulse to measure maximum fluorescence (Kolber *et al.*, 1998). A contrasting instrument is the pump-and probe (P&P) fluorometer, which compares the fluorescence before and after single-turnover (ST) actinic or saturating pump flashes to measure the kinetics of the electron transfer in PSII (Kolber and Falkowski, 1993). This approach uses brief flashes to cumulatively saturate the reaction centre within a single photochemical reaction (Falkowksi and Raven, 1997).

The FRRF instrument is a modification of the earlier pump-and-probe fluorometer. It produces a series of individually sub-saturating pulses that cumulatively saturate the PSII

reaction centres. The excitation source of the FRRF is a bank of blue and green light emitting diodes with a peak at 450nm (Kolber *et al.*, 1998). The fluorescence from weak probe flashes is compared before and after a single turnover actinic flash of known intensity. The weaker flashes before and after stimulate fluorescence but are weak enough not to affect the closure of reaction centres (Kolber *et al.*, 1990). The FRRF is programmed to saturate PSII faster than the time required for Q_A re-oxidation (Suggett *et al.*, 2001). It generates a series of excitation flashes, each with a determined gap in between. Q_A re-oxidation takes 160-400μs and the flash gap is 5-10μs (Greene *et al.*, 1994).

The fluorometer has 'light' and 'dark' chambers. Samples in the light chamber reflect the photochemistry under ambient light. In contrast, samples measured in the dark chamber have experienced 1-2 seconds of darkness, which removes the immediate effect of light and allows some reopening of reaction centres.

The instrument is fully submersible which allows a variety of sampling strategies to be employed. It may be used in the laboratory in 'bench-top' mode, towed behind a boat to gain spatial coverage or used to vertically profile the water column.

1.3.4 Calculating photosynthesis from fluorescence parameters

It is necessary to introduce another level to the terminology. The notation F_v/F_m applies specifically to samples adapted to darkness. The equivalent measurement under ambient light is referred to as F_q'/F_m' if made in the light chamber and F_v'/F_m' if made in the dark chamber. F_q' is equal to the difference between maximum and steady state fluorescence in the light. The subscript 'q' refers to the quenching that occurs in the samples under ambient light

Fluorescence parameters can be used to derive estimates of photosynthetic rates through a two-stage process using photophysiological models. The first is the calculation of the electron transfer rate (ETR) according to equation 4.

$$ETR = PAR \cdot \sigma_{PSII} \cdot F_q' / F_m' \quad (4)$$

where PAR is in units of μmol photons m^{-2} s^{-1}. At saturating irradiances, ($E > E_k$), E is replaced by E_k (or the equivalent value under PAR). The value of E_k is determined by the maximum rate at which electrons can be transferred from water to the terminal electron acceptors (Kolber and Falkowski, 1993) or how quickly components of the ETC can be reoxidised to allow reaction centres to reopen after charge separation. At low irradiance, the primary electron acceptor, Q_A, is reoxidised by the next electron acceptor in the chain, Q_B, a plastoquinone. As irradiance increases, Q_B becomes increasingly reduced and the re-oxidation of Q_A becomes dependent on the
re-oxidation of Q_B, which is a much slower process controlled by the dark reactions of photosynthesis. The irradiance level at which Q_B re-oxidation becomes the rate limiting step is equal to E_k. Values of E_k are estimated according to equation 5 (after Suggett *et al.*, 2001).

$$\frac{F_q'}{F_m'} = \frac{F_v}{F_m} \cdot 1 - e^{\left(-E/E_k\right)} \cdot \frac{E_k}{E} \quad (5)$$

The conversion of ETRs to rates of carbon fixation involves equation 6.

$$PP = ETR \cdot N_{PSII} \cdot PQ \cdot \phi e \cdot [Chl] \quad (6)$$

where PP is primary production , N_{PSII} is the ratio of PSII reaction centres to chlorophyll *a* molecules, PQ is the photosynthetic quotient or ratio of photosynthesis to respiration and ϕe is the quantum yield of electron transport. The N_{PSII} value is needed in order to convert energy flow per unit time per reaction centre to a photosynthetic rate per unit chlorophyll. It is not easily measured and represents one of the areas of greatest ambiguity in the estimation of photosynthesis using the FRRF (Sugget *et al.*, 2001). Currently, for eukaryotes, an assumption of 500 chlorophyll molecules per PSII is assumed, based on laboratory data which suggests 2000 molecules of chlorophyll are involved per molecule of oxygen evolved in each photosynthetic unit and four PSIIs per photosynthetic unit (Kolber and Falkowski, 1993). The quantum yield of electron transfer, for oxygen evolution, ϕe, describes the oxygen yield per photon of light reaching PSII. The maximum value is 0.25 mols O_2 mol photons^{-1} as the transfer of four electrons are required to produce one molecule of O_2. This

value is only true if one photon of light leads to the transfer of one electron from PSII to PSI. At high irradiance, when electrons are wasted due to limitation in re-oxidation of the plastoquinone pool or other factors, ϕe will decrease.

1.3.5 Factors influencing the fluorescence measurement and interpretation

Measurement in ambient light and in darkness

Fluorescence measurements may be made on water samples adapted to ambient light or in darkness. Whilst the dark chamber in the FRRF allows limited relaxation of the PSII reaction centres, only a sustained period of darkness ensures that all reaction centres are open prior to the measurement of fluorescence response. Estimates of how long complete relaxation takes vary from 15 minutes (Flameling and Kromkamp, 1998) to 30 minutes (Geider *et al*, 1993). Samples may be incubated in darkness prior to using the FRRF in the 'benchtop' mode to ensure all reaction centres are open. Alternatively *in situ* night time profiling can also provide dark adapted values. Parameters measured under ambient light are labelled with a prime symbol (').

Quenching

Quenching is the loss of fluorescence due to a competing pathway for the deactivation of an excited chlorophyll molecule including any of those in equation 1. Quenching is typically described in two parts: that due to photochemistry (often called QP) and that due to other factors: 'non-photochemical quenching' (QN) such as thermal dissipation. Photochemical quenching, due to photosynthesis occurs only in light so an understanding of the importance of non-photochemical quenching can be gained by comparing F_m' with F_m. Non-photochemical quenching is not constant and is seen to increase at very high light.

1.4. Remote sensing of primary production

1.4.1 Background and introduction

The application of remote sensing has emerged as a potential way to measure primary production on a scale large enough to be globally significant and to take account of phytoplankton responses to large scale oceanic events (Behrenfeld *et al.*, 2002). Remotely-sensed ocean colour maps provide the ideal tool for the extrapolation of local primary production data from ships to global scale information. As productivity cannot be remotely

sensed directly, the conversion of remotely sensed signals into estimates of primary production relies on the use of algorithms that relate detectable parameters to biological processes. Many models have been developed to estimate production from remotely sensed data. Their complexity varies as well as the methods used to derive values for the variables. However, all models share the requirement for a remotely sensed estimate of chlorophyll concentration derived from ocean colour data.

1.4.2 Ocean colour, SeaWiFS and the calculation of water leaving radiance

Ocean colour and SeaWiFS

The spectral variation of water leaving radiance can be related to concentrations of phytoplankton pigments, coloured dissolved organic matter (CDOM) and suspended particulate matter (SPM)(Hooker *et al.*, 1992). Water leaving radiance (L_w) is downwelling solar irradiance that penetrates the water surface, interacts with the water body and is scattered back into the atmosphere (Lavender, 1996). Satellites orbiting the earth subsequently detect this radiance.

The Orbital Sciences Corporation launched SeaWiFS (Sea-viewing Wide-Field-of-view Sensor) in 1997 on the ORBVIEW-2 satellite and research use of the data was purchased by NASA. SeaWiFS measures radiance in eight wavebands: six in the visible spectrum (at 412 nm, 443 nm, 490 nm, 510 nm, 550 nm and 670nm) and two in the near infra-red or NIR (at 765nm and 865nm). The bands were chosen based on the spectral absorption characteristics of common in-water optical constituents as well as the spectral transmittance of atmospheric particles (Hooker *et al.*, 1992). SeaWiFS produces data at two levels of resolution. The local area coverage or LAC data have pixels of 1.1km x 1.1km at nadir and the global area coverage or GAC data has pixels of 4.5km x 4.5 km at nadir. Images with pixels of 9.0km x 9.0km at nadir are also available. The high resolution data are sent to receiving stations around the world in HRPT form (High Resolution Picture Transmission), referred to as level 0 data. A decoding process converts these to level 1 data (in Hierarchical Data Format (HDF)), which are then transferred to NASA or other licensed research groups where the atmospheric correction is applied and values of biological and geophysical products (level 2 data) calculated.

Atmospheric correction

The radiance signal received by the satellite is a function not only of the radiance leaving the ocean but also of a number of atmospheric components as shown in equation 7 after Barnes *et al.* (2001).

$$L_T(\lambda)=L_R(\lambda)+[L_A(\lambda)+L_{RA}(\lambda)]+T(\lambda)\cdot L_G(\lambda)+t(\lambda)\cdot L_{WC}(\lambda)+t(\lambda)\cdot L_w(\lambda) \quad (7)$$

where $L_T(\lambda)$ is radiance at the top of the atmosphere, $L_R(\lambda)$, $L_A(\lambda)$ and $L_{RA}(\lambda)$ are contributions from scattering by air molecules (Rayleigh scattering, aerosols, and Rayleigh-aerosol interactions respectively), $L_G(\lambda)$is the contribution from sun glint which is attenuated by direct transmittance of the atmosphere, $T(\lambda)$, $L_{WC}(\lambda)$ is the upwelling radiance that arises from whitecaps on the ocean surface and is attenuated by the diffuse transmittance of the atmosphere, $t(\lambda)$ and $L_W(\lambda)$ is the portion of radiance that leaves the surface of the water. Only 5-10% of the signal originates from water so corrections must be applied to account for the atmospheric signal (Lavendar, 1996). Ocean colour imagery is generally corrected by the removal of data where sunglint is present and the use of models that characterise the spectral characteristics of a range of atmospheric constituents. The main atmospheric constituents considered are gases, aerosols, ozone and water vapour (Lavender, 1996). The contribution of each of the components in equation 7 to $L_T(\lambda)$ varies with meteorological conditions so whilst some values can be derived from published data, other corrections must be calculated for each ocean colour image. Such correction values are estimated from spectral radiance values obtained from pixels where $L_w(\lambda)$ is known to equal zero.

The aim of atmospheric correction is to generate the radiance value that would be obtained from a sensor just above the sea surface, $L_w(\lambda)$. $L_w(\lambda)$ is a function of the downwelling light field, interface effects and the inherent optical properties of water column constituents integrated over one to two optical depths (Aiken *et al.*, 1995) and is calculated according to equation 8 after Aiken *et al.* (1995).

$$L_w = F_0 \cdot \left[\frac{(1-\rho)\cdot(1-\tilde{\rho})\cdot R}{n^2 \cdot (1-rR)\cdot Q} \right] \quad (8)$$

where F_0 is extraterrestrial irradiance, n is the refractive index of seawater, R is the irradiance reflectance, r is the air-water reflectance for diffuse irradiance, Q is the ratio of upwelling irradiance to radiance, ρ is Fresnel's reflectivity at normal incidence and $\tilde{\rho}$ is Fresnel's equation for sun and sky irradiance.

Case I and Case II waters

NASA SeaWiFS algorithms and SeaDAS (the NASA SeaWiFS Data Analysis System) are designed for Case I waters where variations in the optical signal are derived from photosynthetic materials alone (Moore *et al.*, 1999). In Case II waters the optical signal is modified by the presence of CDOM and SPM. CDOM decreases reflectance as it absorbs significantly in the blue relative to the red part of the spectrum (Lavender and Groom, 1999). The presence of SPM affects the atmospheric correction of remotely sensed data, which assumes no L_w in the NIR bands. SPM causes otherwise dark pixels, used for the correction, to appear as bright pixels. As a result, Case II waters require special atmospheric correction. The SeaAPS system, developed at Plymouth Marine Laboratory, is based on SeaDAS but has a number of modifications including algorithms to correct for the 'bright-pixel' effect caused by the presence of SPM. A detailed description of the system is given in Moore *et al.* (1999) and Lavender and Groom (1999).

1.4.3 Chlorophyll retrieval

Information on the optically active substances in the ocean can be derived from analysis of L_w values. As phytoplankton concentration increases, the reflectance in the blue decreases and that in the green increases so a ratio of the two can be used to gain quantitative estimates of pigment concentration. However, the performance of the chlorophyll *a* algorithm can never be perfect due to the change in relative abundance of pigments and phytoplankton species with region and season (Aiken *et al.*, 1995). Equations 9 and 10 show the latest algorithm used to calculate chlorophyll concentration (taken from the SeaWiFS website).

$$[Chl]=10^{(0.366-3.067X+1.930X^2+0.649X^3-1.532X^4)} \quad (9)$$

where $$X=\log 10\frac{L_w 443}{L_w 555} \; or \; \frac{L_w 490}{L_w 555} \; or \; \frac{L_w 510}{L_w 555} \quad (10)$$

The maximum of the three ratios (443:555, 490:555, 510:555) is used.

1.4.4 Estimation of production from remote sensing algorithms

Prediction of the profile of biomass with depth

If the satellite derived chlorophyll is used directly in models the assumption of uniform distribution of pigment with depth is usually made. This has been a common feature in primary production modelling (see Behrenfeld and Falkowski, 1997a; Platt, 1986; Rodhe, 1966; Talling, 1957 and Ryther, 1956). Some authors maintain that the volume of biomass in the water is related to its surface concentration so the whole column biomass is reflected in the satellite information (Morel and Berthon, 1989). However, it is argued by others that the assumption of uniform biomass can lead to an error of up to 90% in predictions of total chlorophyll in the photic zone, particularly if a deep chlorophyll maximum is present in the water column (Sathyendranath and Platt, 1989). One approach to overcome this problem has been the use of a shifted Gaussian curve to generate a more realistic profile (Sathyendranath and Platt, 1989). Other similar approaches include the adoption of a triangular biomass profile with depth (Mueller and Lang, 1989) or an asymmetric curve (Li and Wood, 1988).

Look-up tables of production for different types of water bodies are also used (see Antoine and Morel, 1996) and separate tables can be applied to stratified and well mixed water. The rationale is that, when stratification occurs within the euphotic layer, a non-uniform chlorophyll profile results and a deep chlorophyll maximum may occur. In contrast, when the mixed layer is thicker than the euphotic layer, a uniform distribution of pigment results. Antoine and Morel (1996) also suggest that remotely sensed data, such as sea surface temperature, should be used to decide which table is most suitable for the area under consideration.

Prediction of light and the effect of light

One of the areas where there is lack of agreement in modelling primary production is how to account for the effect and variability of light. Models are used to estimate light at the sea surface and at depth. The fundamental importance of light in photosynthesis has lead to a variety of approaches being proposed ranging from simple linear relationships between light and photosynthesis (Platt, 1986) to complex models which attempt to account for the availability and effects of individual wavelengths (Antoine and Morel, 1996; Morel, 1991 and Sathyendranath *et al.*, 1989). The influence of light can be separated into physical and biological categories, the availability to plants and its use by them for driving photosynthesis. In other words, a comprehensive model would account both for the spectral quality of light available to phytoplankton and for the absorption and use of individual wavebands by phytoplankton, at the surface and at depth.

Calculation of surface irradiance

In some models irradiance is not included directly but instead, a coefficient is included to scale down primary production by a value to account for non-optimal light conditions (e.g. Behrenfeld and Falkowski, 1997a; Wright, 1959; Rodhe, 1958 and Talling, 1957). In these models, removal of the light factor would effectively leave a model that returned a primary production value for maximum light conditions. This approach is based on the hypothesis that changes in surface irradiance have relatively minor effects on production variability (Behrenfeld and Falkowski, 1997b).

A number of models use values for the Julian day and latitude to tailor 'standard' solar energy values to the specific time and location to estimate the surface irradiance (e.g.Platt *et al.*, 1990). In this case, the solar irradiance is adjusted to the particular day and location using a calculation of the solar declination angle. Solar declination, derived as a function of Julian day, is 'the angle between the equatorial plane of the earth and the axis joining the centre of the earth and the sun' (Platt *et al.* 1990). The resulting value is corrected for cloud albedo, absorption by water vapour, cloud cover and atmospheric albedo (using a series of constants) to calculate the total surface short-wave radiance.

A more complex approach to light is to split irradiance into direct and diffuse (or sky) components (E_d and E_s respectively, after the notation of Bird (1984) with the 'd' and 's' subscripts referring to direct and sky light respectively) (e.g. Antoine and Morel, 1996;

Morel, 1991; Gregg and Carder, 1990 and Sathyendranath *et al.*, 1989). E_d and E_s are then resolved into individual wavelengths.

Attenuation of light with depth

The value of K, the attenuation coefficient of light with depth, depends not only on the concentration of light attenuating compounds but also on the angular distribution of the light field (Morel and Smith, 1982). It thus varies spectrally and over the course of the day in correspondence with the changing light field. Wavelength specific values of attenuation can be calculated directly from changes in light at depth as in equation 11 (after Morel, 1988).

.

$$K(\lambda) = \frac{1}{z}.\ln\left[\frac{E_0(\lambda)}{E_z(\lambda)}\right] \tag{11}$$

where $K(\lambda)$ is the attenuation at a particular wavelength (m^{-1}); z is the depth (m), $E_0(\lambda)$ is light at sea surface (at a particular wavelength ($Wm^{-2}\ \mu m^{-1}$)) and $E_z(\lambda)$ is light at depth z ($Wm^{-2}\mu m^{-1}$). However, measurements of light are not always available so approximations for attenuation are often used. A common approach is the division of total attenuation, K_{TOT} (m^{-1}), into three separate components: k_w, the attenuation due to pure seawater, k_c, the attenuation due to phytoplankton and co-varying substances and k_x the attenuation due to detritus and other non-photosynthetic substances. Equation 12 shows the general form of the equation used where the three components are considered to have an additive effect (after Morel, 1988).

$$K_{TOT} = k_w + k_c.[Chl] + k_x \tag{12}$$

where [Chl] is the chlorophyll concentration in mg m^{-3}. Equations of this form may be used to calculate the average attenuation for the whole water column or separate values at each depth, with the chlorophyll concentration being altered accordingly (e.g. Lorenzen, 1972). Many authors have noted the strong dependence of K_{TOT} on k_c.[Chl]. As a result standard values are often adopted for the parameters in the equation and k_x is even omitted in some examples. However, K_{TOT} and k_c.[Chl] are not linear and the inclusion of k_x may be required to account for this. This non-linearity can alternatively be accounted for by using two different slopes to describe K_{TOT} at different concentrations of chlorophyll (e.g. Smith and Baker, 1978). In the more complex, spectrally resolved models, K_{TOT} is often calculated

at individual wavelengths (e.g. Sathyendranath *et al.*, 1989). When used to describe the attenuation of broadband PAR, K_{TOT} is referred to as K_{PAR}.

Modelling the relationship between light and photosynthesis

The final stage in the models is the description of the light regulation of photosynthesis. In the complex wavelength resolved models, the distinction between total irradiance and PAR is easily made by simply ignoring wavelengths outside the suitable range. Some models incorporate typical absorption and action spectra to account for the wavelength dependence of photosynthesis (eg. Morel, 1991; Antoine and Morel, 1996). In the simpler models approximations are often made to scale total irradiance to the proportion considered to be PAR (e.g. Platt *et al.*, 1990). Considerable variation exists in the final incorporation of light into the primary production equation. The majority of models incorporate light via the parameters of a PE curve. A large number of models incorporate α^B and P^B_{max}, into models as unchanging or 'generic' values for the whole water column (e.g. Platt *et al.*, 1994; Platt and Sathyendranath, 1993; Platt *et al.*, 1990 and Sathyendranath and Platt, 1989). Alternatively, the amount of light available at the surface may be scaled to the photosynthetic parameters making it dimensionless and normalising it to photoadaptation (see Platt *et al.*, 1990). Variability in photosynthesis has also been described as a polynomial function of temperature (Behrenfeld and Falkowski, 1997b).

The inclusion of photoinhibition in models has not been universal. In the absence of photoinhibition, the maximum rate of photosynthesis would always occur at the surface (Behrenfeld and Falkowski, 1997a) but the incorporation of photoinhibition into primary production models produces more realistic results (Morel, 1991). Some models account for photoinhibition with an equation which leads to a decrease in irradiance dependence as irradiance increases above that need for maximum photosynthesis (Behrenfeld and Falkowski, 1997a; Vollenweider,1966 and Ryther and Yentsch,1957). Others (see Platt *et al.*, 1990) allow for the inclusion of photoinhibition as an optional factor to be subtracted from the original primary production prediction. The overall effect of photoinhibition on final primary production measurements is difficult to separate from the effects of extreme temperature and other factors. As such it can be difficult to include in models (Antoine and Morel, 1996 and Platt *et al.*, 1990).

1.5 Scope of the thesis

A major challenge in comparing the three techniques for estimating primary production is the variability in their scales of measurement and consequently in the parameters measured. Parameter values determined by the ^{14}C technique are often derived from one depth. Additionally, values derived from ^{14}C can be considered an average over the duration of the incubation and may also be affected by photoacclimation or photodamage during the experiment. In contrast, to make measurements at specific stations, the FRRF is usually profiled through the water column and derived photosynthetic values therefore reflect an average value over the whole water column, instantaneous at the time of deployment. Production values from SeaWiFS are derived from one point in the day and are biased to the surface water. A further complication to comparison of the methods is the variety of protocols used for the ^{14}C technique. It follows that a very extensive set of primary productivity measurements exists but comparisons between them are limited due to the uncertainties surrounding the technique and the different properties that they measure.

The study of the techniques is divided into three major sections. The first is an investigation into the variability in measures of photosynthetic fitness and primary production obtained when different types of ^{14}C incubation are used. This is addressed through a series of laboratory studies where incubations will be carried out under different light regimes and for different durations. Additionally, estimates of daily depth-integrated primary production modelled from PE parameters from short-term incubations will be compared with that measured directly from 24h *simulated-in-situ* incubations. The results should allow quantification of the variability expected when different approaches are used and an understanding of how estimates from different experimental protocols relate to each other.

In the second part of the study, production estimates from ^{14}C are compared with those from the FRRF. Estimates of daily depth-integrated production will be derived in a number of different ways from the FRRF data. The variability between results from the different approaches and between measurements made at different times of the day under different light regimes will be assessed. Only one ^{14}C approach will be used but its relation to other ^{14}C estimates will have been established in the previous chapter.

In the third section, chlorophyll and production estimates from remote sensing will be compared with estimates from ^{14}C and the FRRF. Given the requirement of all satellite

production algorithms for a measure of biomass, SeaWiFS chlorophyll estimates at the sites of interest are compared to measurements made on water samples. Finally, three different algorithms for the estimation of primary production from remotely sensed data are compared. These range from a simple empirical algorithm to a complex semi-analytical algorithm.

In addition to the direct comparison of techniques, statistical analysis and modelling will be used to quantify the uncertainty associated with estimates of daily, depth-integrated production from ^{14}C, FRRF and remote sensing approaches. The uncertainty around such production estimates has not been calculated before, due to the complexity of models, and this work demonstrates the importance of understanding the error associated with each approach when considering the merits and limitations of different techniques.

The measurements made during 2001 at L4, a coastal site in the Western English Channel, will allow new estimates of annual production at the site to be made. From these estimates, a new understanding of the importance of the area for carbon fixation will be gained. The contribution of photosynthesis at different times of the year, driven by changing environmental and hydrographic conditions, to the annual carbon fixation at the site will be calculated. This knowledge will help to optimise future studies by identifying times of year when measurements are required frequently, due to rapid changes in production, and times when conditions are more stable and measurements can be made less frequently. It will also help to understand whether the limitations of specific techniques, at particular times of year, are likely to have a major impact on the measurement of annual production.

The specific questions to be addressed are summarised as follows:

1. How variable are estimates of primary production from the ^{14}C technique when different experimental protocols are used and in particular how do incubation time and light regime affect the estimates?
2. How similar are estimates of photosynthetic parameters and daily depth-integrated production from the FRRF to those estimated from short-term ^{14}C incubations?
3. How reliable are SeaWiFS estimates of chlorophyll at coastal sites?
4. How do production estimates from satellite algorithms compare to estimates from ^{14}C and the FRRF and to each other over a seasonal cycle?
5. How confident can we be in the estimates produced from each technique?
6. How much carbon is fixed annually at L4, a coastal site in the Western English Channel?

Chapter 2. Methods

2.1 Background and rationale to sampling strategy

The aims of the work were addressed through measurements in the laboratory and at sea - a cruise and a time series study using weekly sampling to follow the changes in productivity over the course of 2001.

In late May 2000, approximately six weeks after the expected onset of the spring bloom, experiments were carried out in the Celtic Sea from RRS Discovery. The Celtic Sea is a region where high variability in production occurs over short geographic distances. The vertical stability of the water column, controlled by the tidal current velocity is an important factor in determining the spatial and temporal variation of phytoplankton production in the region (Pingree, 1975). The area is characterised by a front that separates the well mixed waters in the north of the region in St.George's channel from the seasonally stratified waters to the south. The thermocline does not form simultaneously over the whole region but starts in the area south of Ireland and spreads eastwards as surface temperature increases (Pingree, 1975). The distribution of phytoplankton populations is related to nutrient concentrations and light availability, maximum production values being associated with the tidal front (Pingree *et al.*, 1982). As the front progresses during April and May, rapid changes in productivity and nutrient concentrations are seen (Rees *et al.*, 1999). The cruise allowed a comparison of photosynthetic characteristics from ^{14}C techniques with those from the FRRF over a range of hydrographic conditions within close proximity to each other. Seven stations were studied over 11 days of sampling but PE parameters were only measured during the second half of the cruise. This study will focus on three stratified stations to the south of the front occupied during the second half of the cruise. The intention was also to compare these field measurements with satellite remote sensing data but, unfortunately, there was only one clear satellite image during this cruise.

Seasonal measurements were made at station L4 throughout 2001, a site to the South of Plymouth Sound in the Western English Channel at 50°15'N, 4°13'W. During the winter, the water column is well mixed and contains relatively high levels of suspended sediment in this region. In the summer, the water stratifies but some weather driven mixing occurs and at some times of the year the site is at the edge of the tidal front in the region (Pingree *et al.*,

1978). The site is also subject to sporadic influence from the river Tamar. L4 is a highly heterogeneous site, classified as Case I or Case II depending on the time of year and prevailing conditions. Weekly sampling over a year (2001) at L4 allowed the three techniques – ^{14}C estimates, FRRF and Remote Sensing - to be used not only in a comparative sense but also as tools to study the seasonal cycle of production. Water was collected from the surface by bucket and poured into a 20l polycarbonate carboy for transfer back to the laboratory. During transfer, it was stored at ambient temperature, in the shade on the deck of the boat. The water arrived at the laboratory within 3h of sampling.

2.2 Chlorophyll concentration

2.2.1 Measurements from water samples

General procedures

The routine determination of chlorophyll *a* concentration involved filtering water samples through 25mm Whatman GFF filters. Analysis was carried out either by High Pressure Liquid Chromatography (HPLC) or using fluorometric techniques. Samples for HPLC analysis were immediately frozen and stored in liquid nitrogen. Those for fluorometric analysis were frozen and stored at –20°C. The majority of measurements of chlorophyll concentration were made by HPLC analysis but in experiments addressing the effect incubation time on measured ^{14}C uptake, fluorometric analysis was used.

Analysis using HPLC[1]

Between 1l and 2l of water was filtered. The defrosted filters were placed in centrifuge tubes with 2ml of 90% acetone. The filters defrosted in the time taken to prepare the samples. Pigments were extracted by ultrasonification and the samples centrifuged. Determination of chlorophyll *a* and other pigments was carried out using the method of Mantoura and Llewellyn (1983).

Fluorometric analysis

Between 40ml and 200ml of water was filtered. The frozen filters were placed in centrifuge tubes and 10ml of 90% acetone added. Samples were left overnight at –20°C, the filters were

[1]James Fishwick (PML) carried out HPLC analysis of L4 samples. Denise Cummings (PML) provided the HPLC measurements from the Celtic Sea cruise.

removed from the acetone and analysis carried out. Samples for fluorometric analysis were not extracted using ultrasonification and this was shown to have a negligible effect on chlorophyll concentration when compared to results from samples extracted by soaking overnight in acetone (data not included here). Chlorophyll *a* concentration was determined in a spectrofluorometer (Perkin-Elmer Luminescence Spectrometer LS 50B) using the technique of Welschmeyer (1994). The fluorometer was calibrated before each batch of analyses with a chlorophyll standard (Sigma-aldrich chlorophyll *a* extract from spinach). The concentration of chlorophyll in the standard was measured in a spectrophotometer using an extinction coefficient of 87.67 for chlorophyll in acetone (from Jeffrey and Welschmeyer, 1997).

2.2.2 Chlorophyll retrieval from SeaWiFS data

Chlorophyll *a* concentration was derived from high resolution (1km x 1km pixels) and low resolution (9km x 9km pixels) SeaWiFS ocean colour images produced by the Remote Sensing Group at Plymouth Marine Laboratory.

The Remote Sensing Group obtained level 1 SeaWiFS data from the satellite receiving station at the University of Dundee. Atmospheric correction and the derivation of SeaWiFS products, including chlorophyll *a* concentration, were carried out using SeaAPS (SeaWiFS Automatic Data Processing System) (see Lavender and Groom, 1999). The chlorophyll estimates used were the averages of the nine pixels surrounding and including the pixel of interest (within which the *in situ* sample was taken). A variety of quality control processes were carried out to remove spurious data and are discussed in chapter 5.

2.3 Production and photosynthetic parameters using the ^{14}C tracer method

2.3.1 General procedures and processing

Experimental protocols for the estimation of primary production

Water samples were decanted into acid washed 1l polycarbonate bottles and distributed to 60 ml polycarbonate bottles that had been cleaned to JGOFS standards (IOC, 1994). Ampoules containing 0.5ml of $NaHCO_3$ with a radioactivity of 37MBq (1mCi) were obtained from Amersham Pharmacia Biotech Ltd. The contents of each ampoule was diluted in 9.5ml of pre-fitered sterile seawater to make 10ml of a stock solution with a radioactivity of

3.7 MBq ml^{-1}. The dilution was carried out using a Pasteur pipette to transfer small aliquots of liquid reciprocally between the ampoule and the bottle containing the sterile seawater to ensure the complete removal of the radioactive liquid from the ampoule. The stock bottle was closed with an airtight seal and stored at 4°C between each use.

The samples were inoculated with 370 KBq (10 μCi) $NaH^{14}CO_3$ dispensed with a P100 Gilsen pipette. The same volume of $NaH^{14}CO_3$ was added to 10ml of a carbon dioxide absorber (Carbo-sorb E supplied by Packard) to measure the total radioactivity added to each sample. Estimates of dark carbon fixation were obtained by covering the polycarbonate bottles with aluminium foil. After incubation, the samples were filtered through 47 mm diameter, 0.2 μm pore-size Nuclepore polycarbonate filters. The filters were exposed to fuming HCl, to remove any inorganic radiocarbon on the filter, and were then transferred to scintillation vials and dried in a dessicator with active silica gel for at least 12 hours before the addition of 2.5ml scintillation cocktail (Wallac OptiPhase 'Hi Safe'3). The ^{14}C content of the filters was measured with a liquid scintillation counter (LKB-Wallac 1219 RackBeta LSC) and carbon fixation rates were calculated using equation 13.

$$PP = \frac{DPM \cdot TCO_2 \cdot 1.05}{Total\ DPM \cdot Hours\ incubation} \tag{13}$$

where PP is primary production (mg C m^{-3} h^{-1}), DPM is the radioactivity of the sample (disintegrations per minute), TCO_2 is the total weight of carbon dioxide present (in mg C m^{-3}) and *Total DPM* is the total radioactivity added to the sample as measured from the carbon dioxide absorber. The factor 1.05 accounts for the isotope discrimination factor - the preferential uptake by plants of ^{12}C over ^{14}C (Strickland and Parsons, 1968). The total weight of carbon dioxide present was calculated according to equation 14 (after Parsons *et al.*, 1984).

$$TCO_2 = ((salinity \cdot 0.067) - 0.05) \cdot 0.96 \cdot 12010 \tag{14}$$

where 0.067 converts salinity (in psu) to total alkalinity (in meq l^{-1}), the subtraction of 0.05 converts total alkalinity to carbonate alkalinity (in meq l^{-1}), multiplication by 0.96 converts carbonate alkalinity into total carbon dioxide (in meq l^{-1}) and multiplication by 12010 converts the units to mg C m^{-3}. At L4, salinity was assumed to be 35 psu as measured values

were not available for much of the year. In the Celtic Sea, measured salinity values were used.

Calculation of photosynthetic parameters

To calculate photosynthetic parameters, data were normalised to the chlorophyll *a* concentration of the sample and a non-linear regression carried out to fit the curve described by equation 15a or 15b depending on whether or not the effects of photoinhibition were included (after Platt *et al.*, 1980). Curve fitting was carried out in SPSS Sigmaplot 2001.

$$PP^{B} = P_S^B \cdot \left(1 - e^{-\left(\frac{\alpha^B \cdot PAR}{P_S^B}\right)}\right) \tag{15a}$$

$$PP^{B} = P_S^B \cdot \left(1 - e^{-\left(\frac{\alpha^B \cdot PAR}{P_S^B}\right)}\right) \cdot e^{-\left(\frac{\beta^B \cdot PAR}{P_S^B}\right)} \tag{15b}$$

where PP^{B} is chlorophyll *a* normalised primary production (mg C [mg Chl]$^{-1}$h^{-1}), P^{B}_{s} is the maximum potential light saturated photosynthetic rate under prevailing conditions (mg C [mg Chl]$^{-1}$ h^{-1}), α^{B} is the light limited rate of photosynthesis (mg C [mg Chl]$^{-1}$ h^{-1} [µmol photons m^{-2} s^{-1}]$^{-1}$), β^{B} is the photoinhibition parameter (mg C [mg Chl]$^{-1}$ h^{-1} [µmol photons m^{-2} s^{-1}]$^{-1}$) and PAR is the incident photosynthetically active radiation (µmol photons m^{-2} s^{-1}). When the equation that did not include photoinhibition (15a) was used, P^{B}_{m}, the specific production rate at optimal light intensity, was equal to P^{B}_{s}. When the equation that included photoinhibition was used, the value of P^{B}_{m} was derived using equation 16 after Platt *et al.*, (1980).

$$P_m^B = P_S^B \cdot \left(\frac{\alpha^B}{\alpha^B + \beta^B}\right) \cdot \left(\frac{\beta^B}{\alpha^B + \beta^B}\right)^{\beta^B/\alpha^B} \tag{16}$$

E_k, in µmol photons m^{-2} s^{-1}, was calculated according to equation 17.

$$E_k = \frac{P_m^B}{\alpha^B} \tag{17}$$

2.3.2 Incubation procedures

Photosynthetic parameter determinations in a large static water tank

Incubations were carried out in large water filled tank in a temperature controlled laboratory. This incubator was used as it allowed the samples to be separated by 50cm of water. This was expected to lead to more realistic spectral attenuation of light than obtained in incubators where only the samples and the incubation bottle walls contribute to the light attenuation. The tank was 5m long by 60cm wide and 30cm deep and was lit by 3 metal halide discharge lamps (Osram POWERSTAR® HQI-TS 150 lamp) at one end. At 50cm intervals from the light source, a rope was fixed horizontally across the tank to attach the sample bottles. Samples could be incubated at ten light intensities, ranging from 10 to 1300μmol photons m^{-2} s^{-1}. The tank was kept at the temperature of the sea at L4 by a refrigeration unit.

The value of α^B is wavelength dependent and a correction was made for the emission spectrum of the lamp using equations 18 to 21 after Arrigo and Sullivan (1992).

$$\alpha^B_{post-correction} = \alpha^B_{pre-correction} \cdot x \tag{18}$$

where
$$x = \frac{A_{in\,situ}}{A_{inc}} \tag{19}$$

where
$$A_{in\,situ} = \frac{\sum_{400}^{700} E_{in\,situ}(\lambda) \cdot a_{phyt}(\lambda)}{\sum_{400}^{700} E_{in\,situ}(\lambda)} \tag{20}$$

and where

$$A_{inc} = \frac{\sum_{400}^{700} E_{inc}(\lambda) \cdot a_{phyt}(\lambda)}{\sum_{400}^{700} E_{inc}(\lambda)} \quad (21)$$

where $E_{in\,situ}(\lambda)$ and $E_{inc}(\lambda)$ are the wavelength specific irradiances from natural sunlight and from the lamp in the incubator respectively and $a_{phyt}(\lambda)$ is the wavelength specific phytoplankton absorption. Measurements of the lamp spectra were made using a spectroradiometer (Trios Ramses-ACC-VIS hyperspectral radiometer). The spectrum was measured at each position in the flume and, given the low variability between values at each position in the flume, an average taken for the light correction. A standard irradiance spectrum of sunlight (after Neckel and Labs, 1984) was corrected for the depth of water collection and used to describe *in situ* irradiance.

Photosynthetic parameter determinations in a portable light gradient incubator

Fifteen bottles were incubated for 3-4h in a portable light gradient incubator, which was cooled with surface seawater or tap water. The sample bottles were packed tightly within a narrow column lit from one end. The light source was a 12V Tungsten-Halogen lamp with a blue filter to simulate the spectra of natural light in seawater (the final spectra is shown in figure 3.1). Unlike the large static water tank, light attenuation in this incubator was mainly due to the samples and their bottles. The spectrum of attenuation is therefore likely to differ from that in the water column. However, incubators such as this allow the easy measurement of photosynthetic parameters at sea. At the end of the incubation period, PAR was measured at each position in the incubator using a PAR meter (Chelsea Technologies Group) fitted with a fibre optic probe and spherical light collector. The probe was placed in a bottle filled with seawater and measurements taken by replacing sequentially the experimental bottle at each position in the column. Spectral correction was carried out on values of α^B as described above.

Simulated-in-situ incubations

Simulated-in-situ incubations are designed to measure the expected daily productivity through the water column without the need to deploy samples at sea. Samples are taken from a number of depths and incubated for 24h in on-deck incubators at irradiance levels equivalent to those expected at the depth of sampling. Water was collected from six depths, corresponding to 1, 5, 14, 20, 55 and 97% of irradiance just below the sea surface. For each

depth, three light bottles and one dark bottle were inoculated and incubated in an on-deck incubator, cooled with surface seawater. Neutral density filters simulated light attenuation in the water column so that the bottles were incubated at irradiance levels approximating those at the depth of sampling. Incubations lasted 24h and were started before dawn to prevent light shock to the phytoplankton.

2.4 Production and photosynthetic parameters from the FRRF

2.4.1 Protocols, deployment and initial processing

A FAST-TRACK (Chelsea Technologies Group. S/N 182018) FRRF with dual 'light ' and 'dark' chambers was used to measure active fluorescence. Vertical profiles of FRRF parameters were obtained[3]. The FRRF was attached to an optical profiler oriented with the LED array facing horizontally. The optical profiler was deployed where possible over the sunward deck to avoid ship shadow and the system profiled slowly at 0.1m s^{-1}. An acquisition sequence of 100 saturation flashes, 20 relaxation flashes and 10 ms sleep time between acquisitions was used. The flash duration was set to either 4 or 8 (instrument units). Filtered seawater blanks were determined for both light and dark chambers and found to be insignificant (<1% of the F_m signals) so no corrections were made to the measurements to account for these values.

During the quality control procedure, data were deleted where the instrument gain setting was greater than 16, where depth was less than 0, where PAR was less than 0 and where the effective absorption cross-section of PSII was greater than 750 x 10^{-20} m^2 $photon^{-1}$. The data were aggregated over fixed 2m depth intervals.

2.4.2 Calculation of photosynthetic parameters and instantaneous primary production

Photosynthetic parameters

Photosynthetic parameters were calculated from equations 22 and 23 using data from the light chamber.

[3] Data collected by James Fishwick and Gerald Moore at L4 and by Tim Smyth and Jim Aiken in the Celtic Sea

$$\alpha^B = 0.00121 \cdot \sigma_{PSII} \cdot \left[\left(\frac{F_q'}{F_m'} \max \right) / 0.65 \right] \quad (22)$$

where α^B is in units of mg C [mg Chl]$^{-1}$ h^{-1} [µmol photons m^{-2} s^{-1}]$^{-1}$. The constant 0.00121 accounts for the conversion of units (from mol C [g Chl]$^{-1}$ mol photons^{-1} m^{-2} to the given units), for the requirement of four electrons to evolve one mol of oxygen and for a PQ value of 1.2.

$$P_m^B = \alpha^B \cdot E_k \quad (23)$$

where P_m^B is in units of mg C [mg Chl]$^{-1}$ h^{-1}. The value of E_k, the light saturation parameter, was obtained from values of F_v/F_m and F_q'/F_m' fitted to an exponential model as shown in equations 24 after Smyth *et al.*, (In prep).

$$\frac{F_q'}{F_m'} = \frac{F_v}{F_m} \cdot \exp\left(\frac{E}{E_k}\right) \cdot \frac{E}{E_k} \quad (24)$$

The values were corrected for the emission spectrum of the FRRF LEDs as described for photosynthetic parameters from ^{14}C in equations 18 to 21.

Primary production

Instantaneous production was calculated from fluorescence parameters using equation 25. Values of F_q'/F_m', σ_{PSII} and PAR were recorded at every depth interval so PP was calculated at every depth and integrated over the water column.

$$PP_z^{FRRF(inst)} = 0.073 \cdot \frac{\left(F_q' / F_m' \right)_{(z)}}{0.65} \cdot \sigma_{PSII(MAX)} \cdot PAR_{(z)} \cdot N_{PSII} \cdot (PQ)^{-1} \cdot [Chl] \quad (25)$$

where PQ was assigned a constant value of 1.2 and N_{PSII} was assumed to be equal to 1/500. The value 0.073 accounts for a number of unit conversions (chlorophyll from mols to mg;

σ_{PSII} from o^2 photon^{-1} to m^2 photon^{-1}; PAR from μmol m^{-2} s^{-1} to photons m^{-2} s^{-1} and time from seconds to hours and the requirement of four electrons to evolve one mol of oxygen.

One profile of production against *in situ* PAR was produced for each cast.

2.5 Assessing primary production algorithms designed for SeaWiFS data

2.5.1 Overview

Three algorithms created for use with SeaWiFS data were used to model primary production. These were 1) a simple empirical model based on chlorophyll concentration, 2) the empirical Vertically Generalised Productivity Model (VGPM) of Behrenfeld and Falkowski (1997a) and 3) a model based on the semi-analytical algorithm of Morel (1991) and Antoine and Morel (1996). Given the potential margin of error associated with chlorophyll estimates obtained from SeaWiFs data, the models were all parameterised using chlorophyll concentrations measured by HPLC. In this way, only the model performance was tested, not the chlorophyll retrieval algorithm. The latter two models were run a number of times to allow modelled parameter values to be replaced by measured values to aid understanding of model performance at each stage of the calculation.

2.5.2 Empirical chlorophyll model

The empirical chlorophyll model was derived from a regression of the log of chlorophyll *a* against the log of daily primary production as estimated by the ^{14}C technique (after Eppley *et al.*, 1985).

2.5.3 VGPM model

The VGPM model, of Behrenfeld and Falkowski (1997a), was implemented in Microsoft Excel in the form shown in equation 26.

$$PP_{Daily} = [Chl] \cdot Z_{eu} \cdot P^{B}_{opt} \cdot D \cdot F \quad (26)$$

where [Chl] is water column averaged chlorophyll *a* concentration in mg m^{-3}, Z_{eu} is the euphotic depth in m, P^{B}_{opt} is the maximum rate of carbon fixation under variable irradiance in mg C [mg Chl]$^{-1}$ h^{-1} and differs from P^{B}_{m} which is measured under fixed irradiance, D is day length in hours and F is a unitless parameter to represent irradiance. Euphotic depth was calculated according to equation 27 after Morel and Berthon (1989) and day length was according to equation 28 after Balch *et al.* (1992).

$$Z_{eu} = 38 \cdot [Chl]^{-0.428} \quad (27)$$

$$D = 12 \cdot \left(1 + \left(-1 \cdot \cos\left(\frac{julian}{57.295} \right) \cdot \sin\left(\frac{latitude}{57.295} \right)^{3} \right) \right) \quad (28)$$

where julian is the Julian day number of the year and latitude is given in decimal degrees. The irradiance parameter, F, was assumed to be 0.55 as in the original publication. P^{B}_{opt} was calculated as a polynomial of measured surface temperature (T°C) as described in equation 29, according to the recommendations of the Behrenfeld and Falkowski (1997a).

$$\begin{aligned} P^{B}_{opt} = {} & 3.27 \times 10^{-8} + 3.4132 \times 10^{-6} \cdot T^{6} - 1.348 \times 10^{-4} \cdot T^{5} + 2.462 \times 10^{-3} \cdot T^{4} \\ & - 0.0205 \cdot T^{3} + 0.0617 \cdot T^{2} - 0.2749 \cdot T + 1.2956 \end{aligned} \quad (29)$$

When measured parameters were used, P^{B}_{opt} was replaced with measured P^{B}_{m} calculated according to equation 15a.

2.5.4 Semi-analytical Morel model

The semi-analytical algorithm was implemented by the Remote Sensing Group at Plymouth Marine Laboratory and is based on the model of Morel (1991) and Antoine and Morel (1996). A detailed account of the algorithm is given in the original paper but an outline of the calculation is described below. The overall algorithm is shown in equation 30.

$$PP_{Daily} = 12 \cdot a^{*}_{\max} \cdot \varphi_{\mu \max} \cdot \int_{0}^{D} \int_{0}^{Z_{eu}} \int_{\lambda 1}^{\lambda 2} [Chl] \cdot PUR(\lambda, z, t) \cdot f[x(z,t)] \, dt \, dz \, d\lambda \qquad (30)$$

(Equation 27 in Morel, 1991)

where $a^{*}_{\max}$, is the maximal value of phytoplankton absorption, in m^2 g Chl^{-1} and $\varphi_{\mu \max}$ is the quantum yield for growth, in mol C mol photons $absorbed^{-1}$. These are assigned constant values (see Table 2.1). PUR (λ) is the photosynthetically usable radiation and is calculated as a function of PAR and the absorption spectrum of algae according to equation 31, after Antoine and Morel (1996).

$$PUR(\lambda) = PAR(\lambda) \cdot A^{*}(\lambda) \qquad (31)$$

where A*λ is the mean absorption cross section per unit of chlorophyll *a*, in m^2 g Chl^{-1}.

The final part of the equation, f[x (z,t)], allows the inclusion of a variable photosynthetic response which is a function of temperature. The function is based on the PE curve equation of Platt *et al.* (1980) but rewritten for the purpose of this model according to equation 32.

$$f(x) = x^{-1} \cdot (1 - e^{-x}) e^{-\beta x} \qquad (32)$$

(Equation 26 in Morel, 1991).

The symbol x represents a dimensionless parameter that describes the ratio of PUR to K_{PUR}. K_{PUR} is a temperature dependent function characterised by a Q_{10} equal to 1.88 as shown in equation 33. Its inclusion in the algorithm allows the effect of temperature on growth rate to be included in the production calculation.

$$K_{PUR}(T) = K_{PUR}(20^{\circ}) \cdot 1.065^{(T-20^{\circ})} \qquad (33)$$

(Equation 29 in Morel, 1991)

The irradiance field just below the sea surface was calculated from latitude and Julian day using the algorithm of Gregg and Carder (1990) with cloud cover assumed to be absent. The attenuation of light with depth (K_{PAR} (λ)) was calculated as a function of absorption (a(λ)) and backscattering (b(λ)) as described in equations 34 to 37.

$$K_{PAR}(\lambda)=a(\lambda)\cdot\mu_0^{-1}\cdot\left[1+(0.425\cdot\mu_0-0.19)^{b(\lambda)/a(\lambda)}\right]^{1/2} \quad (34)$$

(Equation 18 in Morel, 1991)

$$b(\lambda)=b_w(\lambda)+(550/\lambda)\cdot 0.3\cdot[Chl]^{0.62} \quad (35)$$

(Equation 19 in Morel, 1991)

$$a(\lambda)=\left[a_w(\lambda)+0.06\cdot a_{Chl}(\lambda)\cdot[Chl]^{0.65}\right]\cdot[1+0.2\cdot y(\lambda)] \quad (36)$$

(Equation 20a in Morel, 1991)

$$y(\lambda)=e^{(-0.014\cdot(\lambda-440))} \quad (37)$$

(Equation 20b in Morel, 1991)

where μ_0 is the average cosine for downwelling radiation just below the sea surface, $a_w(\lambda)$ and $b_w(\lambda)$ are the wavelength specific scattering and absorption coefficients for pure seawater both in m^{-1}, $a_{Chl}(\lambda)$ is the absorption per unit chlorophyll in m^{-1} g Chl^{-1} and $y(\lambda)$ is a function of wavelength.

All input variables were assumed to be constant with depth. Table 2.1 describes the values assigned to the model variables when run in its default mode. The PAR values used to replace modelled PAR were measured as described in section 2.6.1. The Morel model required spectrally resolved PAR. To approximate this, a factor to account for the proportion of total PAR occurring at each wavelength was calculated using the daylight spectrum recorded in Table 1 of Gregg and Carder (1990). Total PAR was multiplied by this factor at each wavelength to approximate wavelength specific PAR[4].

'Measured' K_{PAR} was calculated according to methods described in section 2.6.1. To calculate K_{PUR}, measured primary production was plotted against PUR and equation 15a

[4] Calculations coded in IDL by Tim Smyth of the Remote Sensing Group at Plymouth Marine Laboratory.

fitted to the data to derive photosynthetic parameters. K_{PUR} is equal to E_k when a PE curve is plotted against PUR rather than PAR. PUR was calculated according to equation 31.

Table 2.1. Values assigned to variables in semi-analytical production algorithm

Variable	Value	Units	Source of value
Chlorophyll *a*	Variable	mg m^{-3}	HPLC analysis of *in situ* samples
a^*_{max}	33	m^2 g Chl $^{-1}$	Morel, 1991
$\phi_{\mu max}$	0.06	mol C mol photons abs^{-1}	Morel, 1991
β	0.01	mg C [mg Chl]$^{-1}$ [µmol photons m^{-2} s^{-1}]$^{-1}$	Morel, 1991
A* (λ)	Wavelength dependent	m^2 g Chl^{-1}	Standard spectrum from Prieur and Sathyendranath, 1981
$a_{Chl}(\lambda)$	Wavelength dependent	m^{-1}	Standard spectrum from Morel, 1988
a_w (λ)	Wavelength dependent	m^{-1}	Standard spectrum from Morel and Prieur, 1977
$b_w(\lambda)$	Wavelength dependent	m^{-1}	Standard spectrum from Morel, 1974
Euphotic depth (Z_{eu})	0.1% light level	m	Calculated from K_{PAR}
K_{PUR}	80	Dimensionless	Morel, 1988

2.6 Other Measurements and procedures

2.6.1 PAR and K_{PAR}

In the Celtic Sea, PAR at the sea surface was measured using an ELE DRP-5 Vector Irradiance PAR sensor mounted high on the ship. Data were logged every 30 seconds and PAR was calculated in Wm^{-2} from volts (using the UKORS calibration equation: Wm^{-2} = V*32310). The data were averaged over 30 minute intervals and converted to units of µmol photons m^{-2} s^{-1} using the equations of Kirk (1983). Surface PAR at L4 was extracted from the University of Plymouth weather station on the University campus, assuming that cloud cover would be the same at L4.

K_{PAR} was calculated empirically as the coefficient of the regression of the natural log of PAR, from the FRRF casts, against depth. The K_{PAR} value used was the average of all the casts on one day.

2.6.2 Particle absorption

For the determination of particle absorption, 1l aliquots of water were filtered onto 25mm Whatman GF/F filters, which were cut into strips the width of a 6ml cryovial. The central strip was immediately frozen in liquid nitrogen and stored for later analysis. At the time of analysis, the diameter of the filter was measured before it was put in a clamp that allowed it to be placed in the spectrophotometer. Particle absorption was measured using the method of Tassan and Ferrari (1998), which involved repeat measurements before and after bleaching (using sodium hyperchloride containing 1% active chlorine) to measure the absorption due to organic matter. The spectrophotometer was a Perkin-Elmer Lambda 2 model.

2.6.3 Coloured dissolved organic matter (CDOM)[5]

The spectral absorption coefficient of CDOM ($a_{ys}(\lambda)$) was calculated using the protocols of the EU Framework IV project COLORS (Coastal region long-term measurements for colour remote sensing development and validation project) shortly to be released as a CD-ROM (G.Moore, Pers. Comm.). The methods are summarised below. Samples were collected in glass bottles and cooled in the dark (to prevent photodegradation) until analysis, which was carried out within 3h of collection. Aliquots of 250ml were filtered through 0.22μm Millipore GSWP filters in a glass filtration system. Roughly 100ml of distilled water was used to wash the filter and remove organic material. The water was discarded from the flask before the sea water sample was filtered and the filtrate was stored in a clean, amber glass storage bottle at 4°C in the dark until analysis. If the samples were stored for more than a few hours before analysis, 0.5ml of an azide solution (1g l^{-1} of NaN_3) was added to inhibit aerobic bacterial growth. Analysis was carried out in the spectral range 350nm to 700nm using a dual beam Perkin Elmer Lambda 12 spectrophotometer. Quartz cuvettes were filled with MilliQ® water and used to 'autozero' the instrument. The absorption spectrum was then measured using the same MilliQ in the cuvettes to check the 'autozero'. The sample was placed in the 'sample cuvette' and a scan performed to get an absorbance ($A_{ys}(\lambda)$) spectrum. The spectral absorption coefficient of CDOM, $a_{ys}(\lambda)$, was calculated according to equation 38.

[5] Measurements of CDOM and SPM made by James Fishwick.

$$a_{ys}(\lambda) = 2.303 \cdot A_{ys}(\lambda) / 0.1 \quad (38)$$

where 0.1 was the pathlength of the cuvette in cm. Absorption by CDOM is maximum at 440nm so this value was used to assess whether the CDOM concentration was high or low.

2.6.4 Suspended particulate matter (SPM)

The concentration of SPM (in mg m^{-3}) was calculated using the protocols of the EU Framework IV project COLORS Project. The methods are summarised below. One litre aliquots were filtered through pre-washed, pre-ashed and pre-weighed 0.7μm Whatman GF/F filters. The filters were washed with distilled water and dried in an oven at 65°C for 24h, after which they were stored in a desiccator before weighing on an electrobalance. Total suspended particulate matter was calculated from the difference in weight before and after filtration divided by the sample volume. After this, the filters were ashed in a muffle furnace for 4 h at a temperature of 500°C and then placed in a desiccator before weighing. The loss of weight is approximately equal to the organic component of the material and the remaining weight is due to the inorganic component.

2.6.5 Nutrient analysis[6]

Water samples were decanted into 60ml polycarbonate bottles. Samples were frozen immediately and stored at –20°C prior to analysis. The nutrient analyser used was a 5 channel Technicon AAII, segmented flow autoanalyser, and the chemical methodologies used were according to Woodward (1994). The chemical methodologies used were: Nitrate, (Brewer and Riley, 1965); Nitrite, (Grasshoff, 1976); Phosphate (Kirkwood, 1989) and Silicate (Kirkwood, 1989).

2.6.6 Algal culture

Axenic cultures of phytoplankton (*Thalassiosira weissflogii*, *Amphidinium sp.* and *Isochrysis galbana*) were obtained from the Culture Collection of Algae and Protozoa (CCAP) at Dunstaffnage Marine Labortatory. Cultures were maintained on a 12h light: dark cycle at 19°C in 250ml conical flasks in F/2 media (Guillard and Ryther, 1962). The cultures were

[6] The nutrient analyses were carried out by Malcom Woodward and Vassilis Kitidis at Plymouth Marine Laboratory.

grown without agitation or aeration but the flasks were gently stirred daily. For experiments, 4.5l of media was made up and autoclaved in 5l glass bottles. After inoculation using clean techniques, the cultures were bubbled with filtered air. Spectrophotometric measurements of absorption showed that the log phase of growth was attained 3 days after inoculation. Experiments with cultures started 3 or 4 day after inoculation. At the beginning of each experiment sub-samples of the culture were analysed under a microscope to ensure that bacteria were absent. This was carried out by staining 1ml aliquots of the culture with acridine orange (a DNA stain) and filtering the stained sample onto 0.2μm pore size, 25mm polycarbonate filters. The filters were placed on glass slides and viewed under an epifluorescence microscope to check for the absence of bacteria.

2.6.7 Phytoplankton cell counts of *Isochrysis galbana* samples

Cell counts were carried out using a Coulter Counter (model Zb) fitted with a tube with an 140μm orifice which had been calibrated for cells between 2 microns and 25 microns. Counts were made on triplicate samples of 1:100 dilutions of culture in filtered seawater. The system was washed with filtered seawater between each sample and these background counts were subtracted from the sample counts.

2.6.8 CHN analysis of *Isochrysis galbana* samples

Samples of 40ml were filtered onto 25mm Whatman GFF filters which were then frozen immediately and stored at –20°C. Samples were analysed in a Carlo Erba analyser using the method of Verardo *et al.* (1990).

2.7 Modelling daily depth integrated production from ^{14}C and FRRF data

2.7.1 Modelling the *in situ* light field

Overall equation

The *in situ* light field was calculated according to equation 39.

$$PAR_{(z,t)} = \left(PAR_{(0,t)} \cdot F_S\right) \cdot e^{-K_{PAR} \cdot z} \tag{39}$$

where $PAR_{(0,t)}$ is measured surface PAR at time t (μmol photons m^{-2} s^{-1}), F_S (surface effect) is a factor to account for the loss of PAR at the sea surface and K_{PAR} is the measured attenuation coefficient of PAR (m^{-1}).

Surface effect (Fs)

The surface effect was calculated[7] as the ratio of total light (diffuse and direct) below the surface to that above the surface as shown in equation 40.

$$F_s = \frac{E_{0-}^{direct} + E_{0-}^{diffuse}}{E_{0+}^{direct} + E_{0+}^{diffuse}} \tag{40}$$

where E_{0-}^{direct} and $E_{0-}^{diffuse}$ are the direct and diffuse components of irradiance just below the surface respectively and E_{0+}^{direct} and $E_{0+}^{diffuse}$ are the direct and diffuse components of irradiance just above the surface respectively. E_{0+}^{direct} and $E_{0+}^{diffuse}$ were calculated according to equations 41 and 42.

$$E_{0+}^{direct} = \frac{P_{direct} \cdot E_{0+}^{diffuse}}{1 - P_{direct}} \tag{41}$$

where P_{direct} is the proportion of total sunlight due to the direct beam. Values for P_{direct} were based on Kirk (1983). At solar zenith angles less than or equal to 20°, P_{direct} = 0.5. At solar zenith angles of 60° and 90°, P_{direct} = 0.75 and 0.85 respectively. A cubic spline interpolation was carried out to calculate intermediate values.

$$E_{0+}^{diffuse} = \sum_{\lambda=0}^{\lambda=90} L(\lambda) \cdot \cos(\lambda) \cdot \sin(\lambda) \tag{42}$$

where L(λ) is the relative radiance at elevation angle λ based on the angular distribution of luminance taken from Kirk (1983) (original reference Robinson, 1966). $E_{0+}^{diffuse}$ is the integral

[7] Surface effect calculated using program developed by Matt Pinkerton (PML).

of values for wavelengths between 0° and 90° at 10° resolution. The direct and diffuse components of total irradiance below the surface were calculated according to equations 43 and 44 respectively.

$$E_{0-}^{direct} = (1-\rho)\cdot E_{0+}^{direct} \tag{43}$$

$$E_{0-}^{diffuse} = \sum_{\lambda=0}^{\lambda=90}(1-\rho)\cdot E_{0+}^{diffuse}\cdot refractive\,index \tag{44}$$

where ρ is the reflectance at the surface calculated by Fresnel's equation shown in equation 45.

$$\rho = \frac{1\cdot\sin^2\cdot(\theta_a-\theta_w)}{2\cdot\sin^2\cdot(\theta_a-\theta_w)} + \frac{1\cdot\tan^2\cdot(\theta_a-\theta_w)}{2\cdot\tan^2\cdot(\theta_a-\theta_w)} \tag{45}$$

where θ_a is the zenith angle of incident light in air and θ_w is the angle to the downward vertical of the transmitted beam in water (Kirk, 1983). θ_a^{direct} and θ_w^{direct} differ for direct and diffuse light. The values for direct light (θ_a^{direct} and θ_w^{direct}) were calculated according to equation 46 and 47.

$$\theta_a^{direct} = zenith - surface\,refraction \tag{46}$$

$$\theta_w^{direct} = zenith + surface\,refraction \tag{47}$$

where *zenith* is the solar zenith angle. The values for diffuse light ($\theta_a^{diffuse}$ and $\theta_w^{diffuse}$) are wavelength specific and were calculated according to equations 48 and 49.

$$\theta_a^{diffuse}(\lambda) = \lambda - surface\,refraction \tag{48}$$

$$\theta_w^{diffuse}(\lambda) = \lambda + surface\,refraction \tag{49}$$

The surface refraction was calculated according to equation 50.

$$surface\ refraction = a\sin\cdot(\sin(zenith))/\ refractive\ index \quad (50)$$

The refractive index was assigned the constant value of 1.33. The solar zenith angle was calculated according to equation 51 after Kirk (1983).

$$zenith = a\cos(\sin(\phi)\cdot\sin(\partial) - \cos(\phi)\cdot\cos(\partial)\cdot\cos(\delta)) \quad (51)$$

where ϕ is latitude, ∂ is the solar declination angle and δ accounts for the effect of the time of day expressed as an angle in radians. The solar declination angle and the effect of the time of day were calculated according to equations 52 and 53 respectively.

$$\partial = 0.39637 - 22.9133\cdot\cos(\psi) + 4.02543\cdot\sin(\psi) - 0.3872\cdot\cos(\psi) + 0.052\cdot\sin(2\psi) \quad (52)$$

where ψ is the date expressed as an angle (Julian day/365).

$$\delta = \frac{360\cdot t}{24} \quad (53)$$

where t is time in decimal hours using a 24h clock and where 360 converts the value into radians.

The cloud cover was unknown so $PAR_{(z,t)}$ was calculated twice, both assuming clear and overcast skies.

2.7.2 Modelling daily, depth-integrated production (PP_{Daily})

Daily, depth-integrated production was modelled using photosynthetic parameters from both ^{14}C and FRRF techniques and using the instantaneous FRRF production values. In both cases, equation 54 was used.

$$PP_{Daily} = \int_{z=0}^{Z_{eu}} \int_{t=0}^{D} PP_{z,t}\, dz\, dt \tag{54}$$

where PP_{Daily} is daily, depth integrated primary production (mg C m^{-2} d^{-1}), z is depth (m), t is time (h from 0 to 24h) and $PP_{z,t}$ is primary production at depth z and time t (mg C m^{-3} h^{-1}).

$PP_{z,t}$ was calculated from the photosynthetic parameters according to equation 55a or 55b depending on whether photoinhibition was included (after Platt *et al.*, 1980).

$$PP_{z,t}^{(psparams)} = \left(P_m^B \left[1 - e^{\frac{\alpha^B \cdot PAR_{z,t}}{P_m^B}} \right] \right) \cdot [Chl] \tag{55a}$$

$$PP_{z,t}^{(psparams)} = \left(P_S^B \left[1 - e^{\frac{\alpha^B \cdot PAR_{z,t}}{P_S^B}} \right] \cdot e^{\frac{\beta^B \cdot PAR_{z,t}}{P_S^B}} \right) \cdot [Chl] \tag{55b}$$

where $PP_{z,t}^{(psparams)}$ is in units of mg C m^{-3} h^{-1} and [Chl] is the average chlorophyll *a* concentration in the water column (mg m^{-3}).

The calculation of daily production based on instantaneous FRRF production values was carried out in two stages. Firstly, the instantaneous production at depth z and time t was plotted against coincident PAR and a non-linear regression fitted to the data using equation 56. The algorithm was based on the PE curve of Platt *et al.* (1980).

$$PP_{z,t}^{FRRF\ PE} = \left(Q \left[1 - e^{\frac{a \cdot PAR_{z,t}}{Q}} \right] \right) \cdot [Chl] \tag{56}$$

where Q and a are parameters of the regression. The second stage was to use the parameters derived from the curve fit, this time in conjunction with modelled PAR ($PAR_{z,t}$') to model production at 1m depth and 1h time intervals throughout the day as shown in equation 57.

$$PP_{z,t}^{FRRF\ PE\ '} = \left(Q \left[1 - e^{\frac{a \cdot PAR_{z,t}'}{Q}} \right] \right) \cdot [Chl] \qquad (57)$$

Equation 57 is identical to equation 56 except that $PP_{z,t}^{FRRF\ PE}$ is replaced with $PP_{z,t}^{FRRF\ PE\ '}$ and $PAR_{z,t}$ is replaced with $PAR_{z,t}$'.

Chapter 3. Variability within the ^{14}C technique

3.1. Introduction and specific methods

Primary production estimates measured from incubations with ^{14}C are often used as "benchmark" values against which to compare production estimates from novel techniques. For this to be a satisfactory approach, it is necessary to understand the variability associated with the ^{14}C technique and in particular the extent to which different experimental protocols can lead to different estimates of photosynthesis and production. Experiments with radiocarbon simply measure the amount of radiocarbon incorporated into organic matter at the end of the incubation. The rate of photosynthesis is then inferred from the radiocarbon assimilated and remaining at the end of the incubation. Differences between the conditions in the incubator and that in the sea lead to differences between the rates of processes measured and those occurring in the sea. This can be further complicated as differences between incubators and experimental protocols can lead to a variety of production estimates from one water sample. For example, different incubator bulbs produce different spectra of irradiance and these are different to that of natural light, which affects the rate of photosynthesis, particularly at low light. Additionally, a lack of understanding of the rates of processes taking place during incubations, such as respiration and recycling of carbon, can make it difficult to interpret the results of experiments. This is made more complex by the non-linear nature of the processes over time.

The work in this chapter investigated the variability in measures of photosynthetic fitness and primary production obtained when different types of ^{14}C incubation were used. In the first section the variability in the photosynthetic parameters (and in daily primary production estimates derived from those parameters) produced from incubations in artificial light gradients is addressed. The effect of using different incubators with different light sources was studied as well as the effect of the duration of the incubation on derived parameters. The incubators used were a large water tank in the laboratory and a portable incubator designed for use at sea. Both incubators provided a light gradient but the large tank, in which light was attenuated by water, was expected to mimic natural conditions more closely than the portable incubator, in which light was attenuated purely by the samples closer to the source. The effect of the different incubators was studied using experiments on natural seawater samples from L4. Both seawater samples from L4 and phytoplankton cultures grown in the laboratory were used to study the effect of the duration of incubation on derived parameters.

Cultures were used to aid the interpretation of the processes taking place during incubations. The rationale was that the response of a single species, rather than a mixed population of both phytoplankton and bacteria, would give a clearer understanding of the physiology of the carbon fixation. Experiments were also done on seawater samples throughout the year, to obtain estimates for natural assemblages of mixed and variable populations of phytoplankton.

Given the effect that different PE curve equations have on the derived parameters, a comparison was made between the photoinhibited and the non-photoinhibited photosynthetic parameter models. The experiments were done at weekly intervals at station L4 and during the Celtic Sea cruise. In the second section of the chapter, production modelled from PE parameters was compared with that from 24h *simulated-in-situ* incubations. The aim was to understand how estimates of daily depth-integrated production vary as a result of the experimental approach used. The data were obtained on the Celtic Sea cruise and the photosynthetic parameter values were the average values of shallow water casts made at dawn and at midday.

3.2. Results

3.2.1 Photosynthetic parameters from incubations under artificial light gradients

The effect of light - Photosynthetic parameters from different incubators

Six experiments were carried out to compare photosynthetic parameters from the different incubators. Figure 3.1 compares the phytoplankton absorption spectrum with the spectra of the lamps used in each of the incubators and the spectrum of sunlight. The lamps had very different spectra to each other and to sunlight. At the peak wavelengths of phytoplankton absorption (440nm and 680nm) the relative intensity of the lamp in the portable incubator was much higher than that in the water tank. The average light correction factor (from equations 18 to 21), used to correct the spectrally sensitive α^B values for the difference between the spectra of the lamps used in incubations and that of PAR were quite different for the two incubators. That from the water tank was 1.08 ± 0.04 compared to 0.90 ± 0.02 from the portable light gradient incubator. This correction led to an 8% increase in α^B values from the water tank and a 9% decrease in those from the portable light gradient incubator. The light correction factor was calculated for all dates on which particle absorption measurements were available and low variability in the measured absorption spectra led to low variability between the light correction factors calculated on different dates. Given this low variability,

the average correction value was applied, rather than those from specific dates, to allow dates to be used when no phytoplankton absorption data were available. Table 3.1 compares the photosynthetic parameter values obtained from simultaneous incubations with identical samples, of natural populations from L4, in each incubator.

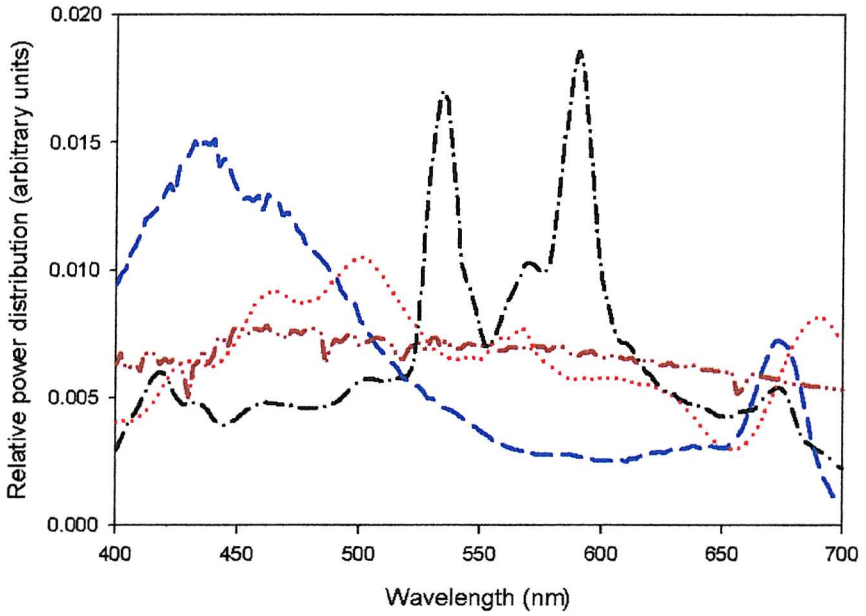

Figure 3.1. Spectra of the lamps used in each of the incubators, of sunlight and the average phytoplankton absorption spectrum from L4 samples. The lines show the spectra within the static water tank ( ), within the portable incubator ( ), of sunlight ( ) and of particle absorption ( ).

Table 3.1. The effect of incubator on photosynthetic parameters. Values obtained from 4h incubations of L4 samples in the water tank (WT) and in a portable incubator (LB). Data are normalised to chlorophyll concentration measured on samples taken at the start of the incubation. α^B,in mg C [mg Chl]$^{-1}$ h^{-1} [µmol photons m^{-2} s^{-1}]$^{-1}$, P^B_m in mg C [mg Chl]$^{-1}$ h^{-1} and E_k in µmol photons m^{-2} s^{-1}

Date	α^B		P^B_M		E_k	
	WT	LB	WT	LB	WT	LB
16/10/2000	0.089	0.054	9.40	6.09	105	113
13/11/2000	0.006	0.007	0.98	0.88	153	121
18/04/2001	0.022	0.024	4.10	4.41	190	182
23/04/2001	0.030	0.018	5.60	6.11	186	337
30/04/2001	0.033	0.051	6.20	6.10	188	119
05/11/2001	0.078	0.047	5.75	7.06	74	150
Average	0.043	0.034	5.34	5.11	149	170

All parameter values obtained with the portable incubator were very similar to those from the water tank. As a result, estimates of daily, depth-integrated production (PP_{Daily}) modelled with these values gave similar primary production rates (Figure 3.2). That is, there was no significant effect of the different incubators on estimated primary production rate.

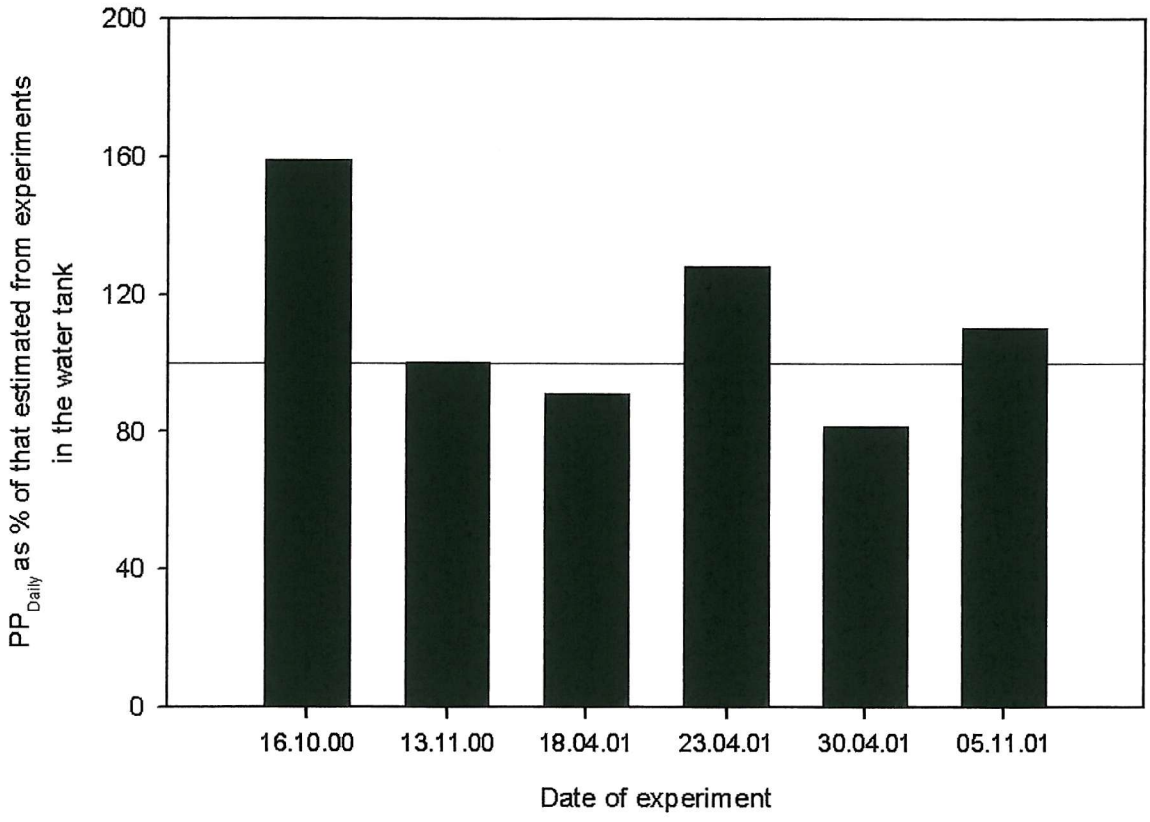

Figure 3.2. PP_{Daily} estimated from photosynthetic parameters derived from incubations of L4 water samples in the portable light gradient incubator. PP_{Daily} is shown as a percentage of the value derived from the incubation in the water tank. The 100% position is indicated by the solid horizontal line.

The effect of duration of incubation on determination of photosynthetic parameters

a) Experiments with cultures

Eight time-series incubations were done with three species of cultured algae: One with *Thalassiosira weissflogii*, one with an *Amphidinium sp.* and six with *Isochrysis galbana*. The first question asked was how much change occurred in chlorophyll concentration over the course of the incubations. There was a general increase in chlorophyll with time (Figure 3.3), and the concentration was always higher at 24h than at 0h. In seven out of the eight experiments, chlorophyll concentration increased during the dark period between the 12h and 24h sampling times. The PE curves determined in each incubation are shown in Figure 3.4. The length of incubation did not appear to have much effect on photoinhibition at high irradiance. However, in all cases there were clear changes in α^B, the initial slope and P^B_m,

the maximum rate of photosynthesis, values from 24h incubations were clearly lower than those from incubations of all other durations (Figure 3.5). The values of α^B and P^B_m after 24h were significantly lower than those measured at all other times ($p < 0.05$ for all comparisons, Wilcoxin's signed rank test). The change in α^B and in P^B_m values between 2 h and 12 h varied between experiments but was always relatively small.

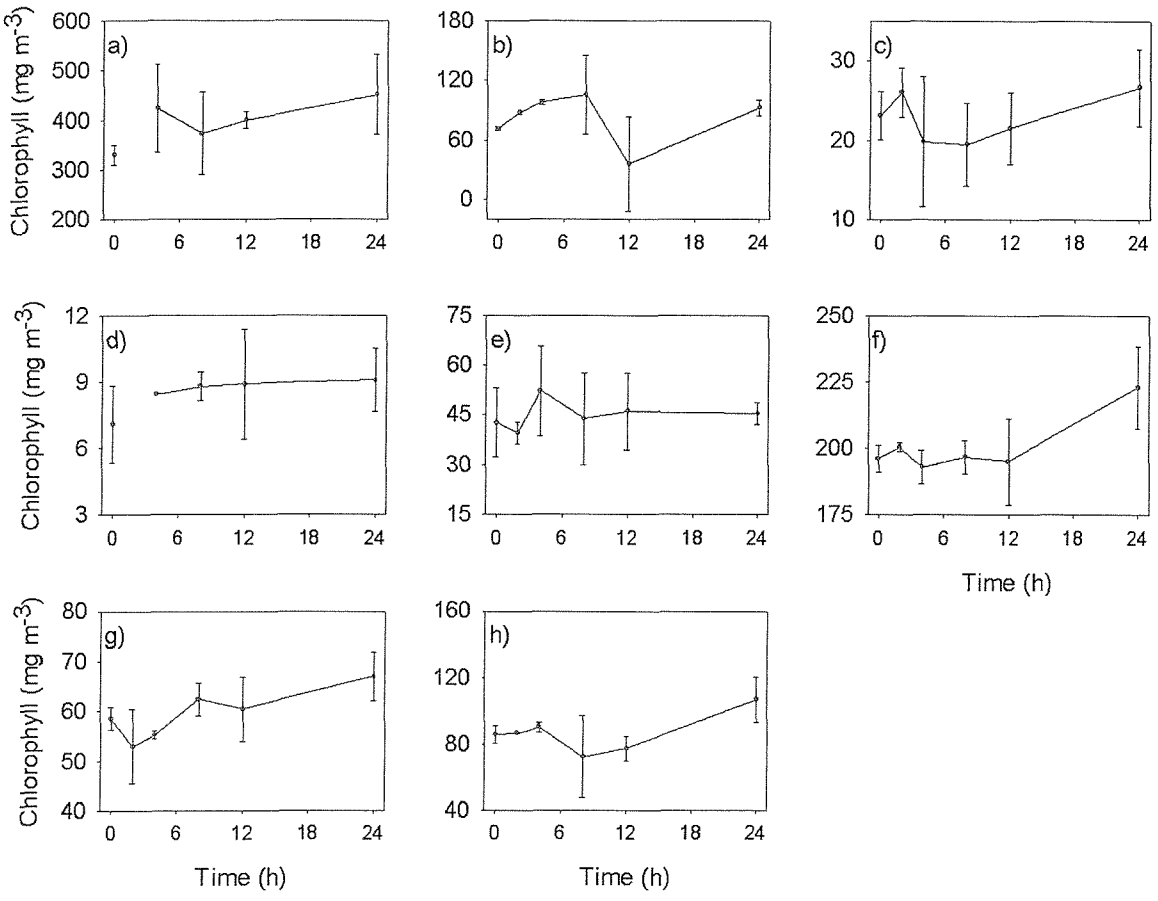

Figure 3.3. Change in chlorophyll concentration in algal cultures over the course of incubations of different durations: a) *Thalassiosira weissflogii*, on 26th April 2001, b) *Amphidinium sp.* on 20th September 2001, c) *Isochrysis galbana* on 22nd August 2001, d) *I.galbana* on 4th September 2001, e) *I.galbana* on 6th September 2001, f) *I.galbana* on 27th November 2001, g) *I.galbana* on 29th November 2001 and h) *I.galbana* on 3rd December 2001.

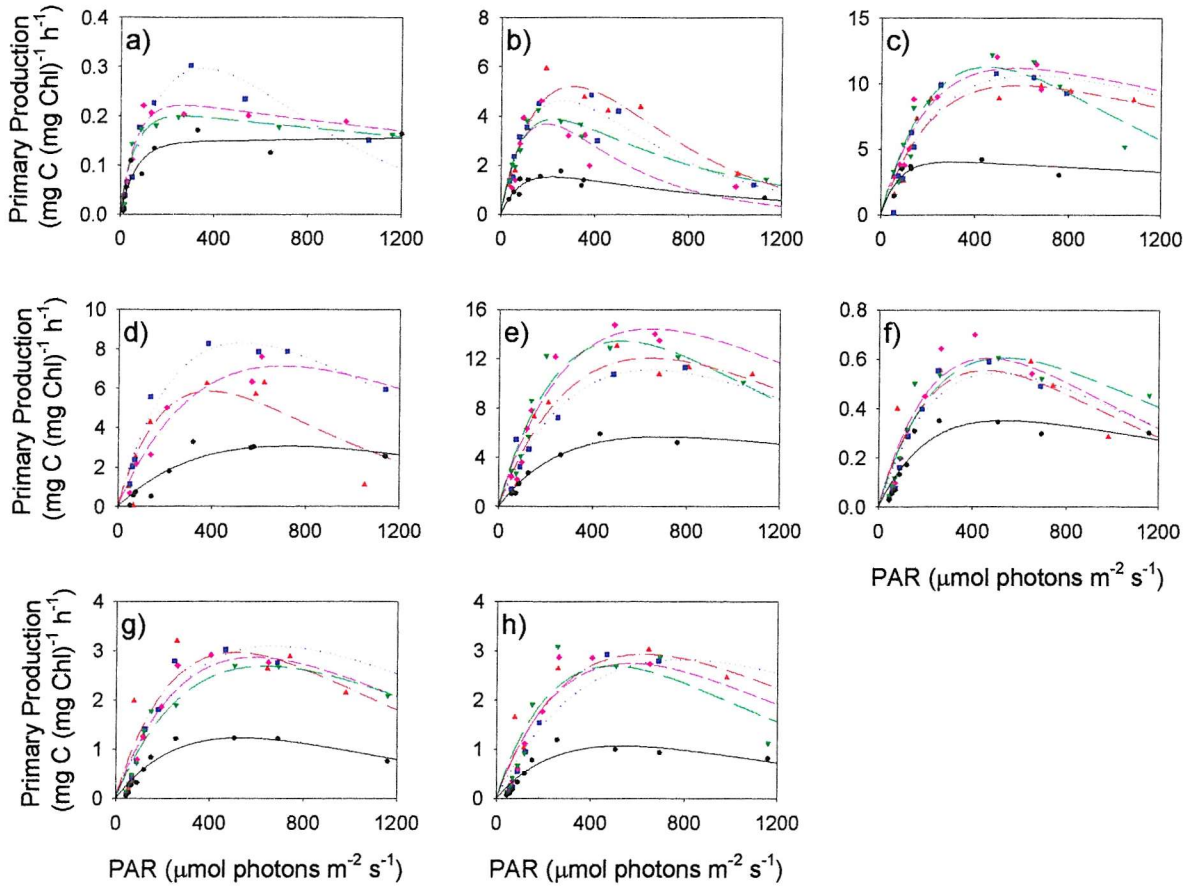

Figure 3.4. PE curves from incubations of cultures for different durations: a) *Thalassiosira weissflogii*, on 26th April 2001, b) *Amphidinium sp.* on 20th September 2001, c) *Isochrysis galbana* on 22nd August 2001, d) *I.galbana* on 4th September 2001, e) *I.galbana* on 6th September 2001, f) *I.galbana* on 27th November 2001, g) *I.galbana* on 29th November 2001 and h) *I.galbana* on 3rd December 2001. The durations of incubation were 2h (▲), 4h (■), 8h(◆), 12h (▼) and 24h (●).

Co-variation of the PE parameters was investigated and Table 3.2 shows the output from regressions between each of the photosynthetic parameters and against chlorophyll. There was some co-variation between α^B and P^B_m with >40% of the variance in α^B being explained by that in P^B_m for seven of the eight experiments. The exception was the experiment with *Thalassiosira weissflogii* on 26th April 2001, which showed a low correlation between α^B and P^B_m. The poor regression was due to an unusually low value of α^B from the 4 h incubation. The relationship between the photoinhibition parameter, β^B and the other parameters was very variable and derived β^B values were often unrealistic. This was a result of the uneven distribution of data points over the range of light levels so that, in most cases, the shape of the curve at high light levels, and hence the value of β^B, was determined by just one data point.

The variable effect of incubation time on PE parameters obviously affected estimates of primary production and Figure 3.6 shows the daily depth-integrated production estimates.

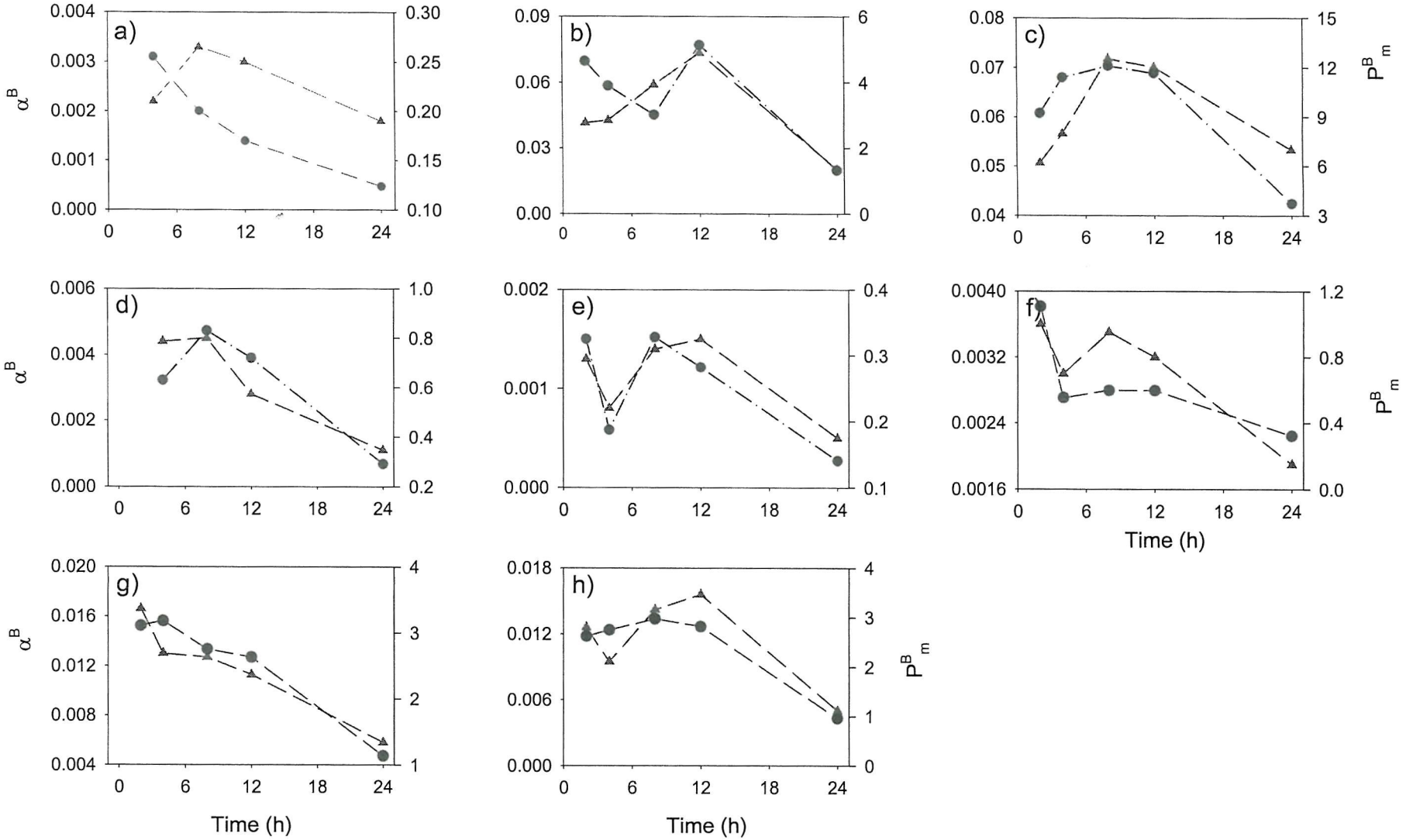

Figure 3.5. Effect of incubation time on photosynthetic parameters measured on cultures of algae: a) *Thalassiosira weissflogii* on 26th April 2001, b) *Amphidinium sp.* on 20th September 2001, c) *Isochrysis galbana* on 22nd August 2001, d) *I.galbana* on 4th September 2001, e) *I.galbana* on 6th September 2001, f) *I.galbana* on 27th November 2001, g) *I.galbana* on 29th November 2001and h) *I.galbana* on 3rd December 2001. Parameters shown are α^B,in mg C [mg Chl]$^{-1}$ h^{-1} [µmol photons m^{-2} s^{-1}]$^{-1}$ (▲) and P^B_m, in mg C [mg Chl]$^{-1}$ h^{-1} (●).

Table 3.2. Variance explained by regressions of photosynthetic parameters against each other and against chlorophyll. Cultures used were *Amphidinium sp.*, *Isochrysis galbana* and *Thallasiossira weissflogii*. α^B is the light limited slope of the PE curve in mg C [mg Chl]$^{-1}$ h^{-1} [mmol photons m^{-2} s^{-1}]$^{-1}$, P^B_m is the assimilation number in in mg C [mg Chl]$^{-1}$ h^{-1}, β^B is the photoinhibition parameter in the same units as α^B and Chl is chlorophyll concentration in mg m^{-3}.

Date	Culture	Variance explained by regression (R^2)					
		α^B vs P^B_m	α^B vs β^B	α^B vs Chl	P^B_m vs β^B	P^B_m vs Chl	β^B vs Chl
20/09/2001	*A. sp.*	0.52	0.00	0.36	0.16	0.35	0.01
04/09/2001	*I. galbana*	0.71	0.24	0.67	0.01	0.22	0.81
06/09/2001	*I. galbana*	0.87	0.28	0.19	0.04	0.40	0.02
22/08/2001	*I. galbana*	0.41	0.30	0.54	0.11	0.72	0.04
26/04/2001	*T. weissflogii*	0.05	0.04	0.92	0.81	0.13	0.01
27/11/2001	*I. galbana*	0.59	0.41	0.70	0.18	0.19	0.33
29/11/2001	*I. galbana*	0.86	0.05	0.81	0.00	0.76	0.04
03/12/2001	*I. galbana*	0.76	0.71	0.91	0.00	0.00	0.78
All data		0.74	0.12	0.12	0.20	0.14	0.03

Primary production estimates from incubations of 24h were significantly lower than all of those from incubations of any other duration. Production estimates from all other durations were statistically similar.

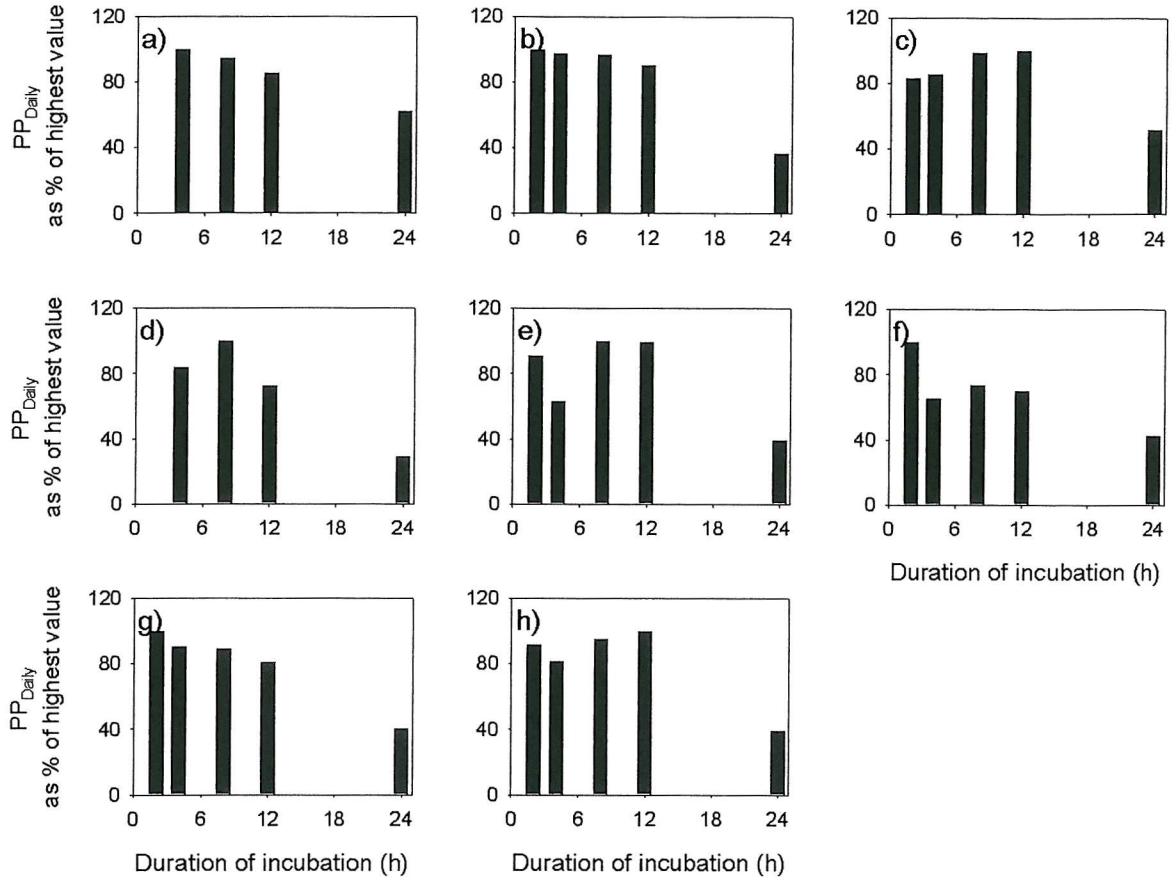

Figure 3.6. PP_{Daily} estimated from photosynthetic parameters of cultured algae derived from incubations of different durations in the water tank: a) *Thalassiosira weissflogii*, on 26th April 2001, b) *Amphidinium sp.* on 20th September 2001, c) *Isochrysis galbana* on 22nd Aug 2001, d) *I.galbana* on 4th September 2001, e) *I.galbana* on 6th September 2001, f) *I.galbana* on 27th November 2001, g) *I.galbana* on 29th November 2001 and h) *I.galbana* on 3rd December 2001.

It was possible that the chlorophyll content of the cells might change during the experiment. Therefore, for three experiments measurements were made of cell numbers and carbon content at each time in the incubations. Results of cell counts and carbon content analysis from the three incubations of *Isochrysis galbana* are shown in Figures 3.7 and 3.8 respectively. There was no consistent pattern of change in cell number or of carbon content during the incubations. Therefore, these experiments with axenic cultures of three phytoplankton species show little effect of incubation period for experiments less than 12h duration. However, 24 h incubations had a significant affect on PE parameters due to the 12h dark period during which no photosynthesis took place but fixed carbon was respired and chlorophyll concentrations changed.

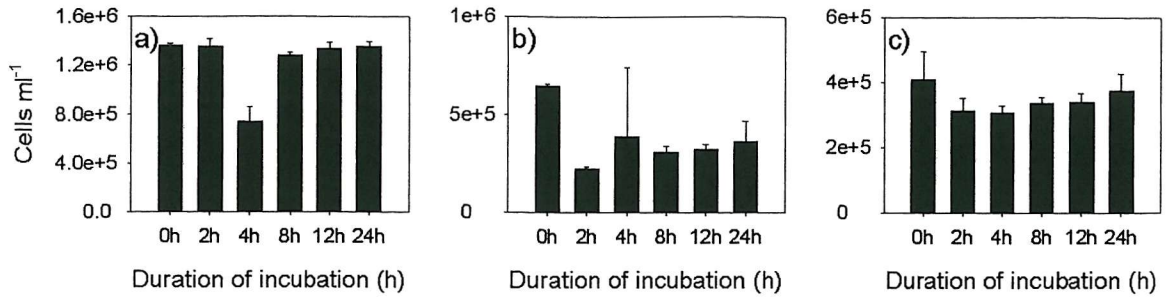

Figure 3.7. Concentration of cells per ml of *Isochrysis galbana* after incubations of different duration: a) 27th November 2001, b) 29th November 2001and c) 3rd December 2001. Values are the averages of three measurements. Error bars show the standard deviation of the mean.

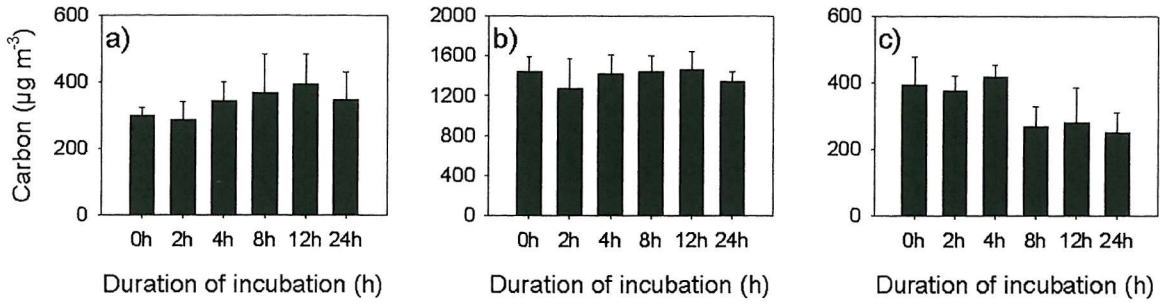

Figure 3.8. Carbon concentration within samples of *Isochrysis galbana* after incubations of different duration: a) 27th November 2001, b) 29th November 2001and c) 3rd December 2001. Values are the averages of three measurements. Error bars show the standard deviation of the mean.

b) Experiments with natural assemblages from station L4

Sixteen time series experiments were carried out on samples from L4. Of these, six included only incubations of 4h and 24h whilst the other ten included at least four different durations of incubation. Since the PE determinations were done on water samples collected the previous day, it was essential to first determine if overnight storage had any effect. The derived PE parameters are shown in Figure 3.9. Generally, there was only a slight decrease in α^B values between day 1 and day 2 but on 1st July 2002, there was a significant decrease in α^B after the overnight storage albeit from a high value of α^B. P^B_m values also showed a general pattern of slight decrease overnight. Again, the exception was on 1st July 2002 when there was a 5% decrease in P^B_m.

In initial experiments, the possibility that chlorophyll concentration might change during the experiment was not considered. However, in later experiments, chlorophyll concentration

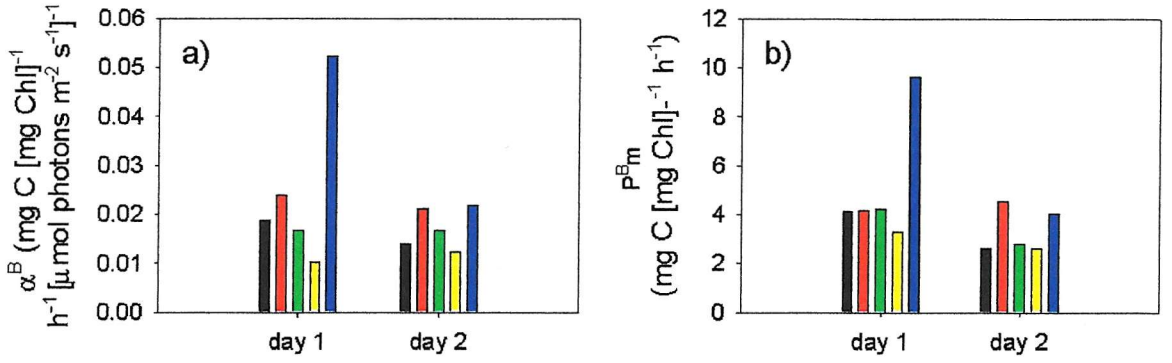

Figure 3.9. Difference in parameter values from incubations made on the day of sampling (day 1) with those stored overnight and measured on the next day (day 2): a) α^B and b) P^B_m from incubations of 4h duration on 13 March 2000 (■), 20th March 2000 (■), 27th March 2000 (■), 2nd April 2001(■) and 1st July 2002 (■).

was determined at the beginning and end of the experiment. Chlorophyll concentrations (at time t0) were measured for all the incubations but for only eleven of the experiments were chlorophyll values also available at the end of the incubation. In all cases chlorophyll values were an average of the concentrations measured in four bottles: two incubated at the high light end of the flume and two at the low light end. The size of the flume prevented incubations, for chlorophyll concentration, from being carried out at all light levels. Where chlorophyll estimates were available at both the start and the end of the experiment, a comparison was made of PE parameter values normalised to chlorophyll at t0 and those normalised to a mean value for chlorophyll concentration during the experiment. The change in chlorophyll concentration with duration of incubations is shown in Figure 3.10. There was no consistent pattern. Of the seven experiments where measurements were taken at 12h and 24h (before and after a period of darkness), chlorophyll decreased on four occasions but showed little change or only a slight increase in three cases. Figure 3.11 shows that normalisation to the different chlorophyll values had little effect on how parameter values changed with experiment duration. Therefore, in order to maximise the number of samples included in the statistics, all variables have been normalised to chlorophyll at t0.

Figure 3.12 shows the PE curves from the incubations. Shorter incubations produced PE curves with steeper initial slopes and higher maximum rates of production. As was found with the cultures, the initial slope of the curve and the maximum rate of photosynthesis were much lower for incubations of 24h than for all other times. There was again no increase in

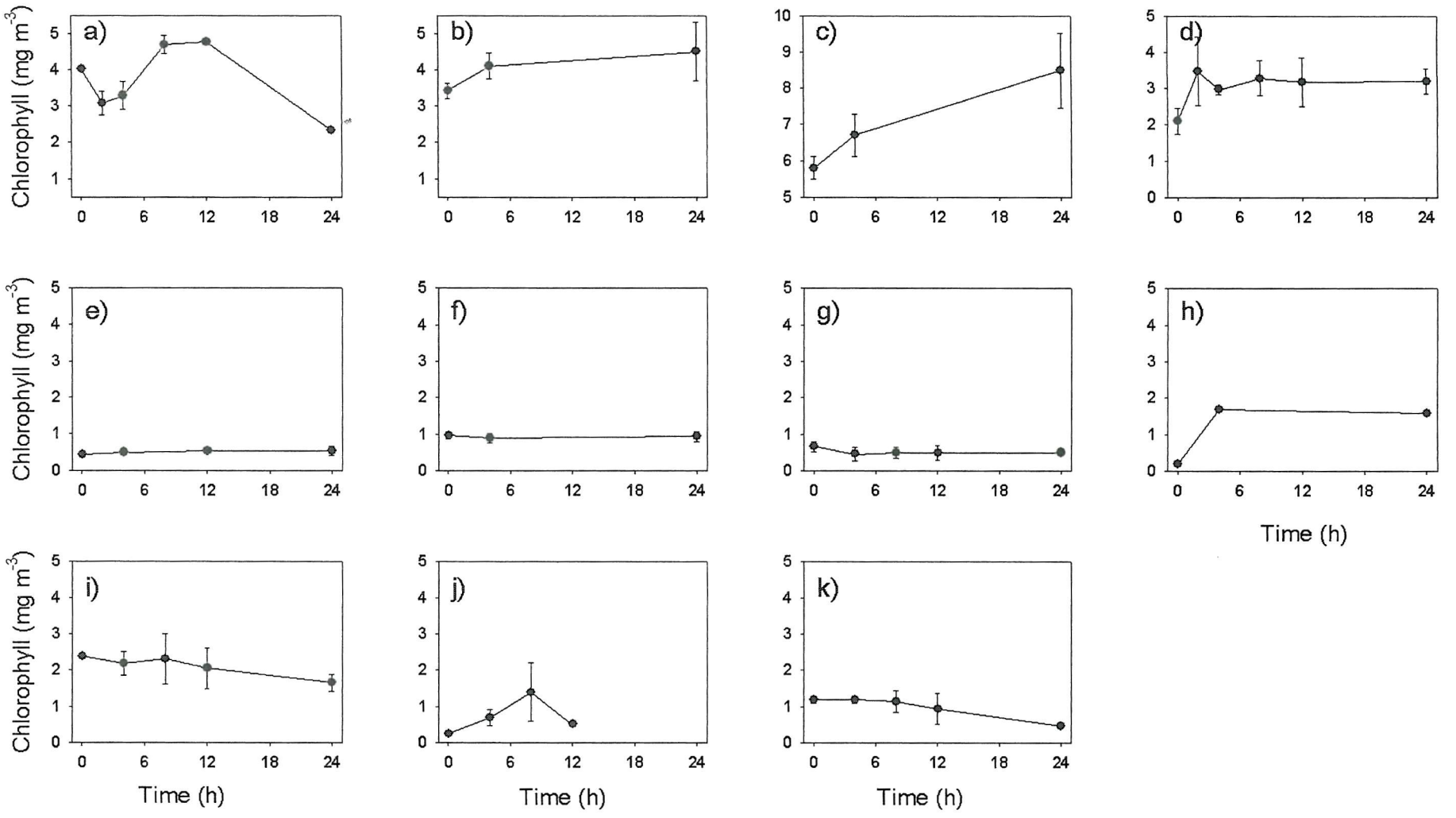

Figure 3.10. Change in chlorophyll in L4 samples over the course of incubations: a) 3rd April 2000, b) 18th April 2000, c) 30th April 2001, d) 5th June 2001, e) 11th September 2001, f) 5th November 2001, g) 20th November 2001, h) 1st July 2002, i) 2nd July 2002, j) 20th August 2002 and k) 3rd September 2002.

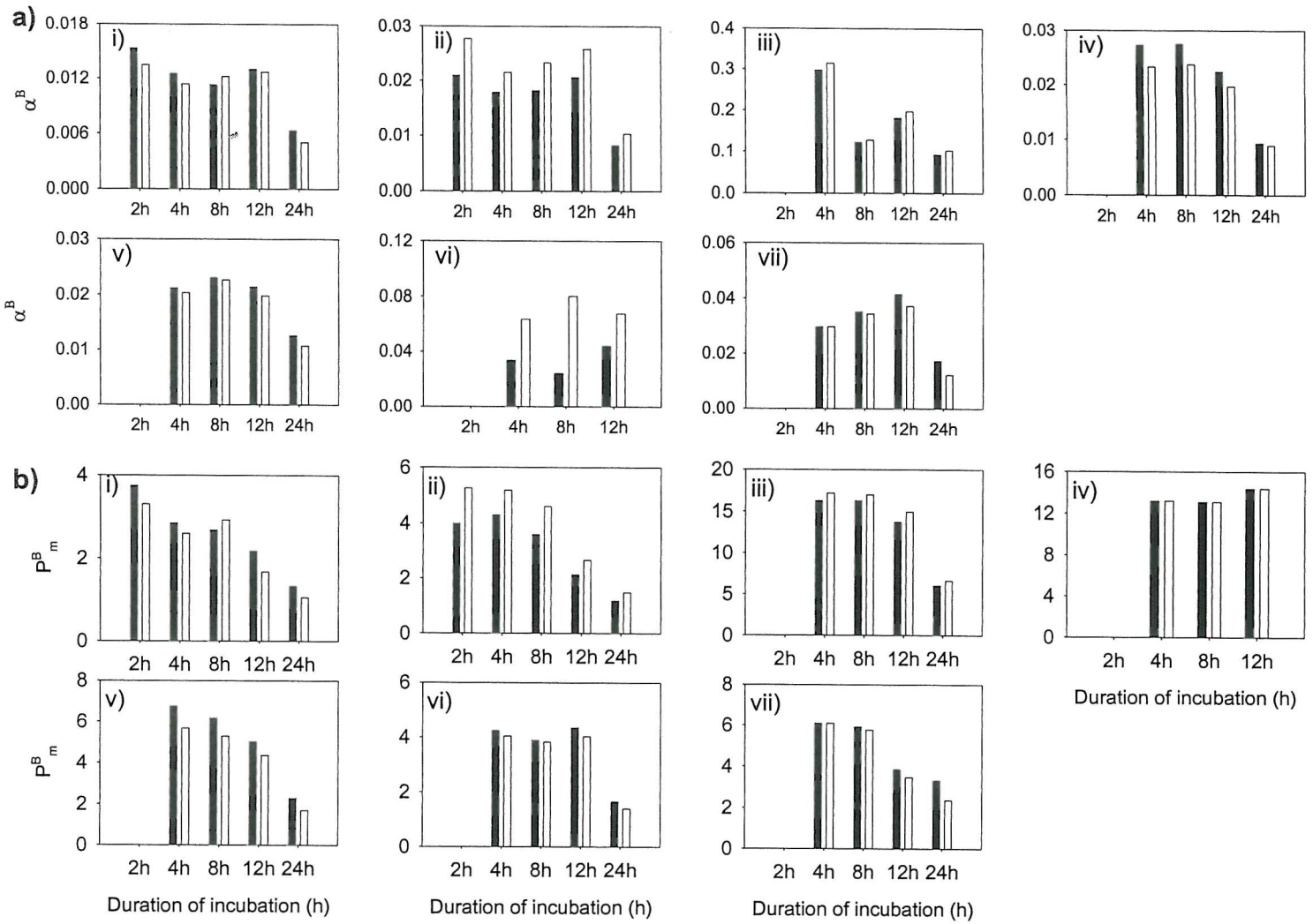

Figure 3.11. Comparison of parameters normalised to average chlorophyll (■) with those normalised to chlorophyll at t0 (□): a) to g) α^B in mg C [mg Chl]$^{-1}$ h^{-1}[µmol photons m^{-2} s^{-1}]$^{-1}$ and h) to n) P^B_m in mg C [mg Chl]$^{-1}$ h^{-1} on a & h) 3rd April 2001, b & i) 5th June 2001, c & j) 11th September 2001, d & k) 20th November 2001, e & l) 2nd July 2002, f & m) 21st August 2002 and g & n) 3rd September 2002.

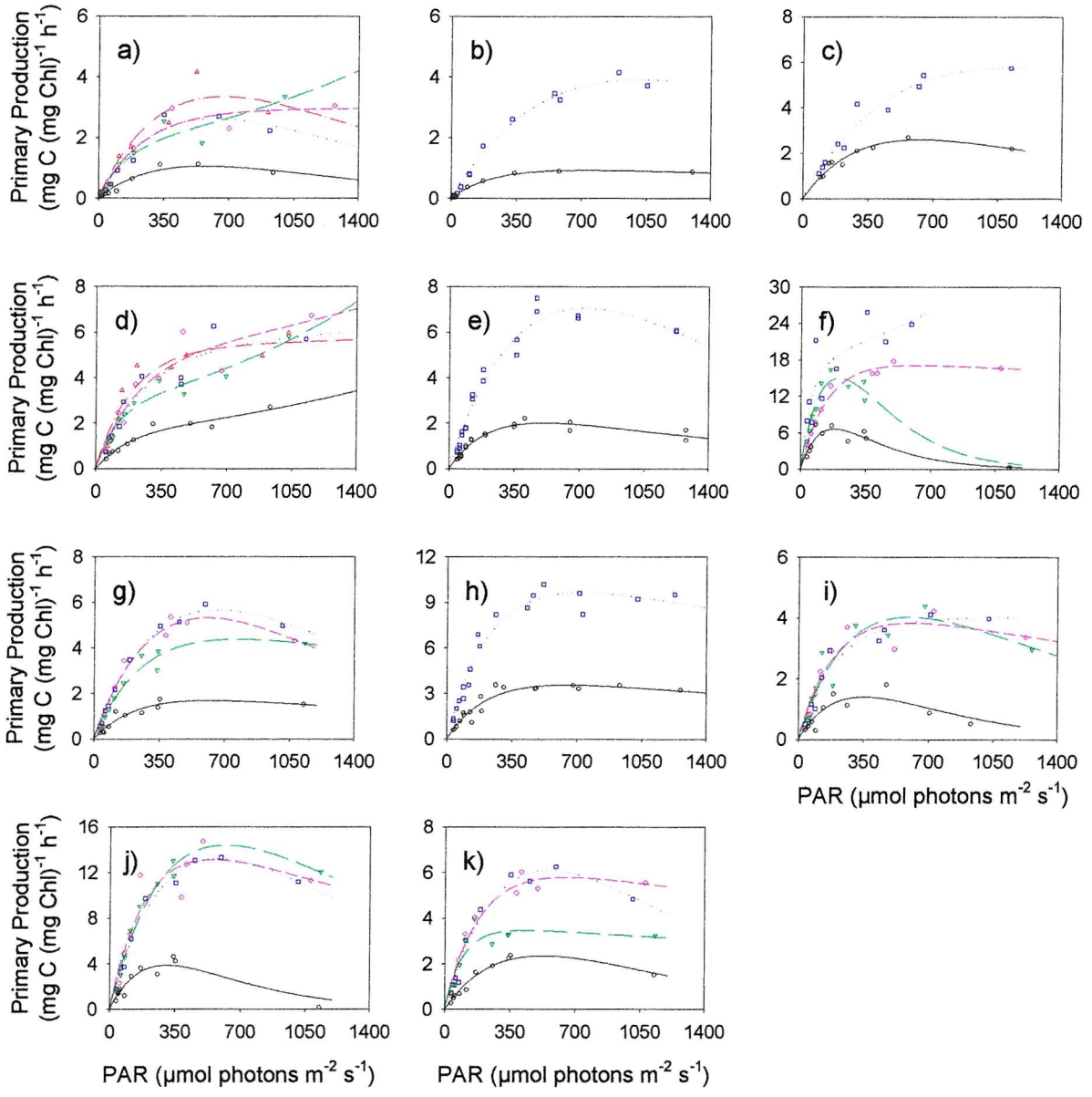

Figure 3.12. PE curves from incubations of L4 water for different durations on a) 3rd April 2001, b) 18th April 2001, c) 30th April 2001, d) 5th June 2001, e) 11th September 2001, f) 5th November 2001, g) 20th November 2001, h) 1st July 2002, i)2nd July 2002, j) 20th August 2002 and k) 3rd September 2002. Durations of incubation were 2h (▲), 4h (■), 8h (◆), 12h (▼) and 24h (●).

photoinhibition at high levels with the increase in the duration of the incubation. In three cases (12h incubations on 3rd April 2001and 4th June 2001 and the 4h incubation on 11th September 2001) the fitted curve suggested that production increased with irradiance even at very high light. In each case, this result is caused by one or two poor data points exerting a strong influence on the shape of the fitted curve. In most cases the PE curves between 2h and 12h were very similar but on 3rd September 2001, the curve from the 12h incubation showed a much lower maximum rate of production than those from the 4h and 8h incubations. This incubation was carried out using water from the autumn bloom when chlorophyll was very

high. High population densities may have led to an increased effect of enclosure in the bottle causing the duration of the incubation to be more important. Alternatively, the chlorophyll concentration at 12h may have been overestimated leading to unrealistically low normalised production values. Figure 3.13 shows the change in photosynthetic parameters over the course of the incubations. There was a general trend of a decrease in parameter values with increasing length of incubation. Values of α^B and P^B_m from 24 h incubations were significantly smaller than those at any other time ($p<0.05$, Wilcoxin's signed rank test). There were no significant differences in α^B for short incubation times. However, P^B_m values at 12h, although not always lower, were significantly different to those at 4h and at 8h. An average of 65 ± 0.26% of the variance in α^B was explained by that in P^B_m.

Figure 3.14 shows the effects of parameter values derived from incubations of different durations on modelled daily, depth-integrated production. The estimates derived with parameters from 24h incubations were significantly smaller than estimates using parameters from any of the other incubations ($p<0.05$, Wilcoxin's signed rank test). The estimates from 24h incubations were an average of 58 ± 10% of the production values from incubations of any other duration. No statistically significant differences were found using parameter values from shorter incubation periods. The model output was very similar when irradiance from different times of year was used. Surprisingly, using irradiance typical of a summer day in the models gave production values very similar to those obtained when winter irradiance was assumed.

Experiments to investigate bottle effects were carried out on five occasions (two in 2001 and three in 2002). On each occasion bottle effects were studied for samples exposed to light for 4h (contained in the bottle for 4h, 8h and 12h) and 8h (contained in the bottle for 8h and 12h). In most cases, the change in chlorophyll over the course of the incubations was small (see Figure 3.15). For two of the experiments a slight increase in chlorophyll was seen and for three, the opposite trend was seen. Figure 3.16 shows plots of PE curves for the samples; figures a) to e) show plots for samples exposed to the light for 4 h and figures f) to j) show plots for samples exposed to the light for 8 h). The apparent increase in production with light at high PAR suggested by the fitted curve for the incubation where the sample was held for 8h in the bottle and 4h in the light on 11th September 2001 (Figure 3.16a) is the result of scatter in the data leading to poor curve fitting. The values of photosynthetic parameters did change with time in the bottle but the pattern was not consistent. P^B_m values

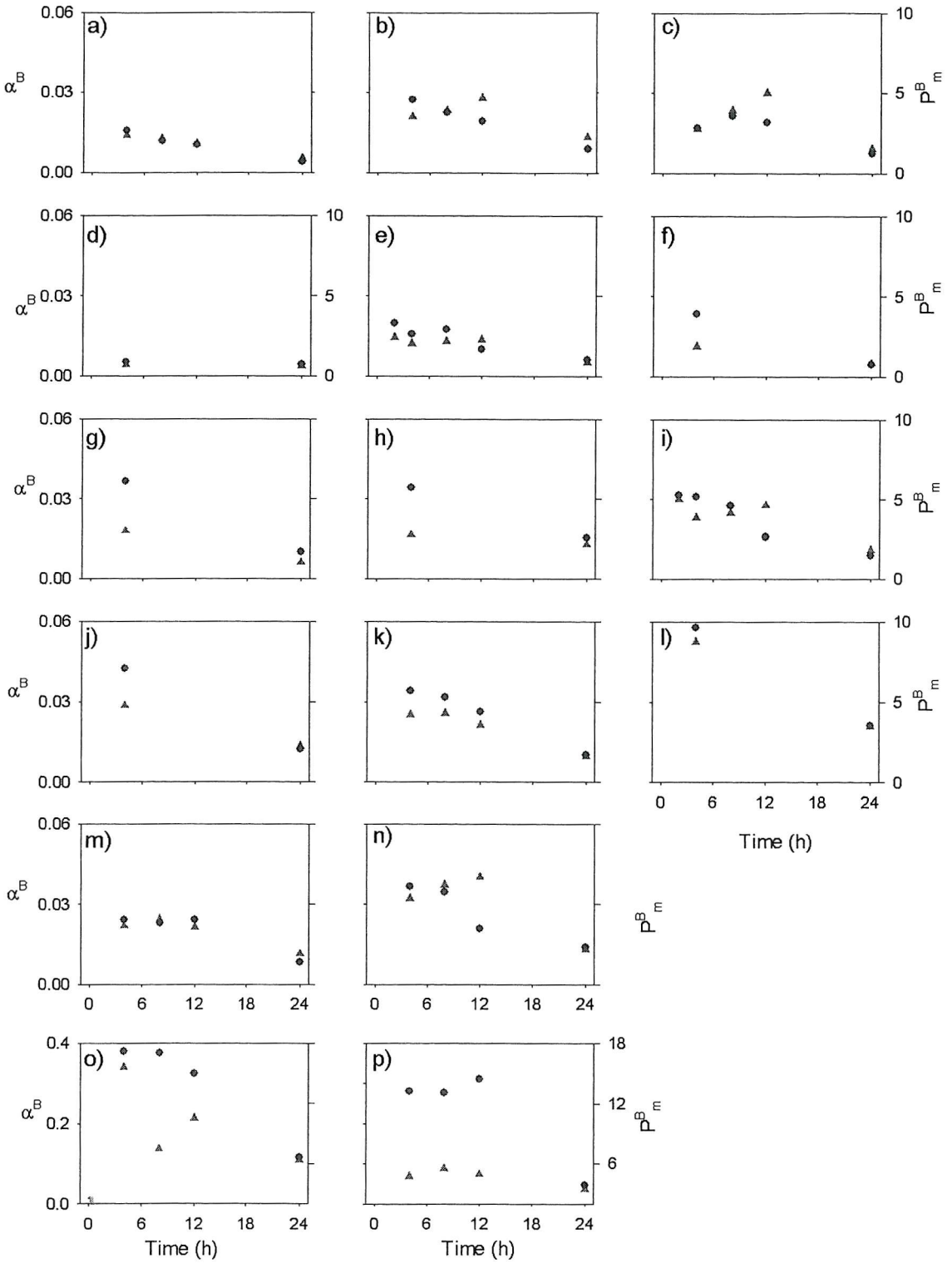

Figure 3.13. Change in photosynthetic parameters, α^B (▲) and P^B_m (●), over the course of incubations with L4 samples on a) 14th March 2000, b) 21st March 2000, c) 28th March 2000, d) 13th November 2000, e) 3rd April 2001, f) 18th April 2001, g) 23rd April 2001, h) 30th April 2001, i) 5th June 2001, j) 5th November 2001, k) 20th November 2001, l) 1st July 2002, m) 2nd July 2002, n) 3rd September 2002, o) 11th September 2001 and p) 20th August 2002. The last two dates (11th September 2001 and 20th August 2002) are shown out of chronological order as the graphs are on different scales to those from the other dates.

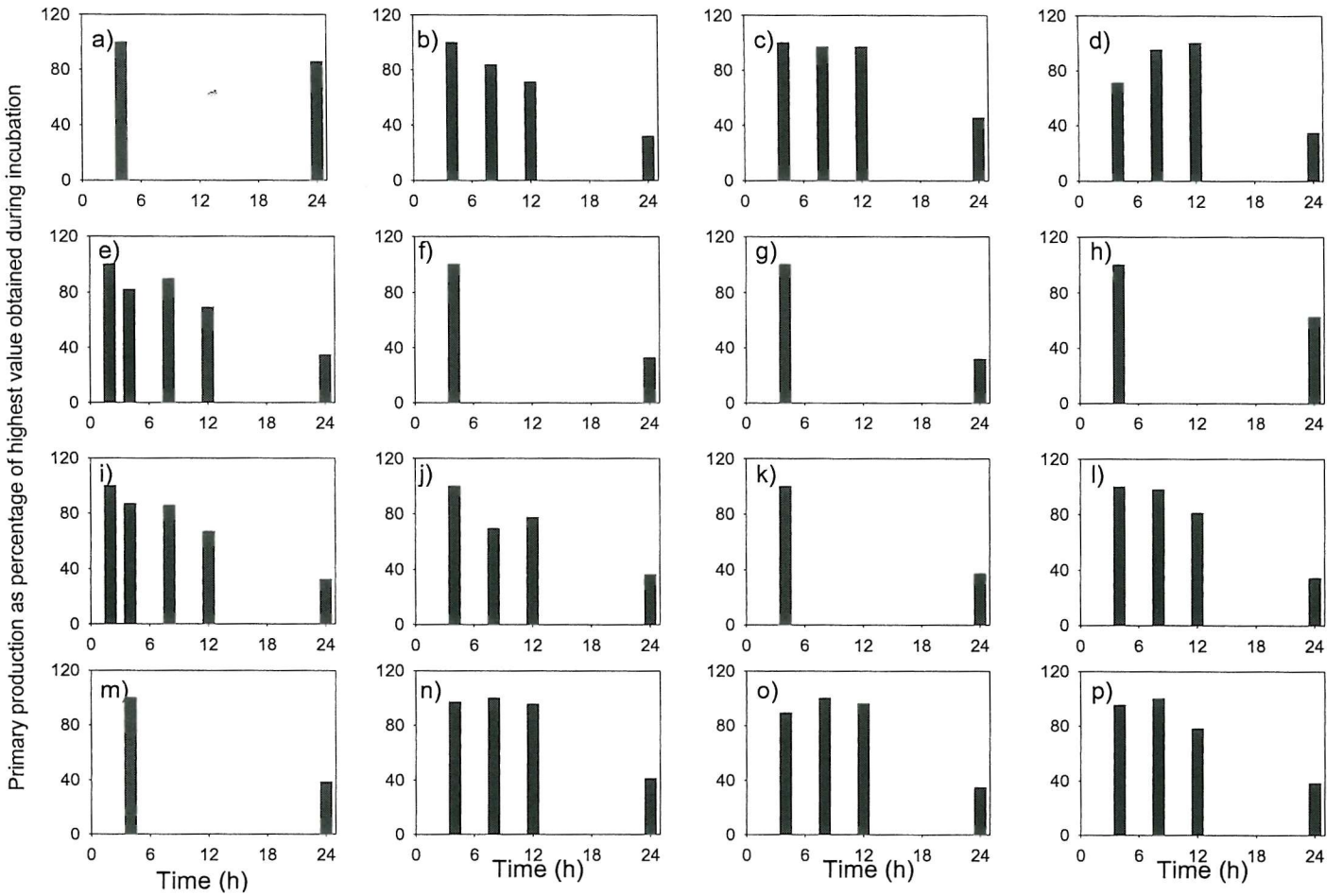

Figure 3.14. Effect of duration of incubation on modelled estimates of daily depth integrated production (L4 samples) on a) 13th November 2000, b) 14th March 2001, c) 21st March 2001, d) 28th March 2001, e) 3rd April 2001, f) 18th April 2001, g) 23rd April 2001, h) 30th April 2001, i) 5th June 2001, j) 11th September 2001, k) 5th November 2001, l) 20th September 2001, m) 1st July 2002), n) 2nd July 2002, o) 20th August 2002 and p) 3rd September 2002.

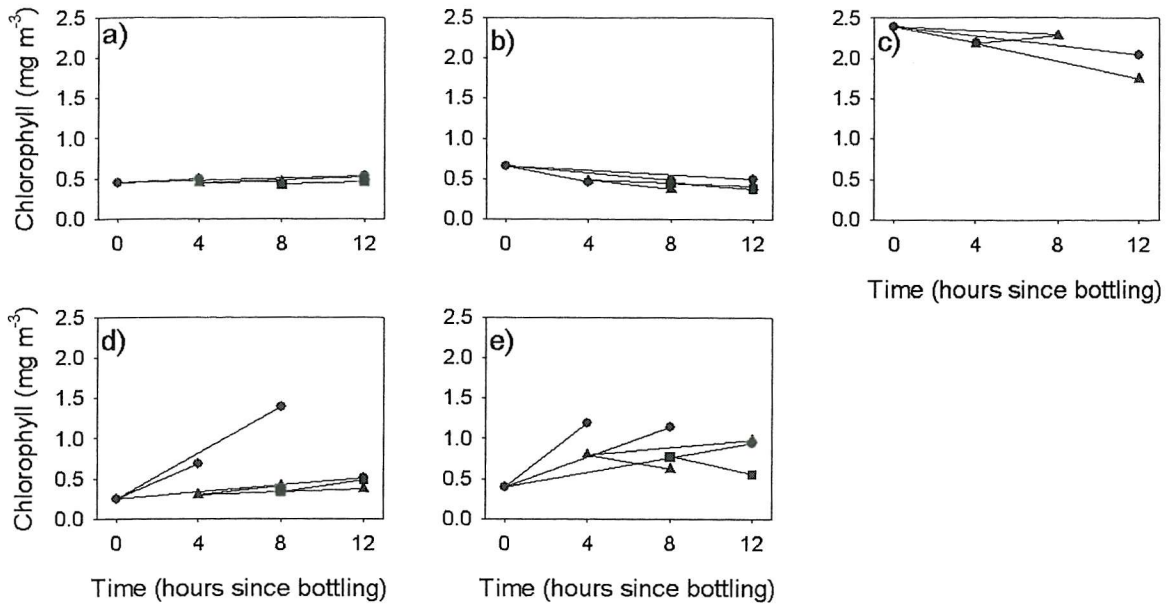

Figure 3.15. Change in chlorophyll concentration over the course of incubations to investigate bottle effects. Samples filtered or exposed to light after 0h (●), 4h (▲) and 8h (■) in bottle on a) 11th September 2001, b) 20th November 2001, c) 2nd July 2002, d) 21st August 2002 and e) 3rd September 2002.

showed no clear pattern of change with time in bottle. The α^B values from samples exposed to irradiance for 8h showed a slight increase with increased time in the bottle but those exposed to irradiance for 4h showed a variable response (a decrease on two occasions, an increase on two occasions and an increase followed by a decrease on one occasion). In most cases, however, there is an increase in curvature, indicative of increased photoinhibition at high light levels with time contained in the bottle.

These experiments showed incubation time to have no effect on the measured rate of production, using natural samples, unless a dark period was included. The lack of effect is thought to be largely due to changes in chlorophyll concentration and in respiration during the dark period. The effect of containment in the bottles was not consistent although there was increased photoinhibition at high light levels as time in the bottle increased. The experiments highlighted the complex nature of the processes taking place in natural samples where populations are mixed and measured results reflect whole community responses.

The effect of the inclusion of photoinhibition in PE models

The models used here were the photoinhibited and the non-photoinhibited equations of Platt *et al.*, (1980) and the photosynthetic parameters derived from each model over the course of each study are shown in Figure 3.17. The parameter values from each model were very

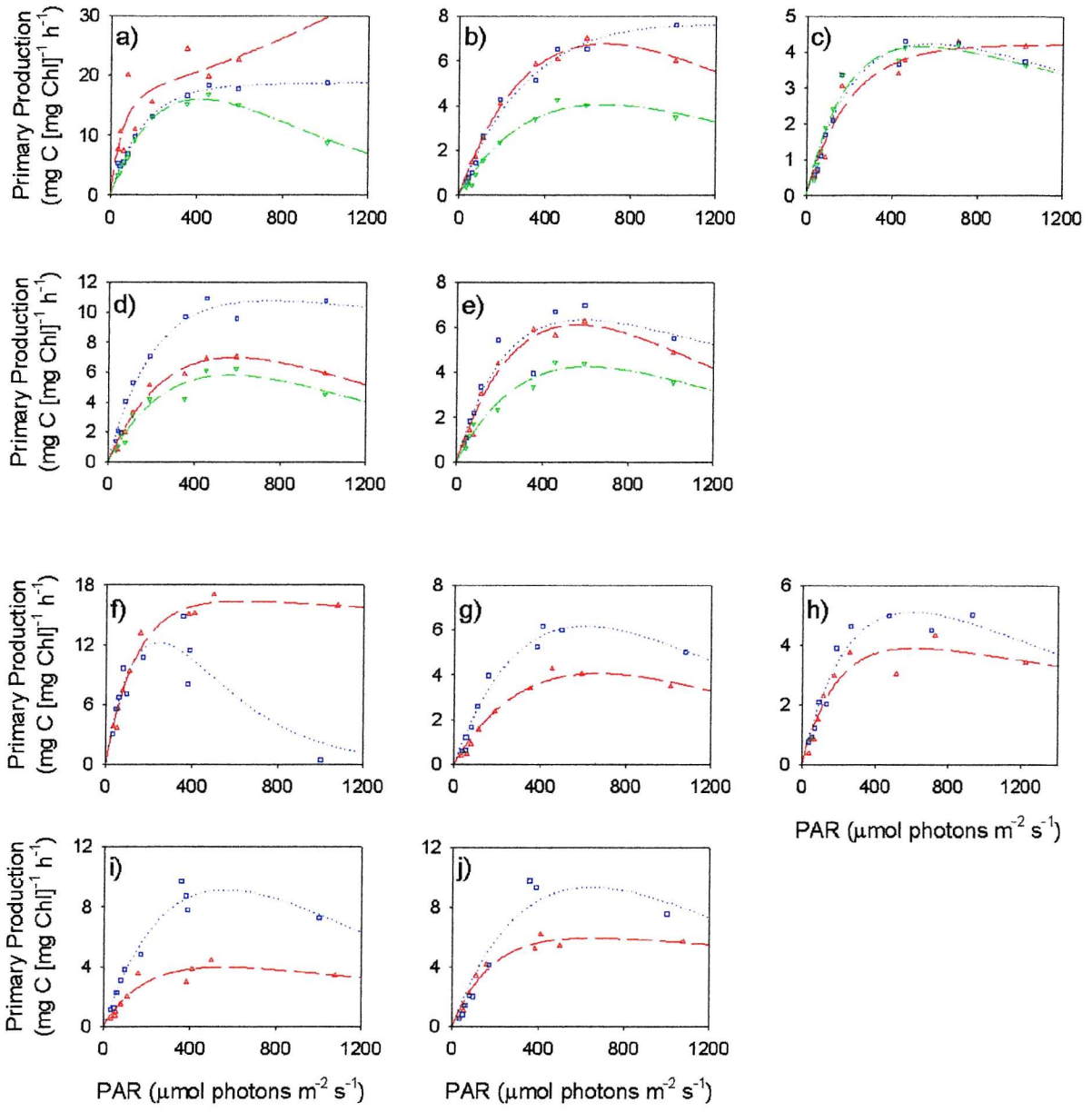

Figure 3.16. Change in shape of PE curve with time contained in bottles: a) – e) Samples exposed to light for 4h and spending a total of 4h in bottle (▲), 8h in bottle (■) and 12h in bottle (▼); f) to j) Samples exposed to light for 8h and spending a total of 8h in bottle (▲) and 12h in bottle (■). Dates of sampling were a & f) 11th September 2001, b & g) 20th November 2001, c & h) 2nd July 2002, d & i) 21st August 2002 and e & j) 3rd September 2002.

similar with over 87% of the variance in the parameters from the photoinhibited model explained by that in parameters from the non-photoinhibited model in all cases. The non-photoinhibited model led to slightly lower $P^B m$ values and slightly higher α^B estimates than the photoinhibited model. This in turn led to higher estimates of E_k from the photoinhibited model than from the non-photoinhibited model. It is important to note that the values in Figure 3.17 are not true photosynthetic parameter values as they were derived from 24h incubations that included a dark period.

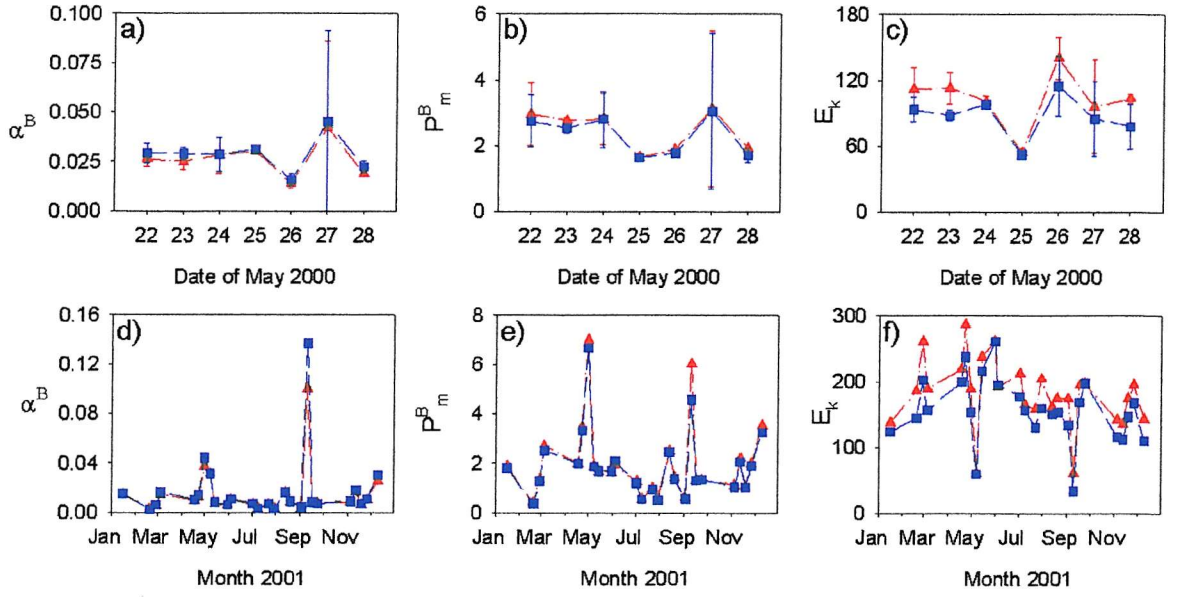

Figure 3.17. Effect of using different models to derive photosynthetic parameters from ^{14}C incubations: a) α^B in Celtic Sea, b) P^B_m in Celtic Sea, c) E_k in Celtic Sea, d) α^B at L4 2001, e) P^B_m at L4 2001 and f) E_k at L4 2001. Data from the photoinhibited model (▲) and the non-photoinhibited model (■). Values of α^B are in mg C [mg Chl]$^{-1}$ h^{-1} [µmol photons m^{-2} s^{-1}]$^{-1}$, P^B_m values are in mg C [mg Chl]$^{-1}$ h^{-1} and E_k values are in µmol photons m^{-2} s^{-1}.

3.2.2 Comparison of PP_{Daily} estimated from photosynthetic parameters with that from 24h *simulated-in-situ* incubations

Extrapolation from measurements of PE parameters from short-term incubations to estimates of PP_{Daily} requires knowledge of how the photosynthetic response changes over the course of the day and of the available light at every hour and every metre of the water column. In this model, diel periodicity was assumed to have little effect and was ignored. The crucial parameters to drive the model were surface PAR at every hour of the day and the attenuation coefficient to describe the loss of light with depth.

Calculation and validation of the light field

Daily values of PAR and K_{PAR} from the Celtic Sea cruise are shown in Table 3.3. Total daily PAR (over 24h) in the Celtic Sea ranged from 2.87 x 10^7 mol photons m^{-2} on 23rd May to 4.57 x 10^7 mol photons m^{-2} on 28th May. On every day, the maximum value of a 30 minute average surface PAR was close to 1500 µmol photons m^2 s^{-1} (average maximum value for all 11days of study = 1458 ± 112 µmol photons m^2 s^{-1}). Average daily K_{PAR} values ranged from 0.124 ± 0.033m^{-1} (28th May) to 0.182 ± 0.019m^{-1} (25th May). The surface effect

Table 3.3. Daily integrated PAR (mol photons m^{-2} d^{-1}) and K_{PAR} (m^{-1}) at each station in the Celtic Sea. K_{PAR} values were averages of all casts on one day. There were a minimum of three casts (on 24th May) and a maximum of seven casts (on 27th May) on each day.

Station	Date	Daily PAR	K_{PAR}
G	22nd May	4.18×10^7	0.134 ± 0.035
G	23rd May	2.87×10^7	0.172 ± 0.021
G	24th May	3.66×10^7	0.179 ± 0.009
E	25th May	3.45×10^7	0.182 ± 0.019
E	26th May	3.71×10^7	0.172 ± 0.016
F	27th May	3.51×10^7	0.147 ± 0.011
F	28th May	4.57×10^7	0.124 ± 0.033

(F_s) was always 0.538 for overcast skies whilst for clear skies the values depended on the time of day. For simplicity, the values at solar noon were used and ranged from 0.721 to 0.730. It is realised that these were the minimum values encountered throughout the day and that the surface effect would increase dramatically towards dawn and dusk.

Estimates of the modelled values of PAR were compared to measured PAR profiles. The model was used to estimate average values for 30-minute periods that included the time of the cast. Figure 3.18 shows typical profiles of measured and modelled PAR using both the

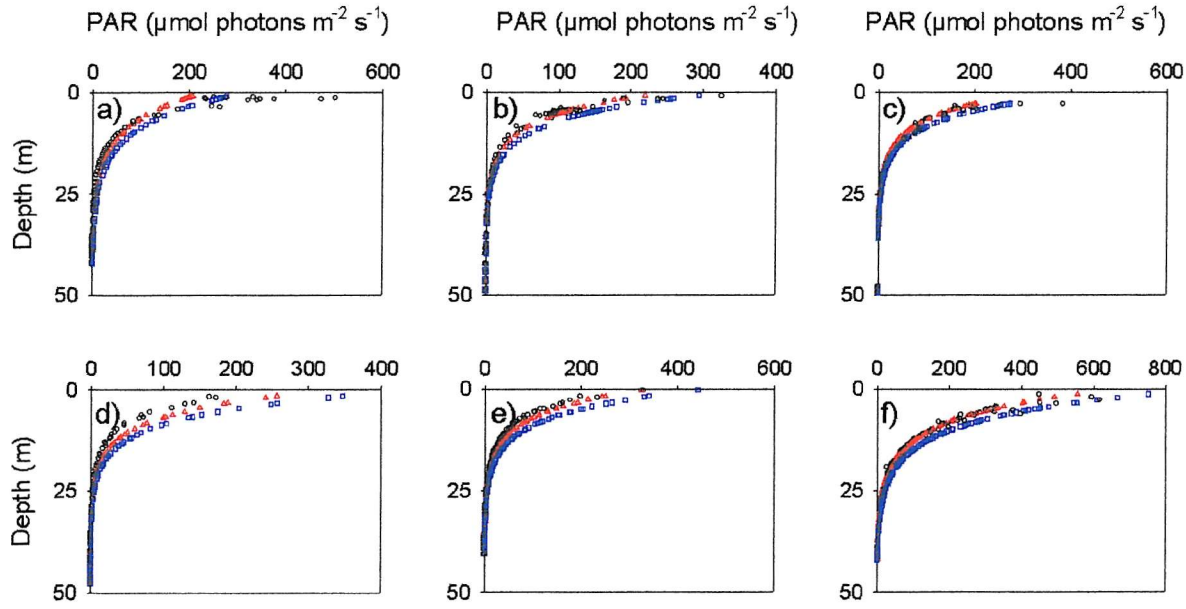

Figure 3.18. Measured (○) and modelled (overcast sky (△) and clear sky (□)) PAR (30 minute averages) from Celtic Sea cruise on a) 22nd May, b) 23rd May, c) 24th May, d) 25th May, e) 26th May and f) 27th May. One typical cast for each day is shown.

overcast and clear sky model and it is clear that modelled PAR agreed well with the measured values. Linear regressions of modelled against measured PAR were carried out for individual casts and for whole days by pooling the data for all casts on each day. Twenty-five regressions from individual casts were carried out using the results from both the overcast and the clear sky models. The PAR values from the overcast model were closer to the measured values than those from the clear sky model. In all but two cases, the variance explained (R^2 value) was greater than 0.89. The slopes of the regressions, when an overcast sky was assumed, ranged from 0.50 (cast 2207) to 2.66 (cast 2710). The average value of the slope was 1.06 ± 0.61. When a clear sky was assumed, the slopes of the regressions ranged from 0.71 (cast 2207) to 3.60 (cast 2710) with an average of 1.45 ± 0.83. Table 3.4 shows the statistics from the regressions of modelled against measured PAR when the data from all the casts on one day were combined (for an overcast sky). In this case, all R^2 values were greater than 0.80 and the slopes of the regressions ranged from 0.69 (22nd May) to 1.39 (25th May), with an average of 0.99 ± 0.25. The average slope value when a clear sky was assumed was 1.23 ± 0.16. Given the lower range of the slopes of the regression and the closeness of the average slope to 1.0, an overcast sky was assumed for the production calculation.

Table 3.4. Statistics from linear regressions of modelled PAR against measured PAR for the Celtic Sea stations. Modelled PAR values are the 30 minute averages for periods including the time of the measurements. Data were pooled over all the casts in one day.

Station	Date (2000)	R^2	Slope	Intercept
G	22nd May	0.95	0.69	0.51
G	23rd May	0.90	1.14	4.44
G	24th May	0.98	0.84	1.85
E	25th May	0.98	1.39	3.28
E	26th May	0.80	0.97	15.69
F	27th May	0.82	0.89	14.83

Comparison of estimates of PP_{Daily}.

The photosynthetic parameter values used in the model are shown in Figure 3.17 (a and b). The values used were averages of the dawn and noon casts. No significant differences were found between the dawn and midday values of any photosynthetic parameters determined for water samples taken near the sea surface (shallow water samples). However, P^B_m values at noon were higher than those determined at dawn in all but one case (24th May). The standard deviation of the average was low in all cases except on the 27th May.

Modelled estimates of PP_{Daily} are compared with estimates from 24h *simultaneous- in-situ* (SIS) incubations in Figure 3.19. The SIS incubations indicated higher production at depth than that estimated by the photosynthetic parameter models. At the surface, production estimates from the SIS incubations were always less than modelled values but below approximately 10m, SIS production was always higher. Figure 3.20 shows the estimates of daily, depth-integrated production from each technique on each day and the average daily estimate with 95% confidence intervals. Production estimates from $^{14}C_{SIS}$ incubations were higher than estimates from the models in all cases. Estimates from the non-photoinhibited photosynthetic parameter model were slightly higher than those from the photoinhibited model. None of the estimates were significantly different to each other. The results of regressions of estimates from the different techniques are shown in Table 3.5. The variance in the *simulated-in-situ* estimates of production explained approximately 40% of that in the equivalent modelled values. The data suggested that 95% of production estimates, whether modelled from PE parameters or from SIS incubations would fall within 21± 14% of the average values.

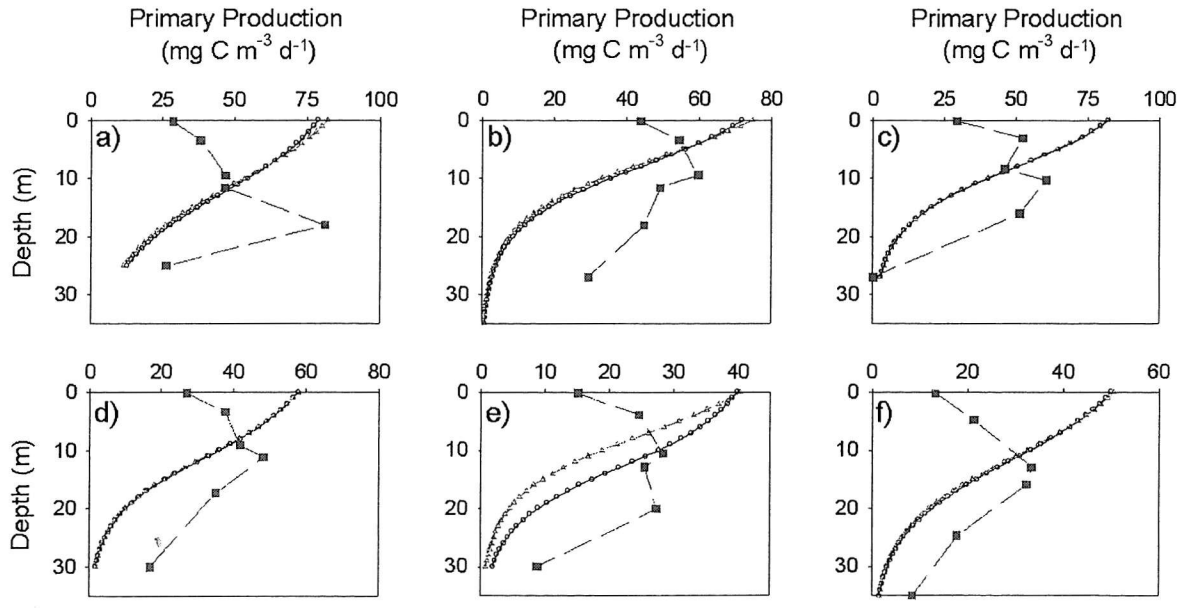

Figure 3.19. Depth specific primary production in the Celtic Sea integrated over the course of the day on a) 22nd May, b) 23rd May, c) 24th May, d) 25th May, e) 26th May and f) 27th May. Data from the photoinhibited photosynthetic parameter model (○), the non-photoinhibited photosynthetic parameter model (△) both based on water from one depth and 24 h *simulated-in-situ* incubations (■) using water from six depths.

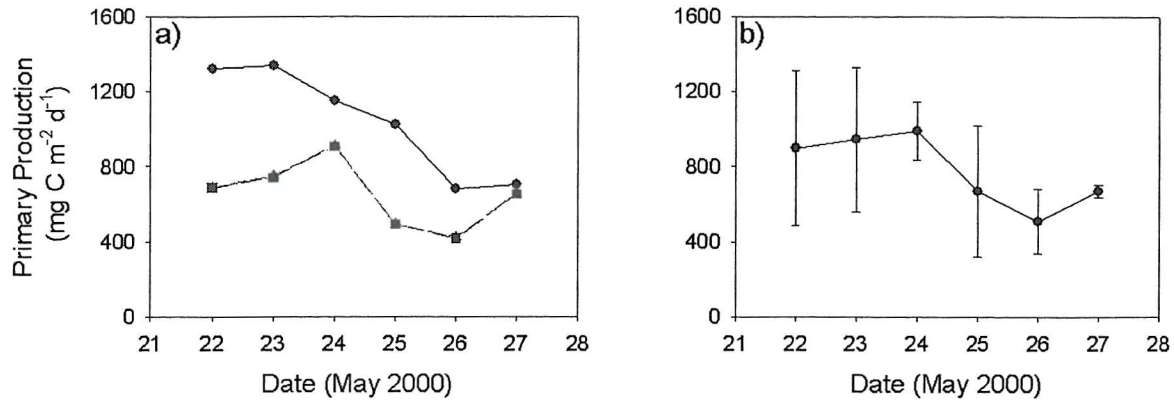

Figure 3.20. a) PP_{Daily} during the cruise in the Celtic Sea estimated from ^{14}C *simulated-in-situ* incubations (●) and ^{14}C photosynthetic parameters with no photoinhibition (■) and with photoinhibition (▲) and b) average PP_{Daily} for each date calculated from all three estimates of production. Error bars show the 95% confidence intervals.

Table 3.5. Statistics from regressions of daily, depth-integrated production from ^{14}C *simulated-in-situ* incubations and ^{14}C photosynthetic parameters for the Celtic Sea stations.

Independent variable	Dependent variable	R^2	Slope	Intercept
SIS	Photoinhibited photosynthetic parameters	0.45	0.51	223
SIS	Non-photoinhibited photosynthetic parameters	0.43	0.42	355
Photoinhibited photosynthetic parameters	Non-photoinhibited photosynthetic parameters	0.97	0.83	167

3.3 Discussion

Photosynthetic parameters from incubations under artificial light gradients

The calculated light correction showed that the spectra of the lamp in the water tank led to an underestimate of α^B whilst that in the portable incubator with the blue filter led to an overestimate compared to that expected under natural light (Figure 3.1). The wavelength dependency of α^B can, if uncorrected, have a large impact on productivity models since the difference between the *in situ* light field and that in the incubator leads to errors in production estimates (Schofield *et al.*, 1996). The ability to use light is a direct function of the light harvesting capability of phytoplankton, itself a function of the types and concentrations of light harvesting pigments. The lamps used had lower proportions of light in the two major absorption peaks of chlorophyll than natural sunlight. Once corrected for the spectra of the

lamps, there were no significant differences between the corrected values of α^B or P^Bm from natural samples incubated in the two different incubators (Table 3.1). However, the average α^B value from the water tank was 0.043 ± 0.033 mg C [mg Chl]$^{-1}$ h^{-1} [µmol photons m^{-2} s^{-1}]$^{-1}$ whilst that from the portable incubator was lower at 0.034 ± 0.020 mg C [mg Chl]$^{-1}$ h^{-1} [µmol photons m^{-2} s^{-1}]$^{-1}$. The correction applied here was investigated by Schofield *et al.* (1996) who compared α^B values derived from wavelength specific incubations with those derived from incubations under broadband irradiances corrected, *post-hoc* for the spectra of the lamp used. They concluded that the technique is an effective way to overcome the technical limitations of measuring α^B using broadband light.

The effect of storing water samples overnight prior to experimentation (Figure 3.9) meant that derived values of photosynthetic parameters were different to those that would have been measured if the experiment had been done on the day of sampling. However, comparison of parameters obtained within any single incubation is still relevant. The work carried out here addressed variability in PE parameters derived from incubations of a minimum of 2h duration. The parameters from the incubations of different durations including only a light period (of 2h, 4h, 8h and 12h duration) were statistically indistinguishable from each other. Only the inclusion of a dark period led to a significant decrease in both parameter values and, hence, derived daily primary production. This was true for both cultures (Figure 3.5) and L4 samples (Figure 3.13). The incubations including a dark period were expected to lead to much lower rates of production than those only in the light, since some fixed ^{14}C would be lost by respiration in the dark. The shorter the incubation, the closer the measured process is to gross production. As incubation time increases, particularly when a dark period is included, the measure moves towards net production. With natural samples, the processes measured from 24h incubations are closer to net community production as grazing and nutrient recycling play an important role in the recycling of fixed ^{14}C.

The main difference between the results from experiments with cultures and those using water from L4 was the increase in chlorophyll during the dark period in the cultures. This might have been associated with cell division during the night. However, a lack of clear change in cell number or carbon content suggests the increase in chlorophyll was due, not to cell division, but to an overnight increase in chlorophyll per cell. The variable overnight changes in chlorophyll concentration in the L4 samples could reflect variability in phytoplankton population composition or the effect of grazing. Interpretation of the time course ^{14}C assimilation is influenced by the metabolism of the various components of various

populations in the microbial food web (Marra *et al.*, 1998). In the dark, there is a net loss of assimilated carbon but estimates vary of the proportion of fixed carbon lost, due to dark respiration (see Williams, 1993a; Harris *et al.*, 1989; Eppley and Sharp,1975 and Ryther,1954). Respiration rates vary between species and with nutrient availability (Laws *et al.*, 2000; Falkowski and Raven, 1997; Langdon, 1993 and Laws and Bannister, 1980) so its quantification is very difficult. Additionally, recycling of fixed ^{14}C during incubations makes it difficult to elucidate the causes of high dark losses (Williams, 1993a and Harris *et al.*, 1989).

PE parameters vary as a result of a range of adaptations that occur over different timescales so the duration of the incubation can have a large effect on derived values. The different timescales of these adaptations have been described by a number of authors. Photoacclimation (also known as rapid photoresponse (Han *et al.*, 2000) or light-shade adaptation (Falkowski and LaRoche, 1991) can occur in minutes and may be important in allowing phytoplankton to exploit turbulent motion in the mixed layer (Han *et al.*, 2000; Franks and Marra, 1994 and Pahl-Wostl and Imboden, 1990). It involves phenotypic or physiological adjustments due to a change in environmental factors (MacIntyre *et al.*, 2002). Photoinhibition, the decrease in photosynthesis at high irradiance, may occur in minutes or over hours (Han *et al.*, 2000). When light varies, subsequent adaptations and changes in the rate of photosynthesis may be delayed or may exhibit complex temporal dynamics (Pahl-Wostl and Imboden, 1990).

As a result, the photosynthetic output measured at any time is not only a function of current conditions but also of conditions to which the phytoplankton have previously been acclimated. Short-term incubations should minimise photoinhibition at high light and should most closely reflect photosynthesis in the water column but may not reflect the irradiance conditions of the incubator, against which they are measured and described. The process measured from a ^{14}C uptake experiment depends not only on the previous light history and other environmental conditions but also on the doubling time of the phytoplankton species. The incubation method can be useful as an indicator of potential photosynthetic capacity under the prescribed conditions but may not always be a true measure of *in situ* primary production. The studies carried out here did not address the previous light or mixing history but this would be of interest for future work as it could aid explanations of the observed results.

A number of studies have documented the change in photosynthetic parameter values with time ranging from 180 minutes (Macedo *et al.*, 1998) to 36h (Marra *et al.*, 1998). Until the introduction of photosynthetron-type incubators, phytoplankton samples were usually exposed to a gradient of light for 3-4h to generate PE curves (Lewis and Smith, 1983). The photosynthetron, introduced in 1983 by Lewis and Smith allows the very short term incubation of very small volumes (~1ml) of samples to generate PE curves, theoretically minimising the artefacts of incubation. Compared to the natural situation in the surface mixed layer, 4h is a long time for a phytoplankton to receive static illumination and significant adaptation occurs within this time (Lizon and Lagdeuc, 1998; Macedo *et al.*, 1998 and Lewis and Smith, 1983). Macedo *et al.* (1998) and Lewis and Smith (1983) showed that after a fast initial adaptation, steady state rates of production are reached. The incubations carried out here did not resolve such short-term adaptations of phytoplankton. The extent of the change in parameter values during the initial minutes of incubations may reflect the extent to which incubator conditions differ from those *in situ* and hence how different the parameter estimates will be to *in situ* populations. However, very short-term incubations are not the answer either since they may measure a transient state of phytoplankton, adapted neither to the *in situ* environment nor to that in the incubator. The difference between the results observed here and those from different authors not only reflect the illumination at the time of the experiment but the environment to which the phytoplankton are adapted over a longer time period. The results from experiments carried out here are expected to differ from those carried out in deep waters as these experiments all used water from less than 40m, which, even at depth, was relatively well illuminated. Mixing would ensure that, for most of the year, the phytoplankton sampled in our studies would experience relatively high light at some point in the day, which may not be true for other sites.

The derived photoinhibition parameter was not considered reliable. This was the result of a low proportion of the data points in the PE curve falling in the light limited region. The exponential decrease of light with distance from the source led to relatively few points being available to dictate the shape of the curve at high light levels so the estimation of β^B was very sensitive to small changes in estimates at just one irradiance. The PE plots gave an indication of the effect of high light and did not show clear increases in photoinhibition, specifically at high light levels with duration of incubation.

The increase in photoinhibition at high light levels with time contained in the bottle (Figure 3.16) could be a result of nutrient limitation. However, nutrient data was only available for

two of the dates and was measured on the day of sampling but in these cases, nutrients were not too low (Nitrate = 0.43μmol l^{-1} and 1.53μmol l^{-1} and Phosphate = 0.04μmol l^{-1} and 0.14μmol l^{-1} on 10th September 2001 and 19th November 2001 respectively). The high light photoinhibition could reflect an adaptive down-regulation of photoprotective pigments with increased time in the darkness before the exposure to light. However, as all samples were contained in the darkness overnight prior to the experiment, it is unlikely that an extra 4h of dark containment would have lead to this down-regulation of specific pigments. A final consideration is that of mechanical damage inhibiting photosynthetic machinery but this would be expected to have an effect at all light levels, not just at high light.

Bottle effects depend greatly on the relative scales of bottle size to dispersal of organisms and the time of incubation related to grazing and remineralisation rates (Harris *et al.*, 1989). Hence, both the container volume and the incubation time are likely to affect the changes within contained populations. Container volume was not addressed here. Harris *et al.* (1989) found that it was difficult to maintain healthy and active tropical autotrophic populations for more than 8 hours in 130ml bottles and that if mishandling occurred during incubation, irreversible changes took place in less than 4 hours. Geiskes and Kraay (1982) looked at the effect of enclosing water in large plastic bags on its content of oxygen, algal cells and pigments. They observed that autotrophic and heterotrophic nanoplankton cells and algal pigments stayed constant or increased slightly in 24h of enclosure. Sornin *et al.* (1990) noted a rapid increase of chlorophyll *a* within bottles whilst at the level of the bulk water from which it was sampled, the increase was not observed. They attributed their observation to the removal of the photoautotrphs from large natural predators (in this case oysters) by bottle enclosure. Marra *et al.* (1988) suggested that a rapid and unexpected increase of autotrophs within bottles in an experiment suggested an unbalanced food web over the period of observation that they suggested might be a result of bottle containment. Venrick *et al.* (1977) looked at the effect of short-term containment of oligotrophic water on plankton and productivity measurements. Their results indicated that changes within the bottles were not merely physiological but were manifested by changes in species abundance to the point that the final contained assemblage often differed markedly from the original sample. Venrick *et al.*, (1977) suggested that parcels of water in bottles might approach equilibrium conditions in which species are excluded by competitive interactions. Other work suggests that diatoms contribute more than expected from initial biomass and that this may result from them being particularly successful within bottles compared to other species (see Thomas and Dodson, 1974). If, as Verduin (1960) suggested, damage can arise from collision with the bottle

surface, then more physically robust species may be more successful in containers. Unfortunately species counts were not made at the start and end of these experiments and definitive explanations of the inconsistent results observed cannot be made.

Comparison of PP_{Daily} estimated from photosynthetic parameters with that from 24h simulated-in-situ incubations

The relatively high production estimates from $^{14}C_{SIS}$ incubations (Figure 3.20) was unexpected. The interpretation of the uptake of carbon during long-term incubations is complex and is related to the extent of respiration and of subsequent reassimilation of respired carbon. However, long-term incubations with ^{14}C are generally thought to measure net community production. In contrast, model derived estimates of production, based on PE parameters derived from short-term incubations, should reflect gross production and as such are expected to exceed *simulated-in-situ* estimates under most conditions (Harrison *et al.*, 1985). However, other experiments comparing *simulated-in-situ* incubations with modelled estimates of production have found similar results to this study. Cullen *et al.* (1992) found that modelled daily production was 34% lower than that measured from *simulated- in-situ* incubations. Harrison *et al.* (1985) found that model estimates were slightly higher in surface waters and significantly lower at the bottom of the euphotic zone than estimates from *simulated- in-situ* incubations. Similarly, in this study, *simulated- in-situ* production was slightly lower than production from the ^{14}C PE models at the surface but much greater at depth.

One cause for the discrepancies between results from different ^{14}C approaches may be spectral differences in the light regime (Harrison *et al.*, 1985). The magnitude of error introduced by spectral differences will be greatest at low irradiances where photosynthesis is light limited (Tilzer *et al.*, 1993). This explains why the highest differences found by Harrison *et al.* (1985) were at the bottom of the euphotic zone. Incubations in artificial light can lead to underestimates of production under limiting irradiance when compared to those measured under natural light (Tilzer *et al.*, 1993 and Harrison *et al.*, 1985). The spectrum of the lamp used in the incubations for the PE curve, even with the blue filter, had a lower proportion of blue light and a higher proportion of red light than natural irradiance. In the sea, light harvested in the blue absorption peak of photosynthetic pigments is the dominant energy source for photosynthesis (Prézelin *et al.*, 1991) so a relative decrease in this part of the spectrum could lead to underestimates of production. It is widely acknowledged that static *simulated- in-situ* incubations, which limit vertical mixing, lead to unrealistic estimates

of production due to unnatural photoacclimation and photoinhibition (Barkmann and Woods, 1996; Gallegos and Platt, 1985 and Marra, 1978). Harrison *et al.* (1985) noted that their relatively lower surface estimates from *simulated- in-situ* incubations could be due to time-dependent photoacclimation at the surface; this could also be true for the results reported by Cullen *et al.* (1992). The profiles of production in this study also suggest time-dependent photoinhibition of surface *simulated- in-situ* samples.

The photosynthetic parameter values were corrected to account for the difference between the spectrum of the lamp and that of natural irradiance. However, production at depth was nevertheless higher from the *simulated-in-situ* incubations than from the photosynthetic parameter models. It is possible that the *post-hoc* application of spectral correction does not fully account for the effect of the lamp spectrum on photosynthesis. It is also possible that production at depth from $^{14}C_{SIS}$ was unrealistically high due to unnatural photoacclimation. Integrated production from *simulated-in-situ* incubations is much higher than modelled estimates because the higher production at depth from the former outweighs the surface photoinhibition. Cullen *et al.* (1992) suggested that the differences between *simulated-in-situ* and modelled estimates were partly due to the accumulation of chlorophyll during long-term *simulated-in-situ* incubations. They found that chlorophyll increased by up to 80% during the incubations. Unfortunately, chlorophyll concentrations were not measured at the end of the incubations in these experiments in the Celtic Sea.

The calculation of $E_{(z,t)}$ assuming completely overcast and clear skies separately was designed to give estimates of PAR that would be considered the extreme values possible on the days studied. In most cases the measured light was closer to that from the overcast than the clear sky model. The regressions also showed that both models tended to over predict $E_{(z,t)}$. One reason for this could be shading of measured values by the ship. Even if the ship were not blocking the direct beam of sunlight to the PAR sensor on the FRRF, diffuse sunlight could decrease. This possibility is supported by comparisons of PAR from the two sensors (that on the FRRF and that mounted high on the ship), which show slightly higher PAR on the ship-board meter. Based on these factors and the weather conditions encountered during the cruise, $E_{(z,t)}$ was estimated using the overcast model to estimate production.

Errors in estimating production may be introduced by relying on a single value to describe the attenuation of a wide band of wavelengths (ie 400-700nm) that are not transmitted

equally through the water. PAR at the red end of the spectrum is absorbed within the first few metres of the water column. The derivation of a whole column value of K_{PAR} could therefore lead to an overestimate of PAR at the surface and an underestimate at depth. However, this did not appear to be a problem here (Figure 3.18). The application of one value of K_{PAR} throughout the course of the day is another potential cause of error in the estimates of daily production. The value of K_{PAR} depends not only on the concentration of light-attenuating compounds but also on the angular distribution of the light field (Morel and Smith, 1982) which varies over the course of the day. However, no clear diel variation of K_{PAR} was seen during the Celtic Sea study (Table 3.3). The daily values used had an average standard deviation of 13%. To investigate the effect of using a single value of K_{PAR} throughout the day, a sensitivity analysis was carried out. When average K_{PAR} values were increased by the value of their standard deviation, PP_{Daily} decreased by between 4% (24th May) and 15% (22nd May). When the K_{PAR} values were decreased by the value of their standard deviation, PP_{Daily} increased by between 4% (24th May) and 20% (22nd May).

Diel periodicity of F_s was ignored in the calculation of $E_{(z,t)}$. This will have had no effect on the overcast model. However, it may have led to an overestimate of light penetrating the surface in the clear sky models as the F_s value used (from midday) was the lowest value over the course of the day. Conversely, the unrealistic assumption of a flat sea surface would have led to an underestimate of F_s.

Diel periodicity in photosynthetic parameters was not included in the models. The parameters from ^{14}C incubations were average values for shallow water samples taken at dawn and noon. Diel periodicity due to physiological adaptation has been observed in a number of species of marine phytoplankton (Lande and Lewis, 1989). P^B_M values at noon were slightly higher than those at dawn in all but one case (24th May) but the difference was not significant. There were no significant differences between the dawn and midday shallow water values of any photosynthetic parameters from the ^{14}C incubations. Periodicity in P^B_M values has been reported with the highest values typically found at noon (Cullen *et al.*, 1992 and MacCaull and Platt, 1977). E_k values have also been reported to exhibit diel periodicity but with unclear patterns of change (MacCaull and Platt, 1977) and diel patterns of change in α^B over the course of the day have not been reported. Some argue (MacCaull and Platt, 1977) that the use of a constant value for P^B_M could induce large errors in models of daily production whilst others (Jitts *et al.*, 1976) find the effect to be small. The depth range of the

model included only the surface mixed layer so the assumption of uniform parameter values is expected to be true.

The conductivity-temperature-depth (CTD) meter was not working for most of 2001 so an assumption of constant salinity at L4 had to be made. This meant that any changes in salinity due to the influence of the Tamar River would not have been resolved in these studies. However, the effect of salinity on the overall production equation is minimal (a change in salinity of 1psu leads to a change in production of less than 3% of the final value) so the results are still considered to be relatively accurate.

3.4 Conclusions

After spectral correction, there were no significant effects of different incubators of experimental outcomes: results from the two incubators led to similar estimates of photosynthetic parameters and daily, depth-integrated production. Parameterising the models with irradiance patterns typical of different seasons had little effect on the ratio of production derived from one incubator to the other.

Experiments using both cultures and seawater samples showed that 24h incubations including a dark period led to significantly lower parameter values and production estimates than those from incubations lasting between 2h and 12h. Estimates of α^B, P^B_m and primary production from 24h incubations were on average 49 ± 15%, 39 ± 14%, and 42 ± 8% of the average values from the shorter experiments in the same incubator respectively. However, there were no significant differences between incubator periods for 2h to 12h. The cause of changes in photosynthetic parameters over the course of incubations was not established. However, in axenic cultures, chlorophyll concentration increased during the dark period. It was also shown that photoinhibition at high light increased with time contained in the bottle.

The daily estimates of primary production from the non-photoinhibited and the photoinhibited photosynthetic parameter models were similar to each other but the $^{14}C_{SIS}$ incubations produced consistently higher estimates than either of the models. This was despite the fact that the models did not include a respiration term and should therefore have produced an estimate much closer to gross production than the $^{14}C_{SIS}$ incubations. Primary production estimates at depth from the *simulated-in-situ* incubations were much higher than those from the models. The relatively low photosynthetic rates from models under light

limiting conditions may indicate that, despite the correction applied to the photosynthetic parameters, spectral differences in incubation may have been important. Conversely, production under light limiting conditions from $^{14}C_{SIS}$ may have been unrealistically high as a result of unnatural photoacclimation due to the static nature of the incubation. Photoinhibition was seen in surface samples from $^{14}C_{SIS}$ incubations and is thought to be an artefact of unnaturally long exposure to high irradiance. Production from the photosynthetic parameter models was not statistically different to that from $^{14}C_{SIS}$ incubations. The results from the comparison of estimates of PP_{Daily} from the Celtic Sea suggested that 95% of production estimates, whether modelled from PE parameters or from SIS incubations would fall within 21 ± 14% of the average values.

The effect of irradiance and the duration of experiments on estimates of photosynthetic capacity and production are not consistent and the variability between estimates depends on a number of factors including ambient illumination, species composition and nutrient availability. In these experiments, neither the incubator (when spectral correction was applied) nor the duration of the incubation, for incubations of up to 12h, had a significant effect on estimates of photosynthetic parameters or of daily production derived from these values. Incubations in light gradients measure different processes to *simulated-in-situ* incubations and the choice of approach used should depend on what aspects of phytoplankton productivity are of interest.

Chapter 4. A comparison of FRRF and ^{14}C approaches

4.1 Introduction and specific methods

The speed and ease with which fluorescence data can be collected using the FRRF offers great potential for making large scale and high-density measurements of photosynthesis and primary production. The relationship between fluorescence and photosynthesis is neither linear nor simple but the measurements of *in vivo* fluorescence that can be made with the FRRF provide key information on the photosynthetic capacity of phytoplankton populations. The conversion of such fluorescence information into relevant measures of photosynthetic capacity requires the use of algorithms based on known photophysiology and parameterised with a mixture of measured and published parameter values. As with the ^{14}C technique, a variety of models can be used to derive estimates of photosynthetic capacity and to estimate daily production from instantaneous fluorescence measurements.

In the first part of this chapter, four different approaches for deriving instantaneous photosynthetic parameter values from FRRF data were investigated: Two different curve fitting procedures were applied to data from the light chamber and the dark chamber. The derived photosynthetic parameters were compared with each other and with parameter values derived from the ^{14}C technique. An alternative approach for the calculation of photosynthetic parameter values was also used. In this approach, PE type curves were fitted to plots of measured $PP_{z,t}^{B}$ against coincident $PAR_{z,t}$ and the parameters of the curve were used to describe the photophysiological state of the phytoplankton community. This is the same method used for deriving photosynthetic parameters from ^{14}C data but differs to the standard approach used for FRRF data where curves are fitted to F_v/F_m and (F_q'/F_m') and σ_{PSII} data. (See section 2.4.2). The variability in FRRF measurements over the course of a day was also considered in order to assess the reliability of extrapolating from a single instantaneous measurement to daily estimates of photosynthetic characteristics and production. In the final section a simple model was used to calculate daily depth integrated production (PP_{Daily}) from the FRRF data. These estimates of PP_{Daily} are compared with each other and with estimates from the ^{14}C technique.

The study was carried out using data from the Celtic Sea cruise in May 2000 and from station L4 throughout 2001. During the Celtic Sea cruise, repeated casts were made during each day which allowed the effects of diel variability and the assumption of uniform photosynthetic

response throughout the day to be studied. Conversely, at station L4 the FRRF was deployed only once a week from RV Squilla or RV Sepia. The assimilation of data over a whole year allowed the variability in fluorescence measurements due to seasonal changes in environmental variables and the floristic composition of the phytoplankton to be studied and compared with the changes measured by the radiocarbon method. Given that the FRRF parameter models assume no photoinhibition of photosynthesis, the ^{14}C data used were those derived from the non-photoinhibited model.

4.2 Results

4.2.1 Comparison of photosynthetic parameters

Variability between photosynthetic parameters derived using different FRRF models

Photosynthetic parameter values from the FRRF were derived for seven dates during the Celtic Sea cruise and for 26 dates at L4 over the course of 2001. The α^B values derived from the Celtic Sea data using the four approaches (two models and two data sets) were very similar to each other (see Figure 4.1a) and over 98% of the variance in α^B derived from any one model was explained by that in estimates derived from any of the other models. The different models led to similar estimates of P^B_m and Ek values when light chamber data were used but the model estimates diverged when dark chamber data were used. The dark chamber data led to consistently higher values of all parameters than data from the light chamber.

The photosynthetic parameters derived from the L4 data were more sensitive to the choice of model than the Celtic Sea data. There was also a greater difference between values derived from light chamber data and those based on dark chamber data. Parameter values derived from the dark chamber data from L4 were all unrealistically high. Values of P^B_m rarely exceed 20 mg C [mg Chl]$^{-1}$ h^{-1} (Behrenfeld *et al.*, 2002) and Falkowski (1981) calculated the maximum theoretical value to be 25 mg C [mg Chl]$^{-1}$ h^{-1} based on the size and turnover time of photosynthetic units. The average P^B_m value from the exponential (Exp) model was 32.07 ± 25.99 mg C [mg Chl]$^{-1}$ h^{-1} and that from the hyperbolic tangent (Tanh) model was 31.71± 25.95 mg C [mg Chl]$^{-1}$ h^{-1}. The average value of E_k from the Exp model was 706 ± 578 µmol photons m^{-2} s^{-1} and that from the Tanh model was 1059 ± 1465 µmol photons m^{-2} s^{-1}. As seen

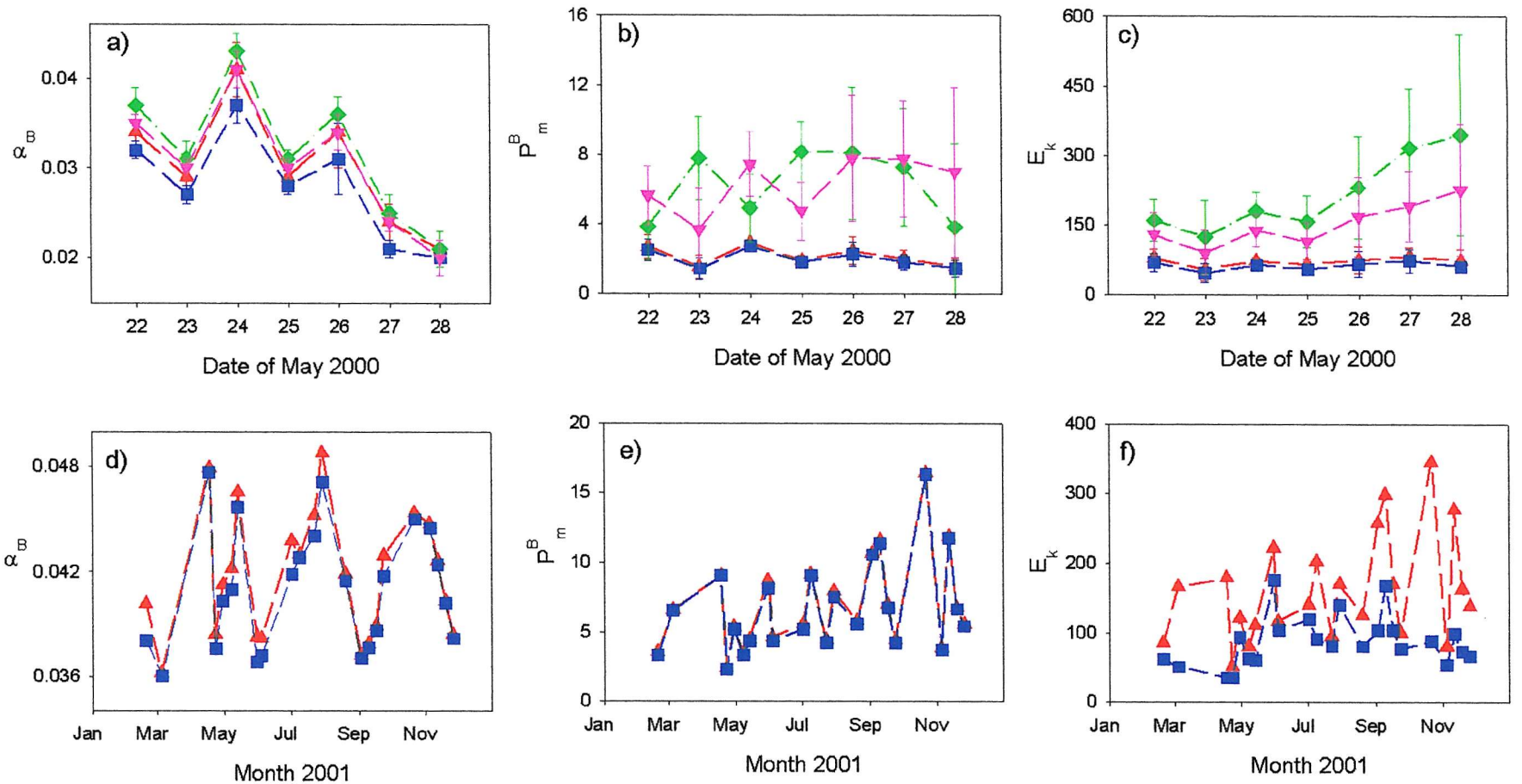

Figure 4.1. Effect of using different models to derive photosynthetic parameter values from the FRRF: a) α^B in the Celtic Sea, b) P^B_m in the Celtic Sea, c) E_k in the Celtic Sea, d) α^B at L4, e) P^B_m at L4 and f) E_k at L4. Data and processing used: Exp L (▲), Tan L (■),Exp D (◆) and Tan D (▼). Dark chamber data not included in L4 data as the values were unrealistically high.

in the Celtic Sea, at L4 the parameter values derived from the different models applied to light chamber data agreed well with a covariance of over 97% for both α^B and P^B_m values. Conversely, only 27% of the variance was explained by a regression of light chamber E_k values from the Tanh model against those from the Exp model.

Given the poor estimation of photosynthetic parameters from the L4 data, the raw fluorescence data from the two cruises was examined to see if the cause of the problem with the L4 data could be identified. The F_q'/F_m' and σ_{PSII} profiles from the Celtic Sea show a clear inflection point above which there is a clear decrease of values towards the surface but the L4 data vary little with depth (see Figure 4.2). The patterns shown in Figures 4.2b, c, e and f were typical of the data from the Celtic Sea. Whilst a number of data sets from L4 did show similar quenching at high light (Figure 4.2k), many of the casts were similar to that shown in Figure 4.2h. The plots of PAR show that the irradiance levels during the Celtic Sea casts were much higher than those during the L4 casts. The data suggest that, in a number of cases, the irradiance levels were too low to induce the saturation of the photosytems, which led to the lack of variability in fluorescence parameters with depth. The photosynthetic parameter model failed in such cases, as it was designed to fit a curve, not a linear distribution. As a result of these problems, the photosynthetic parameter values from L4 were considered unreliable and were not used further.

For the Celtic Sea data, parameter values derived using light chamber data and the Exp model were used for all subsequent comparisons. The Exp model was chosen as an exponential model describes the PE curve used for ^{14}C data. Data from the light chamber were used as they reflect the photosynthetic capacity of the phytoplankton under ambient light condition, which for these studies, was the process of interest.

Diel variability in FRRF photosynthetic parameters

The data from the Celtic Sea allowed the variability in photosynthetic parameters over the course of the day to be studied. This was important as the production models are run with photosynthetic parameter values that are constant over the day. The pattern of change within each day was variable (see Figure 4.3). The variability in α^B values over one day ranged from a minimum of 0.002 mg C [mg Chl]$^{-1}$ h^{-1} [µmol photon m^{-2} s^{-1}]$^{-1}$ on 28th May to a maximum of 0.120 mg C [mg Chl]$^{-1}$ h^{-1} [µmol photon m^{-2} s^{-1}]$^{-1}$ on 26th May. The lowest daily range of P^B_m values was 0.279 mg C [mg Chl]$^{-1}$ h^{-1} on 24th May and the highest was

2.15 mg C [mg Chl]$^{-1}$ h^{-1} on 26th May. P^B_m and E_k had a covariance of 96% but α^B values were not significantly correlated with either E_k or P^B_m.

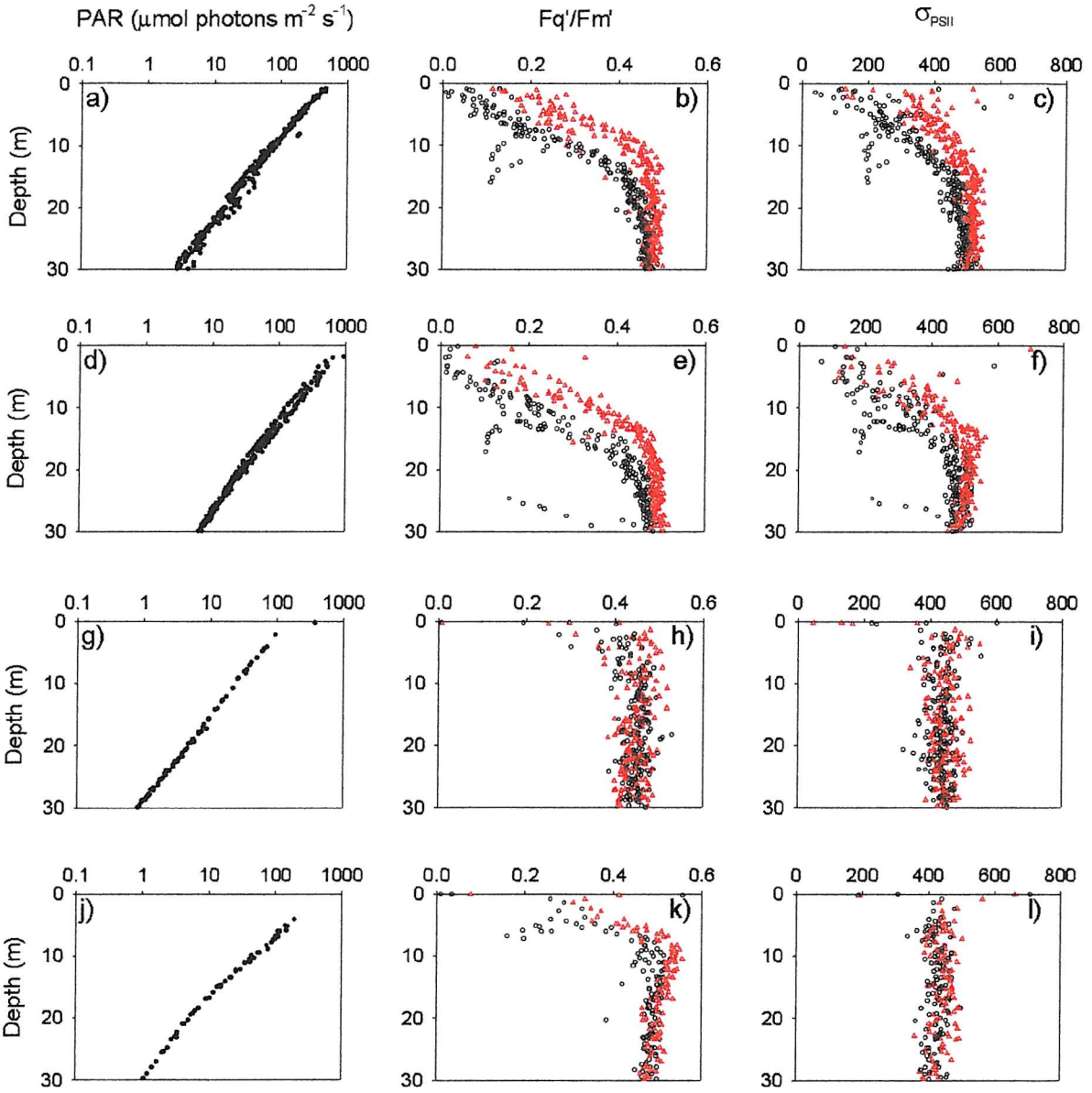

Figure 4.2. Plots of PAR (a, d, g and j), F_q'/F_m' (b, e, h and k) and σ_{PSII} (c, f, i and l) to show the different patterns with depth in the Celtic Sea and at L4. Data are from a, b & c) cast 2413 on 24th May in the Celtic Sea; d, e & f) cast 2211on 22nd May in the Celtic Sea; g, h & i) L4 on 5th March 2001 and j, k & l) L4 on 30th April 2001. Light chamber (○) and dark chamber (△) data are shown. PAR in µmol photons m^{-2} s^{-1}, F_q'/F_m' in dimensionless units and σ_{PSII} in m^2 photon^{-1}.

Comparison of photosynthetic parameter values from ^{14}C with those from the FRRF

In the Celtic Sea, the radiocarbon incubations produced similar values of α^B to the FRRF (see Figure 4.4a) for all but two dates (26th May and 27th May). On 26th May, the radiocarbon [µmol photons m^{-2} s^{-1}]$^{-1}$ compared to 0.030 mg C [mg Chl]$^{-1}$ h^{-1} [µmol photons m^{-2} s^{-1}]$^{-1}$ from

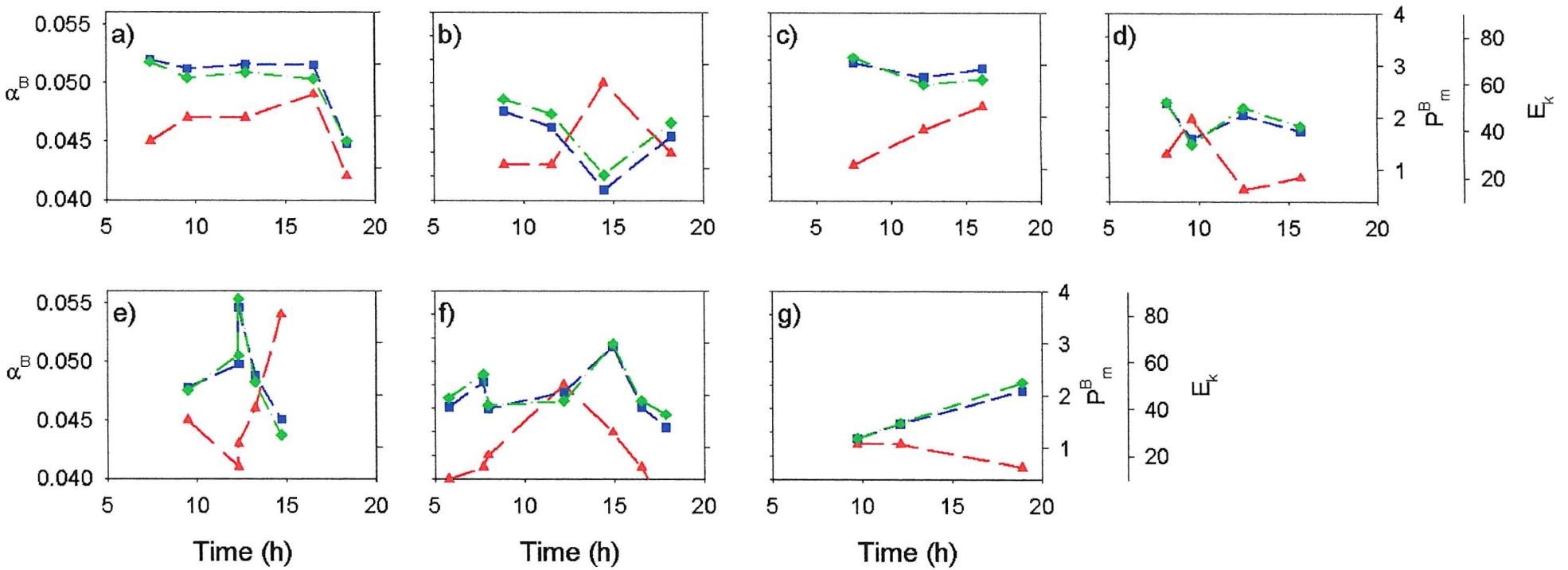

Figure 4.3: Change in FRRF photosynthetic parameter values over the course of the day in the Celtic Sea: a) 22nd May, b) 23rd May, c) 24th May, d) 25th May, e) 26th May, f) 27th May and g) 28th May. Parameters shown are α^B, in mg C [mg Chl]$^{-1}$ h^{-1} [µmol photons m^{-2} s^{-1}]$^{-1}$ (▲), P^B_m in mg C [mg Chl]$^{-1}$ h^{-1} (■) and E_k in µmol photons m^{-2} s^{-1} (◆).

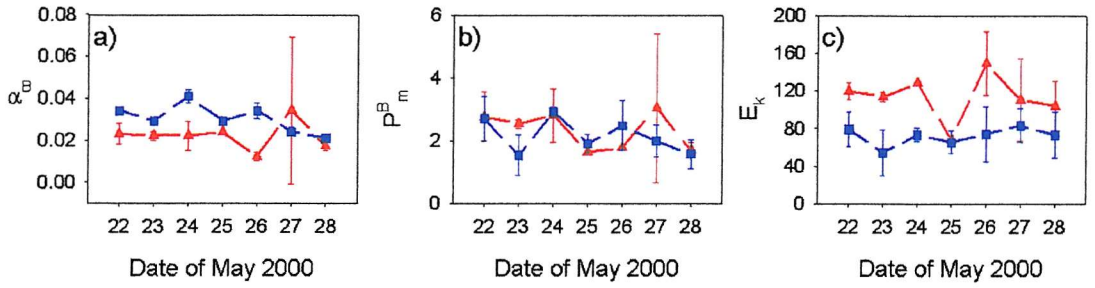

Figure 4.4. Comparison of photosynthetic parameters in the Celtic Sea from ^{14}C incubations (▲) with those from the FRRF (■). Parameters shown are a) α^B in mg C [mg Chl]$^{-1}$ h^{-1} [µmol photons m^{-2} s^{-1}]$^{-1}$, b) P^B_m in mg C [mg Chl]$^{-1}$ h^{-1} and c) E_k in [µmol photons m^{-2} s^{-1}]$^{-1}$. The ^{14}C data are from the non-photoinhibited model and FRRF data are from the Exp L model

the FRRF) whilst on the 27th May the reverse was true (the ^{14}C estimate was 0.043 mg C [mg Chl]$^{-1}$ h^{-1} [µE m^{-2} s^{-1}]$^{-1}$ compared to 0.026 mg C [mg Chl]$^{-1}$ h^{-1} [µmol photons m^{-2} s^{-1}]$^{-1}$from the FRRF). The standard deviation of the estimate from radiocarbon was very high on the 27th May and was the result of a relatively low value from the dawn cast (0.011mg C [mg Chl]$^{-1}$ h^{-1} [µmol photons m^{-2} s^{-1}]$^{-1}$) and an extremely high value from the noon cast (0.073mg C [mg Chl]$^{-1}$ h^{-1} [µmol photons m^{-2} s^{-1}]$^{-1}$). The cause of the high noon value is not clear but it is a result of high photosynthesis rather than normalisation to a low chlorophyll concentration. The E_k values derived from radiocarbon were all higher than those from the FRRF (the ^{14}C average was102 ± 26 µmol photons m^{-2} s^{-1}and the FRRF average was 62 ± 14 µmol photons m^{-2} s^{-1}). The average value of P^B_M over the course of the cruise from ^{14}C was 2.43 ± 0.6 mg C [mg Chl]$^{-1}$ h^{-1} compared to 2.00 ± 0.51 mg C [mg Chl]$^{-1}$ h^{-1} from the FRRF but the high average does not reflect the fact that the ^{14}C values were lower than those from the FRRF on some days. The photosynthetic parameter values from each technique were regressed against each other to quantify their covariance and similarity (see Table 4.1).

Table 4.1. Statistics from regression of FRRF photosynthetic parameters (Exp L) against those derived from incubations with ^{14}C (non-photoinhibited model). Data are from the Celtic Sea cruise.

Parameter	R^2	Slope	Intercept
α^B	0.06	-0.24	0.04
$P^B m$	0.13	0.33	1.39
E_k	0.08	0.11	59.44

The regression statistics suggested a poor relationship between parameter values from the different techniques despite the graphs suggesting covariance. However this was likely to be a result of the small number of data points and the low range of data.

4.2.2 FRRF PE type curves

The estimation of daily production from the instantaneous FRRF production and coincident PAR (PP_{zt} and PAR_{zt}) was carried out for both data sets (Celtic Sea and L4) and is referred to as the FRRF PE model. In the Celtic Sea, there were multiple casts on each day so a number of PE curves were produced. The FRRF PE curves for each cast on 22nd May are shown in Figure 4.5 and as seen for this date, on all days, the parameters of the fitted curves showed no clear diel

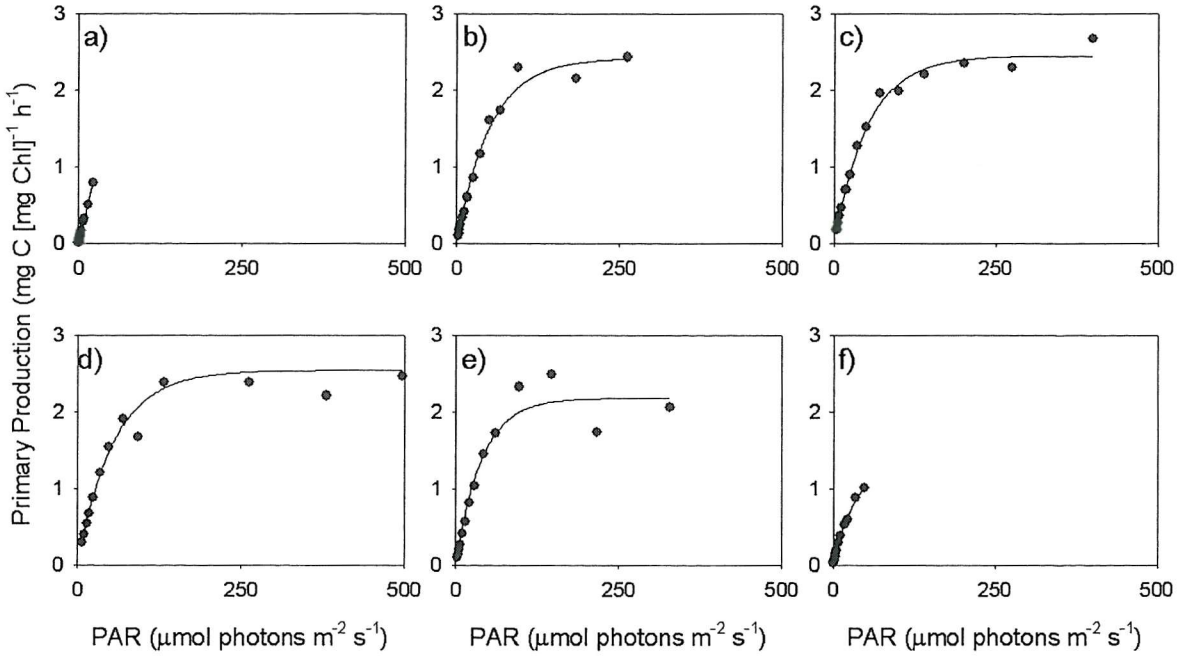

Figure 4.5. Plots and fitted curves of instantaneous, chlorophyll normalised FRRF production against coincident PAR on 22nd May in Celtic Sea: a) Cast 2203 at 03:40 GMT, b) cast 2207 at 07:30 GMT, c) cast 2209 at 09:32 GMT, d) cast 2211 at 11:56 GMT, e) cast 2219 at 16:03 GMT and f) cast 2222 at 18:11 GMT.

patterns within each day. However, where ambient light was low, early and late in the day, (see figures 4.5a and 4.5f) the curve did not reach a plateau as light was not saturating. In addition to the individual curves, 'daily' PE curves were derived by pooling all the data from one day to see if it could be described by a single curve. Casts were excluded from the pooled data sets for any of three reasons: (1) where the incomplete PE curves did not show light saturation (i.e. the curve did not plateau), (2) where saturation did occur but shading of

direct sunlight by the ship was evident as determined from large differences between surface PAR measured from the FRRF sensor ($E_{(0)FRRF}$) and from the sensor on the ship ($E_{(0)Ship}$) and (3) where high variability of PAR during a cast led to highly scattered data. Figure 4.6 shows the curves fitted to the pooled data for each day of the study. The highest rate of production was calculated for 22nd May (2.14 mg C [mg Chl]$^{-1}$ m^{-2} h^{-1}) and the lowest on 28th May (0.88 mg C [mg Chl]$^{-1}$ m^{-2} h^{-1}) as shown in Figure 4.6. All the data on 28th May were collected with the ship blocking the direct sunlight so most of the resulting PE curves were incomplete, showing no light saturation and as a result, data from this day were excluded from the study.

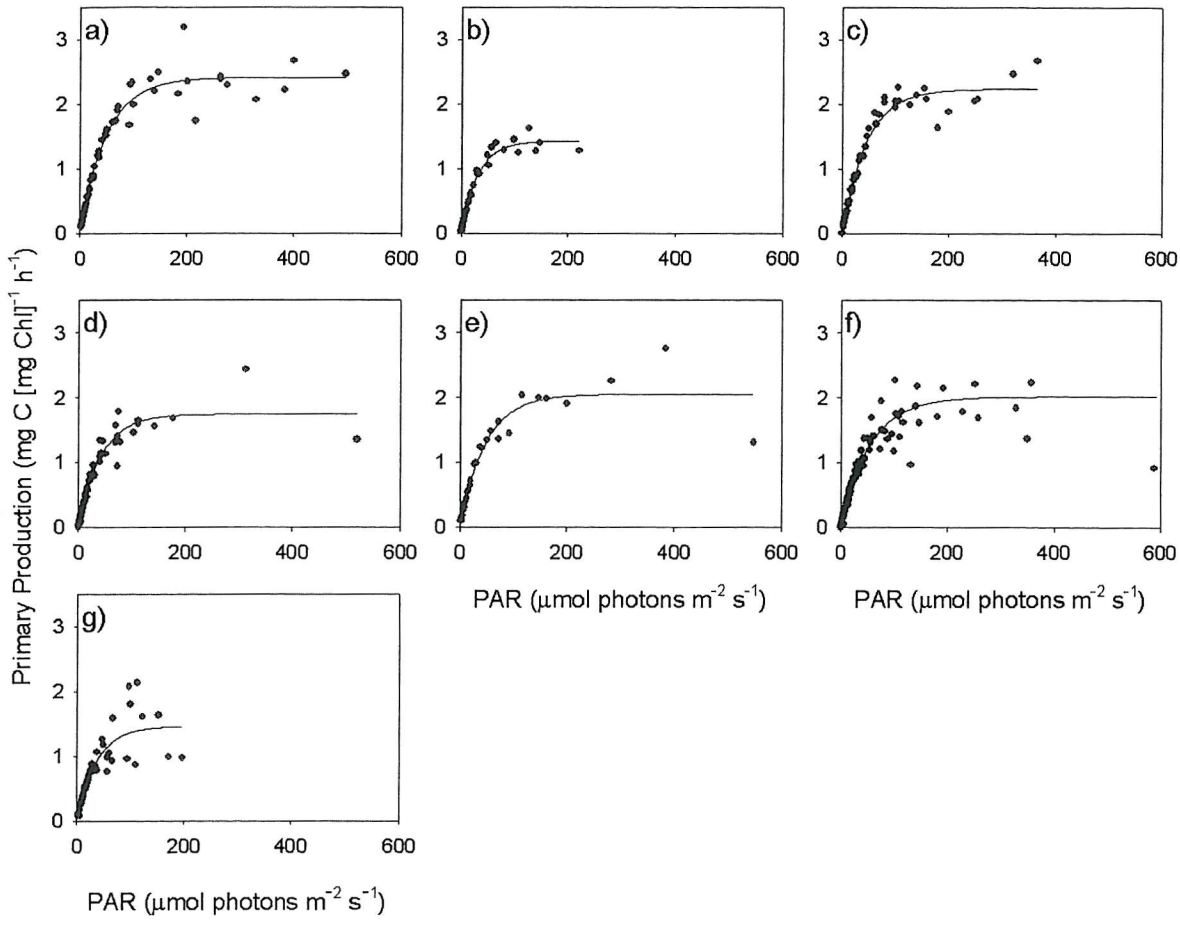

Figure 4.6. Pooled instantaneous, chlorophyll normalised FRRF production plotted against coincident PAR for each day of the Celtic Sea cruise: a) 22nd May, b) 23rd May, c) 24th May, d) 25th May, e) 26th May, f) 27th May and g) 28th May.

The plots of instantaneous production against coincident PAR for the L4 data showed that on many occasions light saturation was never reached and only the initial slope of the curve was measured. In order to overcome this problem, data were pooled within seasons with the aim of deriving four standard curves from which production could be calculated. However, as shown in Figure 4.7, limited data and low irradiance levels in autumn and winter meant that

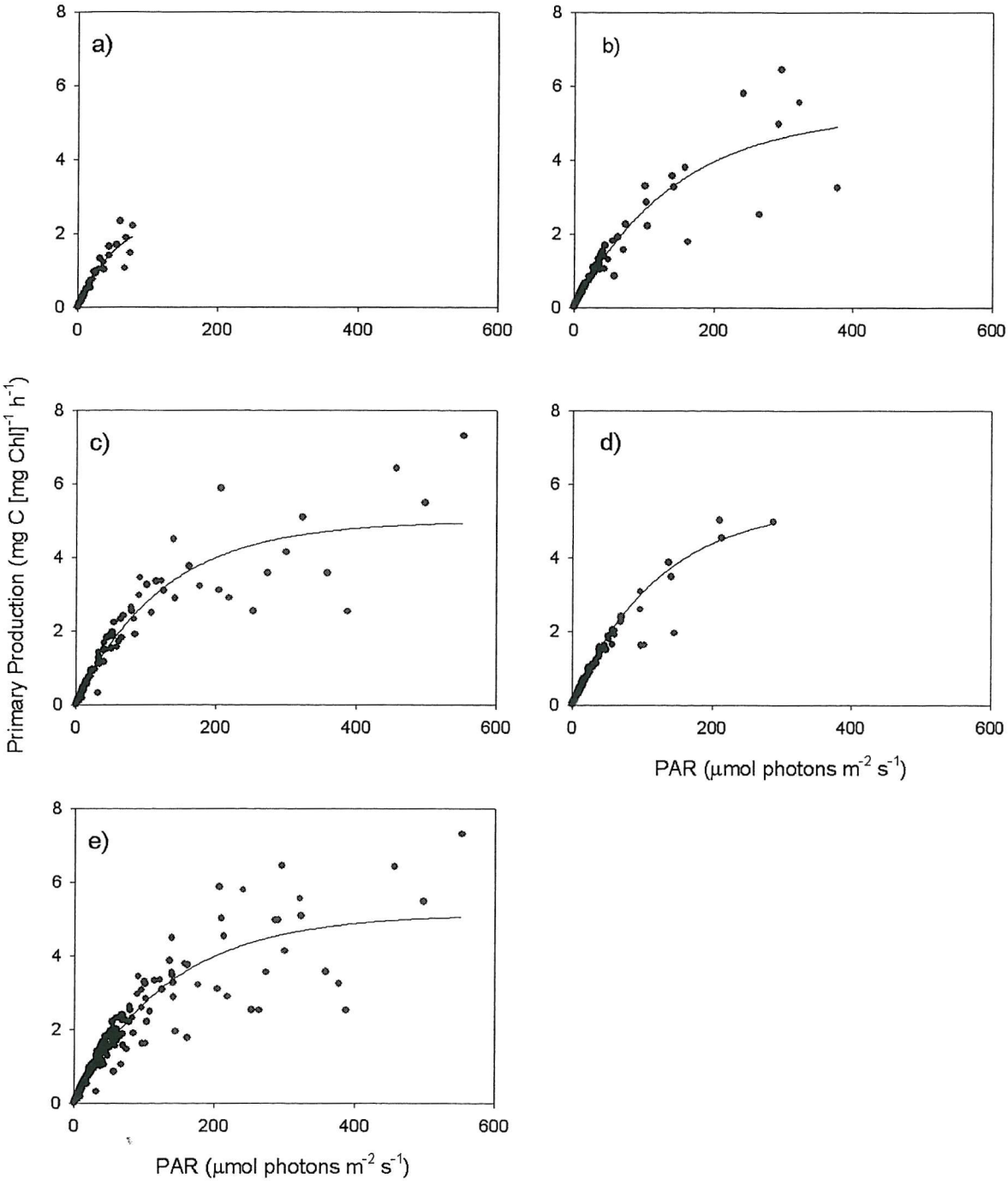

Figure 4.7. Instantaneous, chlorophyll normalised FRRF production against coincident PAR at L4 in 2001: a) all winter casts (December-February), b) all spring casts (March-May), c) all summer casts (June-August), d) all Autumn casts (September-November) and e) all casts.

the PE relationship, over a range of light conditions was still not clear. As a result, all the data for 2001 at L4 were pooled to derive a general annual PE relationship (see Figure 4.7e). The maximum rate of production on the curve was 3.02 mg C [mg Chl]$^{-1}$ h^{-1} and the initial slope was 0.041 mg C [mg Chl]$^{-1}$ h^{-1} [µmol photon m^{-2} s^{-1}]$^{-1}$. Given the difficulties of incomplete curves, estimates of PP_{Daily} from the PE relationship at L4 were derived twice, once using the parameters of the generic curve for the whole year and once using the curve parameters derived using only the data from the specific date.

4.2.3 Comparison of different estimates of FRRF PP_{Daily}

When estimates of PP_{Daily} derived from Celtic Sea light chamber data and each of the FRRF photosynthetic parameter models were compared, 92% of the variance was explained and the slope was 1.14 (see Figure 4.8).

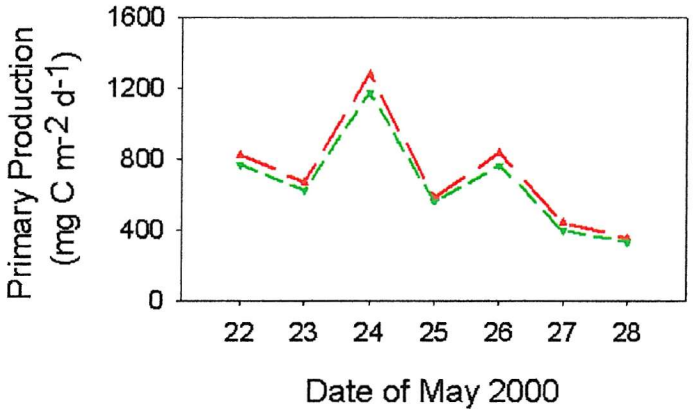

Figure 4.8. Daily, depth-integrated primary production in the Celtic Sea from different FRRF photosynthetic parameter models and using light chamber data. Exp L (▲) and Tan L (▼).

The production estimates obtained when the PE relationship from each cast in the Celtic Sea was used to estimate PP_{Daily} are shown in Table 4.2. Values of coincident surface PAR are shown and the tendency of models to produce extreme estimates of daily integrated production when they were run with data measured under low ambient light is clear. The PP_{Daily} estimate derived from the pooled data for each day is also shown. The standard deviation of PP_{Daily} estimates from FRRF PE curves ranged from 32% (on 24th May) to 63% (on 25th May and 26th May) of the daily average when all casts were included. However, when only casts used in the pooled data sets were included, the standard deviations decreased and ranged from 3% (24th May and 25th May) to 20% (22nd May) of the mean. When only

Table 4.2. Daily, depth-integrated primary production calculated using PE curve parameters derived from each FRRF cast and from the pooled data for each day. Coincident $PAR_{(0)}$ is also shown. PP is primary production in mg C m^{-2} d^{-1}. Averages and pooled data sets include all casts except those marked with an asterisk. Time in GMT.

22/05			23/05			24/05			25/05			26/05			27/05		
Cast	PAR (0)	PP	Cast	PAR (0)	PP	Cast	PAR (0)	PP	Cast	PAR (0)	PP	Cast	PAR (0)	PP	Cast	PAR (0)	PP
2203*	0	883	2308	219	842	2403*	0	2850	2503*	0	807	2603*	1	2426	2703*	1	1604
2207	458	887	2310	343	765	2407	260	1153	2507	188	665	2604*	12	2521	2705*	35	1337
2209	996	901	2316*	93	365	2413	500	1170	2509*	78	546	2605*	86	631	2707*	170	541
2211	1468	879	2320	200	772	2423	534	1228	2512	831	634	2607	254	772	2708*	133	466
2219	821	571							2520*	139	588	2610a*	1224	723	2710*	139	440
2222*	202	2244							2522*	61	741	2610b*	349	873	2713	946	535
									2524*	20	2089	2610c*	1025	1075	2719	992	644
												2610d*	601	883	2721*	448	470
												2612	792	846	2723*	253	507
												2614*	84	640	2725*	57	489
Average		1061			686			1600			867			1139			703
SD		593			217			834			546			716			413
Pooled		**890**			**770**			**1179**			**642**			**816**			**533**

these pooled casts were included, the averages of all the estimates were very similar to the production estimate derived from the pooled data set.

The two approaches used to calculate primary production from the L4 FRRF PE type curves (date specific and general curves) led to similar estimates of PP_{Daily} throughout the year (see Figure 4.9). The slope of the regression of one set of data against the other was 0.93 and over 70% of the variance was explained. On April 18th and April 30th, the estimate from the date specific curve was much lower than that from the standard curve but on all other dates, the estimates were very similar. The differences on these two dates reflect that the measured data were not well described by the standard PE relationship that described the pattern over most of the year.

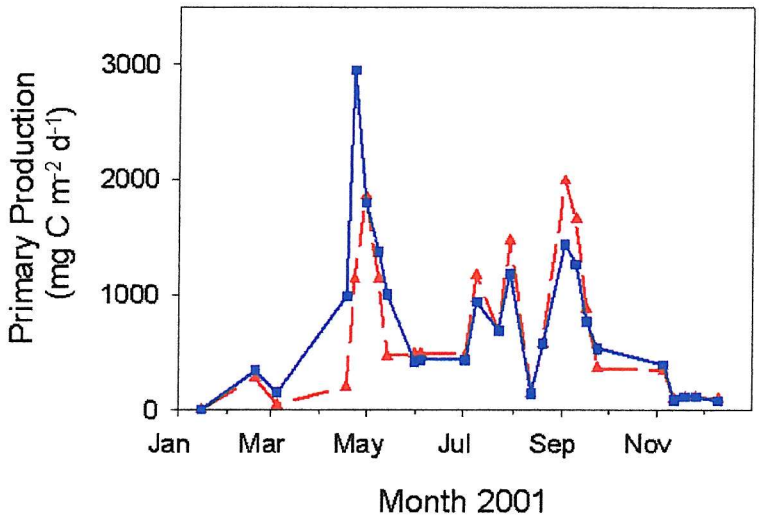

Figure 4.9. PP_{Daily} for L4 in 2001 from FRRF PE type curves: Date specific curve (▲) and general curve derived from data pooled from the whole year (■).

The different techniques led to different profiles of production over the water column. As no photoinhibition was seen in the raw data and was therefore not included in the models, the maximum production over the water column was at the surface for all the models. In the Celtic Sea (Figure 4.10), below the surface layer the production profiles mirrored that of PAR, decreasing exponentially with depth. However, at the surface, where light is saturating and production is light independent, the production profiles deviate from that of PAR. In the Celtic Sea, the profiles were similar on each day but at L4 (Figure 4.11), the shape of the profiles varied between dates. On all dates at L4, the highest production was seen from the FRRF PE curve models whilst the profiles showed very low production from ^{14}C.

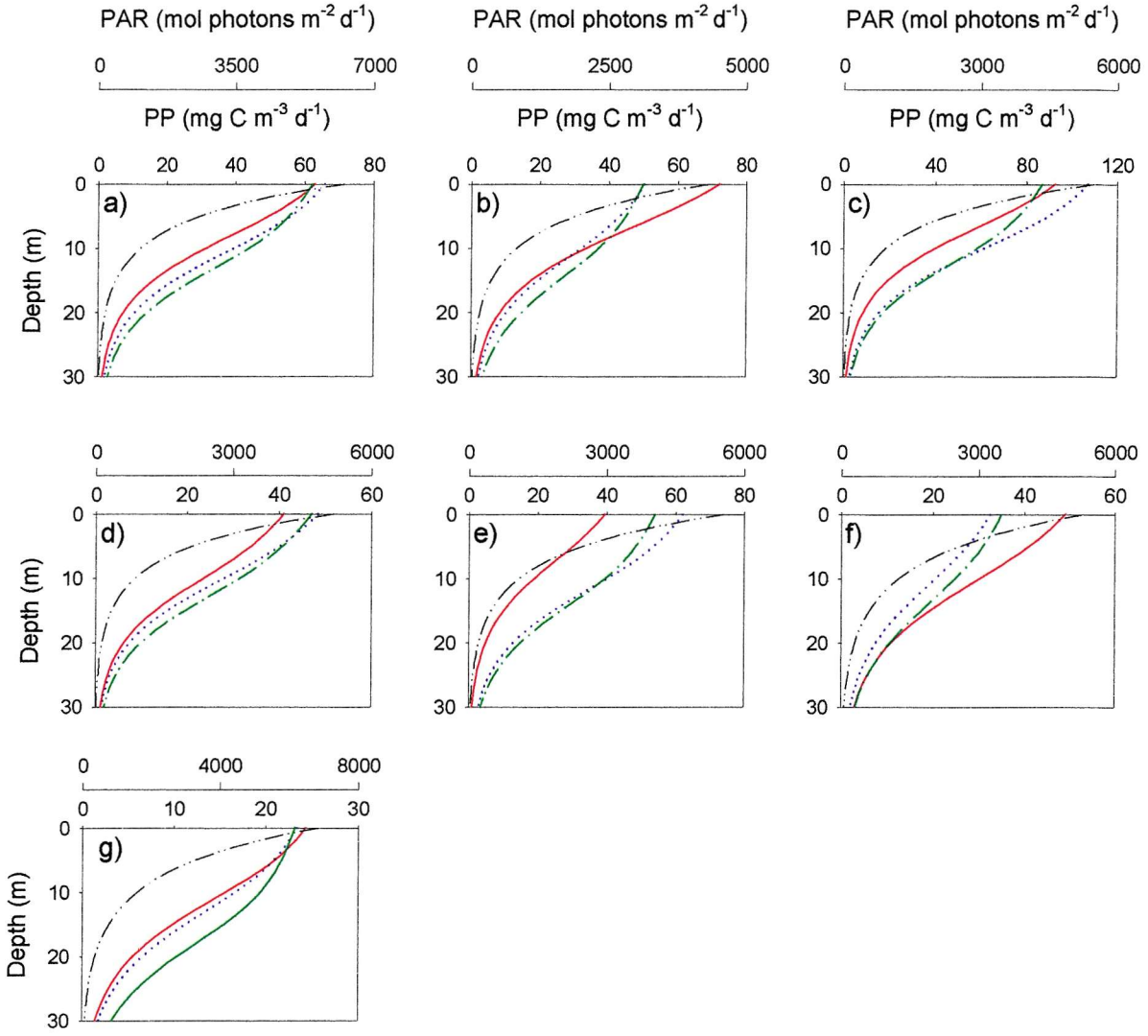

Figure 4.10. Profiles of primary production (PP), from ^{14}C and FRRF techniques, with depth on each date in the Celtic Sea: a) 22nd May, b) 23rd May, c) 24th May, d) 25th May, e) 26th May, f) 27th May and g) 28th May. The lines show PAR (—··—), ^{14}C photosynthetic parameters (———), FRRF photosynthetic parameters (·····) and FRRF PE type curve (———).

Daily depth-integrated production from each technique is shown in Figure 4.12. In most cases in the Celtic Sea, the highest production estimates were derived using the FRRF data. Production from the two FRRF approaches (photosynthetic parameters and PE curves) showed similar patterns of change and a regression of one data set against the other had a covariance of 98% (see Table 4.3). The relationship between PP_{Daily} from ^{14}C parameters and each of the two FRRF techniques was different with the ^{14}C estimates explaining 46% and 55% of the variance in estimates from FRRF photosynthetic parameter and FRRF PE curve models respectively. At L4 the annual pattern of production was reflected similarly by the measurements from ^{14}C and the FRRF over most of the year. However, production over the summer measured by ^{14}C was constantly low but the FRRF measurements showed

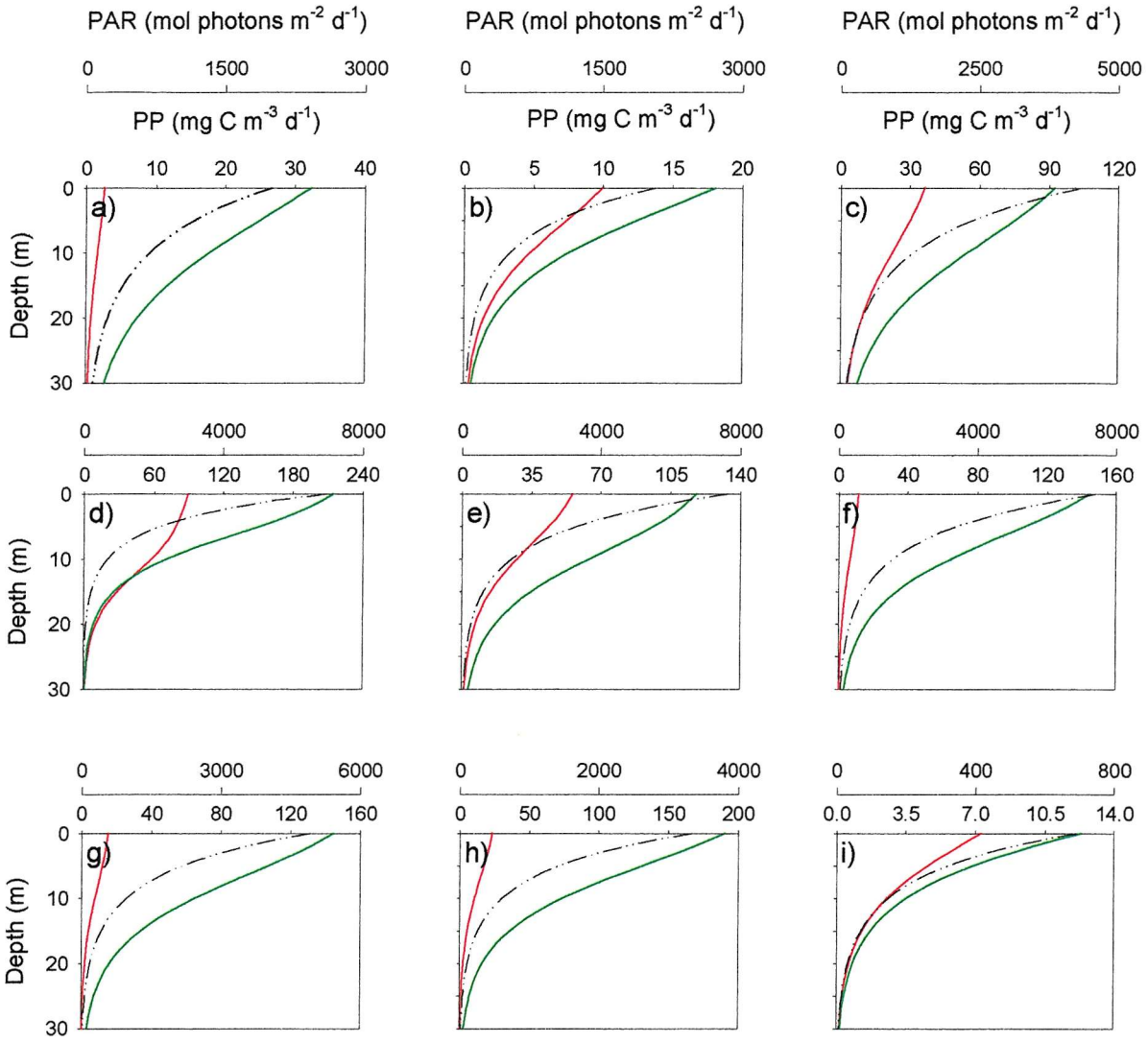

Figure 4.11. Representative profiles of PP_{Daily} at L4, from ^{14}C and FRRF techniques, for every month where measurements from both techniques were available: a) 19th February 2001, b) 5th March 2001, c) 18th April 2001, d) 8th May 2001, e) 4th June 2001, f) 2nd July 2001, g) 1st August 2001, h) 3rd September 2001 and i) 12th November 2001. The lines show PAR (—··—··), ^{14}C photosynthetic parameters (——) and FRRF PE type curve (——).

blooms separated by periods of low productivity. The autumn bloom was much more significant in the ^{14}C pattern over the year than in that from the FRRF but both methods showed a similar decline to low levels over winter.

Figure 4.13 shows the average and the 95% confidence interval (CI) for production that could be expected from any of the techniques. In the Celtic Sea, this value was the average of estimates from ^{14}C and FRRF photosynthetic parameter models and from the FRRF PE curve model and the confidence limits are relatively low. At L4, the averages were calculated from estimates from the ^{14}C photosynthetic parameter model and the FRRF PE curve model. The

standard deviations are much higher at L4 than in the Celtic Sea and may reflect the long incubations or the time taken to transport water back to the laboratory.

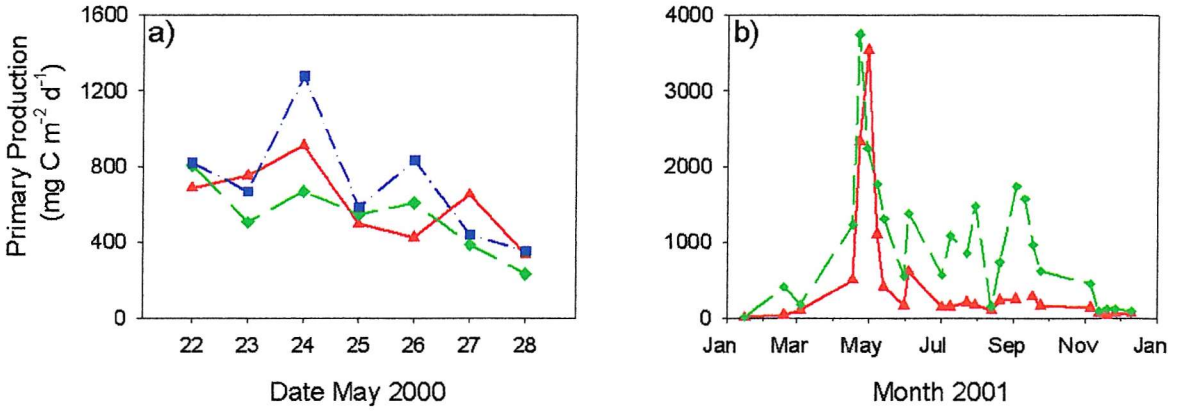

Figure 4.12. PP_{Daily}, over the course of the studies as measured by the ^{14}C and FRRF techniques: a) Celtic Sea and b) L4 in 2001. The models used were the ^{14}C photosynthetic parameter model (▲), FRRF photosynthetic parameter model (■) and FRRF PE type curve model (◆).

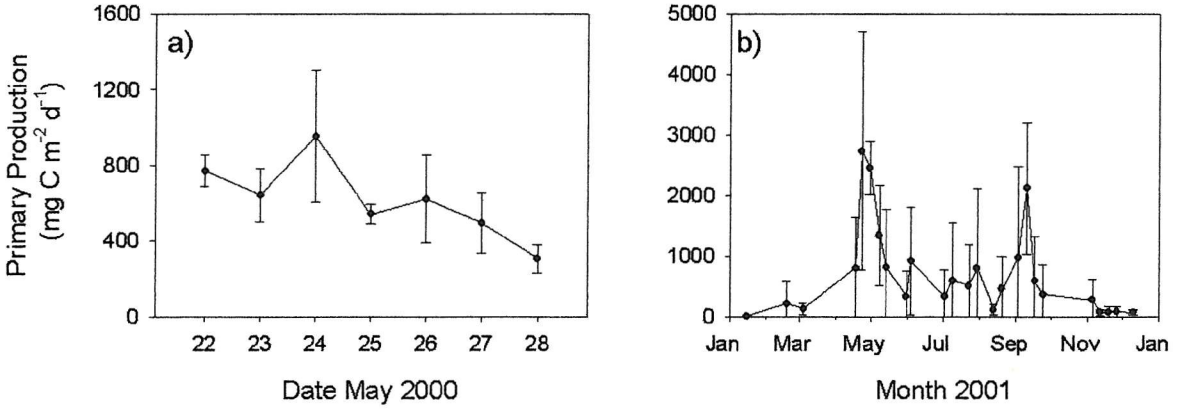

Figure 4.13. Average PP_{Daily}, from ^{14}C and FRRF techniques, with 95% confidence intervals: a) for the Celtic Sea and b) for L4.

The production estimates were regressed against daily integrated PAR and against average chlorophyll concentration (both as used in the models) and regression statistics are shown in Table 4.4. For both studies, the relationship between production and chlorophyll was much more significant than that between production and PAR. Regressions against chlorophyll alone accounted for a similar proportion of the variance in production estimates from the ^{14}C model as did the regressions against either FRRF model. Adding PAR to a regression, originally only including chlorophyll, increased the variance explained by only a small amount.

Table 4.3. Statistics obtained when estimates of PP_{Daily} from the three techniques (^{14}C photosynthetic parameters, FRRF photosynthetic parameters and FRRF PE curves) were regressed against each other.

a) Celtic Sea

Independent	Dependent	R2	Slope	Intercept
^{14}C	FRRF PE curve	0.55	0.92	192.52
^{14}C	FRRF photosynthetic parameters	0.46	1.04	78.55
FRRF photosynthetic parameters	FRRF PE curve	0.98	1.22	-205.96

b) L4

Independent	Dependent	R2	Slope	Intercept
^{14}C	FRRF PE curve	0.51	0.63	582.34

Table 4.4. Statistics obtained when estimates of PP_{Daily}, from the three techniques (^{14}C photosynthetic parameters, FRRF photosynthetic parameters and FRRF PE curves), were regressed against PAR and chlorophyll.

Independent	Dependent	R^2 value	
		Celtic Sea	L4
PAR	^{14}C	0.23	0.10
PAR	FRRF curve	0.05	0.33
PAR	FRRF photosynthetic parameters	0.03	
Chlorophyll	^{14}C	0.46	0.51
Chlorophyll	FRRF curve	0.70	0.90
Chlorophyll	FRRF photosynthetic parameters	0.65	
PAR & Chlorophyll	^{14}C	46.50	51.50
PAR & Chlorophyll	FRRF curve	84.90	96.00
PAR & Chlorophyll	FRRF photosynthetic parameters	83.50	

4.3 Discussion

The work included in this chapter aimed to compare estimates of photosynthesis (and PP_{Daily} derived from these values) from the FRRF with those from the ^{14}C method. In order to carry out these comparisons, a number of complications, related to the different styles of the two techniques, had to be considered. These included the different ways in which photosynthetic parameters could be derived from the FRRF data (light or dark chamber and hyperbolic tangent or exponential models), the requirement for light saturation in order to obtain profiles that included the full range of expected fluorescence responses and the variability in parameters over the course of the day. An additional consideration was whether the ^{14}C values used in the comparison were measuring the same processes as the FRRF. This discussion is divided into three major areas: in the first, the overall comparison of results from the FRRF and ^{14}C approaches is discussed; the second section is a discussion of the issues associated with deriving measurements of photosynthesis from the FRRF and in the final section, the validity of the approaches used here to compare the techniques are discussed.

Comparison of results from the ^{14}C and FRRF approaches

Radiocarbon measurements (neglecting the obvious difference that they are chemical rather than fluorescence measurements) are integrated over time and potentially affected by photoacclimation, which leads to an expected difference between the values from the two techniques. Suggett *et al.* (2001) also found α^B values from ^{14}C measurement to be lower (by

2-2.5 times) than those from the FRRF. They discussed possible reasons for the difference, which included incorrect assumptions about the size of the photosynthetic unit used in the FRRF calculations; error in the estimate of E_k from the FRRF; failure to account for the uncoupling of electron transfer and carbon fixation and errors in ^{14}C assimilation associated with bottle effects. The standard deviation of the average α^B derived from the radiocarbon method in the Celtic Sea is much higher than the FRRF estimate but is dominated by the results of 27 May. In the Celtic Sea, the P^B_M values from the two techniques were very similar with those from ^{14}C incubations being slightly higher in four of six cases. E_k values in the Celtic Sea from the FRRF were lower than those from ^{14}C incubations, in agreement with the findings of Suggett *et al.* (2001) and of Boyd *et al.* (1997). They suggested that the conventional method used to derive E_k from plots of F_q'/F_m' against PAR might be flawed as a result of the inflection in the curve sometimes being indistinct.

The differences between gross and net photosynthesis have been discussed earlier with regard to the duration of ^{14}C incubations and it was emphasised that even the relatively short incubations of 4h duration may measure net rather than gross production. The greater constancy of α^B from the FRRF than from ^{14}C methods may be due to the instantaneous nature of the FRRF measurements and a result of electron transfer rather than carbon fixation, being measured. The higher variability in ^{14}C derived measurements may be linked to processes further downstream in the photosynthetic pathway than electron transfer although this is unlikely as the value of α^B is controlled by the absorption of light energy and not the dark reactions of photosynthesis. The variability may also be linked to the relatively long incubations in which artefacts of enclosure and exposure to constant light could have led to increased variability in final measured values. However, the variability in P^B_m values from ^{14}C is lower than that in the values derived from the FRRF which does not support this hypothesis. The high variability in P^B_m from the FRRF is caused by a higher variability in Ek from the FRRF than from ^{14}C.

For estimates of photosynthetic parameters and production from the FRRF and ^{14}C techniques to agree, every electron passed to the ETC would have to be used for the production of reductant, all the reductant would have to be used to carbon fixation and for none of the newly fixed carbon could be respired (either in the light or the dark) during the incubation. Obviously this is never the case. The use of reductant for processes other than carbon fixation is accounted for via the PQ quotient in the FRRF calculation but respiration and the loss of electrons due to the Mehler reaction are not. The Mehler reaction (the light

driven consumption of oxygen in the electron transfer chain) is only likely to be important at irradiance levels above E_k (Suggett *et al.*, 2001) so should not affect α^B but would have an effect on P^B_m, measured at higher irradiance. The difference between estimates of photosynthetic capacity from the FRRF and ^{14}C are also due to the former being made from a measure of the whole water column and the latter from samples taken from fixed depths - in most cases, at the surface. The lowest photosynthetic efficiency is likely to occur at the surface which could explain the discrepancies between α^B values from the two techniques but would not explain the higher E_k values from ^{14}C.

The difference between estimates from the FRRF and ^{14}C techniques are obviously dependent on the extent of stratification in the water column. In a well mixed system where photophysiology may be assumed to be uniform with depth, the discrepancies between the two techniques should be at their lowest. It would be useful to compare estimates of photosynthetic capacity derived from a whole column profile from the FRRF with measurements made with the FRRF on-deck using water sampled at discrete depths. This could help the understanding of the relationship between estimates from whole column FRRF profiles and ^{14}C estimates. Boyd *et al.* (1997) suggested that the large differences they observed between photosynthetic parameters from ^{14}C incubations and those from the FRRF were mainly due to spectral differences of the light regime. However, in this study the data were spectrally corrected so this is unlikely to be the cause of any discrepancies.

The high variance explained by the regressions of the results from the two FRRF models (the photosynthetic parameter model and the PE curve model) against each other is not surprising as the same raw data were used to derive each model parameters. As expected, the FRRF gave higher estimates of PP_{Daily} than ^{14}C and explained between 46% and 55% of the variance in estimates from ^{14}C (FRRF PE curve and FRRF photosynthetic parameter models respectively). Similarly, Suggett *et al.* (2001) found that 59% of the variance in estimates of depth specific primary production from ^{14}C incubations was explained by the variance in the FRRF. The results suggested a high level of the variance in all of the production estimates was due to changes in chlorophyll and, to a much lesser extent, to changes in PAR.

In the L4 data, the observed similarities between estimates of production from the ^{14}C and FRRF methods were considered promising but there were clear discrepancies between the estimates over the course of the summer. Summer estimates of PP_{Daily} from ^{14}C incubations were consistently low while those from the FRRF were variable, with occasional peaks

throughout the summer. In this way, the FRRF revealed a pattern previously unrecorded by ^{14}C techniques. This may reflect that the peaks are only indicative of high gross production and that net production remains fairly constant throughout the summer, when the water stratifies. Alternatively, it may be a result of the ecology of the summer phytoplankton community, often dominated by dinoflagellates and highly dependent on recycled nutrients (Joint *et al.*, 1986). A high dependence on recycled nitrogen may lead to large discrepancies between the instantaneous FRRF measurements and those from ^{14}C incubations. Similarly, if the phytoplankton population are subject to high grazing pressure, the relatively long enclosure in a bottle required for ^{14}C incubations may mean that a large proportion of fixed carbon is lost to grazers. However, for this grazed carbon to be ignored in the final ^{14}C count it would have to have been excreted as DOC during the course of the incubation.

The derivation of photosynthetic parameters from the FRRF

The study raised a number of issues concerning the best approaches to use for the derivation of photosynthetic parameters from the FRRF. These included the suitability of data from the light and dark chambers, the effect of low ambient light on derived parameters and the requirement, during quality control processes, for the removal of data measured at the surface.

The two different models (exp and tanh) led to similar estimates of production when light chamber data were used but results diverged with dark chamber data. The FRRF dark chamber measurements are made on samples briefly removed from the ambient light for approximately 0.5-1.0 seconds, depending on the speed of deployment. The consistently higher values from the dark chamber than from the light chamber confirm some relaxation of photosynthesis but the extent of the relaxation is unclear. The period of darkness is not enough for complete dark adaptation and it is known that light energy can leak into the dark chamber from the light chamber, further compounding the interpretation of this measure. The re-opening of some reaction centres is expected in this time and the measured values may reflect the potential photosynthetic capacity of the populations sampled, rather than the actual capacity under measured light. The increased variability between models when applied to dark chamber data reflect more scatter in these data, which may be due to an inconsistent response to the period of darkness. The light chamber data are therefore recommended for studies of phytoplankton photosynthesis.

A large number of incomplete FRRF PE curves, where no light saturation was measured, were produced. Extrapolation using parameters from incomplete curves led to estimates of daily production that were very different to the estimates made from complete curves with the same initial shape. In most cases, the incomplete curves were due to low ambient light conditions where $E_{(0)FRRF}$ was less than 200μmol photons m^{-2} s^{-1} and $E_{(0)Ship}$ was always less than 300μmol photons m^{-2} s^{-1}. In other cases, the incomplete curves resulted from the ship blocking the direct sunlight. The results of this study highlighted the effect that shading by the ship, both of direct and diffuse PAR, can have on the shape of fluorescence profiles and derived parameters. The equations used to process FRRF data and to calculate production from those data mean that underestimating PAR leads to an underestimate of production.

The increased tendency for incomplete curves to be produced from FRRF data at the start and end of the day should be considered when planning sampling strategies. At L4, the casts were always made in the mornings and the low ambient light led to a number of profiles where light saturation was never reached and this resulted in the failure of the model used to derive photosynthetic parameters and in the production of incomplete FRRF PE curves. This was particularly evident during the winter months when all casts were made at light levels less than 200 μmol photons m^{-2} s^{-1} and none of the curves showed any saturation. Similarly, the production of complete curves with unrealistically low rates of maximum production due to severe ships shading also raises issues about deployment protocols. If only one cast was made during the day and was shaded from the direct sunlight by the ship, the subsequent estimate of daily production would be much too low.

The curves used to derive the PE curve model showed no clear decrease in production at high irradiance so the model did not include a photoinhibition parameter. Data recorded in the top few metres at the surface are removed by the quality controls included in data processing, designed to remove quenched data. This means that if photoinhibition occurs near the surface, it will not be recorded. This presents an area of confusion over whether photoinhibition and fluorescence quenching occur as a result of the same physiological responses. It is often argued that photoinhibition is an artefact of artificial long-term exposure to high light levels, such as is often encountered in incubations with ^{14}C and does not exist in nature. Given the equation used here to calculate production from the FRRF data, any decrease in production at high irradiance must be due to decreases in F_q'/F_m', the parameter that reflects the rate of non-cyclic electron transfer in PSII (Genty *et al.*, 1989). Plots of F_q'/F_m' are typically uniform over a range of low irradiance and then show a steady

decrease with increasing PAR above a particular light level as shown in Figure 4.2. If the assumption, that this inflection point occurs at E_k, is correct, the range of light levels above this point should include irradiances at which photosynthesis is light saturated (but not photoinhibited) and, if it occurs, irradiances at which photosynthesis is photoinhibited. If photoinhibition affected F_q'/F_m',, there would be another inflection point in the curve within the light saturated region at PAR levels above E_k and this is not typically seen in the quality controlled data. Photoinhibited data would therefore only be observed from FRRF data if it affected the relationship between F_q'/F_m', and PAR within the photo-saturated region of the water column. It would not be observed if the photoinhibited data was removed during quality control or if it occurred via non-photochemical processes such as increased loss of energy by heat or by the use of electrons, passed along the electron transfer chain for processes other than carbon fixation.

Validity of the approaches used here to carry out the comparisons

The limitations of the sampling strategies possible for each of the two studies raise a number of issues concerning the validity of the comparisons. These include the use of one value to describe photosynthesis for the whole day, the need to pool all the data at L4 for the whole year, the suitability of the ^{14}C measurements from L4 given the long incubations and the assumption of a fully mixed water column.

One daily value of each photosynthetic parameter was derived from the FRRF so diel periodicity was not included in the models. In the Celtic Sea, the FRRF parameter values used were calculated as the average values from all the profiles made throughout the day whilst the parameters from ^{14}C incubations were averages of the values derived from shallow water samples at dawn and at noon. Diel periodicity due to physiological adaptation has been observed in a number of species of marine phytoplankton (Lande and Lewis, 1989) and details of such periodicity seen in results from ^{14}C incubations were discussed in chapter 3. The inconsistency of the diel variability in photosynthetic parameters from the FRRF made it difficult to assess the impact of using single values to describe the photochemical response over the whole day. However, the standard deviations of the daily averages were used to get an indication of the effect of averaging over the day. The largest standard deviations of the averages of the FRRF photosynthetic parameter values were seen for α^B on 26th May (average = 0.046 ± 0.005 mg C [mg Chl]$^{-1}$ h^{-1} [µmol photon m^{-2} s^{-1}]$^{-1}$) and for P^B_m on the same day (average = 2.47 ± 0.79 mg C [mg Chl]$^{-1}$ h^{-1}). Increasing or decreasing α^B by this

amount lead to an increase of 4.0% or a decrease of 4.5 % in PP_{Daily} respectively. Similarly, increasing or decreasing P^B_m by its maximum standard deviation lead to an increase of 17.7 % or a decrease of 24.8 % in PP_{Daily} respectively. Altering both simultaneously led to an increase of 22.9% or a decrease of 24.8% in PP_{Daily}.

The need to pool all the L4 data from 2001 to derive a 'standard curve' had surprising results. The scatter of data around the fitted curve was high. However, the results from models using the standard curve, and those where the curve from a specific date, were very similar and showed the same pattern of production over the course of the year. The similarity between results from the two models was thought to be because the model was insensitive to values of photosynthetic parameters or because, despite the changes in floristic composition, the photosynthetic response varied little over the course of the year. To address the former hypothesis, a sensitivity test was carried out to see how PP_{Daily} was affected by 10%, 25% and 50% changes in curve parameters. Increases and decreases in curve parameters led to similar increases and decreases on final daily production. Changing all parameters at the same time by 10%, 25% and 50% led to equivalent changes in final production so the model was shown to be sensitive to parameter values. Changing α^B alone had a greater effect on final PP_{Daily} than changing P^B_m alone suggesting that photosynthesis was often light-limited.

The ^{14}C parameter values derived at L4 were expected to significantly underestimate the rate of gross production as the incubations lasted 24h and included a dark period. In chapter 3 it was found that α^B and P^B_m values derived from 24h incubations were on average only 49 ± 15% and 39 ± 14% respectively, of the average values from shorter experiments in the same incubator. In order to see what values could be expected if these data had been derived from short-term incubations and how these compared with the FRRF values the ^{14}C derived photosynthetic parameters measured at L4 were adjusted by the percentages noted above. The resultant average values of α^B and P^B_m were 0.040 ± 0.06 mg C [mg Chl]$^{-1}$ h^{-1} [µmol photons m^{-2} s^{-1}]$^{-1}$ and 4.85 ± 3.51 mg C [mg Chl]$^{-1}$ h^{-1} respectively. These averages are much closer to the estimates from the FRRF but on occasions where the originally measured production rates were relatively high (23rd April 2001, 30th April 2001 and 10th September 2001) during bloom periods, this experimental correction led to unrealistically high parameter estimates. For example, on 10th September 2001, the corrected values of α^B and P^B_m were 0.325 mg C [mg Chl]$^{-1}$ h^{-1} [µmol photons m^{-2} s^{-1}]$^{-1}$ and 11.74 mg C [mg Chl]$^{-1}$ h^{-1} respectively. Similarly on 30th April 2001, the corrected values of α^B and P^B_m were 0.104 mg

C [mg Chl]$^{-1}$ h^{-1} [μmol photons m^{-2} s^{-1}]$^{-1}$ and 17.07 mg C [mg Chl]$^{-1}$ h^{-1} respectively. This highlights a problem with assigning an average or standard correction factor to parameters that show clear variations with changing environmental conditions. These results suggest that during bloom periods, the 24h incubation measures a higher proportion of the production that would be measured from 4h incubations; this is not the case at other times of the year. This is difficult to explain and could only be due to less autotrophic respiratory carbon loss in the dark period or less grazing and subsequent respiration or excretion by heterotrophs during bloom conditions. An alternative explanation is that the relationship between estimates made at 4h and 24h still holds true during bloom periods but that chlorophyll concentration is underestimated at high levels leading to an underestimate of the chlorophyll normalised parameters.

The models assumed a fully mixed water column in which chlorophyll and photosynthetic response were both uniform with depth. This is obviously not always true and at L4, fluorescence profiles indicated distinct stratification on eight dates of the year. To investigate the effect of the assumption of a single mixed layer in such cases, the models were re-run : once for the surface layer and once for the deep layer and the results integrated over the water column. Chlorophyll at depth was estimated from fluorescence profiles and the measured concentration at the surface. The results suggested that the mixed layer assumption had little effect on PP_{Daily}. For the ^{14}C model, PP_{Daily} increased by between 0.74% and 7.56% when stratification was introduced and for the FRRF PE curve model, PP_{Daily} increased by between 1.19% and 5.72%.

4.4 Conclusions

This work showed that the FRRF estimates of photosynthetic parameters are comparable to those produced from incubations with ^{14}C. Estimates of α^B and P^B_m from the FRRF were higher than those from ^{14}C reflecting the measurement of gross rather than net photosynthesis. As expected, the use of photosynthetic parameters in primary production models led to higher estimates of PP_{Daily} from the FRRF than from the ^{14}C technque. Roughly half of the variance in PP_{Daily} from ^{14}C incubations was explained by that in PP_{Daily} from the FRRF. The greatest differences between FRRF and ^{14}C estimates were seen over the summer. During this period the FRRF measurements suggest variable production whilst the ^{14}C method suggested consistently low values. This may reflect variability in gross

production over the summer months that have not been recorded before by long-term ^{14}C incubations measuring net community production.

The reliable derivation of photosynthetic parameters from the FRRF was shown to be dependent on ambient light high enough to induce saturation of the photosystems. The FRRF photosynthetic parameter data measured at L4 were unreliable as a result of low ambient light failing to saturate photosynthesis, leading to vertically uniform profiles of fluorescence parameters. It is thought that this led to the failure of the curve fit models used to derive the parameters.

The Celtic Sea data showed the choice of FRRF photosynthetic parameter model to have little effect on the derived parameters when light chamber data were used. Data from the dark chamber data led to higher estimates of photosynthetic parameters than light chamber data. The light chamber data reflect photosynthetic capacity under ambient light but the interpretation of the dark chamber data is less clear. The dark chamber data are likely to reflect the potential photosynthetic capacity of phytoplankton adapted to the ambient conditions. In the Celtic Sea, the use of a single generic daily relationship under the conditions experienced is thought to have led to up to 25% error in the overall PP_{Daily} estimate. The use of a generic annual curve at L4 led to a similar pattern of production over the year to the use of specific parameters derived from individual dates, despite the curves from individual dates often being incomplete. This was unexpected but may reflect the relatively low variability of photosynthetic response, despite floristic changes, over the course the year at the station.

The quality controls used in the processing of FRRF data results in the removal of surface data. PAR decreases a lot in the first few metres and the need to remove surface data could mean that important information on the photophysiology of phytoplankton at saturating light is lost.

Chapter 5. A comparison of remotely sensed with measured estimates of chlorophyll and production

5.1 Introduction and specific methods

The use of remote sensing to measure ocean primary production relies upon the ability of satellites to retrieve biomass estimates. All production algorithms share the requirement for remotely sensed estimates of biomass derived from ocean colour data but this is also the source of the greatest error in production modelling. The conversion of ocean colour data to estimates of chlorophyll concentration relies on changes in the reflectance at different wavelengths of light due to changes in phytoplankton concentration. It requires complex atmospheric correction and is made particularly difficult in Case II waters where the optical signal is modified by the presence of coloured dissolved organic matter (CDOM) and suspended particulate matter (SPM). Difficulties in atmospheric correction and the presence of optically active constituents in the water can sometimes cause poor quality satellite data that leads to incorrect estimates of chlorophyll.

Many production models exist and have varying levels of complexity. They range from simple empirical models, where production is considered to be directly proportional to chlorophyll concentration, up to complex semi-analytical models, where individual wavelengths of light and their effects on phytoplankton photophysiology are included. The application of satellite production models over the whole water column is difficult as the signal is derived only from the surface water and a number of approaches are used to describe the shape of the biomass profile. There is also considerable variation in the way in which light is included in the models. In simple models a constant value for irradiance at the sea surface is assumed whilst in the most complex, surface light is divided into diffuse and direct components and into individual wavelengths within these groups. A variety of approaches also exist for the estimation of the attenuation of light with depth. The majority of models incorporate the effect of light on photosynthesis via the parameters of a PE curve but the remote estimation of these parameter values is not simple and is a major limitation to the modelling of primary production from satellite data.

In the first part of this chapter, the satellite retrieval of chlorophyll concentration is investigated using data from L4 in 2000 and 2001. Only one SeaWiFS image was available from the Celtic Sea cruise so these data were not included in the comparison. A quality control process on high resolution (1km x 1km pixels) data was carried out to remove

unreliable data. These SeaWiFS chlorophyll estimates were then compared with low resolution (9km x 9km pixels) SeaWiFS data and with measured estimates of chlorophyll concentration to assess their consistency and accuracy. The relationship between SeaWiFS and measured data was compared to that observed in a standard NASA dataset to see whether these results were typical. The effects of the CDOM and SPM on remotely sensed chlorophyll estimates were also considered due to their impact on reflectance in Case II waters.

In the second section of this chapter, three different production models are assessed. The models were run for station L4 in 2001 and for the stations of the Celtic Sea cruise. The first model was a simple empirical algorithm derived from the measured relationship between measured chlorophyll and production from ^{14}C incubations. The second was the Vertically Generalised Productivity Model of Behrenfeld and Falkowksi (1997a) (described in section 2.5.3 and hereafter referred to as the VGPM model), which is comprised of a suite of empirical relationships. The final model was the complex semi-analytical model of Morel (1991) and Antoine and Morel (1996), which included wavelength resolution and phytoplankton absorption (See section 2.5.4 for a description of the model, hereafter referred to as the Morel model). For the Morel model, estimates of PAR at the surface were required and were calculated using a separate algorithm. All of the models were parameterised with measured chlorophyll in order that their performance could be attributed directly to the model and not complicated by uncertainties in chlorophyll retrieval. The latter two models were run a number of times using different combinations of modelled and measured supporting parameters. For the VGPM model, the parameters altered were P^B_{opt} (which was replaced with measured P^B_{max}) and the euphotic depth (which was replaced with a fixed maximum depth of 30m). For the Morel model, the parameters altered were K_{PAR}, Zeu and K_{PUR}. These parameter alterations were carried out to aid the understanding of the model performance at each stage of the calculation. The results from the models were compared with each other and with estimates from the ^{14}C and FRRF techniques.

5.2 Results

5.2.1 Comparison of remotely sensed and measured chlorophyll estimates

Quality controls on SeaWiFS chlorophyll data

a) Local scale images

The total number of days in 2000 and 2001 was 731 but even before quality control, SeaWiFS chlorophyll estimates were available for only 199 of those dates. Table 5.1 shows the number of pixels present after different types of quality control on high resolution SeaWiFS data. Depending on which of the four approaches was used, the total number of dates remaining after the quality control process ranged from 143 (72% of the original number of images) to 87 (44% of the original number of images). The type of quality control used affected the range of chlorophyll values measured as shown in Table 5.2. Where the standard deviation of the yearly mean was high, this tended to correlate with the presence of unlikely extreme estimates of chlorophyll in the data set. Given the statistics and the values of the post-quality control data sets, the quality control chosen was the requirement for at least three of the nine pixels to be present and for the standard deviation of the mean estimate from these pixels to be less than 25% of the mean value. This quality control process left 93 dates for 2000 and 2001 (47% of the original number of images and 13% of the total dates).

b) Global scale images

A total of 53 chlorophyll estimates were available from NASA 8-day composite images for L4 in 2000 and 2001 (23 from 2000 and 30 from 2001). These were NASA derived estimates and no further quality control was carried out on the data. The average chlorophyll estimate for the period of study was 2.14 ± 1.97 mg m^{-3} which compared well to that from the high resolution SeaWiFS data (2.26 ± 2.22 mg m^{-3}).

Comparison of chlorophyll estimates from fluorometric and HPLC techniques

A comparison of fluorometric and HPLC methods to determine chlorophyll concentration was done in 2001 (see Figure 5.1). For most of 2000, only HPLC measurements were made. The fluorometric estimates for dates between 19th Aug 2001 and 19th Nov 2001 are considered to be suspect due to problems with the fluorometer (see discussion) and were not used in these analyses. A regression of the data showed measurements from the two

Table 5.1. Number of dates for which SeaWiFS data were available at L4 in 2000 and 2001 after different types of quality control. SD refers to the standard deviation around the mean value.

Year	Quality control				
	None	At least 3 pixels	At least 3 pixels SD < 25% of ave.	At least 3 pixels L4 pixel present	At least 3 pixels L4 pixel present SD < 25% of ave.
2000	111	93	48	77	46
2001	88	77	45	66	41
Sum	199	170	93	143	87

Table 5.2. Effect of different types of quality control on the range of chlorophyll values measured throughout 2000 and 2001. SD refers to the standard deviation around the mean value.

	Quality control				
	None	At least 3 pixels	At least 3 pixels SD < 25% of ave.	At least 3 pixels L4 pixel present	At least 3 pixels L4 pixel present SD < 25% of ave.
Average	3.04	3.09	2.01	2.26	2.05
SD	4.70	5.46	1.67	2.22	1.71
SD as % of average	155	177	83	98	84

techniques to be closely correlated with 88% of the variance explained. HPLC chlorophyll = fluorometric chlorophyll*0.66 + 0.02, n = 19 (see Figure 5.2). An average of the two estimates was used in cases where both *in situ* measurements were available for comparison with SeaWiFS data. In all other cases the estimate from HPLC analysis was used.

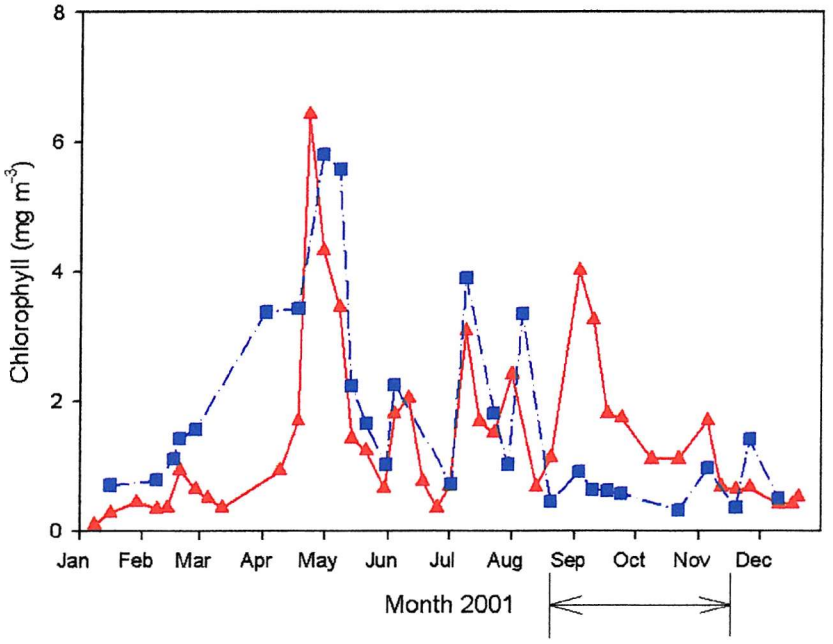

Figure 5.1. Chlorophyll concentrations derived from HPLC (▲) and fluorometry (■) at L4 in 2001. Fluorometric measurements between the dates marked by arrows are considered unreliable due to problems with the spectrofluorometer discussed in the text.

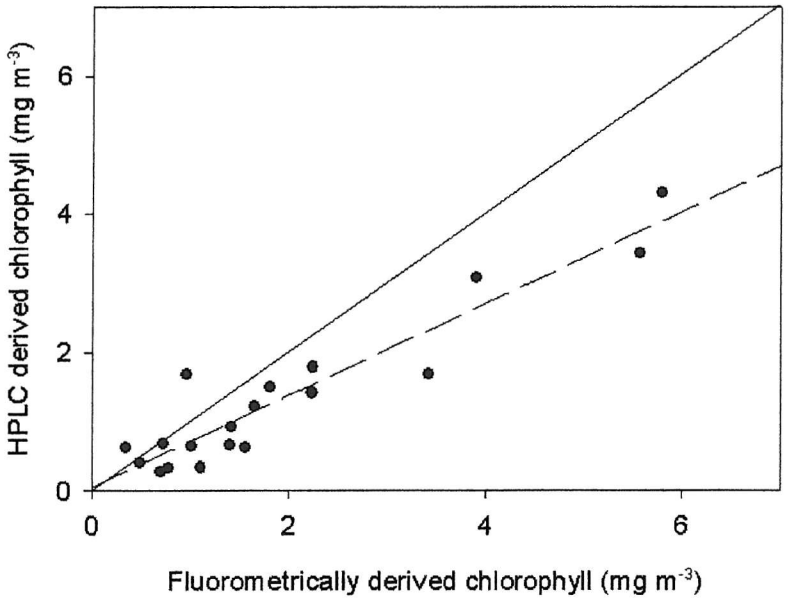

Figure 5.2. Plot of chlorophyll estimates from HPLC against those measured using fluorometry over 2001. The dotted line shows the line of the regression and the solid line is the 1:1 line.

Comparison of SeaWiFS chlorophyll data with measurements from water samples

The annual variations of chlorophyll concentration at L4 in 2000 and 2001, as measured by the extraction of pigments and SeaWiFS, are shown in Figure 5.3. Over the two-year period of study, chlorophyll was measured on sixty days but on only ten dates did local scale (1km x 1km pixels) SeaWiFS chlorophyll estimates coincide with water sampling. Where this occurred, all SeaWiFS images, except that for 21st Mar 2000 show clear skies all around

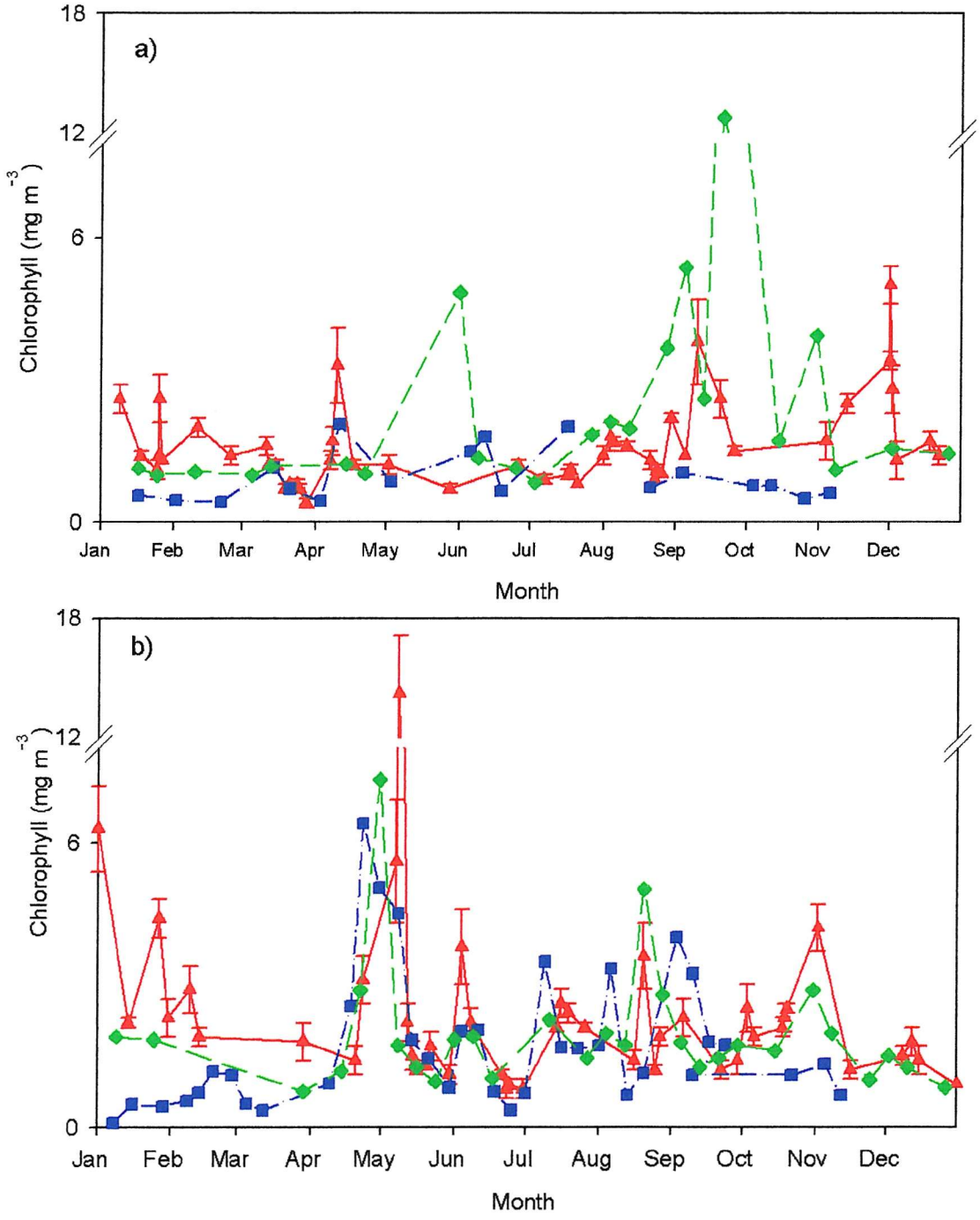

Figure 5.3. Comparison of SeaWiFS and measured chlorophyll estimates at L4 a) in 2000 and b) 2001. Measured values are from HPLC or fluorometric techniques and averages used where estimates from both techniques were available. SeaWiFS 1.1km pixels (▲), SeaWiFS 9km pixels (◆) and *in-situ* measurements (■).

the L4 site (see Figure 5.4). The cloud cover was almost complete on 21st Mar 2000, except for a couple of pixels just south of L4 so the chlorophyll values retrieved may be unreliable, despite passing the quality controls. There were 28 dates on which SeaWiFS global estimates coincided with water sampling and 37 occurrences where local SeaWiFS estimates coincided with global SeaWiFS estimates. All statistics of the regressions of the three chlorophyll estimates against each other were poor but the fits of the data around the 1:1 line suggested reasonable agreement (Figure 5.5). The local scale satellite values originally used were those from the L4 pixel itself. However, due to the time delay between water sampling (which was always in the morning) and the satellite overpass (which was between 1100h and 1500h local time), a tidal excursion model was used to predict the drift of the sampled water. SeaWiFS chlorophyll estimates were extracted at the new position, calculated to allow for the movement of water between *in situ* sampling and the satellite overpass. The tidal drift would not have affected the global scale estimates as the water body always remained within the 9km x 9km box. For three dates, chlorophyll values were not available at the new pixel (21st Mar 2000, 31st May 2001 and 16th Jul 2001) so the regression, using the new SeaWiFS data, was only carried out on seven data points and the relationship between remotely sensed chlorophyll at the new location and *in situ* measurements was poorer than originally calculated using data from the L4 pixel (Figure 5.6).

In order to see how this relationship between SeaWiFS estimates and measurements compared with values from other research, these data were superimposed on plots of the SeaBAM data set (see O'Reilly *et al.*, 1998). The SeaBAM data set (from the SeaWiFS Bio-Optical Algorithm Mini-Workshop) was acquired from the NASA/SeaWiFS Bio-optical Archive and Storage System (SeaBASS) and contains comparisons of expected SeaWiFS and measured chlorophyll from a wide range of oceanic conditions. The SeaWiFS data are not real but are simulated from measured water leaving radiance and as such they are optimistic estimates as they do not include any errors from atmospheric correction. The data from this study lie slightly outside the limits of the SeaBAM data but the scatter of the data falls on both sides of the 1:1 line (see Figure 5.7).

Measurements of CDOM and SPM were available for 36 and 39 dates in 2001 respectively (Figure 5.8). Unfortunately, on only six dates when CDOM, and ten dates when SPM

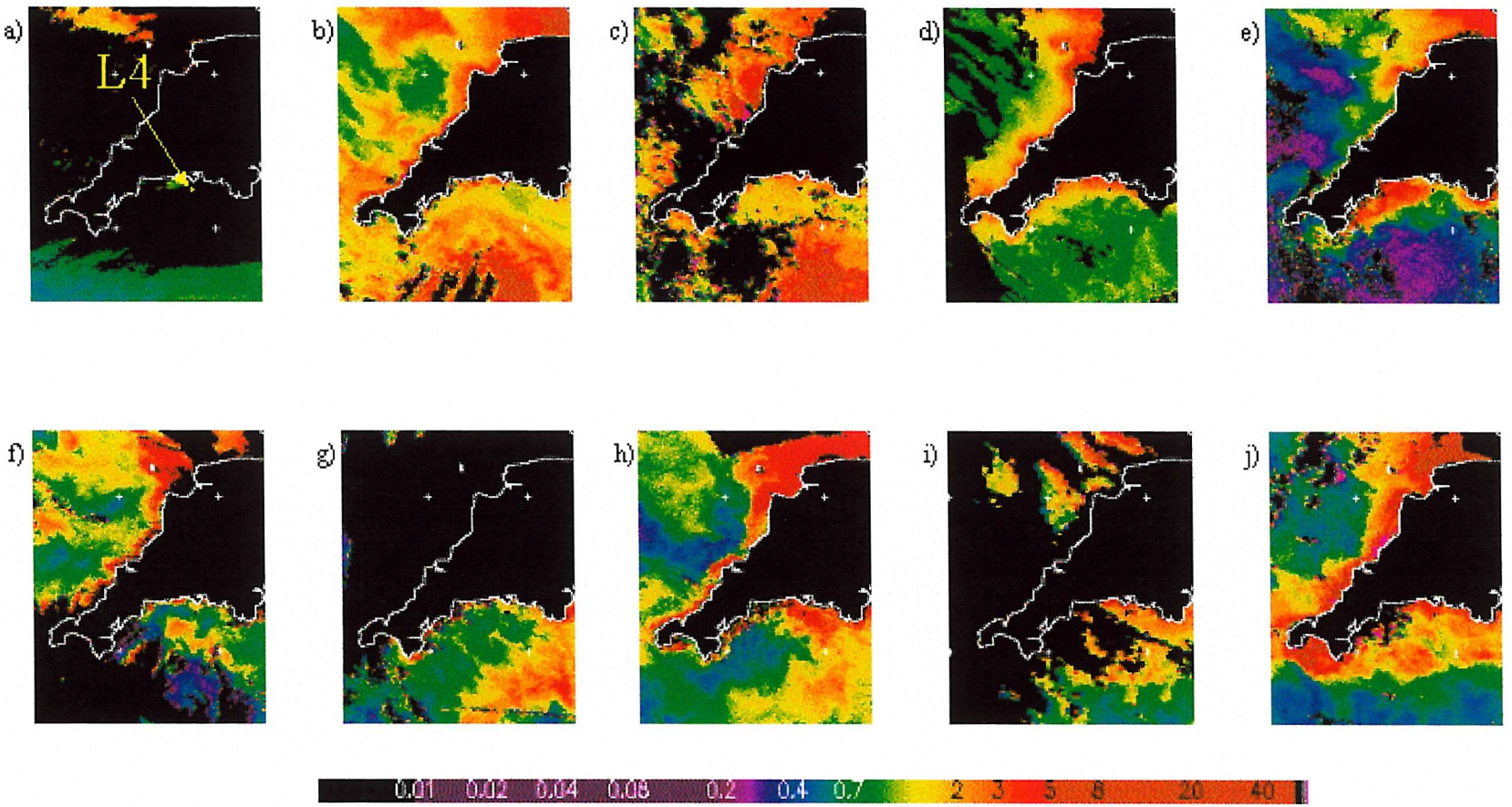

Figure 5.4. Satellite images of chlorophyll concentration around the South West of England on days when measured estimates coincided with satellite estimates of chlorophyll: a) 21st Mar 2000, b) 17th July 2000, c) 21st Aug 2000, d) 13th Feb 2001, e) 23rd Apr 2001, f) 14th May 2001, g) 30th May 2001, h) 4th Jun 2001, i) 16th Jul 2001 and j) 20th Aug 2001. The position of L4 is marked with a dot as indicated on the first figure.

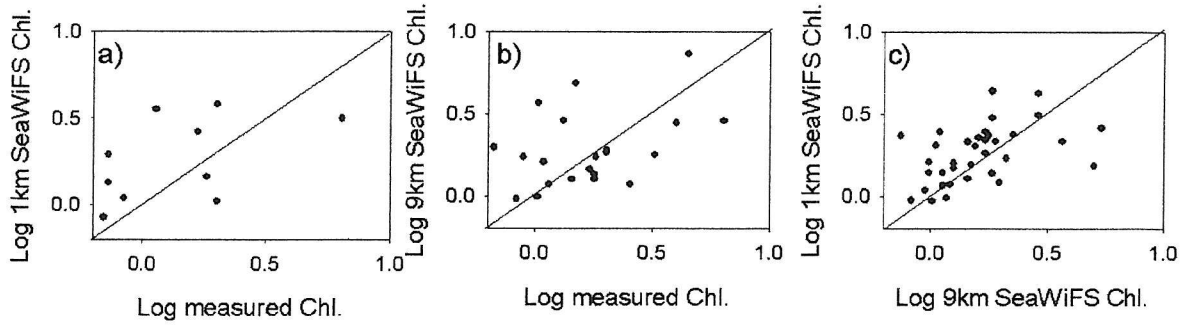

Figure 5.5. Plots of log chlorophyll estimates from different sources against each other. Data from 2000 and 2001 at L4: a) chlorophyll estimates from 1km SeaWiFS pixels against measured values, b) chlorophyll estimates from 9km SeaWiFS pixels against measured values and c) chlorophyll estimates from 1km SeaWiFS pixels against those from 9km SeaWiFS pixels. Chlorophyll is in units of mg m^{-3}. The 1:1 lines are shown.

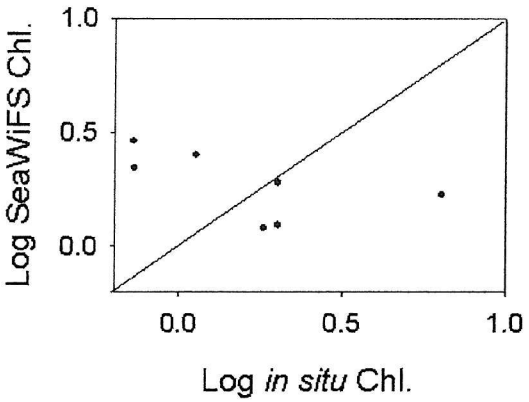

Figure 5.6. Log chlorophyll estimates derived from SeaWiFS at the new position after displacement by tidal drift, plotted against log measured chlorophyll estimates. Data are from L4 in 2000 and 2001. Chlorophyll is in units of mg m^{-3}. The 1:1 line is shown.

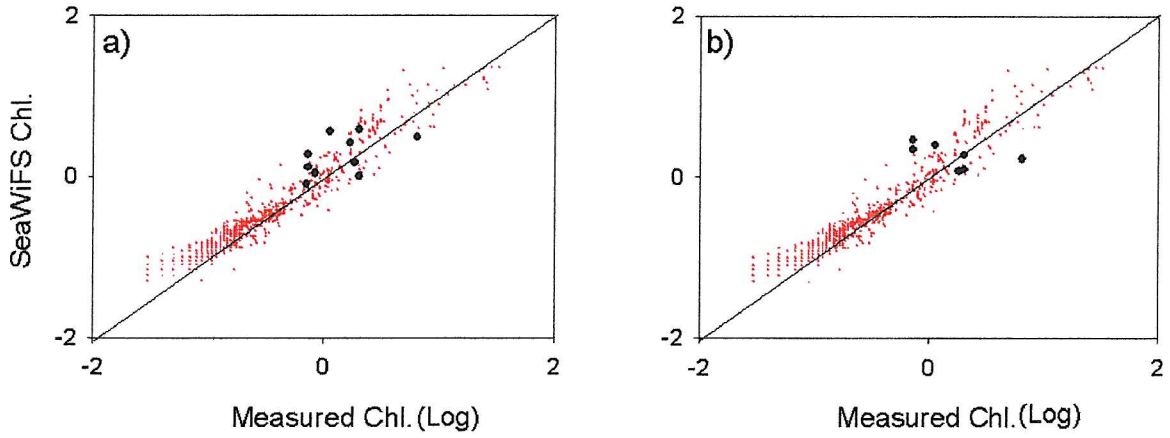

Figure 5.7. Comparison of the relationship between SeaWiFS and measured data from the SeaBAM data set (·) with that at L4 over 2000 and 2001 (●): a) data at L4 position (before allowance for tidal displacement) and b) data at new position post-tidal displacement (b). Chlorophyll is in units of mg m^{-3}. The 1:1 line is shown.

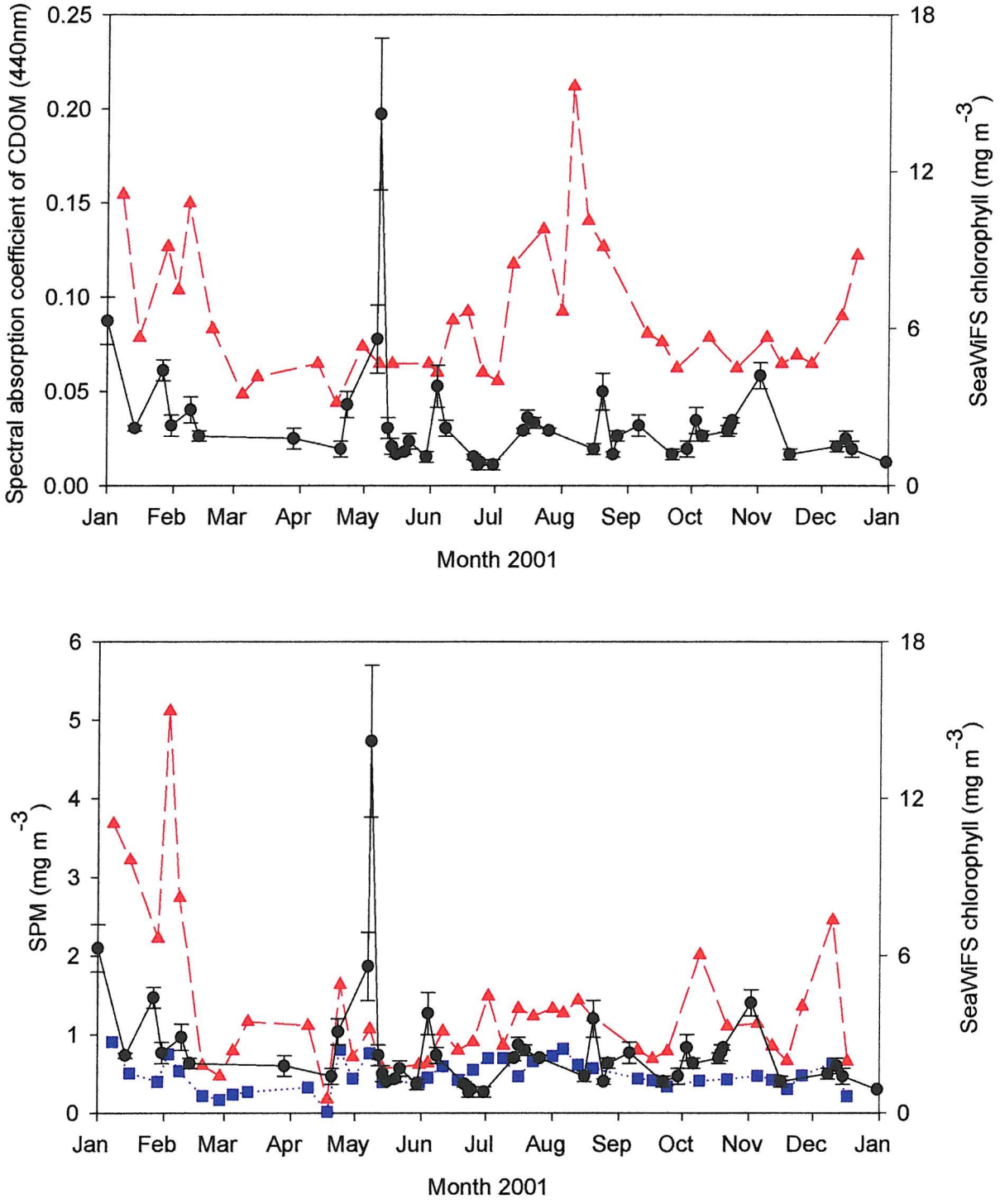

Figure 5.8. Plots of a) Coloured dissolved organic matter (CDOM)(▲) and b) Suspended particulate matter (SPM) (total (▲) and organic (■)) both shown with estimates of chlorophyll from SeaWiFS (●) over the course of 2001.

were measured were SeaWiFS derived chlorophyll estimates available, so little could be learnt about the relationship between chlorophyll concentration and these two interfering substances. Scatter plots of the measured values of CDOM and SPM against SeaWiFS chlorophyll did not reveal a clear relationship (Figure 5.9).

5.2.2 Comparison of PP_{Daily} from satellite models with PP_{Daily} from ^{14}C and FRRF approaches

PP_{Daily} from an empirical model

The empirical model was based on the relationship between chlorophyll concentration and PP_{Daily} from the ^{14}C photosynthetic parameter model (Figure 5.10). The regression against log chlorophyll explained 43 % and 66 % of the variance in log production in the Celtic sea and for L4 respectively.

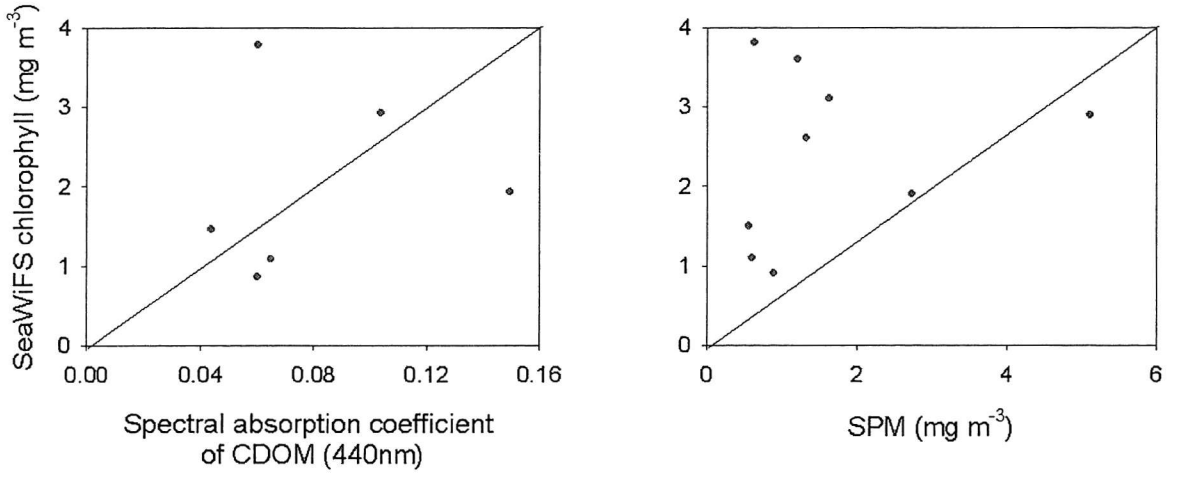

Figure 5.9. Plots of SeaWiFS chlorophyll against a) CDOM absorbance and b) SPM at L4 in 2001. The 1:1 line is shown.

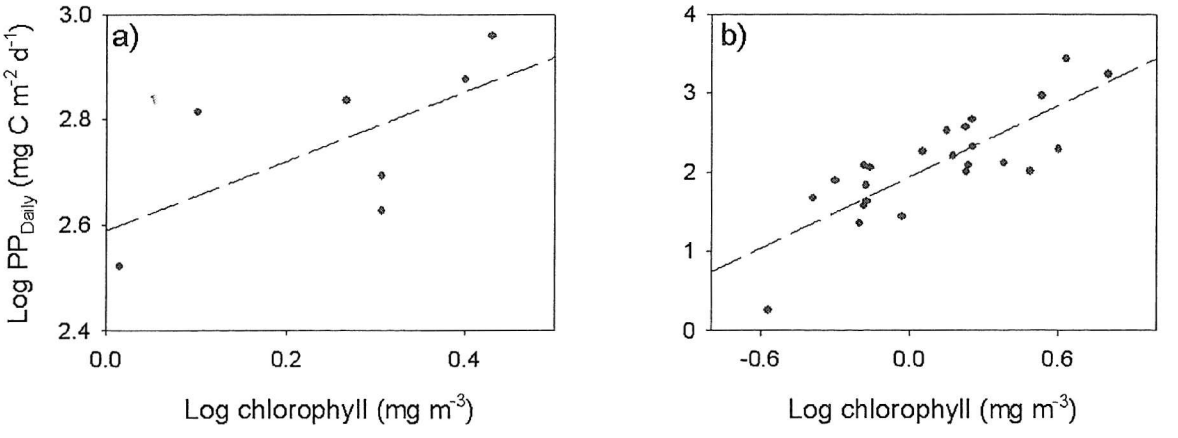

Figure 5.10. Plots of log PP_{Daily} from ^{14}C against coincident log chlorophyll measurements a) in the Celtic Sea and b) at L4. The line describing the regression is shown.

The outlying data point in the regression of the L4 data was from 16th Jan 2001 and production on this date was lower than expected given the chlorophyll concentration. The magnitude of the empirically modelled values were very similar to the estimates from ^{14}C as shown in Figure 5.11. However, this was not very surprising as the ^{14}C data were used to derive the model. The regression of the empirically modelled estimates against production from the ^{14}C method was carried out using the data in its original linear form and 45% and 58% of the variance was explained was for the Celtic Sea and L4 respectively. As expected, if the data were logged prior to the regression, the statistics were the same as the original chlorophyll-production relationship ($R^2 = 0.42$ for the Celtic Sea and $R^2 = 0.66$ for L4). Figure 5.12 shows plots of the empirical modelled estimates against those from the ^{14}C method. Neither data set showed a good fit around the 1:1 line. The range of values encountered over the whole year at L4 was much higher than in seven days in the Celtic Sea hence the higher R^2 values obtained for the former. The obvious outlier at L4 was from the 30th Apr 2001 when very high PP_{Daily} was predicted from the ^{14}C measurements.

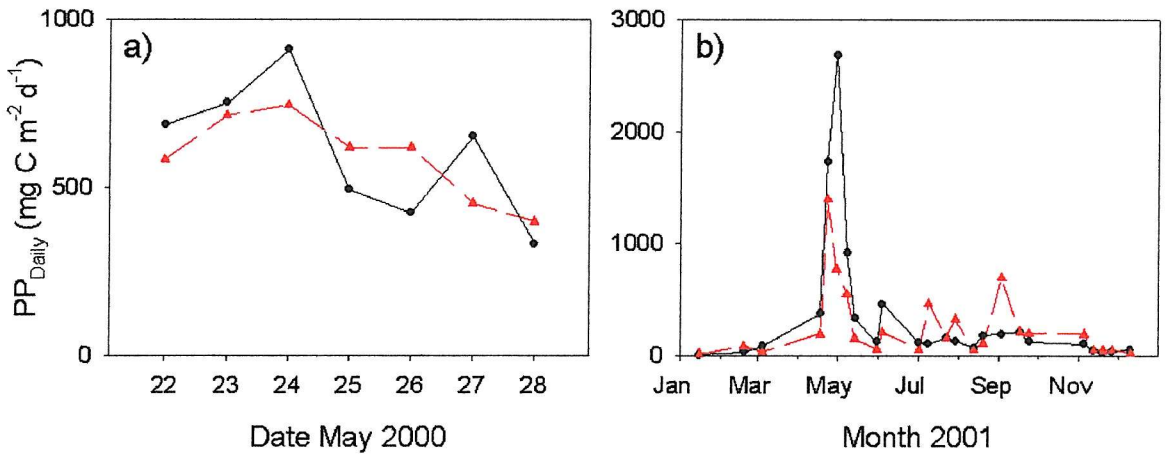

Figure 5.11. Plot of PP_{Daily} from the ^{14}C technique (●) and from the Empirical model (▲) over the course of each study, a) for the Celtic Sea and b) for L4.

PP_{Daily} from VGPM model

The estimates of euphotic depth used in the VGPM model, based on chlorophyll concentration, were lower than the estimates from *in situ* measurements of light in both the Celtic Sea and at L4 (Figure 5.13). When the modelled and *in situ* estimates were compared, the equation describing the regression line showed a very poor fit to the data in both cases ($R^2 = 0.008$ in the Celtic Sea and $R^2 = 0.009$ at L4) so the regression statistics were not considered further. The modelled value of P^B_{opt} was much higher than the measured value of

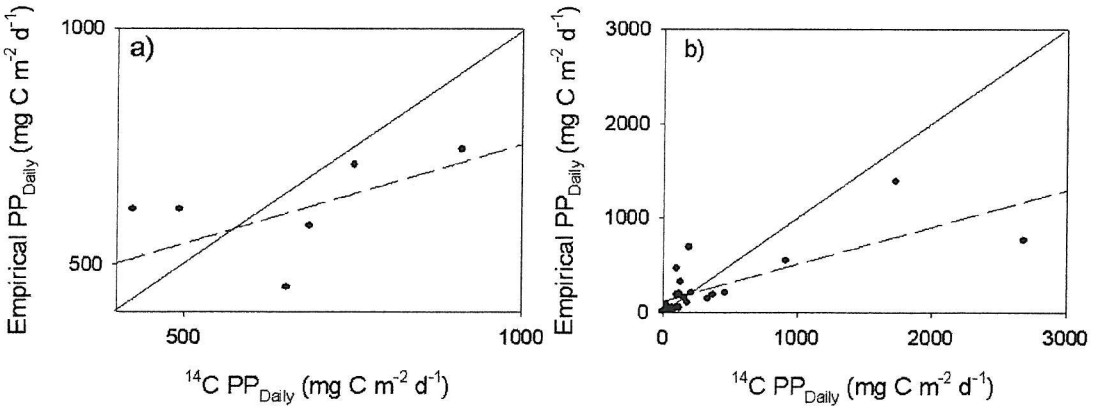

Figure 5.12. Plots of PP_{Daily} from the empirical model against estimates from ^{14}C a) for the Celtic Sea and b) for L4. The dotted line describes the regression and the solid line is the 1:1 line.

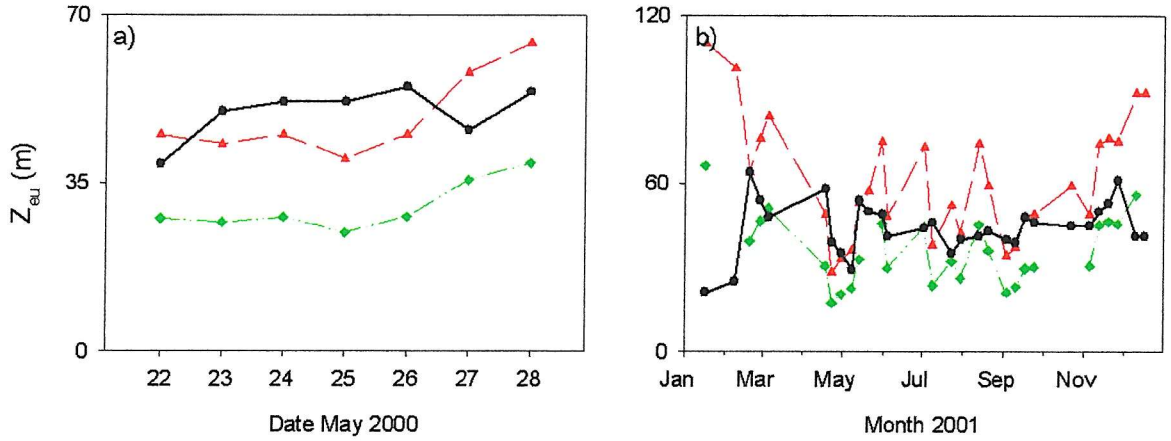

Figure 5.13. Depth of the euphotic zone (Z_{eu}) as predicted by different approaches a) for the Celtic Sea and b) for L4 : Z_{eu} used in VGPM model (◆), Z_{eu} used in Morel model (▲) and Z_{eu} measured from PAR data (●).

P^B_m (Figure 5.14) and modelled P^B_{opt} was much less variable than measured P^B_m. Again the variances explained by the regression of P^B_{opt} against P^B_m were very low ($R^2 = 0.06$ for the Celtic Sea and $R^2 = 0.09$ for L4). The four runs of the VGPM model differed in euphotic depth (either calculated as a function of chlorophyll or fixed at 30m) and in the calculation of P^B_{opt} (either as a function of temperature or direct use of the P^B_m value measured from ^{14}C incubations) and the results are shown in Figure 5.15. A fixed euphotic depth of 30m was included as this would be used later in comparisons with estimates from the ^{14}C method and the FRRF and estimates from the Morel model. In most cases the highest production values were obtained assuming a euphotic depth of 30m and when modelled P^B_{opt} was used and the lowest values were obtained using the modelled euphotic depth and measured P^B_m. When regressions of modelled production were carried out against ^{14}C and FRRF estimates of

production, the highest R^2 values were always obtained from estimates obtained using P^B_m rather than P^B_{opt} (See Table 5.3). However, in all except two out of 8 cases (both for regressions against Celtic Sea FRRF data) the slopes of the regressions were closer to unity when P^B_{opt} was used in the models. A large proportion of the variance in the modelled production was explained by that in chlorophyll (67%) and euphotic depth (61%) and 76%

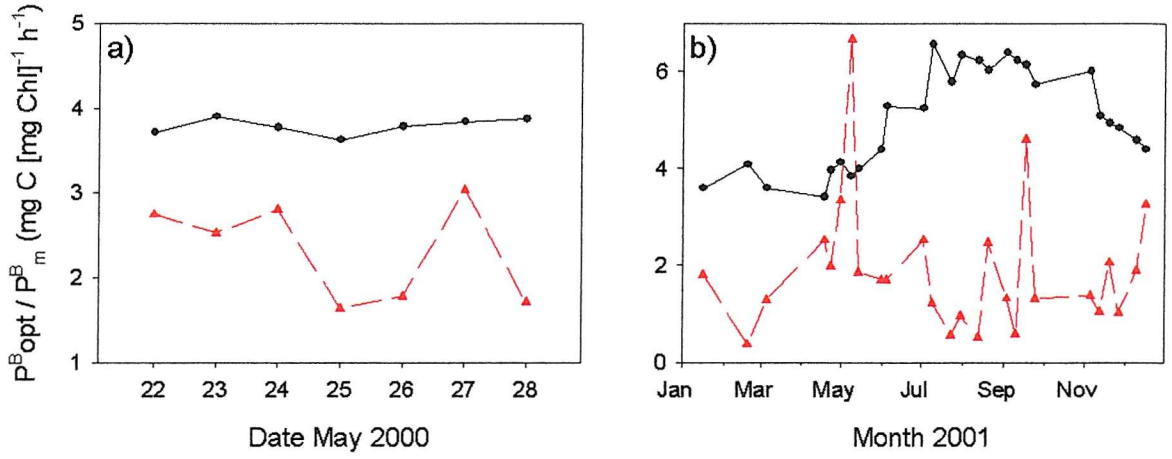

Figure 5.14. Modelled values of P^B_{opt} from the VGPM model (●) and measured values of P^B_m (▲), a) for the Celtic Sea and b) for L4.

Table 5.3. Statistics from regressions of PP_{Daily} estimates from the VGPM model against estimates from the ^{14}C and FRRF methods. PP_{Daily} from the VGPM model was always the dependent variable. MOD Z_{eu} and 30m Z_{eu} refer to modelled estimates of euphotic depth and euphotic depth fixed at 30m respectively. Photosynthetic parameter models are indicated by 'psp'.

Study	Independent variable	P^Bopt / P^Bm	Depth of euphotic zone			
			30m	Modelled	30m	Modelled
			R^2	R^2	Slope	Slope
Celtic	^{14}C psp	P^Bopt	0.71	0.15	1.8	0.68
Celtic	^{14}C psp	P^Bm	0.11	0.87	1.05	1.55
Celtic	FRRF curve	P^Bopt	0.47	0.50	2.28	1.32
Celtic	FRRF curve	P^Bm	0.66	0.53	1.88	1.30
Celtic	FRRF psp	P^Bopt	0.24	0.28	0.98	0.61
Celtic	FRRF psp	P^Bm	0.48	0.42	0.97	0.71
L4	^{14}C psp	P^Bopt	0.32	0.21	1.37	0.70
L4	^{14}C psp	P^Bm	0.86	0.89	2.03	1.32
L4	FRRF curve	P^Bopt	0.50	0.56	1.12	1.32
L4	FRRF curve	P^Bm	0.58	0.76	1.89	2.37

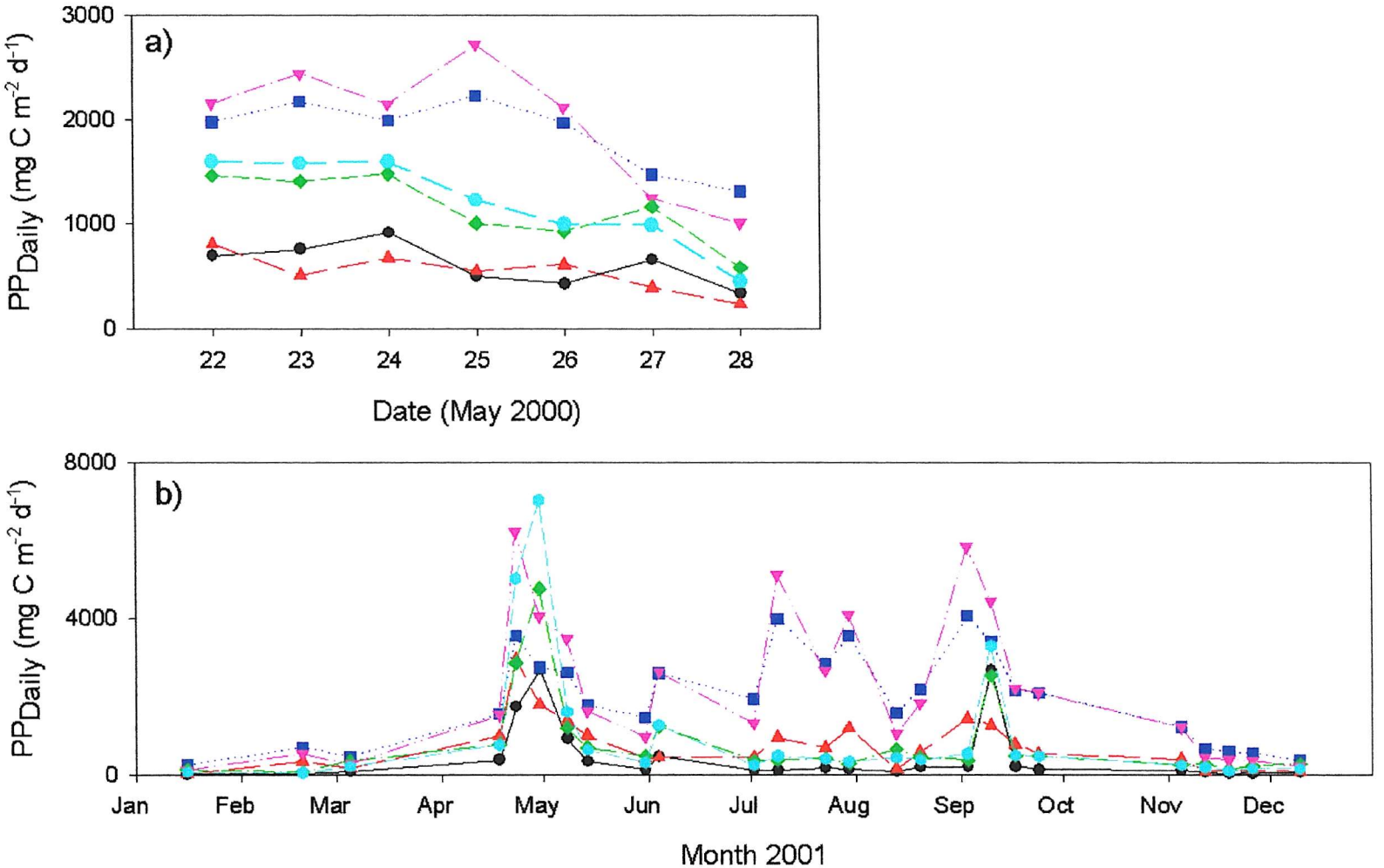

Figure 5.15. PP_{Daily} estimated from VGPM model parameterised with different combinations of modelled and measured data a) in the Celtic Sea and b) at L4: ^{14}C photosynthetic parameters (●), FRRF PE curve (▲), VGPM modelled Z_{eu} and modelled P^B_{opt}, (■), VGPM modelled Z_{eu} and measured P^B_m (◆), VGPM Z_{eu} fixed at 30m and modelled P^B_{opt} (▼) and VGPM 30m Z_{eu} fixed at 30m and measured P^B_m (●). ^{14}C and FRRF values were integrated over the top 30m of the water column.

of the variance was explained by the product of the two. Variance in P^B_{opt} only explained 37% of that in modelled production.

PP_{Daily} from Morel model

The model was run with different combinations of modelled and measured PAR, K_{PAR}, K_{PUR} and with the euphotic depth both modelled (to the 0.1% light level) and fixed at 30m to aid comparisons with other techniques.

The PAR model was run assuming no cloud cover so PAR was calculated simply as a function of Julian day and latitude (Figure 5.16). This explains the smoothness of the curves of the modelled PAR estimates compared to the measured values and why modelled PAR is higher than the measured values. When the two data sets were regressed against each other, different results were seen from each study (Figure 5.17). At L4 (Figure 5.17b) the variance explained by the regression was high ($R^2 = 0.89$) but modelled PAR was approximately twice the measured values. However, the R^2 value from the Celtic sea data (Figure 5.17a) was only 0.16 and the fitted regression line (not shown) suggested a decrease in measured PAR with an increase in modelled PAR. It is thought that the regression was particularly poor due to the low number of data points (n = 7) and the low variability in PAR over the course of the study.

In the Celtic sea, K_{PAR} from the model was higher than measured K_{PAR} in most cases but at L4, the relationship between the modelled and measured values varied with season (See Figure 5.18). Over most of the year, the K_{PAR} estimates were comparable but in winter, the measured values were much higher than the modelled estimates. The plot of modelled K_{PAR} against the measured estimates for the L4 data (Figure 5.19) shows two outliers (labelled z1 and z2) and these were estimates for 8th Feb 2001 and 16th Jan 2001 respectively. The K_{PAR} value was inversely correlated to the calculated euphotic depth, which is shown in Figure 5.13. In the Celtic Sea, modelled estimates of euphotic depth were similar to measured values. At L4, relatively deep euphotic depths were estimated from the Morel model in winter when modelled K_{PAR} was lower than measured.

Modelled K_{PUR} was compared to that estimated both from ^{14}C and FRRF data in the Celtic Sea but, due to the previously discussed problems with FRRF photosynthetic parameter estimates at L4, modelled K_{PUR} was only compared with ^{14}C estimates for the L4 study. In the Celtic Sea, modelled K_{PUR} was similar to that from the FRRF (Figure 5.20) but generally much lower than that from ^{14}C. At L4, modelled values were lower than measured for

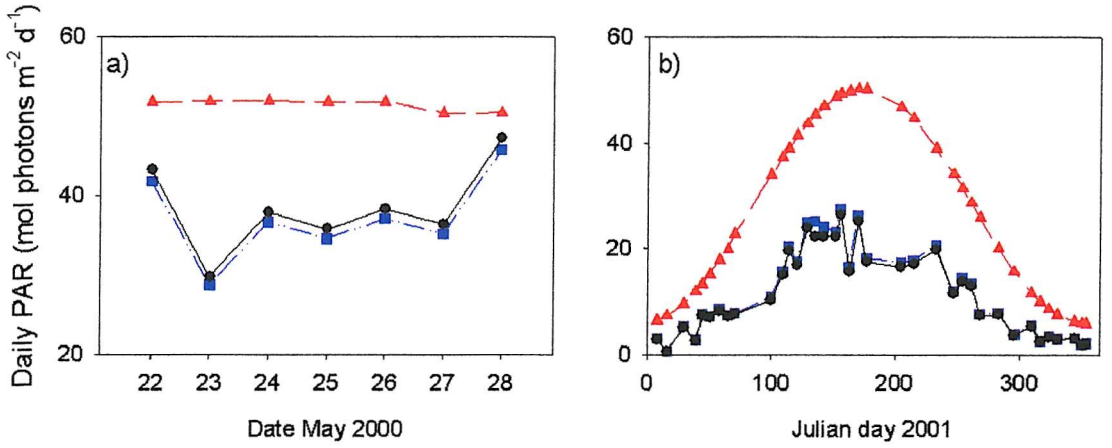

Figure 5.16. Modelled (▲) and measured (■ and ●) PAR a) in the Celtic Sea and b) at L4. Measured PAR is shown in its original, broadband values (■) and 'post-conversion' (●) where it was processed into individual wavelengths and then reintegrated.

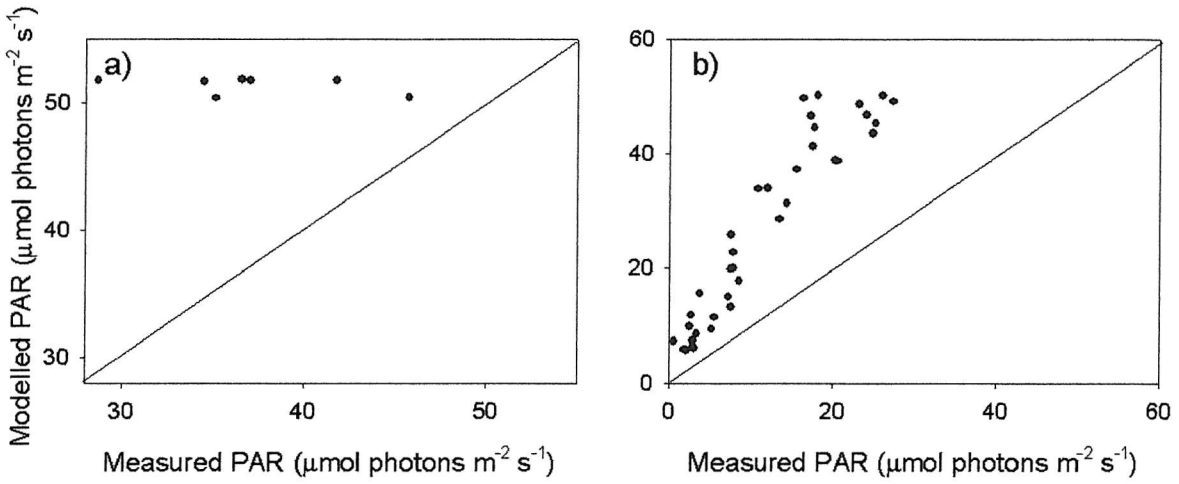

Figure 5.17. Plot of modelled PAR against measured PAR a) for the Celtic Sea and b) for L4. The 1:1 line is shown

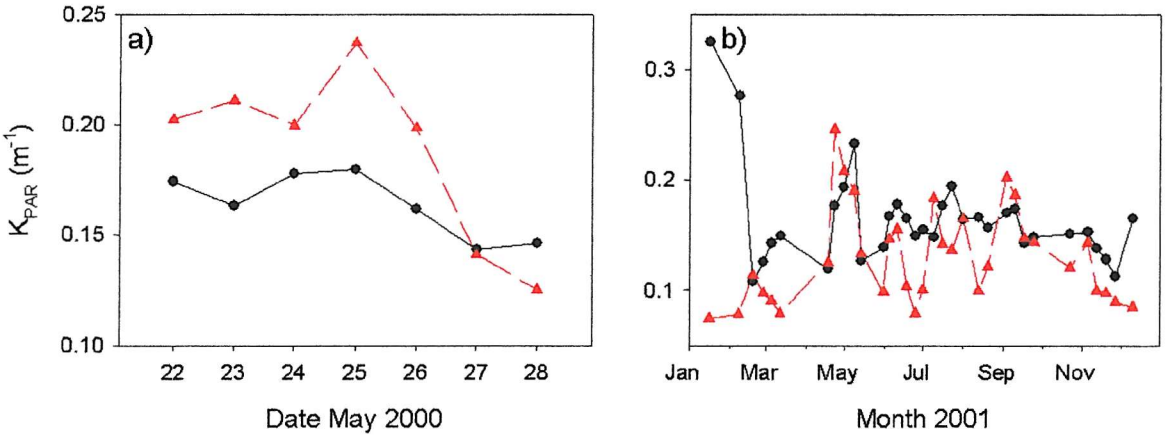

Figure 5.18. Comparison of K_{PAR} derived from PAR measurements (●) with that estimated using the Morel model (▲), a) for the Celtic Sea and b) for L4.

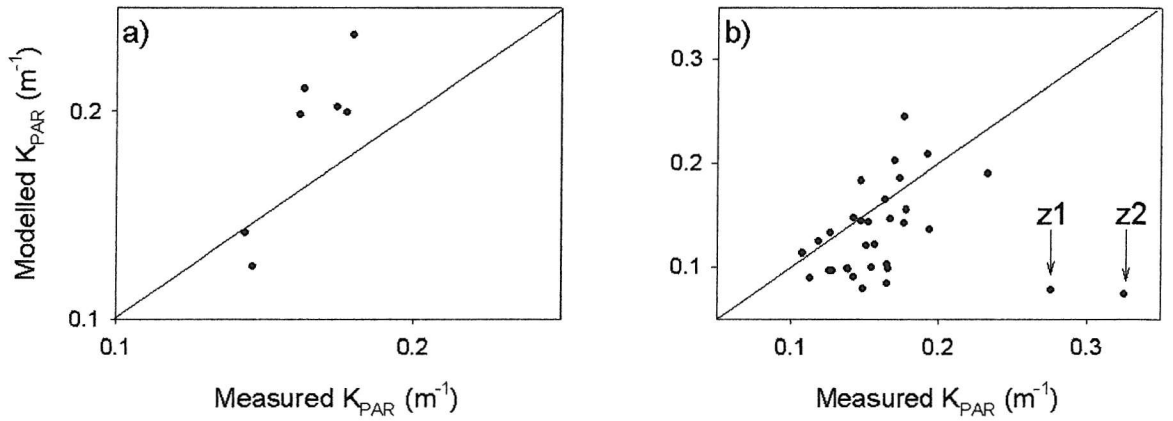

Figure 5.19. K_{PAR} values calculated from the Morel model plotted against those derived from *in situ* PAR measurements a) for the Celtic Sea and b) for L4. The symbols z1 and z2 indicate the outlying points from 8th Feb 2001 and 16th Jan 2001 respectively. The 1:1 line is shown.

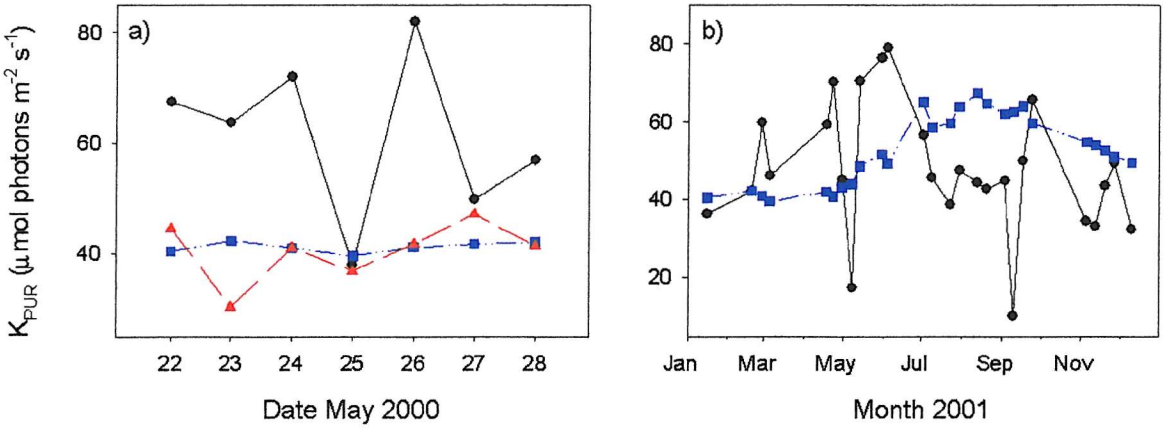

Figure 5.20. Comparison of measured (from ^{14}C (●) and the FRRF (▲)) and modelled (■) K_{PUR} over the course of each study a) for the Celtic Sea and b) for L4.

most of the first half of the year but increased to higher values than measured from the summer onwards. When modelled K_{PUR} values were plotted against measured estimates (Figure 5.21) the scatter around the 1:1 line was quite high reflecting poor agreement between the data.

The relationship between production in the Celtic Sea from the ^{14}C and FRRF techniques and that estimated from the Morel model varied, depending on the date and on the parameters used in the model (Figure 5.22) but estimates were of a similar magnitude.

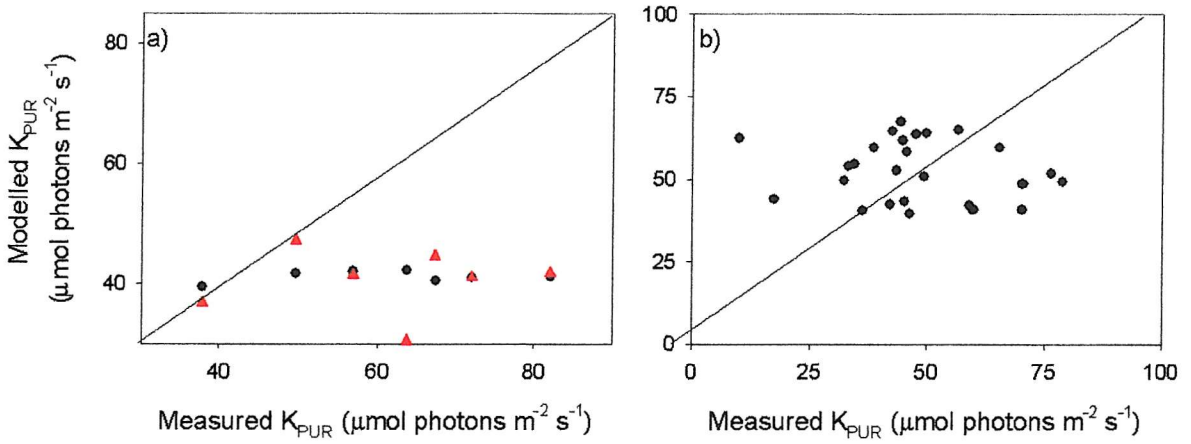

Figure 5.21. Plots of modelled against measured K_{PUR} (from ^{14}C (●) and the FRRF (▲)), a) for the Celtic Sea and b) for L4. The 1:1 line is shown.

For most of the year at L4, the ^{14}C estimates fell slightly below the estimates from the satellite model. The clear exception is the data from the 30th Apr 2001 where ^{14}C estimates are as high as those from the model. The FRRF estimates, being slightly higher than those from ^{14}C are closer to the satellite estimates for most of the year. The statistics from the regressions of the different Morel models against the ^{14}C and FRRF estimates are shown in Table 5.4. Fixing the euphotic depth at 30m had very little effect on the depth integrated production estimates or how well they described production from the ^{14}C and FRRF methods. The Celtic Sea data were more scattered around the 1:1 line than the L4 data (not shown) and the range of the modelled estimates was much lower than that of the ^{14}C and FRRF data. The modelled data compared very similarly to both sets of FRRF estimates for L4 (from photosynthetic parameters and FRRF PE curves) and a high variance was explained. In contrast, the statistics for regressions of estimates from the Morel model against the ^{14}C estimates for L4 were poor but also misleading as they are strongly influenced by only two of the 24 points (23rd Apr 2001 and 30th Apr 2001). For example, despite the slopes of these regressions being less than one, suggesting that the higher estimates were predicted by the ^{14}C technique, the satellite model predicted higher production than ^{14}C in 23 of the 24 cases. There is very good agreement between production estimated from the Morel model and from the FRRF at L4. The variance explained increased when measured PAR was used and the slope of the curve was closer to 1 when modelled K_{PAR} values were replaced with measured values. When modelled K_{PUR} was replaced with measured K_{PUR}, the percentage of the variance in FRRF estimates decreased because the measured values were derived from ^{14}C, not the FRRF.

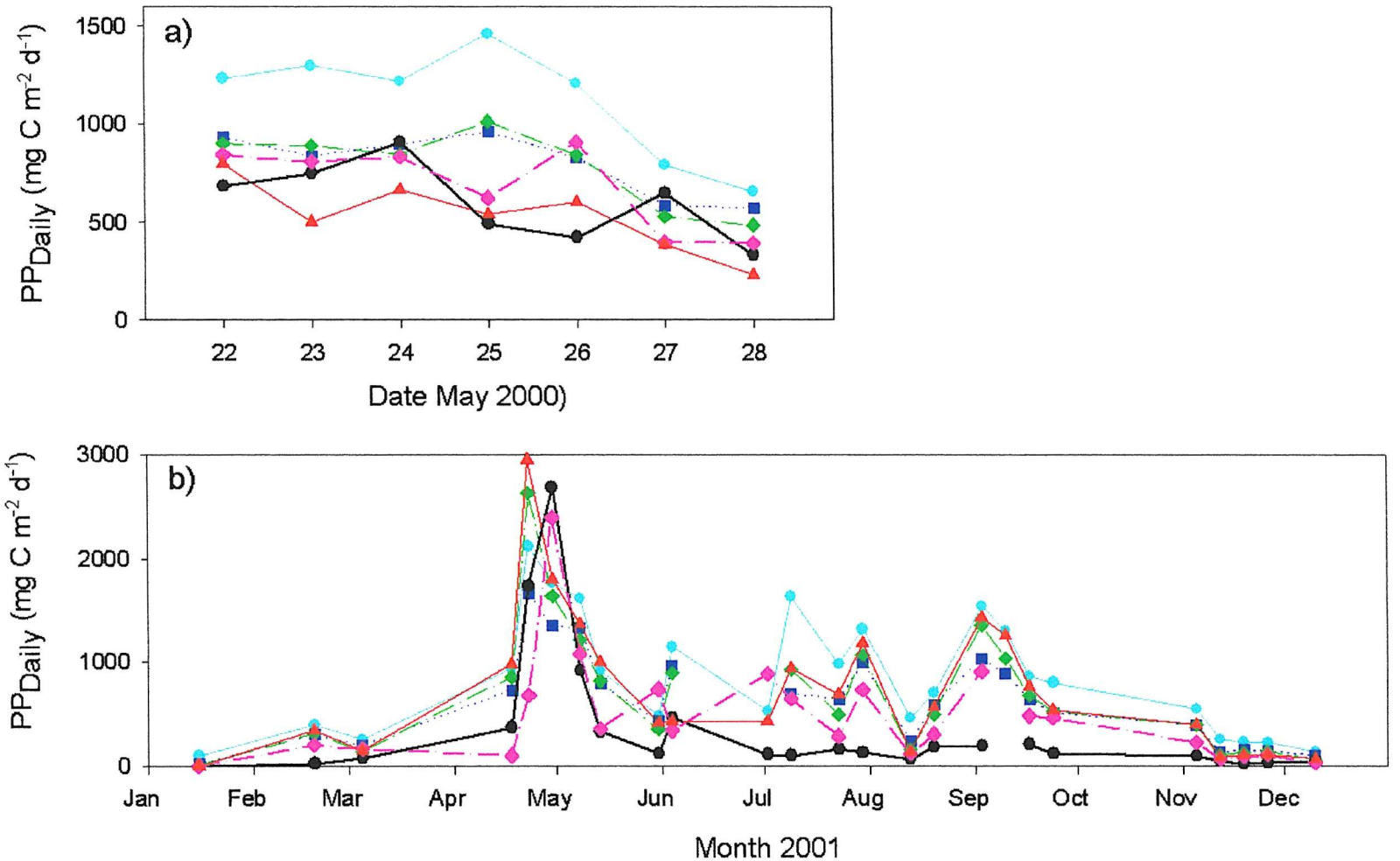

Figure 5.22. PP_{Daily} modelled from ^{14}C , the FRRF and from the Morel model run using different combinations of modelled and measured parameters a) in the Celtic Sea and b) at L4: ^{14}C photosynthetic parameters (●), FRRF PE curve (▲), Morel model with modelled PAR, modelled K_{PAR} and modelled K_{PUR} (●), Morel model with measured PAR, modelled K_{PAR} and modelled K_{PUR} (■), Morel model with measured PAR, measured K_{PAR} and modelled K_{PUR} (◆) and Morel model with measured PAR (▼). All values were integrated over the top 30m of the water column

Table 4. Statistics from regressions of PP_{Daily} estimates from the Morel model against ^{14}C and FRRF estimates. PP_{Daily} from the Morel model was always the dependent variable. All combinations of modelled and measured data were repeated with the depth of the euphotic zone modelled and with it fixed at 30m. Key: psp = photosynthetic parameter model, FRRF PE = FRRF PE curve type model. The K_{PUR} value used was calculated using data from the appropriate technique (^{14}C or FRRF) for each comparison in the Celtic Sea but only from ^{14}C at L4.

Study	Independent variable	Parameters used in Morel model			Depth of euphotic zone			
		PAR	K_{PAR}	K_{PUR}	30m R^2	Modelled R^2	30m Slope	Modelled Slope
Celtic	^{14}C psp	MOD	MOD	MOD	0.12	0.11	0.50	0.40
Celtic	^{14}C psp	MEAS	MOD	MOD	0.15	0.10	0.31	0.32
Celtic	^{14}C psp	MEAS	MEAS	MOD	0.10	0.10	0.31	0.32
Celtic	^{14}C psp	MEAS	MEAS	MEAS	0.17	0.16	0.45	0.85
Celtic	FRRF PE	MOD	MOD	MOD	0.53	0.52	1.13	0.91
Celtic	FRRF PE	MEAS	MOD	MOD	0.72	0.71	0.73	0.64
Celtic	FRRF PE	MEAS	MEAS	MOD	0.59	0.58	0.82	0.85
Celtic	FRRF PE	MEAS	MEAS	MEAS	0.82	0.83	0.57	1.06
Celtic	FRRF psp	MOD	MOD	MOD	0.28	0.27	0.49	0.39
Celtic	FRRF psp	MEAS	MOD	MOD	0.42	0.42	0.34	0.3
Celtic	FRRF psp	MEAS	MEAS	MOD	0.29	0.28	0.35	0.36
Celtic	FRRF psp	MEAS	MEAS	MEAS	0.39	0.38	0.24	0.44
L4	^{14}C psp	MOD	MOD	MOD	0.47	0.45	0.64	0.60
L4	^{14}C psp	MEAS	MOD	MOD	0.56	0.53	0.53	0.53
L4	^{14}C psp	MEAS	MEAS	MOD	0.58	0.56	0.75	0.77
L4	^{14}C psp	MEAS	MEAS	MEAS	0.63	0.66	0.65	0.65
L4	FRRF PE	MOD	MOD	MOD	0.84	0.82	0.78	0.73
L4	FRRF PE	MEAS	MOD	MOD	0.87	0.82	0.60	0.60
L4	FRRF PE	MEAS	MEAS	MOD	0.97	0.95	0.87	0.90
L4	FRRF PE	MEAS	MEAS	MEAS	0.14	0.37	0.16	0.44

For comparisons between the remote sensing algorithms the models were run in their default modes (i.e with modelled parameters) and assuming a euphotic depth of 30m (Figure 5.23). The empirical model has not been shown to make the graphs clearer. The VGPM model gave estimates over twice as high as either the Morel model or the ^{14}C or FRRF approaches.

Results from the Morel model, even in its default mode, showed good agreement with those from the ^{14}C and FRRF techniques. The satellite production estimates were plotted against ^{14}C and FRRF estimates as shown in Figure 5.24. As noted earlier, the estimates from the empirical model were of a similar magnitude to those from ^{14}C but the model is of limited applicability in areas outside the one for which it was developed. In plots of production from the VGPM model against the ^{14}C and FRRF data, all the data points lie above the 1:1 line (Figures 5.24b, c, g and h). The estimates from the Morel model compared reasonably well with the ^{14}C estimates but were always much higher than them when the Morel model was run in its default mode. The best comparisons were seen between the Morel model and the estimates from the FRRF. For L4 data, 84% of the variance was explained by the regression of production estimates from the Morel model against those from the FRRF and the slope of the line was 0.78 (see Table 5.5). The confidence intervals on average production from all the techniques were very high due to the high production estimates from the VGPM model (see Figure 5.25). In the Celtic Sea, the standard deviations around the mean production

Table 5.5. Statistics from regressions of PP_{Daily} estimates from both ^{14}C and FRRF techniques against one example from each of the satellite models. All data were integrated to 30m and satellite models were run using modelled parameter values. ^{14}C values were from photosynthetic parameter models and FRRF were from PE type curve models. FRRF estimates were not run against the empirical model as it was empirically derived from ^{14}C data.

Study	Independent	Dependent	R^2	Slope
Celtic	^{14}C	Empirical	0.45	0.42
Celtic	^{14}C	VGPM	0.32	1.37
Celtic	^{14}C	Morel	0.12	0.24
Celtic	FRRF	VGPM	0.50	1.12
Celtic	FRRF	Morel	0.53	0.56
L4	^{14}C	Empirical	0.58	0.39
L4	^{14}C	VGPM	0.71	1.80
L4	^{14}C	Morel	0.63	0.65
L4	FRRF	VGPM	0.47	1.88
L4	FRRF	Morel	0.84	0.78

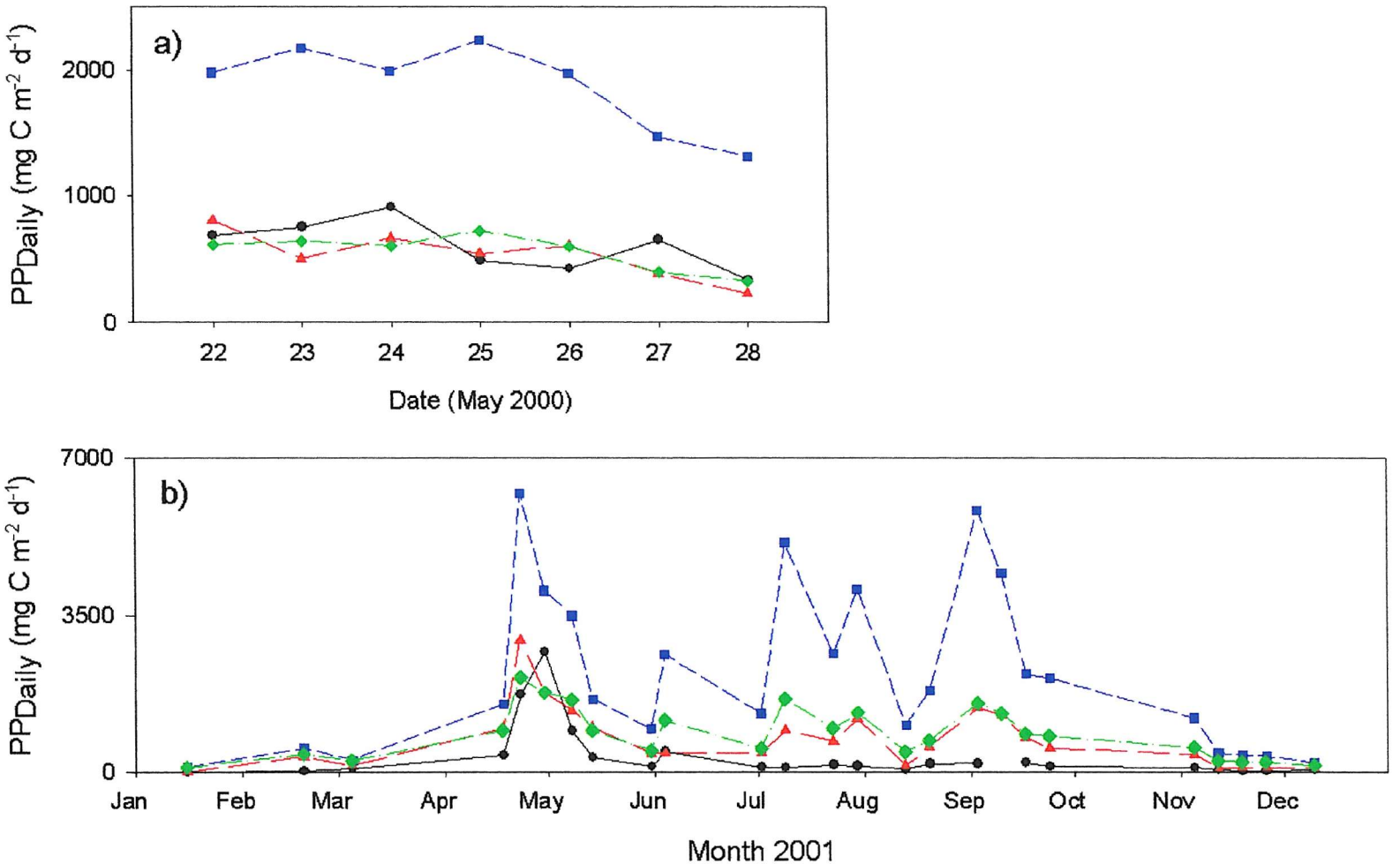

Figure 5.23. PP_{Daily} modelled using the each of the models in their default modes a) in the Celtic Sea and b) at L4. ^{14}C (●), FRRF (▲), VGPM model (■) and Morel model (◆). All data were integrated over the top 30m of the water column. Results from the empirical satellite model not shown to keep results clear.

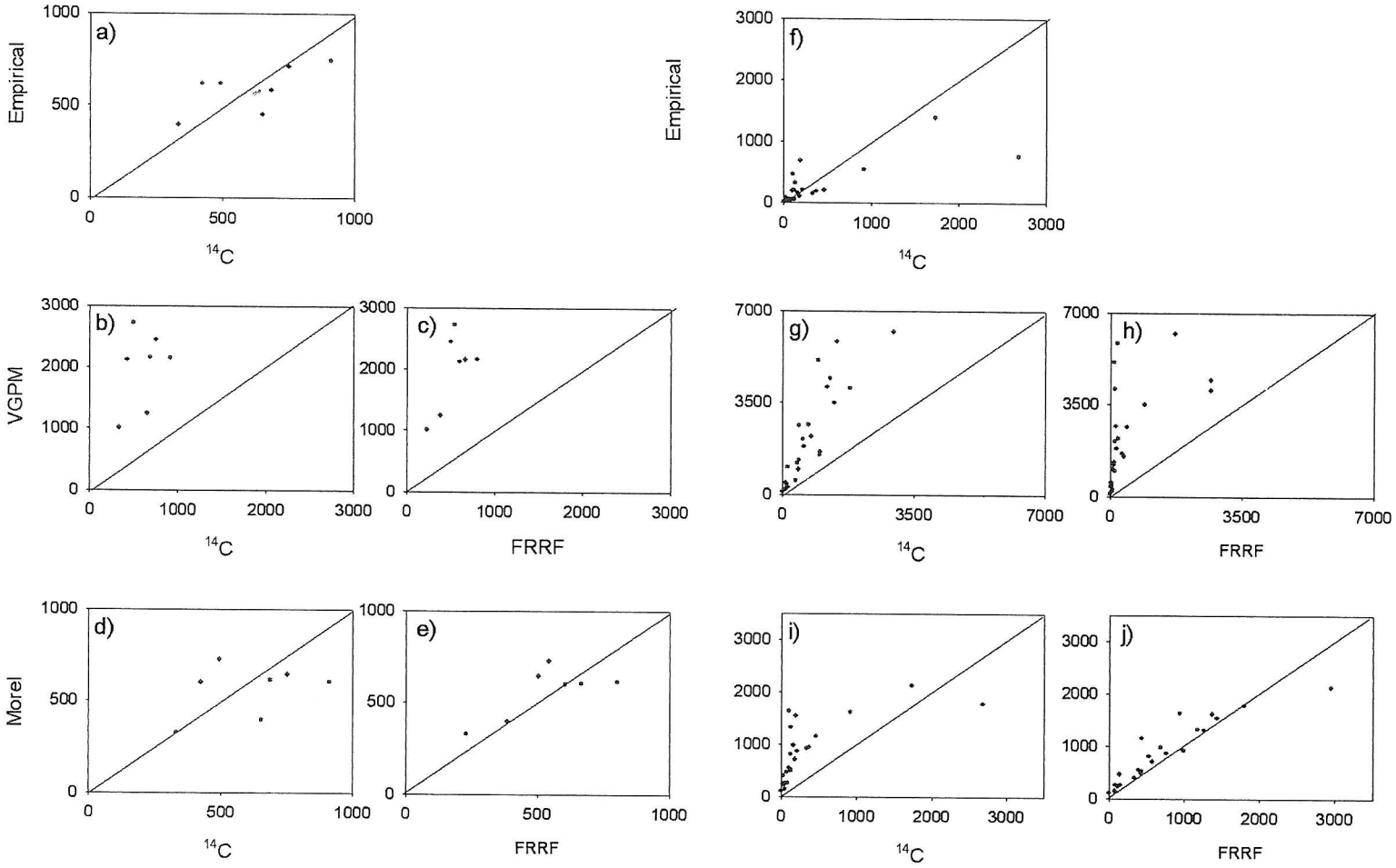

Figure 5.24. Plots of PP_{Daily} form satellite models against that derived from ^{14}C and FRRF approaches a) to e) for the Celtic Sea and f) to j) for L4. All axes show production in mg C m^{-2} d^{-1}. The 1:1 lines are shown.

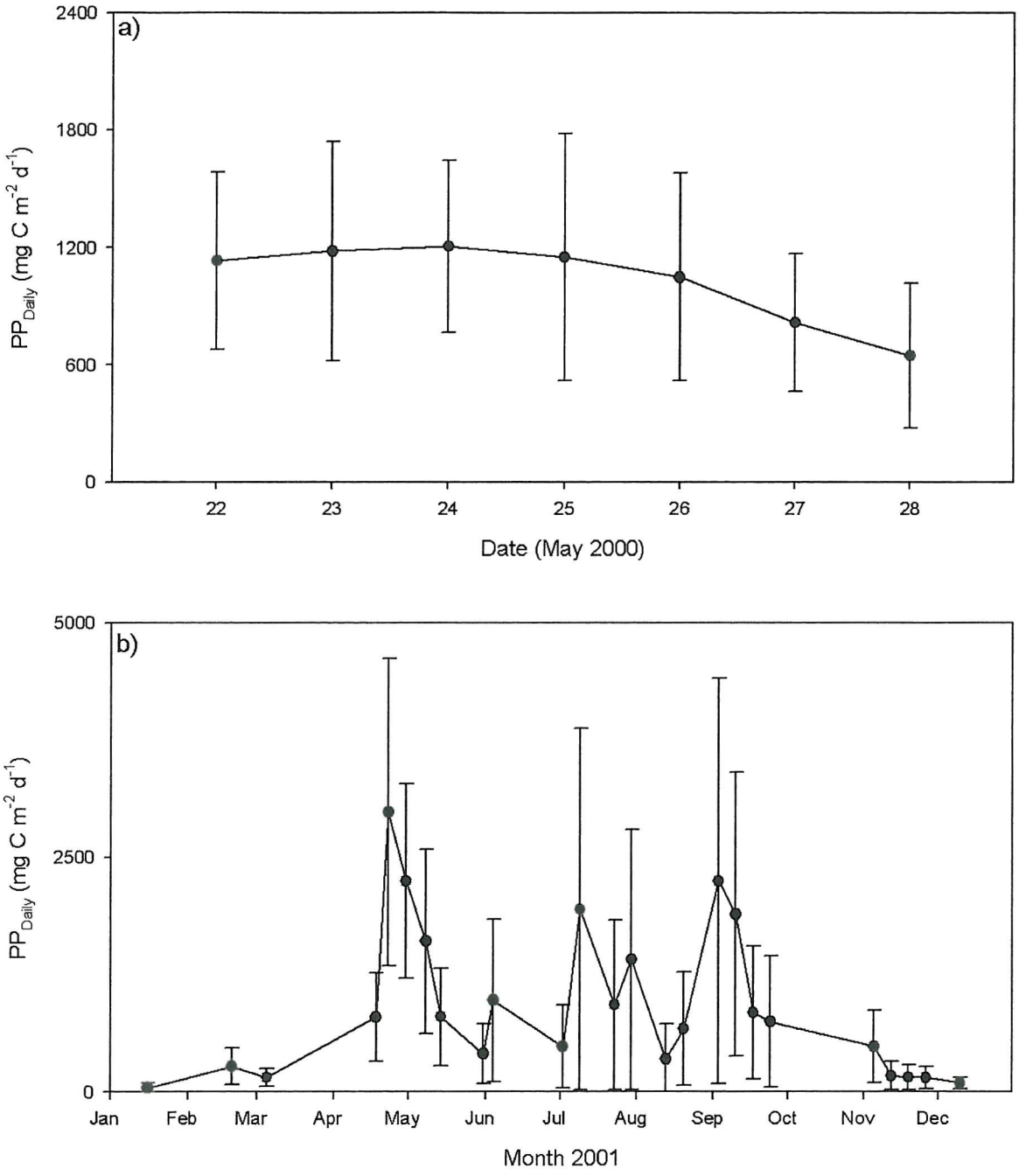

Figure 5.25. Average PP_{Daily} calculated from all the techniques a) for the Celtic Sea and b) for L4. All data were integrated over the top 30m of the water column and satellite models were run in their default modes. Results from the empirical satellite model were included in the average. The error bars show the 95% confidence intervals.

estimates were fairly constant over the course of the cruise. At L4 the time of greatest discrepancy between models was during the summer months and this is reflected in the relatively large error bars at this time.

5.3 Discussion

The data collected highlight the impact of cloud cover on the use of satellite remote sensing in the region studied. The proportion of dates where *in situ* sampling coincided with quality controlled high resolution satellite images was very low (17% of days studied which means that for 83% of the days on which *in situ* measurements were made, no satellite data were available). At L4, after the quality control process, satellite data were only available for 13% of the total number of days over 2000 and 2001. There was only one satellite image available from the Celtic Sea cruise. For satellite remote sensing to provide a suitable alternative to *in situ* measurements, the frequency with which satellite data are available needs to be high enough to reliably monitor the time scales of the oceanic processes under study.

The chlorophyll values used were the averages of the nine clear pixels surrounding and including the pixel of interest (within which the sample was taken). For the SeaWiFS validation process, NASA applied stringent exclusion criteria to remove potentially unreliable data. The details of these are listed in McClain *et al.* (2000) but the main criteria were as follows: 1) *in situ* measurements had to be taken at the time of the satellite overpass ± 180 minutes to ensure reasonable illumination and comparable atmospheric conditions, 2) pixels were removed where flags indicated the failure of atmospheric correction or the occurrence of sun glint, unusually high total radiance, high satellite zenith angle, clouds, ice or coccolithophores, 3) five of the nine pixels had to be present and 4) the standard deviation of the nine pixels had to be less than the absolute value of 0.2. In this study the exclusion criteria were less rigorous: 1) *in situ* samples were taken at the time of the satellite overpass ± 240 minutes (4 hours), 2) only pixels affected by cloud were automatically flagged and removed, 3) three of the nine pixels had to be present and 4) the standard deviation of the nine pixels had to be less than 25% of the average value. The relaxed criteria used in the study were necessary due to the inflexibility of the water sampling times and the difficulty in obtaining satellite data.

The high resolution (1km x 1km pixels) SeaWiFS data may be more susceptible to errors from patches of spurious reflectance than the low resolution (9km x 9km pixels) data.

If satellite remote sensing is to be used for large-scale studies both spatially and temporally then the 9km 8-day composite images may provide the most useful information. Any spurious patches of reflectance are not likely to cover the whole pixel nor to endure over the whole week so should not count significantly in the final value. However, if smaller scale processes are of interest, the high-resolution data are required. The high day-to-day variability between the high-resolution pixels means that these data are not routinely merged to make weekly composite images. The smaller pixels provide more information but the information is more susceptible to small-scale errors in the chlorophyll estimate from the satellite. The choice of resolution must depend on the type of study being carried out. Unsurprisingly, despite the good fit of most data around the 1:1 line, there are cases where low-resolution data and high resolution data show very different estimates of chlorophyll concentration (Figure 5.5c). This variability may be real, reflecting short term and small spatial scale variability or it may reflect unusual or spurious estimates from high-resolution data, which has been smoothed over in the larger scale data. It could alternatively reflect that the composite value in the large scale image was dominated by dates other than the one from which the high resolution data was extracted.

The regression of chlorophyll determined by HPLC against that from fluorometric techniques suggested a consistent relationship between the two data sets but that the fluorometric estimates were consistently higher than those from HPLC (Figure 5.1). Traditional fluorometric techniques can overestimate chlorophyll *a* due to interference from chlorophyll *b* but the Welschmeyer technique used here is thought to significantly reduce the interference from chlorophyll *b* and pheopigments and therefore increase the accuracy of the fluorometric estimates (Mantoura *et al.*, 1997). However, the higher chlorophyll *a* concentrations measured from fluorometry here probably do reflect interference from other pigments that are separated from the chlorophyll *a* by HPLC and not included in its total concentration. The necessity to remove data between 19th Aug 2001 and 19th Nov 2001 is highlighted and was due to suspiciously low fluorometric response at this time, despite ongoing calibration. A fault with the fluorometer power board was identified as the cause of the problem. Increased fluorometric response and a return to the expected relationship between HPLC and fluorometric estimates of chlorophyll suggested that the problem was resolved when the power board was replaced with a new one. An intercalibration exercise between the HPLC instrument and the spectrofluorometer was carried out to confirm this (see Appendix I).

Given the restrictions of the sampling regime at L4, it was not possible to collect water at the same time as the satellite overpass. Water samples were taken in the morning, 2-3h before the overpass so it is likely that the water body sampled at L4 was not the same one from which SeaWiFS chlorophyll estimates were retrieved. The good observed relationship between the measured data and the SeaWiFS estimates at the L4 pixel is likely to be coincidental. The poor relationship between measured chlorophyll and SeaWiFS chlorophyll estimates, at the position calculated to allow for tidal drift, may be the result of a number of problems. The discrepancies may reflect poor performance of the tidal drift model in calculating the expected new position of the water and, as samples were taken at the surface, strong winds may have led to deviations from the expected position. If the new positions are correct, then the poor agreement could be due to a change in atmospheric conditions between *in situ* sampling and the satellite overpass. It is possible that both the position is correct and the atmospheric conditions were the same as for *in situ* sampling but that the poor relationship reflects poor chlorophyll retrieval by SeaWiFS. This could be due to the turbid nature of the L4 site relative to the Case I waters for which the chlorophyll retrieval algorithm was designed. However, the data compared reasonably to the SeaBAM data set, which was dominated by samples from Case I waters. Not only that but the satellite estimates of chlorophyll used in the SeaBAM data were simulated based on water leaving radiance to give the value that would theoretically be obtained if atmospheric correction were perfect.

The two-band ratio satellite algorithm produces anomalously high chlorophyll values where high levels of CDOM, composed mainly of humic and fulvic particles of terrestrial origin, are present because its absorbance cannot be distinguished from that due to chlorophyll. The bright pixel approach (Moore *et al.*, 1999), despite improving chlorophyll retrieval in turbid waters is unlikely to entirely solve the problem of backscatter from SPM. The limited number of dates on which both measured CDOM or SPM values and satellite chlorophyll data were available made it difficult to determine their relationship. In particular, it had been of interest to see if poor correlations between measured and satellite chlorophyll coincided with high measurements of SPM or CDOM. High concentrations of both CDOM and SPM in January and February coincided with high estimated chlorophyll (Figure 5.8). However, CDOM absorbance also increased toward the end of the year but this was not seen in the satellite estimates of chlorophyll. The high scatter in the plots of SeaWiFS chlorophyll against CDOM and SPM suggest that the chlorophyll estimate is not uniquely dependent on

either of them. An additional problem in winter is the low sun angle, which can lead to poor atmospheric correction and unreliable SeaWiFS data.

A consistently anomalous data point occurred on 23rd April when the measured chlorophyll concentration was 6.41 mg chlorophyll m^{-3}, roughly three times the satellite estimate. The satellite estimate showed low standard deviation but no replicates were measured for the HPLC data so the expected variance associated with the measured value is unknown. However, the fluorometric measurement from the previous week (18th April) was also high (5.80 mg chlorophyll m^{-3}) which supports the high values measured by HPLC on 23rd April. On 30th April, assuming the HPLC measurements were correct, the signal received by SeaWiFS led to an extreme underestimate of chlorophyll concentration. The image was cloud free around the L4 site and the reason for the low chlorophyll estimate is unclear. The satellite measurements showed a chlorophyll peak roughly two weeks after the bloom measured by HPLC. On this date (8th May) the satellite estimated 14.2 mg chlorophyll m^{-3}, much higher than the measured value on the same day (3.44 mg chlorophyll m^{-3} and 5.58 mg chlorophyll m^{-3} from HPLC and fluorometry respectively) and twice as high as the satellite estimate from the previous day so it is probably incorrect. The very high SeaWiFS chlorophyll estimate is difficult to explain. Three of the pixels on the image near L4 are cloud covered so the possibility of stray light causing the error was considered. Stray light errors occur in two ways but both are due to the proximity of a bright pixel close to the pixel of interest. The first effect is caused by light from the bright pixel being scattered by the atmosphere into the area above the pixel of interest. The second effect occurs because the SeaWiFS sensor takes time to regain sensitivity after it has been saturated so chlorophyll concentration in pixels adjacent to bright pixels may be overestimated. A large patch near station L4 also shows very high concentrations of chlorophyll and the L4 pixel was close to the edge of this patch so may have suffered from stray light.

Another cause of discrepancies between satellite estimates and measured values of chlorophyll is deviation from the expected ratio of chlorophyll *a* to accessory pigments (Aiken *et al.*, 1995). This ratio is thought to be constant over a wide range of ocean types and this consistency is essential for chlorophyll retrieval to be accurate as it provides the ability to measure chlorophyll *a* concentrations based on the absorption of accessory pigments (particularly carotenoids). However, the ratios of individual accessory pigments to chlorophyll *a* can vary as a function of taxonomic composition, physiological state, nutrients, temperature, light intensity and spectral composition and photoperiod (Trees *et al.*, 2000).

Trees *et al.* (2000) studied the relationship between accessory pigments and chlorophyll *a* and observed that Case II waters showed statistically different slopes and intercepts to global patterns and such deviations could lead to incorrect estimates of chlorophyll concentration. Where total pigment concentration is low, a higher proportion of it is made up of accessory pigments and *vice versa* (Trees *et al.*, 2000), which would lead to the satellite overestimating chlorophyll *a* in cases of low total pigment and underestimating it in areas of high total pigment concentration. Unfortunately, the accessory pigment data were not compared as part of this study.

A strong relationship between chlorophyll and production (from ^{14}C) was seen in the data from both the Celtic Sea and at L4 (Figure 5.10). The lower number of data points in the Celtic Sea and the low variability of data may have been the reason for the poorer regression statistics compared to those from L4 data. The relatively low measured production on 16th January at L4 is likely to have been due to light or temperature limitation of photosynthesis. The relationship between the results from the empirical model and the ^{14}C measured production reflect the importance of biomass in determining the magnitude of carbon fixed in photosynthesis. However, the high scatter around the 1:1 line seen for the L4 data reflects the importance of other environmental variables, such as light and nutrients, in modifying the photosynthetic response per unit biomass over the changing seasons. The outlying point, on 30th April, showed higher production measured by ^{14}C per unit chlorophyll than described by the model. This date was during the spring bloom when nutrient concentrations are high and there is enough light to allow phytoplankton to rapidly increase in number; the higher production per unit chlorophyll, measured on this date may be due to an underestimate of chlorophyll. The empirical model has the advantage of being very simple and it explained 66% of the variance in values measured by the ^{14}C method. However, the variable relationship between chlorophyll concentration and carbon fixation are major disadvantages leading to a limited applicability outside the time and location of the original data collection.

The VGPM model always overestimated production compared to ^{14}C and FRRF estimates and explained between 11% (model run with Z_{eu} of 30m and P^B_{opt} against ^{14}C estimates for the Celtic Sea) and 89% (model run with modelled Z_{eu} and P^B_m against ^{14}C estimates for L4) of the variance in production estimates from ^{14}C and the FRRF. The euphotic depth calculated for the VGPM model, using the relationship described by Morel (1988) was generally shallower than that calculated from PAR measurements. This model, therefore, predicted higher attenuation than observed which was contrary to the expected results. Since

only chlorophyll was included in the calculation of the euphotic depth, whilst in reality the water contained other light scattering substances, it was expected that the predicted euphotic depth would be higher than measured. For the VGPM model, the modelled euphotic depth was low so integrating to 30m led to an increase in estimates of PP_{Daily}. The way algal physiology was included in the VGPM and Morel models were different. No method is available for the remote sensing of photosynthetic parameters so that bio-optical modelling requires equating measurable environmental variables to physiological fitness. Behrenfeld and Falkowski (1997a), noted that the P^B_{opt} factor in their model is responsible for most of the unexplained variability observed in the model results. P^B_{opt} is regulated mainly by P^B_m, itself determined by the enzymatically controlled Calvin cycle and, therefore, by temperature (Behrenfeld and Falkowski, 1997a). The high order polynomial model used to calculate P^B_{opt} as a function of temperature is described as only a preliminary model but is easy to implement as temperature is a variable that can be remotely sensed and is theoretically a good indicator of potential productivity given no other limiting conditions. P^B_{opt} was found to be much higher than measured P^B_m values. In the Celtic Sea, the low range of temperatures led to very consistent values of P^B_{opt} over the study whilst for L4, the dependence on temperature was clear and P^B_{opt} increased over the summer with water temperature. As a result, the expected summer depression in productivity due to nutrient limitation was completely absent in the model predictions.

The Morel model explained between 10% (model run with measured PAR, measured K_{PAR} and modelled K_{PUR} against ^{14}C estimates for the Celtic Sea) and 97% (model run with measured PAR, measured K_{PAR} and modelled K_{PUR} against FRRF estimates for L4) of the variance in production estimates from ^{14}C and the FRRF and the magnitude of the estimates were similar to each other. The modelled surface PAR values, required for the Morel model, were clearly affected by the lack of the inclusion of cloud cover (Figure 5.16). A study into the atmospheric aspects of PAR modelling was outside the remit of this study but the data sets emphasised how important cloud cover is in controlling the day-to-day variability of PAR. The PAR model was designed for marine aerosols but at coastal sites, such as L4, aerosols from land are likely to have had an impact on the irradiance at the surface of the water. However, where wide ranges of PAR were included such as at L4, the modelled and measured values compared well when regressed against each other. The poor regression statistics from the Celtic Sea reflected the limited range of the data. In all cases, replacing modelled PAR with measured values in the Morel model led to an increase in the variance

explained by a regression, of the output against ^{14}C and FRRF data, but the effect on the slope of the regression was minimal.

The euphotic depth value from the Morel model was a direct function of the calculated attenuation coefficient, K_{PAR}. The K_{PAR} algorithm used in the Morel model was designed for Case I waters and was based on measured chlorophyll concentrations and published descriptions of the spectral attenuation of light by chlorophyll and water. In Case I waters, the non-linear effect of phytoplankton substances (chlorophyll and phaeophytin) are reasonably well understood and described by models (Morel, 1988) but the absorption by non-biological particles is not well understood and was not accounted for in the Morel model. In the Celtic Sea, the sites sampled were relatively far from terrestrial input and the modelled K_{PAR} estimates were generally higher than the measured values (Figure 5.18). At L4, the modelled K_{PAR} values were similar, but slightly lower, than the measured estimates for most of the year. The regressions for L4 showed two clear outliers where measured attenuation was much greater than predicted by the model and both these measurements were made in the winter when high levels of suspended particulate matter were present. The deviation in modelled K_{PAR} from the measured values was reflected by anomalously high predicted euphotic depths from the Morel model. For comparisons with each other and with ^{14}C and FRRF estimates, the models were all subsequently run to a standard depth of 30m to overcome the variability in euphotic depths estimated in each of the models.

In the Morel model, similar to P^B_{opt} in the VGPM, standard values of photosynthetically relevant parameters (a^*_{max} and $\phi_{\mu max}$) are modified by a temperature dependent function, K_{PUR}. The dependence of K_{PUR} on temperature differs from the temperature dependence of P^B_{opt} in a number of ways and the examples given below are taken directly from Behrenfeld and Falkowski (1997a). Firstly, the K_{PUR} model was derived for growth and P^B_{opt} for photosynthesis, the difference being related to the effect of temperature on the carbon to chlorophyll ratios. Secondly, the K_{PUR} curve describes maximum rates whilst the P^B_{opt} model describes median rates. Finally, the K_{PUR} model shows an exponential increase between –1 and 29°C but P^B_{opt} decreases above 20°C. Behrenfeld and Falkowski note that above 20°C, the electron turnover rate of light reactions still increases with temperature so the observed decrease in P^B_{opt} above this temperature must reflect secondary controls of photosynthesis. These could include coincident nutrient limitation, increased susceptibility to photoinhibition, increased respiration rates and changes in species composition. As K_{PUR} describes the E_k values when primary production is plotted against PUR rather than PAR (Antoine and Morel,

1996), it was possible to compare the modelled values with measured estimates. This approach did not separate error due to the temperature function from that due to the initial assumption of a K_{PUR} of 80 units at 20°C but it was clear that the relatively high modelled K_{PUR} values at L4 from the summer onwards reflected a similar temperature dependence to that seen for P^B_{opt}.

As chlorophyll estimates at L4 were only made at the surface, the effect of the assumption of uniform biomass in the models was difficult to assess. However, as the site is well mixed for most of the year, the assumption is likely to be realistic for most of the year. In chapter 4 it was shown that adding stratification did not significantly change estimates of PP_{Daily} from ^{14}C and the FRRF models. Stratification in the Celtic Sea occurred at depths greater than 25m so the uniform biomass assumption was likely to have had a low impact as the depths at which the assumption was incorrect were also regions of low light where photosynthesis was likely to account for only a small fraction of total water column integrated values. A limitation of satellite sensors is that they offer no vertical resolution of the water column. The data is retrieved from only the first optical depth (Gordon and McCluney, 1975) – a value related to visibility that ranges from 20m in oligotrophic waters to 1-2m in coastal waters (Aiken *et al.*, 1992). In some conditions this could mean that an important portion of the total depth integrated primary production is not accounted for whilst in others, low light may limit the importance of production and hence of the biomass below the depth range of the detector.

The measurements made over the course of these studies have allowed not only the comparison of three different techniques but also have given an insight into the controls on primary production in the regions studied. In the Celtic Sea, changes in production were shown over one short period of time but for a relatively small geographical area whilst the study of L4 followed seasonal changes in primary production.

A large fraction of the annual production in the Celtic Sea occurs during the spring bloom, in April and May, with the formation of the seasonal thermocline, (Joint *et al.*, 2001 and Joint *et al.*, 1986). The phytoplankton spring bloom does not develop simultaneously over the whole region but starts to the south of Ireland and spreads eastwards as surface temperature increases (Pingree, 1975). The current study took place in late May 2000, about one month after the expected onset of the bloom. All stations experienced similar weather conditions and would have had comparable nutrient concentrations before the stratification of the water column (Pingree *et al.*, 1976).

The primary production measurements from ^{14}C in the Celtic Sea are discussed, in conjunction with measurements of nutrient concentration, information on phytoplankton species and satellite imagery of fronts, in a manuscript entitled "The influence of water mass characteristics on phytoplankton production in the Celtic Sea" (submitted to Continental Shelf Research. See Appendix IV). The following discussion summarises the findings and compares the measurements of production by the ^{14}C method, the FRRF and from satellite models, in the context of the hydrographic and nutrient conditions encountered. The whole study was carried out over 10 days at seven stations but this discussion will only focus on the second half of the cruise when photosynthetic parameters from ^{14}C and the FRRF were both obtained. The stations considered were to the south of the tidal front between the Celtic and Irish Seas and were seasonally stratified. At station G, experiments were done over a 72h period (22 to 24 May) and at both stations E and F, sampling took place over 48 h periods (25 to 26 May and 27 to 28 May respectively).

The similarity between photosynthetic parameter values from ^{14}C and the FRRF at these stations was recorded and discussed in sections 4.2.1.3 and 4.3 respectively. In the context of the controls on production, it is interesting that the large changes in photosynthetic parameter values, as recorded by ^{14}C, over the two dates of sampling at stations E and F were not apparent in the FRRF data (Figure 4.4). The day-to-day variability recorded by the FRRF was similar within each of stations G, E and F. As discussed earlier and in more detail, the differences in the patterns of change shown by the two techniques may reflect the difference between fluorometric and chemical measurements and between instantaneous measurements and those that represent integrated values over the duration of an incubation. The overall variability in parameters during the cruise was low so the different patterns of day-to-day variability recorded by each technique may not be important when considered in the context of larger scales. However, understanding the controls on production is very important and the two techniques could lead to different conclusions in this context.

Primary production measurements were made from 24h *simulated-in-situ* incubations with ^{14}C as well as using the ^{14}C and FRRF models previously discussed. In section 3.2.2.2 estimates of PP_{Daily} from this technique were compared with those from ^{14}C photosynthetic parameter incubations and were higher than them. In section 4.2.3 PP_{Daily} estimates from the ^{14}C photosynthetic parameter model were shown to be generally lower than those from the FRRF models, as expected given the different processes measured by each technique. In all

but two cases (24th and 26th May), the production estimates from the 24h *simulated-in-situ* incubations were higher even than the FRRF modelled values. Reasons for the consistently higher values from *simulated-in-situ* incubation were discussed (in the context of their comparison with production estimates from ^{14}C photosynthetic parameters) in section 3.3 and included differences in the light regimes and possible photoacclimation of samples in the *simulated-in-situ* incubations (Harrison *et al.*, 1985) as well as the possibility of unnatural build up of chlorophyll in the *simulated-in-situ* samples (Cullen *et al.*, 1992). It is remarkable that the *simulated-in-situ* values are higher than FRRF estimates and suggests either that the measurement from the on-deck incubations is closer to gross primary production than net community production, contrary to popular opinion, or reflects extreme artefacts introduced during incubations on deck for such long periods of time. When considering the reliability of these production estimates, it is worth remembering that the ^{14}C *simulated-in-situ* values are the only estimates that were measured directly, rather than extrapolated from short-term estimates using a model.

Production estimates from the empirical and Morel satellite algorithms were of a similar magnitude to those from ^{14}C and the FRRF (see sections 5.2.2 and 5.3). However, the VGPM model consistently over predicted production, especially when it was run with only modelled parameter values.

A large range of chlorophyll concentrations and production was measured over the small geographical area in the Celtic Sea. The stations were depleted of nutrients in the surface mixed layer and dominated by dinoflagellates. In the stratified waters, the flux of nutrients from below the thermocline to the surface mixed layer was low and most primary productivity is thought to depend on nutrients regenerated within the surface waters. There were no consistent differences in the photosynthetic parameters between different sites but a high degree of day-to-day variability was observed within each station and is thought to be a result of horizontal advection, due to tides or currents, having led to different phytoplankton populations being sampled in each case. With the exception of the *simulated-in-situ* measurements on the 22nd and 23rd May, the overall pattern of production over the course of the cruise was similar from the ^{14}C and FRRF techniques and similar conclusions would be drawn from the results of either. Satellite data was not considered, as only one image was available for the whole cruise, but production estimates from the empirical and Morel models, run with HPLC chlorophyll, were of similar magnitude to the ^{14}C and FRRF estimates.

The seasonal studies at L4 showed how the different techniques recorded the changes in production over the course of the year. All techniques showed similar changes in production over the seasons and agree with previous reports (Rodriguez *et al.*, 2000; Maddock *et al.*, 1981 and Holligan and Harbour, 1977). The changes in phytoplankton and chlorophyll are determined by variations in the vertical stability of the water column and its control on the availability of light and nutrients (Pingree, 1975). The stabilisation of the water column allows phytoplankton sufficient time in the surface layer to utilize light energy to allow increased production and the timing of the spring and autumn diatom blooms depend on the timing of thermocline development. This is, in turn, dependent on the turbulence derived from the tides and subsequent tidal stream amplitudes (Pingree, 1975).

Production increased from March to the spring bloom at the end of April. This increase reflects the onset of stratification creating a shallow surface layer where nutrients are replete and cells maintained in high light. Previous studies have reported the spring bloom in this region to be diatom dominated (Maddock *et al.*, 1981and Holligan and Harbour, 1977). From mid-May, the bloom declined as nutrients were used up in the surface layer. Over the summer, episodic blooms separate periods of otherwise low production. The blooms could be the result of episodic breakdowns of the thermocline and the subsequent injection of nutrients into the surface layer. Holligan and Harbour (1977) and Rodriguez *et al.* (2000) observed that during this period, the phytoplankton are dominated by dinoflagellates due to their high competitive ability in nutrient depleted conditions. The autumn diatom bloom occurred in early September and is likely to have been triggered by the breakdown of the thermocline and re-supply of nutrients to the surface layer. After the autumn bloom, a steady decline in production rates to low values over winter was recorded by all techniques.

The pattern of production rates measured using the FRRF is much more variable over the course of the summer than that from ^{14}C measurements. This variability is also seen in the estimates from remote sensing. The summer production peaks have been observed before at coastal stations in the Western English Channel (Rodriguez *et al.*, 2000 and Holligan and Harbour, 1977). It is unclear why they were not shown using the ^{14}C estimates but could be an artefact of the long incubations and may reflect high rates of dark respiration and therefore loss of assimilated carbon. This would suggest that, net production is less variable than gross production.

The spring and autumn blooms were recorded at the same time by both ^{14}C and FRRF techniques but these were both strongly influenced by the measured chlorophyll estimate so the similarity is not surprising. As previously discussed, the late April chlorophyll peak was not recorded by SeaWiFS. For the full potential of satellite oceanography to be realised, full confidence in the estimation of chlorophyll from space is required and the failure of SeaWiFS to measure the spring bloom at the site highlights current limitations

5.4 Conclusions

The frequent occurrence of clouds combined with the fixed dates of sampling (irrespective of weather conditions) limited the comparisons, between satellite estimates and measured chlorophyll values, that could be made during the study. Cloud cover is likely to be an important factor when considering the application of SeaWiFS for point comparisons in temperate regions. It is important both in terms of the number of clear images available and in terms of the effect of clouds on the values obtained from apparently 'cloud-free' pixels. The complex nature of the optics of Case II waters and particularly the nature of water at the L4 site makes it very difficult to suggest a clear cause of inaccuracy in satellite estimates of chlorophyll. The discrepancies between SeaWiFS and measured chlorophyll were greatest in winter when high levels of CDOM and SPM were present in the water and the angle of the sun was very low making atmospheric correction difficult. Combinations of the many variables (SPM, CDOM, the chlorophyll: carotenoid ratio) can lead to a whole variety of impacts on chlorophyll retrieval by SeaWiFS and it is very difficult to separate the individual effects.

The VGPM model overestimated production compared to the other techniques. It underestimated the euphotic depth but vastly overestimated the maximum rate of production in the water column (P^B_{opt}). The change in production estimates from the VGPM and Morel models over the year at L4 reflected the change in temperature and this led to unexpectedly high predicted production during the nutrient depleted summer months. The estimates from the Morel model generally compared well with ^{14}C and FRRF estimates, particularly with those from the FRRF. Replacing modelled PAR with measured PAR always improved model predictions. This is partly due to the lack of cloud cover assumed when PAR was modelled. The modelled estimates of light attenuation were higher than those measured in the Celtic Sea but agreed well with the data measured at L4 except during periods when high levels of suspended particulate matter were present. Given the nature of the two study sites,

it appears that the modelled K_{PAR} was suitable for water bodies that fall between Case I and Case II classification. Using measured K_{PUR} in place of the modelled values also improved model estimates. Modelled values of K_{PUR} agreed much better with those estimated from FRRF data than from the ^{14}C data. This could reflect that the K_{PUR} model describes gross rather than net production. Variability in modelled K_{PUR} was much lower than in measured estimates. The temperature dependent photosynthetic parameters used in both models (P^{B}_{opt} and K_{PUR}) showed much less variability than the measured values, which reflects the multitude of environmental factors, other than temperature that affect photosynthetic performance.

The production estimates from satellite algorithms explained a greater proportion of the variance in estimates from the ^{14}C and FRRF methods, for data obtained from L4 than for the Celtic Sea data. This is thought to be due to the low range of conditions experienced in the Celtic Sea and to the low number of data points.

The satellite algorithms showed similar changes in production over the year to the estimates from ^{14}C and the FRRF. The estimates from the VGPM were, however, much higher than those from the other approaches. The complex semi-analytical Morel model did show improved performance in primary production estimation over the simpler models and this was even true when it was parameterised only with modelled values. Improved modelling of PAR should greatly improve the overall performance of the production models and should be possible given the availability of cloud cover data from meteorological stations. It is crucial to remember that the good performance of the satellite models is due, in a large part, to their parameterisation with measured chlorophyll values. Were the SeaWiFS chlorophyll estimates used instead, the pattern of production over the season would have been very different to that from the measured techniques and in particular, the spring bloom would have been recorded at a different time.

Chapter 6. Estimation of the uncertainty associated with estimates of PP_{Daily}

6.1. Background and introduction

To derive daily, depth-integrated production from the results of short-term experiments, algorithms are used for extrapolation from measured values using the changing irradiance field as the controlling parameter. The models require values to describe photosynthetic parameters, estimates of PAR at the sea surface over the course of the day and descriptions of how PAR decreases through the water column. All of these have associated errors and the uncertainty around the modelled value of primary production reflects the combined variability around each of the mean values used in the model. The complexity of the production models makes this variability difficult to calculate precisely but in order to understand the level of confidence in production estimates, some measure of the uncertainty associated with them is required. The main sources of uncertainty include errors on the measured values, the effect of aggregating parameters over time or space and, most seriously, the failure of the model to accurately describe the process of interest.

In the first part of this chapter, two different approaches are used to estimate the uncertainty associated with production estimates from the ^{14}C photosynthetic parameter model and from the FRRF photosynthetic parameter and PE curve models. The first is a theoretical approach (Taylor series) where error is calculated from a polynomial equation based on an understanding of the model and of the importance of each parameter in the final production estimate. In the second approach (Monte Carlo), repeated calculations of production are made using randomly generated numbers to parameterise the model and the error around the mean of the repeats is used as an indicator of the model uncertainty. The two different methods were chosen because they use different approaches to the same problem. It was assumed that if both approaches led to similar results, we could be confident in the values obtained.

In the second part of the chapter, the uncertainty of satellite derived production estimates is considered. The confidence limits on production estimates from the empirical chlorophyll model are calculated. Error was not calculated for estimates from the other satellite models

(VGPM and Morel) due to their complexity and the difficulty in estimating the error on each of the individual parameters in the algorithms.

6.2. Results

6.2.1 Development of Taylor series algorithm to calculate error on PP_{Daily} from ^{14}C incubations and the FRRF

Explanation of the calculation

The Taylor series was used to estimate the variance around the production estimate by weighting the error associated with each individual parameter in the production model (equations 55a or 57, repeated below for convenience) according to its overall importance in the production calculation.

$$PP_{z,t}^{(psparams)} = \left(P_m^B \left[1 - e^{\frac{\alpha^B \cdot PAR_{z,t}}{P_m^B}} \right] \right) \cdot [Chl] \qquad (55a)$$

Where $PP_{z,t}^{(psparams)}$ is depth and time specific primary production (mg C m^{-3} h^{-1}), P_m^B is the maximum potential light saturated photosynthetic rate under prevailing conditions, written as P_S^B in the earlier version of the equation and equal to it in this case of no photoinhibition (mg C [mg Chl]$^{-1}$ h^{-1}), α^B is the light limited rate of photosynthesis (mg C [mg Chl]$^{-1}$ h^{-1} [µmol photons m^{-2} s^{-1}]$^{-1}$), [Chl] is the average chlorophyll *a* concentration in the water column (mg m^{-3}).

$$PP_{z,t}^{FRRF(PE)'} = \left(Q \left[1 - e^{\frac{a \cdot PAR_{z,t}'}{Q}} \right] \right) \cdot [Chl] \qquad (57)$$

where $PP_{z,t}^{FRRF(PE)'}$ is depth and time specific primary production (mg C m^{-3} h^{-1}) and Q and a are parameters of the regression with the same units as P^B_m and α^B respectively. For a parameter to be included in the overall error calculation, the standard deviation associated with that parameter had to be known.

The error on the photosynthetic parameters from ^{14}C (α^B and P^B_m) was produced in the PE curve fitting procedure (see section 2.3.1.2) and that associated with K_{PAR} was the error on the fitted regression line used to describe K_{PAR} from the profile of light against depth (see section 2.7.1.1). The standard deviation was squared to calculate the variance. It was assumed that no error was associated with the HPLC chlorophyll measurements, as replicates were not made, nor with the measured PAR values at the sea surface.

The error (SD) on the photosynthetic parameters from the FRRF was calculated indirectly from the error on the parameters from which α^B and P^B_m were derived as shown in equations 58 and 59 respectively (see equations 22 and 23 for FRRF photosynthetic parameter equations).

$$SD\alpha^B(FRRF) = \alpha^B(FRRF) \cdot \sqrt{\left(\frac{SD\,F_v/F_m}{F_v/F_m}\right)^2 + \left(\frac{SD\sigma_{PSII}}{\sigma_{PSII}}\right)^2} \tag{58}$$

$$SD\ P_m^B(FRRF) = P_m^B(FRRF) \cdot \sqrt{\left(\frac{SD\alpha^B}{\alpha^B}\right)^2 + \left(\frac{SDE_k}{E_k}\right)^2} \tag{59}$$

The overall importance of each parameter in the equation was calculated using partial differentials of the production equation (equation 55a or 57). When an equation is partially differentiated it is done so with respect to one parameter, x for example, in that equation. The result (known as the "partial differential with respect to x") can be solved to calculate how much the solution to the original equation will change if all the parameters, except x, are held constant. This procedure shows the extent to which parameter x influences the result of the overall equation. This process was repeated for all the parameters included in the equation, for which error could be calculated.

The final part of the equation was the correlation factor for α^B and P^B_m. This step accounted for the fact that high variance in one parameter may always co-occur with high or low variance in another. In cases where parameters are negatively correlated, the inclusion of the correlation factor will lead to a decrease in the overall error and, conversely, the overall error will increase in cases where parameters are positively correlated. K_{PAR} was not correlated to the photosynthetic parameters so was not included in this section.

The Taylor series approximation was solved for every metre and every hour (to give $Variance\,PP_{z,t}$) and these values were integrated over the day and over the water column to calculate the overall daily variance ($Variance\,PP_{Daily}$). The standard error (SE) for the overall model was calculated as the square root of the variance and the 95% confidence intervals as 1.96*SE.

The Equations

The model was written in IDL version 5.3 and is included as Appendix II. The form of the calculation is shown in equations 60 to 62.

$$Variance\,PP_{Daily} = \int_0^D \int_0^{Z_{eu}} Variance\,PP_{(z,t)} \tag{60}$$

$$\text{where } Variance\,PP_{z,t} = \sum_{n=1}^{N} \left(\left(\frac{\partial PP_{z,t}}{\partial n} \right)^2 \cdot \text{var}\,iance(n) \right) + correlation\ factor \tag{61}$$

$$\text{where } correlation\ factor = \sum_{n=1}^{N} \left(\left(2 \cdot \left(\left(\frac{\partial PP_{z,t}}{\partial n1} \right) \cdot \left(\frac{\partial PP_{z,t}}{\partial n2} \right) \right) \right) \cdot Cov(n1, n2) \right) \tag{62}$$

The two production models (equations 55a and 57) have different inputs parameters but share the same form. The parameters included in the calculation of variance were P^B_m or Q, α^B or a and K_{PAR}. For simplicity, the parameters used in equation 55a will be used in the following explanation but the models are also relevant to the equivalent parameters from equation 57. In order to simplify the differentiation of the production equation, it was split into two subsections, termed A and B as shown in equations 63 and 64.

$$A = \exp\left(\left(-\frac{\alpha^B}{P_m^B} \right) \cdot PAR_0 \cdot e^{-K_{PAR} z} \right) \tag{63}$$

$$B = PAR_0 \cdot e^{-K_{PAR} z} \tag{64}$$

The overall production equation could then be described according to equation 65.

$$PP_{Daily} = \int_{0}^{D} \int_{0}^{Z_{eu}} P_m^B (1-A) \tag{65}$$

The partial differentials of the equations with respect to the parameters P_m^B, α^B and K_{PAR} are shown in Equations 66 to 68.

$$\frac{\partial PP_{z,t}}{\partial P_m^B} = (1-A) - \frac{A\alpha^B B}{Q} \tag{66}$$

$$\frac{\partial PP_{z,t}}{\partial \alpha^B} = BA \tag{67}$$

$$\frac{\partial PP_{z,t}}{\partial k_{PAR}} = -AB\alpha^B z \tag{68}$$

Equations 69 and 70 show the form of the correlation factor and the equation used to calculate the covariance (*Cov*) between $P^B{}_m$ and α^B respectively.

$$Correlation\ factor\left(P_m^B, \alpha^B\right) = \left(Cov\left(P_m^B, \alpha^B\right) \cdot SD\, P_m^B \cdot SD\, \alpha^B \cdot \frac{\partial P}{\partial P_m^B} \cdot \frac{\partial P}{\partial \alpha^B} \right) \tag{69}$$

$$Cov\left(P_m^B, \alpha^B\right) = Correlation\left(P_m^B, \alpha^B\right) \cdot SD\, P_m^B \cdot SD\, \alpha^B \tag{70}$$

6.2.2 Development of Monte Carlo model to calculate error on PP_{Daily} from ^{14}C incubations and the FRRF

Explanation of the calculation

The Monte Carlo approach was based on repeat calculations of production using randomly generated numbers. Random numbers, of normal distribution and within the expected limits, were generated for each of the parameters in the model (α^B, $P^B{}_m$ and K_{PAR}) and primary production calculated for each group of random numbers. One hundred replicate estimates of

production were calculated for each depth and time interval and the standard deviation of the replicate estimates around the mean taken to equal the error associated with the model. The overall daily error was calculated by integrating these values over depth and over the day.

The generation of normally distributed random numbers, within the expected limits required three stages. In the first, normally distributed numbers with values between 0 and 1 were generated using an in-built function in IDL. In the second stage, the random value assigned to α^B was altered to account for its correlation with the value of P^B_m. Finally, the measured parameter values and their associated standard deviations were used to convert the random numbers into values within the expected ranges.

The equations

The model was written in IDL version 5.3 and is included as Appendix III. Normally distributed random numbers, with mean of 0 and standard deviation of 1, were generated using an inbuilt IDL function (RANDOMN), which was based on the Box-Muller method. These numbers are referred to x1, x2 and x3 and correspond to parameters P^B_m, α^B and K_{PAR} respectively. The correlation between P^B_m and α^B was included by converting x1 and x2 to a pair of correlated normal variables, y1 and y2, according to equations 71 and 72.

$$y1 = x1 \tag{71}$$

$$y2 = \rho \cdot x1 + \left(\sqrt{1-\rho^2}\right) \cdot x2 \tag{72}$$

where ρ is the correlation between P^B_m and α^B. K_{PAR} was not correlated to the other variables so y3 was calculated according to equation 73.

$$y3 = x3 \tag{73}$$

Finally, y1, y2 and y3 were converted to the random numbers for use in the model by an adjustment to make the mean and standard deviation fall in the expected range as shown in equations 74 to 76.

$$rP_m^M = \mu\left(P_m^B\right) + \left(SD\left(P_m^B\right) \cdot y1\right) \tag{74}$$

$$r\alpha^B = \mu(\alpha^B) + (SD(\alpha^B) \cdot y2) \quad (75)$$

$$rK_{PAR} = \mu(K_{PAR}) + (SD(K_{PAR}) \cdot y3) \quad (76)$$

Where rP^B_m, $r\alpha^B$ and rK_{PAR} refer to the random estimates of P^B_m, α^B and K_{PAR} respectively and the parameter values on the right hand side of the equation relate to the measured means (μ) and standard deviations (SD).

6.2.3 Calculated error on PP_{Daily} from ^{14}C incubations and the FRRF

The error on daily production estimates was integrated over the top 30m of the water column. Both approaches (Taylor series and Monte Carlo) led to similar estimates of the 95% confidence intervals (see Figures 6.1 and 6.2) and in all but one case (the Celtic Sea FRRF PE curve model), the errors from the Monte Carlo approach were higher than those from the Taylor series approach. The maximum relative confidence intervals (as percentages of the means) were found for the production estimates from the photosynthetic parameter models in the Celtic Sea. The maximum confidence interval from the FRRF photosynthetic parameter model (from the Monte Carlo approach) was 109% of the average production estimate whilst that from the ^{14}C photosynthetic parameter model was 49% of the average production estimate (see Table 6.1). Generally the confidence intervals from L4 were much lower than those from the Celtic Sea but they were highly variable around the ^{14}C data at L4 where they ranged from 8% to 60% of the mean.

Table 6.1. The 95% confidence intervals associated with estimates of PP_{Daily} from ^{14}C and FRRF approaches. The values are the minimum and maximum relative confidence intervals where the relative confidence interval is the 95% confidence interval as a percentage of the production estimate. Confidence intervals were calculated using the Monte Carlo modelling approach.

Study	Model ^{14}C photosynthetic parameters	FRRF photosynthetic parameters	FRRF PE curve
Celtic Sea	27-49	55-144	5-13
L4	8-60	NO DATA	3-40

The estimated errors were derived from the standard deviations of the estimates of P^B_m, α^B and K_{PAR} (see Figure 6.3). In the Celtic Sea, the standard deviations were highest on the

photosynthetic parameters from the FRRF whilst the error on the FRRF PE curve parameters was relatively constant and low over the course of the cruise. At L4, the magnitudes of the standard deviations of the means were highly variable. The standard deviations on P^B_m values from ^{14}C were generally higher than those from the FRRF PE curve but the errors on estimates of α^B were similar from both techniques.

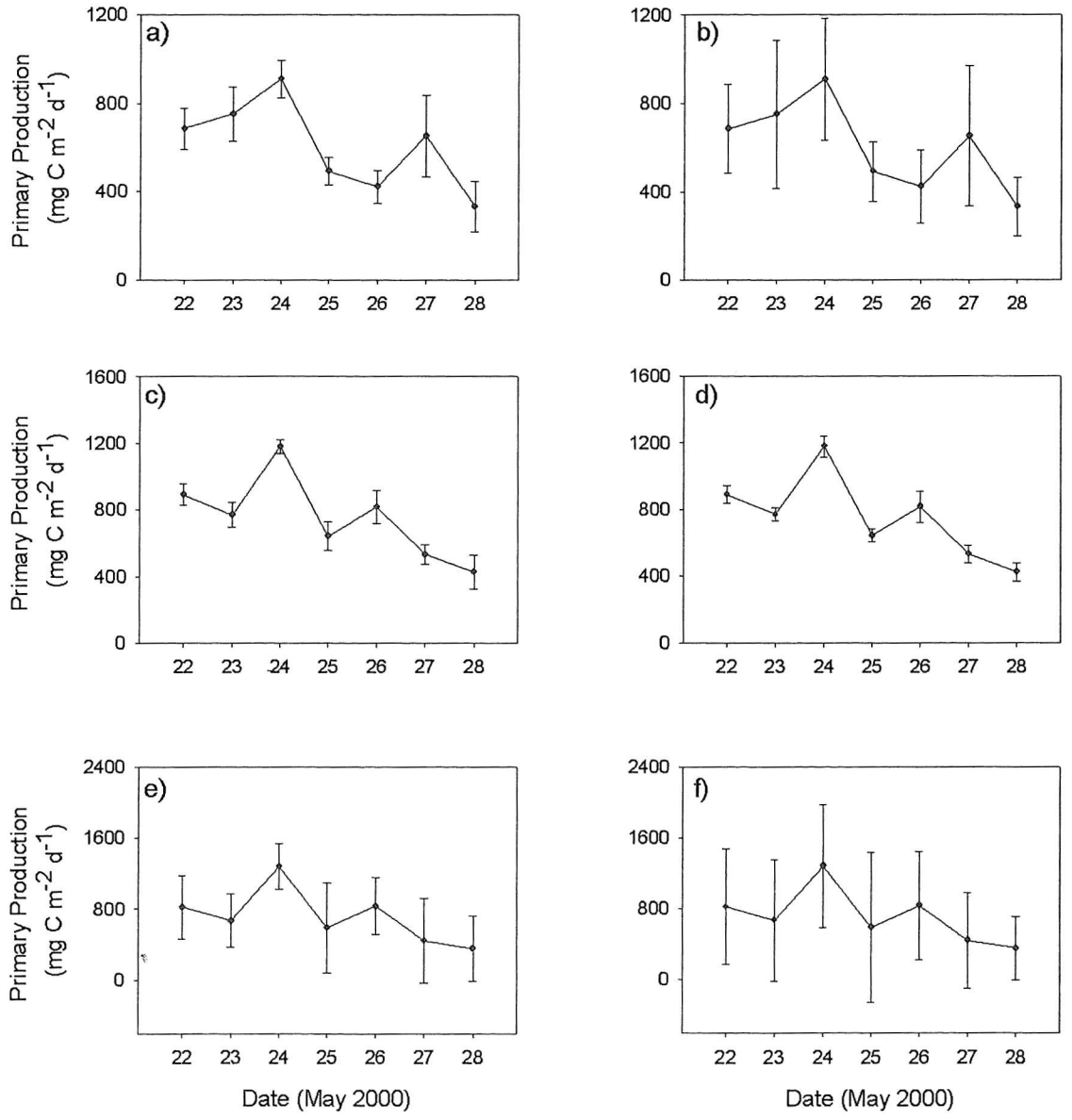

Figure 6.1. The 95% confidence intervals associated with production estimates for the Celtic Sea. Production was modelled from a & b) ^{14}C photosynthetic parameters, c & d) FRRF PE curve parameters and e & f) FRRF photosynthetic parameters. The confidence intervals were calculated from a, c & e) the Taylor series and b, d and f) Monte Carlo modelling approaches.

6.2.4 Calculated error on estimates of PP_{Daily} from the empirical satellite algorithm

The confidence limits calculated for the empirical chlorophyll model of production are shown in Figure 6.4. The potential errors are very high, increasing as the production estimates increase and highest for L4 during the Spring and Autumn blooms. The form of the calculation means that this error is purely due to how well the derived equation described the relationship between chlorophyll and primary production. It does not account for any error in satellite chlorophyll retrieval as the model was run using chlorophyll measurements from HPLC.

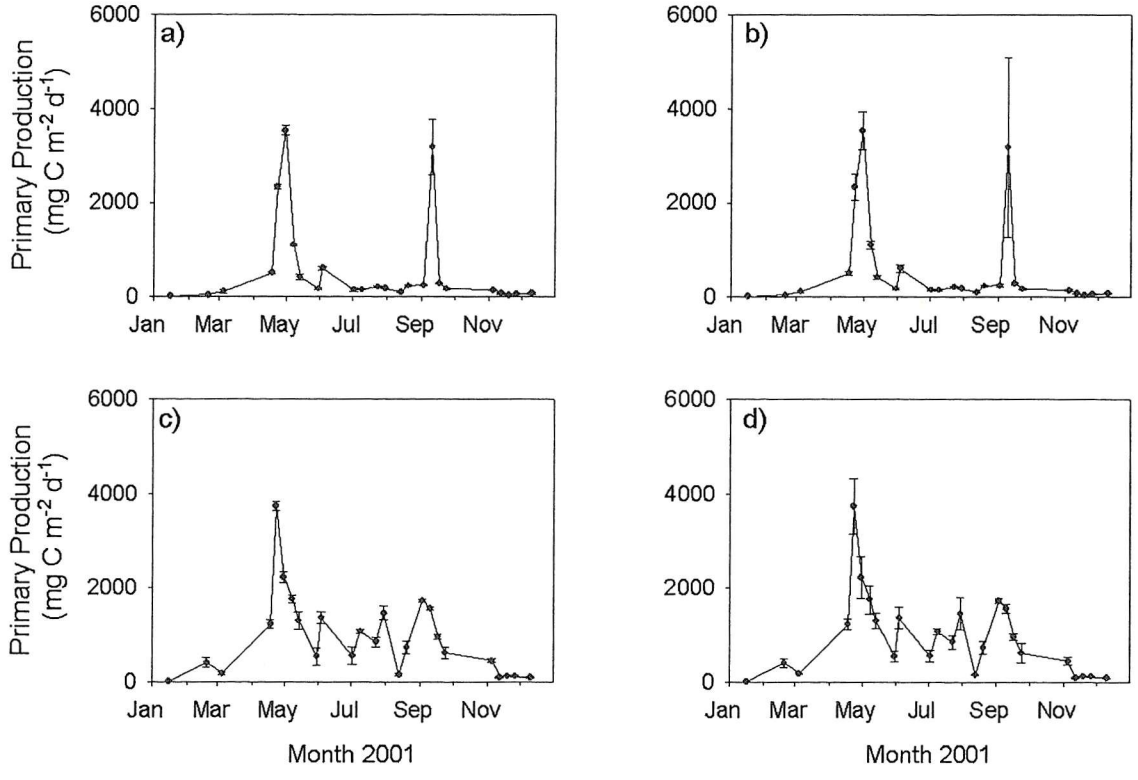

Figure 6.2. The 95% confidence intervals associated with production estimates for L4 in 2001. Production was modelled from a & b) ^{14}C parameters and c & d) FRRF PE curve parameters. The confidence intervals were calculated from a & c) the Taylor series and b & d) Monte Carlo modelling approaches.

6.3 Discussion

The way in which the error from the Taylor series approximation was combined over depth and time led to lower integrated error than predicted by the Monte Carlo model. The Taylor

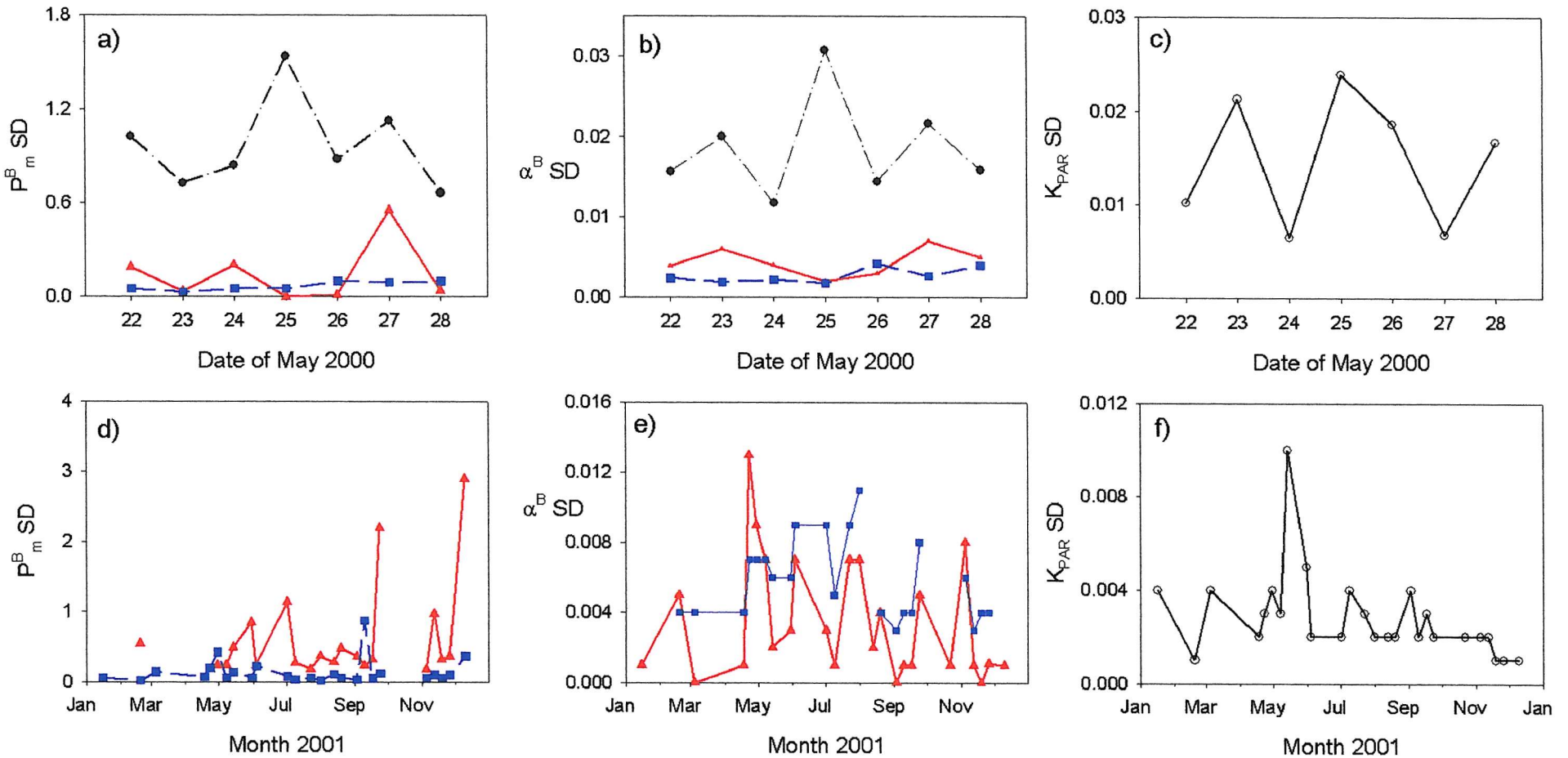

Figure 6.3. Standard deviations of parameter values used in models. Data from: a, b & c) the Celtic Sea and d, e & f) L4 in 2001. a & d) P^B_m in mg C [mg Chl]$^{-1}$ h^{-1}, b & e) α^B in mg C [mg Chl]$^{-1}$ h^{-1} [µmol photons m^{-2} s^{-1}]$^{-1}$ and c & f) K_{PAR} in m^{-1}. Modelled estimates were from ^{14}C photosynthetic parameters (●), FRRF photosynthetic parameters (▼) and FRRF PE curve (○). The standard deviations on parameters from ^{14}C at L4 are not included in four cases where the error was too high to show on the graph. These cases were the values for P^B_m on 16th January 2001, 5th March 2001 and 18th April 2001 and the α^B value on 10th September 2001.

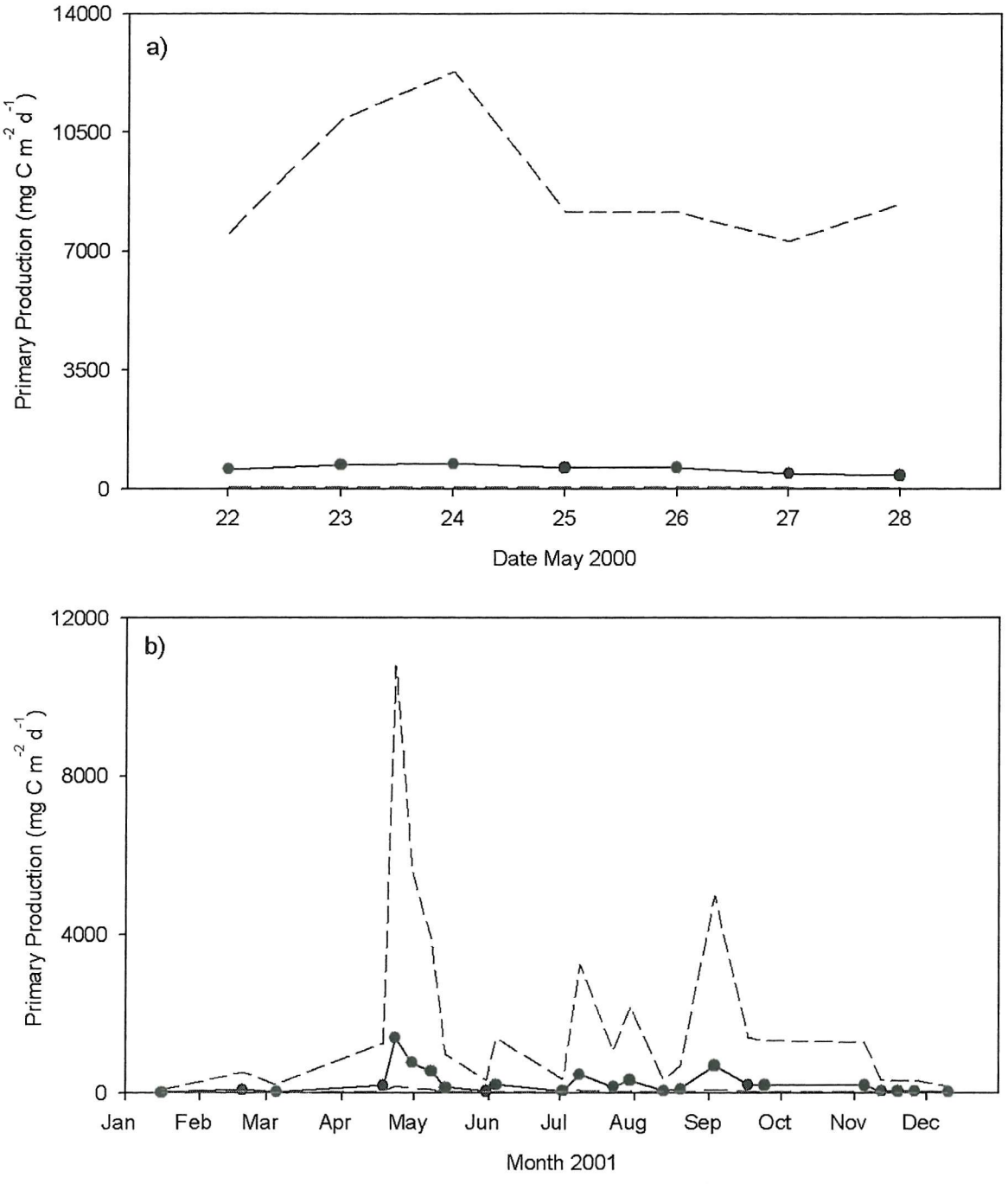

Figure 6.4. Daily primary production (——) and 95% confidence limits (— —) on estimates from the empirical model for remote sensing a) for the Celtic Sea and b) for L4.

series was used to calculate depth and time specific variance for every metre and every hour and these values were simply integrated to estimate error for the whole day and water column. This simple integration was a non-conservative approach, as it assumed, unrealistically, complete independence of the individual error estimates. The data are not independent due to the assumption in the model that parameter values (and their standard deviations) remain constant over the course of the day and over the whole water column.

This means that high errors at one depth are likely to coincide with high errors at other depths and times. The magnitude of the error is affected by PAR so error decreases with depth and towards dusk and dawn but estimates will still be correlated over the water column and over the day. As a result, when integrations are carried out in this way, the Taylor series underestimates the daily, depth-integrated error. The Monte Carlo approach does not suffer such limitations and, assuming that 100 replicates were enough to provide a realistic measure of the range of estimates possible, is expected to provide the more realistic estimate of the confidence intervals around production. However, the process of error calculation via the Taylor series offers more resolution of the importance of the various parameters in the overall error model.

The relatively high error associated with the production estimates from the ^{14}C and FRRF photosynthetic parameter models in the Celtic Sea is explicable. These cases were the only ones where parameter values were the averages of more than one measurement made over the course of the day. The standard deviations of these parameters therefore reflected not only the deviations from each individual measurement but also the differences between measurements from different times of the day (see Methods section for details of the calculation). The ^{14}C parameter values were averages from two measurements, one made at dawn and one made close to midday and the FRRF parameter values were the averages of values from at least three casts taken over the course of the day. The photosynthetic parameters from the FRRF are derived indirectly from the values of F_v/F_m, σ_{PSII} and E_k. As a result, the errors on the FRRF values of α^B and P^B_m had to be derived indirectly from the errors on the original parameters. The calculation required summing the relative errors from each of the original parameters then multiplying the sum by the photosynthetic parameter values. This need to combine numerous errors is the probable cause of the high error on the FRRF photosynthetic parameters compared to those from ^{14}C where error on α^B and P^B_m were derived directly as part of the curve fitting process.

The Celtic sea production estimates from the FRRF PE curve model were also made using the data measured throughout the day but the data were pooled before parameters were derived so only one parameter estimate and associated standard deviation was produced for each day. Although the standard deviations on the PE curves were relatively high, they were smaller than the combined deviations from numerous casts throughout the day. This led to smaller confidence intervals on production estimates from the PE curve model than from the photosynthetic parameter model.

The confidence intervals on the L4 data are relatively small, probably because a single measurement was used to calculate the photosynthetic parameter values used in the model, rather than taking the average of multiple measurements and having to sum all of the errors. High error was associated with the ^{14}C photosynthetic parameter values on the 10th September 2001 as a result of high scatter of the data around the fitted PE curve.

It is important to realise that the errors calculated here reflect only the standard deviations of the parameter values and not how well the chosen model describes the relationship between primary production and PAR. The measurements of surface PAR and chlorophyll are assumed to be error free and there is no inclusion of the error due to the assumption of a uniform chlorophyll profile.

The wide confidence limits on the estimates of production from the empirical satellite algorithm reflect the limitations of using chlorophyll as a descriptor of production. These large limits were calculated assuming perfect chlorophyll retrieval by SeaWiFS but biomass retrieval is likely to be the biggest source of error in satellite production models (Joint and Groom, 2000 and Platt *et al.*, 1995). The aim of the SeaWiFS project was to retrieve accurately chlorophyll concentrations for Case I waters to within ± 35% of real values (Hooker and McClain, 2000) but such uncertainty is still high and will be even higher for coastal areas where the water is often classified as Case II. Any error in biomass estimates will increase when concentrations at the surface do not reflect those at depth, particularly in cases where a deep chlorophyll maximum exists. Even if an algorithm can be formulated to accurately describe the relationship between chlorophyll and primary production, the final estimates will still have a high degree of uncertainty as long as errors in chlorophyll retrieval remain at their current levels.

Antoine and Morel (1996) and Behrenfeld and Falkowski (1997a) carried out sensitivity studies on their respective models. These studies are used to quantify the effect of altering parameter values on the production estimate and they provide information on the importance of different parameters in the model. The results of sensitivity studies apply only to the data sets used and do not provide generic estimates of the reliability of the model when run over a range of conditions. It is likely that increasing complexity in models increases the potential for errors in model predictions. However, the complexity of the models, and the difficulty in

assigning estimates of error to the parameters included in them make it difficult to calculate confidence limits on their predictions.

Small errors in models at local scales will be amplified when applied at basin scales, especially when model parameters have to be extrapolated from values measured under different environmental conditions. For example, when photosynthetic parameters are aggregated over large spatial scales, the values used in the model will have a component of error from the measurement itself and one from the aggregation of the data (Platt and Sathyendranath, 1993).

6.4 Conclusions

This attempt to calculate the error on a typical production model provides a clear indication of the uncertainty associated with modelling daily production from instantaneous measurements. It highlights the importance of understanding how overall error has been calculated and in particular, which sources of error have been included in or excluded from the calculation.

Calculation of the error on production estimates from satellite algorithms is very difficult given the numerous stages and assumptions made. The models are often complex and the uncertainty in parameters used in them unknown. However, the poor retrieval of chlorophyll is currently responsible for the highest degree of error in remotely sensed estimates of production. Until this changes, the errors due to the models themselves, despite the expectation that they are probably very high, are masked by the uncertainty in chlorophyll estimates.

Chapter 7: Discussion

7.1 Rationale of the study

Measurements of marine primary production are required in order to gain a better understanding of the global carbon cycle to predict production in previously unstudied areas or seasons. This information is needed to answer two major questions: 1) what is the flux of CO_2 from the atmosphere to the oceans and how much atmospheric CO_2 can be sequestered in the deep ocean? And 2) how much primary production is available to support secondary production related to fisheries? We will be unable to predict future changes in ocean biology and their effects on atmospheric CO_2 levels until we have a complete understanding of present day controls on productivity (Pahlow and Riebesell, 2000).

Ocean primary production is currently measured on discrete water samples. The time required and the cost of such measurements means that, although such measurements have been made all over the world for many years, the available data set is highly scattered in space and time. In order to improve our understanding of phytoplankton productivity and the controls on it, we need to be able to make more frequent measurements in space and time and to be able to extrapolate from local scale estimates to basin- or global-scale values. There are two novel techniques that appear to offer the potential for making primary production measurements at wider scales than the standard ^{14}C technique – the FRRF and satellite remote sensing. In this thesis, the advantages and limitations of these novel techniques but have also considered the inherent limitations of the ^{14}C approach were addressed. A necessary first step was an investigation into the expected variance within the ^{14}C technique to understand the constraints of these primary production estimates used as "benchmark" values. Production estimates from the FRRF to those from the ^{14}C method and estimates from remote sensing to those from both the ^{14}C and FRRF approaches were then compared. Finally the calculation of error associated with modelled estimates of daily, depth-integrated production was investigated.

7.2 Limitations of each method

7.2.1 The ^{14}C technique

The ^{14}C method is the most widely applied procedure to measure production and is used as a benchmark in this study. However, the method has uncertainties, which are not normally critically evaluated when using the method in a routine way. The length of incubation, light source and fundamental approach (*in situ* vs PE) all vary in different studies. Each of these variables were investigated and uncertainty value were assigned to them. Also, it was shown that by utilising an understanding of algal physiology, the methodology could be improved. For example, in this study, the absorption spectrum of the phytoplankton was used to correct for the differences in the spectra of different incubator lamps. This method, derived by Arrigo and Sullivan (1992) was tested by Schofield *et al.* (1996) who concluded that it successfully overcame the problems of using broadband PAR to measure α^B, a wavelength specific parameter.

More difficult to correct are differences in length of incubations. In this work it has been shown that incubation time has a large effect on production estimates. An attempt to calculate a correction factor to account for incubations of different lengths was not successful for all seasons. The myriad of factors controlling ^{14}C uptake rates, and the way they relate to photosynthesis and primary production, mean that empirically derived correction factors for the duration of incubations are unlikely to apply to all conditions. However, general patterns are evident and are useful when comparing data from different sources. For example, in this study, results from incubations of between 2h and 12h duration were statistically similar to each other and gave higher estimates than those from 24h incubations that included a dark period. It could be argued that short-term incubations are more realistic simulations of events influencing natural assemblages. Mixing in the sea means that phytoplankton are unlikely to receive constant illumination for periods equal to even the shortest incubation time used here (2h) and a number of authors have recorded adaptation of phytoplankton within short-term incubations (Lizon and Lagdeuc, 1998; Macedo *et al.*, 1998 and Lewis and Smith, 1983). However, these changes often take place in the initial minutes of the incubation after which steady states are reached (Lewis and Smith, 1983) and are likely to be specific to the conditions in the sea at the time of each study. The experiments used here were all relatively

long term and did not record changes in rates of ^{14}C uptake between 2h and 12h in the light. Similarly, Marra *et al.* (1988) showed ^{14}C uptake to be linear over time during daylight hours.

Extrapolating from individual parameters measured at one point in the day, to get estimates of daily production, does not take into account diel variability in photosynthesis. One average daily value of each photosynthetic parameter was used in the models. Diel periodicity due to physiological adaptation has been observed in a number of species of marine phytoplankton (Lande and Lewis, 1989). No significant differences were found between the dawn and midday shallow water values of any photosynthetic parameters from the ^{14}C incubations. However, P^B_m values at noon were higher than those at dawn in all but one case (24th May). Periodicity in P^B_m values has been reported with the highest values typically found at noon (Cullen *et al.*, 1992, MacCaull and Platt, 1977). E_k values have also been reported to exhibit diel periodicity but with unclear patterns of change (MacCaull and Platt, 1977). However, diel patterns of change in α^B over the course of the day have not been reported. MacCaull and Platt (1977) suggest that the use of a constant value for P^B_m could induce large errors in models of daily production. Conversely, Jitts *et al.* (1976) found the effect to be small.

One long standing area of contention is what to do about the dark period (Morris *et al.*, 1971). The inclusion of a dark period makes the interpretation of results more difficult than short incubations that include only a light period. The observed high loss of carbon during the dark period was expected. A loss of assimilated carbon in the dark period has been widely reported (Williams, 1993a; Harris *et al.*, 1989; Eppley and Sharp, 1975 and Ryther, 1954) and is due to respiration of fixed carbon by autotrophs as well as grazing and subsequent respiration by heterotrophs (Harris *et al.*, 1989). The quantification of each of the losses is complicated as the extent to which respired ^{14}C is recycled during incubations is poorly understood (Williams, 1993a). The complex food webs contained in natural samples means that fixed ^{14}C may be respired by autotrophs or grazed and then excreted or respired by heterotrophs; the measurement of this cycling is not easy. However, models have been created to track the fate of fixed carbon (Jackson, 1993; Williams, 1993a; Smith *et al.*, 1984; Smith and Platt, 1984; Dring and Jewson, 1982 and Hobson *et al.*, 1976). These models offer insight into the physiology behind the dark loss of ^{14}C but lack of consensus on the fate of fixed ^{14}C during incubations has led to models based on different physiological descriptions. For example, Dring and Jewson (1982) and Hobson *et al.* (1976) assumed that all carbon was

part of a single pool and that newly fixed ^{14}C was respired at the same rate as ^{12}C. Conversely, Jackon (1993), Williams (1993a), Smith *et al.* (1984) and Smith and Platt (1984) included multi-compartments of carbon flow where the respiration of ^{12}C was favoured over newly fixed ^{14}C. Improvements to these models rely on improvements in our understanding of the use of carbon within algal cells. Measurements from ^{14}C incubations, whether of gross or net primary production, are dependent on the ecological conditions in the sea and the interpretation of processes occurring within enclosed natural samples of mixed populations remains very difficult.

A number of experiments in the past have addressed the differences between production estimates from the parameters of PE curves and *simulated-in-situ* incubations. The experiments reported here have shown that estimates of production from *simulated-in-situ* incubations were consistently higher than those from PE models. This is in agreement with the findings of a number of authors (Cullen *et al.*, 1992; Harris, 1978, 1980, 1984 and Marra, 1978, 1980) but is contrary to the findings of others (Lizon and Lagdeuc, 1998; Harrison *et al.*, 1985; Eppley and Sharp, 1975 and Eppley *et al.*, 1973). Lizon and Lagdeuc (1998) compared production estimates from 40 minute PE incubations with those from 4h *simulated-in-situ* incubations and found the relationship between the two estimates varied between stations according to the mixing and irradiance regime. Similarly, Harrison *et al.* (1985) found the relationship between estimates from PE curves and from 24h *simulated-in-situ* incubations to differ with depth in the water column. The experiments carried out here all used water from less than 40m, which, even at depth, was relatively well illuminated. Results from such experiments are expected to differ from those carried out in deep, poorly illuminated water columns. The different and opposing results obtained by different authors demonstrate that observed relationships may be specific to the particular conditions in the sea at the time of sampling. It also confirms that correction factors for different types of incubations cannot be applied universally.

To summarise the investigation into the ^{14}C techniques, different experimental procedures can give different estimates. Some corrections can be applied to account, for example, for changes in spectral regimes within incubators. Allowance for incubation time is more difficult and corrections to compensate for incubations of different duration, cannot be made. However, there are patterns to the changes that occur as the duration of incubations increase and these can be useful in understanding how results from an incubation of one duration

relate to those of another. Model methods for computing primary production from photosynthetic parameters offer an alternative to conventional 24h *simulated-in-situ* incubations. However, the differences between results from PE curve models and 24h *simulated-in-situ* approaches are not consistent but vary with the populations and their environmental history. Theoretically, 24h incubations, which include a dark period provide a useful measure of net community production, which could be argued to be the parameter most applicable to processes on global scales. However, artefacts introduced by long incubation periods can mean that measured processes bear little similarity to those in the sea and models based on short-term experiments may, in some cases, offer results closer to the true values. Providing that the experimental approach used to derive values from ^{14}C incubations are known, they can continue to provide a useful benchmark against which to compare new approaches and will undoubtedly continue to be used to understand algal physiology. The concurrent measurement of supporting data, such as chlorophyll concentration, the phytoplankton absorption spectrum and species composition, greatly increases the usefulness of the data.

7.2.2 The FRRF

It was shown here that the successful derivation of photosynthetic parameters from the FRRF is dependent on good profiling and the presence of ambient light high enough to induce photosaturation. This work demonstrated that when used correctly, the instrument produces estimates of photosynthetic parameters comparable to those produced by the ^{14}C method. Similar results were found by Moore (2002), Suggett *et al.* (2001) and Boyd *et al.* (1997). It has also been shown by others, as was found here, that α^B values from the FRRF are consistently higher than those from ^{14}C incubations and E_k values are lower (Suggett *et al.*, 2001and Boyd *et al.*, 1997). The reliable calculation of photosynthetic parameter estimates was dependent on clear vertical distributions of fluorescence parameters in the water column and particularly a clear definition of the inflection point in the F_v/F_m curve.

Minor discrepancies between photosynthetic parameters from different techniques become larger when models are used to calculate daily, depth-integrated production. In these experiments, roughly half the variance in primary production estimates from the ^{14}C method was explained by those from the FRRF. The FRRF always gave higher production estimates than ^{14}C but this was expected, given that the FRRF measures gross rather than net

production. Similarly, Suggett *et al.* (2001) found FRRF, depth-specific production to explain 59% of the variance in the equivalent values from ^{14}C incubations and the FRRF values were roughly twice those from ^{14}C. Moore (2002) also found similar results but the variance explained by a regression of the two data sets was not stated. Given the known variability within ^{14}C estimates, the observed performance of the FRRF was considered very promising.

The clearest patterns of photosynthesis were obtained when profiling was carried out slowly and outside the shade of the ship. The potential of the FRRF for making measurements, over large horizontal scales, of photosynthetic fitness has already been considered but the deployment requirements found here limit the potential for large scale monitoring by opportunistic towing. However, the FRRF has already been used in a number of large-scale studies to monitor changes in the efficiency of phytoplankton photosynthesis. Greene *et al.* (1994) used the FRRF to make measurements over the Eastern equatorial Pacific and linked photosynthetic efficiency to iron limitation. Olaizola *et al.* (1996) carried out a nine-day transect of the North Atlantic Ocean and showed that over large areas of the ocean, nutrient supply limits photosynthetic performance. Both the above studies used the FRRF in bench top mode with discrete water samples. Strutton *et al.* (1997) employed the instrument in "flow-through" mode on a towed transect from Tasmania to the Antarctic coast. Their measurements were, however, averaged over 100km transects and they noted the need to focus on analysis techniques that are able to exploit the temporal resolution of the raw data measurement. Despite the rapid speed with which data can be acquired from the FRRF, more research is needed to understand how the fluorescence signal recorded over a horizontal transect should be interpreted in relation to the primary production within small sections of that transect. It will also be very important to understand how values recorded over a horizontal transect can reflect the different distributions of fluorescence and photosynthesis over the water column.

As with all data, FRRF data is only useful if it is of good quality. The data from this study suggest that the instrument currently requires maintenance too frequently and measurements to be made too slowly to make it suitable for attachment to ships of opportunity. However, improvement of the FRRF as understanding of its limitations become clearer, is likely to lead to an instrument with the capability to make the large scale measurements that meet the criteria discussed above.

7.2.3 Remote sensing

The potential use of SeaWiFS images for biological oceanography is immense. However, in this study, the potential was not realised, at least for high resolution data, because of cloud cover. Clear SeaWiFs images were available on only 10 of the 60 days (17%) when *in situ* measurements were made. This is likely to be a common problem for UK waters. Pinkerton (2000) compared estimates of water leaving radiance from SeaWiFS with those from a mooring buoy at a site close to L4. Similar to the results here, he obtained cloud-free images on only 24 of 262 (9%) of days where *in situ* measurements were made. Cloud cover could be a serious limitation to the temporal applications of satellite remote sensing for biological oceanography in temperate water.

Where coincident SeaWiFs and measured chlorophyll data were available, the relationship between the two was poor but only fell slightly outside the range of relationships recorded for the NASA SeaBAM data set (O'Reilly *et al.*, 1998). The discrepancies between measured and SeaWiFS chlorophyll were greatest in winter when the sun angle was low and the concentrations of CDOM and SPM were high. The high proportion of optically active substances in Case II waters are well known to lead to problems in chlorophyll estimates (Moore *et al.*, 1999). Mitchelson *et al.*, (1986) showed that the presence of CDOM and SPM had a negligible influence on the colour signal of pigments in Case II waters in the Irish Sea. They observed, however, that this result was specific to their study and may not hold true elsewhere as it depended on the concentration of suspended matter.

There is a strong relationship between chlorophyll concentration and primary production and biomass is used as the basis of all primary production models designed for remote sensing. Three different algorithms for the estimation of primary production from remotely sensed data were compared. They ranged from a simple empirical algorithm to a complex semi-analytical algorithm. The empirical satellite model explained 66% of the variance in depth integrated production. Joint and Groom (2000) used a similar model and compared model estimates with *in situ* incubations in the Celtic Sea. They found that the model explained 75% of the variance in measured production. Eppley *et al.* (1985), using a similar approach, found that chlorophyll concentration explained 33% of the variance in production in their data set. So it appears that simple empirical models can be used to derive primary production estimates. The great advantage of such empirical models is that they are easily derived, but

their simplicity means that they are only likely to be specific to the ocean province and time from which they were derived.

The VGPM model is more complex than the empirical chlorophyll model and the model output explained very little of the variance in production from ^{14}C incubations or the FRRF. Better results were obtained when modelled P^B_{opt} was replaced by measured P^B_m. The P^B_m value was different to P^B_{opt} because it was measured under constant irradiance. In contrast P^B_{opt} reflects the maximum carbon fixation rate under variable irradiance as would be experienced over the course of the day. The euphotic depth was fixed so that production estimates were compared for the same volume of water. The estimation of euphotic depth is obviously important but was considered separately here to the calculation of production per unit depth. A large proportion (76%) of the variance in modelled production was explained by the product of chlorophyll concentration and euphotic depth whilst the variance in P^B_{opt} only explained 37% of that in modelled production. Behrenfeld and Falkowski (1997a) found the VGPM explained 58% of the variance in measured values and 86% of the variance when modelled P^B_{opt} was replace with by measured P^B_{opt}. However, by contrast, they found only 38% of the variance in production was explained as the product of chlorophyll and euphotic depth. The data set of Behrenfeld and Falkowksi had many more data points than this study (272 compared to 32: 7 in the Celtic Sea and 25 at L4), and the wider range of their data set may have led to the higher regressions statistics than found here. However, their plot of modelled (from the VGPM) against measured production (Figure 5 in their paper) shows that the relationship between modelled and measured values is close to the 1:1 line. In contrast, in this study the VGPM model consistently over-estimated production compared to the ^{14}C method and the FRRF.

The semi-analytical model of Morel is more complex than the VGPM. When run in its default mode, the Morel model explained 12% and 53% of the variances in production from ^{14}C and the FRRF respectively in the Celtic Sea and 63% and 84% of the variances in production from ^{14}C and the FRRF respectively at L4. Antoine and Morel (1996) and Morel (1991) did not carry out direct comparisons with *in situ* measurements so it is not known whether these results are typical. In these simulations, model performance was improved when measured values were used in place of modelled PAR and K_{PAR}. Modelled K_{PAR} compared well with measured values at L4 except in the winter when the water column

contained high concentrations of suspended particulate matter, and the model underestimated the true value.

Both the VGPM and the Morel model contained temperature-dependent functions to control photosynthetic parameters. The inclusion of temperature masked the effect of other factors, such as nutrients, on primary production and at L4, led to predictions of high production throughout the nutrient-depleted summer. Improved estimates of P^B_m or P^B_{opt} are expected to vastly improve production estimates. In a recent paper, Behrenfeld *et al.* (2002) introduced the possibility of making better estimates of P^B_{opt} by classifying areas into empirically derived categories that reflect the nutrient status of the water column.

The complex semi-analytical model (Morel model) did perform better than the simple empirical approaches in the estimation of primary production. The Morel model produced production estimates very similar to those from the FRRF. Both were higher than estimates from the ^{14}C method and may indicate that they estimate gross rather than net production. When measured PAR and K_{PAR} were used, the Morel model explained 97% of the variance in estimates from the FRRF PE curve for L4. The regression had a slope of 0.87. Regression statistics from the Celtic Sea were lower but can be attributed to the small data set and the low range of the data.

7.2.4 Estimation of the error associated with estimates of PP_{Daily}

The calculation of error on estimates of production modelled from short-term measurements (from the ^{14}C method or the FRRF) has not been carried out before. The approaches used here were very conservative as they only included sources of error that could be easily described or have values assigned to them. The models did not attempt to account for errors inherent to the techniques used i.e. they assumed that values from both the ^{14}C and FRRF techniques were accurate measurements of production. The models also did not account for any error due to the assumption of constant values of photosynthetic parameters over the course of the day and through the water column. The highest errors were associated with production estimates from the FRRF photosynthetic parameter model where the maximum 95% confidence interval was equal to 109% of the production value. The maximum 95% confidence interval around the ^{14}C photosynthetic parameter model was equal to 49% of the production estimate. In the Celtic Sea, the parameter values used in the models were

averages of all the measurements made over the course of the day and the error associated with them was combined from the errors on all individual values. It thus represented the difference between measurements from different times of the day. There was an additional level of error associated with the photosynthetic parameters from the FRRF as their values were derived indirectly from other derived parameters (F_v/F_m, σ_{PSII} and E_k). This necessary procedure is the cause of the particularly high errors associated with the FRRF photosynthetic parameter model.

The uncertainty around measurements made at L4 was less than that in the Celtic Sea but this only reflects the greater number of measurements made in the Celtic Sea on each day. As a result of only one measurement being made each day at L4, the calculated or known error was low but the true uncertainty is likely to be much greater than that from the Celtic Sea where more measurements were made. These results show how important it is to understand which sources of error are accounted for in models. The uncertainty associated with individual parameters in productivity models leads to very high uncertainties around modelled production estimates. It is common to make no account of these errors, and this can present misleading impressions of the relationships between estimates from different sources.

It is difficult to calculate the error on the complex models to derive production from satellite remote sensing data since overall error can only satisfactorily be calculated when uncertainty in all the parameters can be quantified. However, at present, chlorophyll retrieval is the greatest source of error in satellite production estimates (Joint and Groom, 2000 and Platt and Sathyendranth, 1991) and until problems with chlorophyll retrieval are overcome, the errors associated with the production models themselves are likely to have minimal effect on the overall uncertainty associated with satellite-derived production estimates. The precision of the biomass estimates is no greater than a factor of 2 and the accumulation of error in chlorophyll estimates, from atmospheric correction, cloud cover, instrument calibration and irradiances, make it difficult to assign a figure to the precision of the result (Gregg and Conkright, 2001and Platt and Sathyendranath, 1988).

All the techniques used in this study measure different processes over different time scales and the most widely used method for the comparison of results, linear regressions, is not ideal. Many of the comparisons carried out during this work have included model I linear

regression analyses but given the sparseness of the data in many cases, it was noted that the regression statistics did not reflect the true relationship. Model I linear regression theory is often used in the analysis of data under conditions when model II theory is required. Model II regressions should be used when there is some uncertainty in the measurement of the known variable. Assumptions of model I linear regression are that the values on the x axis are measured without error, that they are chosen or set by the experimenter and that the relationship between x and y is best fitted by a straight line. One reason that type I models are used so widely is that type II models are not available in commercial statistical packages. Model I regressions were used in this study, in keeping with common practice but statistics were only accepted if the fitted line closely followed the scatter of the data: plots of data were always regarded as being more important. The similarity or dissimilarity between estimates are often best compared by plots of the data and their distribution around the 1:1 line. Such plots also provide a good indication of correlations between parameters and may be more suitable than regression statistics.

7.3 Annual production at station L4 in the Western English Channel

The measurements made during the study allowed not only the assessment of the individual merits and limitations of the different techniques but also resulted in new estimates of the amount of carbon fixed annually at L4. It was shown (chapter 5) that the water at L4 contains many optically active substances and estimates of chlorophyll concentration from SeaWiFS data are often poor. As a result, the satellite algorithms for production were parameterised with measured chlorophyll values so that errors in chlorophyll retrieval were not confused with poor model performance. Also, SeaWiFS estimates of chlorophyll were available on very few days that coincided with sampling at L4 so comparisons between production estimates using chlorophyll from the two different sources would have been limited. However, in order to obtain production estimates from remotely sensed data, for comparison with measurements made on water samples, the models were parameterised using SeaWiFS chlorophyll estimates as well as chlorophyll measured by the HPLC technique.

Estimates of annual production were obtained by linear interpolation between each data point and integrated to calculate the amount of carbon fixed at L4 over the year (Figure 7.1). In all

cases, the estimated carbon fixation was highest when the satellite production algorithms were parameterised with SeaWiFS chlorophyll estimates rather than HPLC chlorophyll measurements.

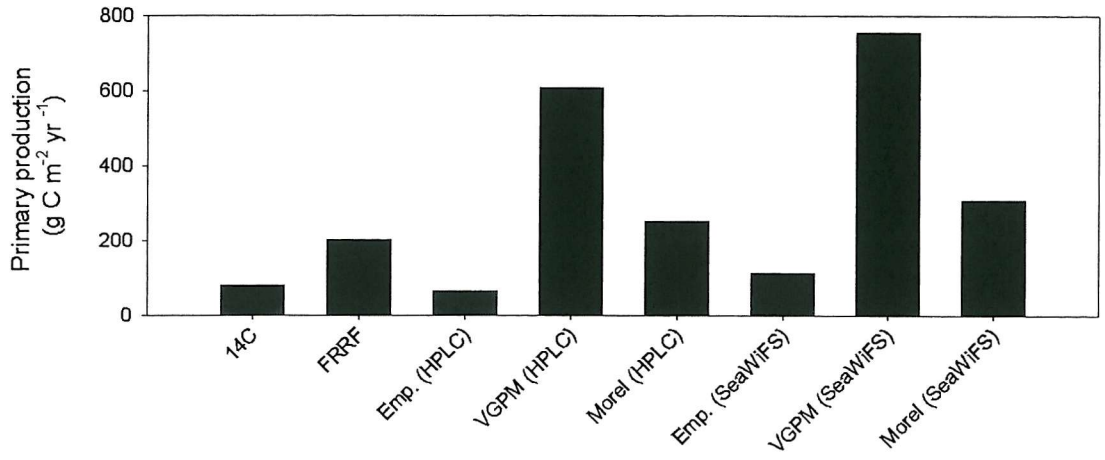

Figure 7.1 Annual carbon fixation estimated for L4 by the different approaches. Emp. refers to the empirical satellite algorithm. HPLC and SeaWiFS refer to the source of chlorophyll used in the model.

Annual estimates of carbon fixation ranged from 64 g C m^{-2} (empirical model using HPLC chlorophyll) to 756 g C m^{-2} (VGPM using SeaWiFS chlorophyll). However, estimates from the VGPM are considered unreliable, given the results of chapter 5, so the maximum estimate of annual production is probably about 310 g C m^{-2}, as indicated by the Morel model using SeaWiFS chlorophyll. Similarly, it is possible that results from other approaches may be too low. Pingree and Pennycuik (1975) estimated annual production in the Western English Channel at a station close to L4 (station E1 at 50°02.05'N, 04°22.5'W). Based on mixing rates and the transfer of inorganic phosphate through the thermocline, they estimated that approximately 100 g C m^{-2} was fixed annually. This suggests that the estimates made here from the empirical model (64 g C m^{-2}) and the ^{14}C method (82 g C m^{-2}) could be too low. This is unsurprising as both these estimates were based on 24h incubations with ^{14}C which, given the dark loss of fixed carbon by autotrophic and heterotrophic respiration, are expected to underestimate gross production.

A greater understanding of the ecology of the region can be gained from the annual patterns of production. Figure 7.2 shows that, in winter, the erroneously high estimates of chlorophyll from SeaWiFS led to high estimates of production compared to those based on measured

chlorophyll. The high winter production suggests that limitation by light and temperature did not control model predictions as expected and highlights a limitation of estimating production using algorithms that are highly dependent on chlorophyll. Also when SeaWiFS chlorophyll estimates were used, the satellite algorithms did not predict the sporadic summer blooms that were seen when measured chlorophyll was used. High estimates of chlorophyll from SeaWiFS were recorded during the summer but the majority failed the quality control (QC) process and were removed from the data set. It may be that the QC procedures cannot deal with the high spatial variability associated with the blooms since there were large differences between adjacent pixels surrounding and including L4, or high cloud cover may influence some pixels but not others. As discussed earlier, an additional discrepancy is that the maximum chlorophyll concentration estimated by SeaWiFS occurred at a different time of year to those in water samples. As a result, SeaWiFS chlorophyll estimates lead to different seasonal patterns of productivity.

In 2001, HPLC measurements of chlorophyll suggested that the spring bloom occurred between 18th April and 31st May. The spring bloom accounts for a significant fraction of total annual production and estimates of the percentage of total annual carbon fixation that occurs during the spring bloom varied considerably with techniques. The Morel model with SeaWiFS chlorophyll suggested only 19% of the annual production occurred in the spring bloom but the ^{14}C method suggested 52% of the total annual value (Table 7.1). The FRRF also reduced the significance of the spring bloom to 29% of annual production because the FRRF detected sporadic blooms during the summer but the ^{14}C method measured low production throughout the summer. As discussed in section 5.3, this may reflect the measurement of gross production by the FRRF and net production by the ^{14}C method.

During the summer months, the water column is stratified. The method used here, where production throughout the water column is described using one value for each chlorophyll and photosynthetic parameters, is likely to have led to errors when applied to stratified water. In section 4. 3, it was shown that considering the water column above and below the thermocline separately, had very little effect on the overall daily depth-integrated production estimate. However, only the chlorophyll concentration was varied, with the rate of

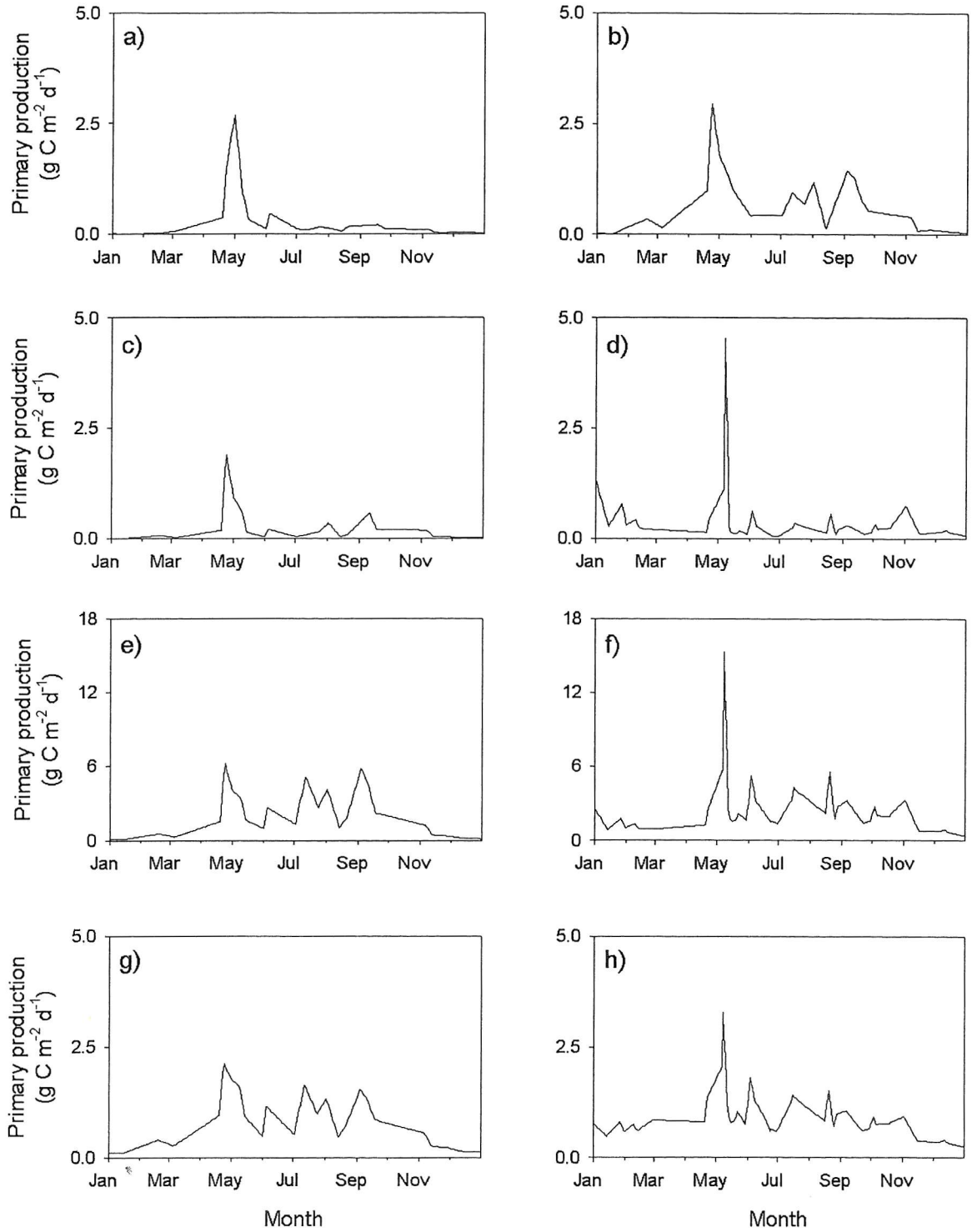

Figure 7.2 Production estimated for L4 over 2001: a) ^{14}C, b) FRRF, c) Empirical model with HPLC chlorophyll, d) Empirical model with SeaWiFS chlorophyll, e) VGPM model with HPLC chlorophyll, f) VGPM model with SeaWiFS chlorophyll, g) Morel model with HPLC chlorophyll and h) Morel model with SeaWiFS chlorophyll. Note the different scale used for the VGPM model (e & f).

Table 7.1 The percentage of annual primary production in 2001 occurring during the Spring bloom between 18th April and 31st May as estimated by the different techniques for L4.

Approach	% of annual production occurring in Spring bloom	
^{14}C photosynthetic parameter model	52	
FRRF PE curve model	29	
	HPLC chlorophyll	SeaWiFS chlorophyll
Empirical model	40	24
VGPM	20	20
Morel model	22	19

photosynthesis only described by a single value. Phytoplankton are likely to be adapted to different states above and below the thermocline and this should, ideally, be included in future models. Unfortunately, this would necessitate sampling throughout the water column for both chlorophyll measurements and the ^{14}C method. An additional problem with the FRRF, particularly in structured water columns, is that only one value can be obtained for the whole water column because of the way in which photosynthetic parameters relying on the natural attenuation of light with depth. At the surface, light saturation can be ensured by making measurements at the brightest time of the day. However, in stratified water columns, photosynthesis may never be light saturated so FRRF casts may have to be made at other times in the day, under lower irradiance, to reflect the ambient light in layers below the surface. So the creation of a model to incorporate stratification is relatively simple but the derivation of data to parameterise it is difficult.

Primary production in the Western English Channel has also been estimated by Joint and Groom (2000) for station E1, close to L4. Using an empirical model they estimated that 122g C m^{-2} in 1998 and 124 g C m^{-2} in 1999 were fixed between April and September. Table 7.2 shows the estimates of total carbon fixation for the same time period in 2001 calculated using the approaches of this study. Joint and Groom (2000) derived their estimate from an empirical (chlorophyll) satellite model which was derived from 5h incubations with ^{14}C. Their estimates are over twice that from the empirical satellite model used in this study (51 g C m^{-2} using HPLC chlorophyll and 57 g C m^{-2} using SeaWiFS chlorophyll) but are similar to the estimates from the FRRF and the Morel model. It has already been suggested that the empirical model used here underestimates gross primary production as it is based on

Table 7.2 Total primary production between April and September 2001, as estimated by the different techniques for L4.

Approach	Total carbon fixed ($g\ C\ m^{-2}$)	
^{14}C photosynthetic parameter model	70	
FRRF PE curve model	160	
	HPLC chlorophyll	SeaWiFS chlorophyll
Empirical model	51	57
VGPM	495	507
Morel model	189	193

measures of net community production. The estimates from the VGPM model are much higher than those of Joint and Groom (2000). It is important to note that, although these absolute values of carbon fixed, as predicted by the satellite models, were similar when either HPLC or SeaWiFS chlorophyll estimates were used, they accounted for different percentages of the total annual production. When SeaWiFS estimates of chlorophyll were used, a lower proportion of annual production occurred between April and September reflecting the unusually high SeaWiFS estimates of chlorophyll during the winter.

In conclusion, the use of SeaWiFS chlorophyll values at L4 leads to overestimates of production during the winter months and therefore over the course of the year. The temporal distribution of production in the months between April and September was different when satellite algorithms were parameterised with HPLC and SeaWiFS chlorophyll but the absolute estimates of carbon fixed during the period were similar. Therefore, SeaWiFS is not recommended for estimating production between October and April but could be used to estimate production between April and September. The empirical model is suitable for use at L4 but due to its specificity to the data used to derive it, the Morel model is recommended. The VGPM consistently overestimated production and is not recommended.

It is difficult to assess the importance of the variability between the estimates from different approaches without knowing how much estimates may vary within an individual technique. Unfortunately, it was not possible to calculate the uncertainty associated with the annual estimates of production. Calculations of the error associated with daily production estimates were made in chapter 6. However, in order to calculate the error associated with annual

production it would be necessary to know the error associated with production for every day of the year, including those on which experiments were not carried out. For these, non-sampled dates, estimates of primary production were made by interpolation between the values from days on which sampling was carried out. However, interpolation to obtain error assumes that the error is related to the date or more specifically to the way in which the ambient conditions change with date. This was not the case: As discussed in chapter 6, the error was associated with how well the measured data fitted the curves used to describe the PE relationship and this was independent of the date or ambient conditions.

Estimating production during the winter months is particularly difficult. Fixation of ^{14}C during the winter months was low at L4 and showed little temporal variation. This may be a consequence of infrequent sampling during the winter due to poor weather conditions which restricted sampling, but is more likely to be real, reflecting the low light and temperature. As a result, between November and February *in situ* measurements are not likely to be acquired frequently. Most production occurs between April and September. The different methods give estimates between 51 g C m^{-2} and 189 g Cm^{-2} during this period. In 2001, the spring bloom lasted for six weeks and accounted for an important fraction of the annual production at the site. The absolute importance of the bloom was different by the different approaches but it was estimated to account for between 19% and 52% of the annual production. It is particularly important that future studies should make frequent measurements from the end of March so as to fully document the bloom development.

The greatest disagreement between the techniques was in their predictions of production during the summer. This may reflect the unsuitable application of a model, particularly the VGPM that was designed for a well-mixed water column, to a site, which stratifies at this time of year. The stratification can lead to a relatively shallow sub-surface chlorophyll maximum which cannot be discounted, due to light limitations, as not contributing to production. Despite the difficulties discussed, future estimates of annual production should aim to account for summer stratification. Overall the study at L4 suffered from limitations typical for coastal work. Sampling was carried out from small boats so the data set was limited to days when the weather was calm. The sampling days were pre-planned so opportunistic measurements on cloud-free days could not be made. As water had to be returned to the laboratory as quickly as possible, only surface water sampling was carried out. It also meant that sampling was carried out as early as possible in the day, often in low light.

Given the time required to transport water back to the laboratory, the FRRF may offer more reliable measurements of production at L4. However, FRRF sampling will only offer a viable alternative if carried out during the brightest part of the day or if detailed studies are undertaken to understand diel changes in photosynthetic parameters measured by the FRRF.

7.4 The future for global estimates of primary production

The feasibility and reliability of making global scale estimates of primary production using each of the three techniques is an important issue arising from these studies. The available dataset of ^{14}C measurements is very large but the spatial distribution of the archive is uneven in space and time (Platt *et al.*, 1995). The FRRF has the potential to make large scale measurements over useful timescales but further research is needed before this is potential is achieved. Remotely sensed data offers the necessary spatial coverage and acceptable spatial resolution for making global scale measurements (Platt and Sathyendranath, 1988) but to be confident in estimates of primary production, we must first be confident in the retrieval of biomass from the satellite.

It has been suggested that chlorophyll concentration may not provide a sound basis for estimating photosynthetic production since, even with sufficient nutrients, available chlorophyll may not be fully utilised due to wide ranges in incident PAR (Aiken, 1980). Some authors maintain that research should focus on obtaining estimates of phytoplankton absorption from remote sensing rather than chlorophyll as this is a more important factor in determining primary production (Lee *et al.*, 1996). It is clear that the retrieval of accurate chlorophyll estimates has not yet been achieved for coastal or Case II waters. There is an increasing awareness of the importance of coastal water bodies both in terms of their contribution to global production and with respect to their susceptibility to impacts from land. Assuming that chlorophyll continues to be used as the basis for production models, the problems associated with its retrieval in Case II water must be solved before we can be confident in global estimates of primary production.

One of the objectives of this study was to compare some of the wide range of models available for deriving primary production from satellite derived chlorophyll concentrations. As simple empirical models, based on chlorophyll concentration alone, are rather limited in their applicability, research has focussed on the development of algorithms that include

empirically derived descriptors of photosynthetic performance. The problem associated with this approach is the difficulty in the parameterisation of the models over areas of great oceanographic and atmospheric variation. The problem is compounded by the incompatibility of the spatial scales of measurement at sea and satellite data (Platt and Sathyendranath, 1993). Global models that include parameters which vary between water bodies, must somehow account for this variation. Clearly it would be unrealistic to try and derive global values for photosynthetic parameters or, in the models incorporating non-uniform pigment profiles, for chlorophyll distribution with depth. The current approach to the problem is the division of the oceans into 'biogeochemical provinces'.

The 'biogeochemical province' approach assumes that within a defined province, in any given season, the photosynthetic parameters and the shape of the pigment profile can be considered relatively constant (Platt and Sathyendranath,1988). Photosynthetic parameters can then be combined with remotely-sensed data on a pixel by pixel basis. Longhurst *et al.* (1995) produced an estimate of net primary production in the oceans from mean near-surface chlorophyll values using this approach. They initially divided the oceans into four domains (Polar, Westerlies, Trade winds and Coastal) that were further divided to produce a total of 57 provinces based on oceanography. Seasonal primary production estimates were calculated for each province using seasonal averages of photosynthetic parameters (from data archives) at each grid point. However, holding photosynthetic parameters and thus the rate of photosynthesis constant over such large areas neglects the scale of many hydrographic process important in controlling primary production (Balch, 1993). There are both systematic and random errors associated with the biogeochemical province approach, the main one being that photosynthetic parameter estimates must be taken from archived data and are non-dynamic. Another problem is that the accuracy of the province approach cannot be tested as there are no values to which it can be compared i.e. it cannot be proven. It is argued that poor short-term estimates made using the province approaches do not reflect poor overall performance as one would not expect the rate of production on one day to reflect that over a whole province and whole season. So their performance should not be tested at scales shorter or smaller than those for which they are designed.

It may be that the future of remote sensing requires the move away from models based on empirically derived relationships to analytical equations and this requires the remote sensing of parameters that reflect photosynthesis. Comprehensive knowledge of all kinds of

physiological responses and their causes is far from being sufficiently documented and quantified (Morel *et al.*, 1996) so analytical solutions are difficult to derive. However, the recent launches of the satellites MODIS (the MODerate resolution Imaging Spectrometer) by NASA and MERIS (the MEdium Resolution Imaging Spectrometer) by ESA with their increased numbers of wavebands offers the potential for much improvement in the detection of biological responses using remote sensing. They offer increased opportunity for accessory pigment resolution and potentially the measurement of phytoplankton fluorescence from space.

The future is likely to involve the combination of coupled physical-biological 3-dimensional models with remotely sensed data. The remotely sensed data could be assimilated into models as a means to prevent them from diverging from reality (Longhurst *et al.*, 1995). Platt and Sathyendranth (1991) addressed the possibility of inserting terms describing carbon fixation into global circulation models (GCMs) and concluded that the approach could extend the knowledge of how the ocean functions as a coupled physical-biogeochemical system. A source of parameters for the models is mooring arrays, which could offer measurements of water properties, PAR and even phytoplankton fluorescence. Alternatively, in the future the FRRF may offer a means to make frequent, measurements of phytoplankton photosynthetic parameters over ocean basins.

7.5 Recommendations for further studies.

It is worth considering whether or not we are carrying out the studies that will help advance our understanding of primary production. There are three aspects to primary production: biomass, yield and rate. In order to answer the questions we are asking, we need to know the loss terms due to phytoplankton respiration and grazing and to know what proportion of the total production is new and available for processes at higher trophic levels.

The discussion has focussed on the measurement of total primary production but in terms of carbon transport from the atmosphere to deep water, new production is the relevant ecological flux (Platt and Sathyendranath, 1988). New production is the fraction of production resulting from new sources of nitrogen, for example nitrate in subthermocline water advected into the upper euphotic zone, as opposed to nitrogen regenerated within the

euphotic zone (Dugdale and Goering, 1967). The input of new nitrogen determines the maximum export of nitrogen and carbon from phytoplankton to the deep water and therefore sets limits to the amount of CO_2 taken up and incorporated into biological particles. A number of studies have used satellite derived temperature data to estimate the proportion of total production that is new, the so-called f-value. These f-values can then be combined with satellite-derived estimates of total production to calculate new production. This value is simply derived by dividing new production by total production and the basis of these studies is the assumption that the f-value is correlated to nitrate concentration which correlates with sea surface temperature. Dugdale *et al.* (1989) carried out such a study at Cap Blanc off North West Africa, Sathyendranath *et al.* (1989) employed the technique on St.Georges Bank and Dugdale *et al.* (1997) estimated new production at Point Conception in California using this approach. The use of temperature to estimate nutrient concentrations and sources is obviously a coarse approach but estimates of the proportion of total production that is new must be determined if the draw down of atmospheric carbon into the deep ocean is to be estimated. New production is often intense at coastal sites (Dugdale and Wilkerson, 1998), which highlights the importance of adapting current satellite algorithms to make them applicable to the Case II waters bodies often typical in coastal regions.

It may be argued that you cannot predict tomorrow's carbon from today's primary production, as the measurement of production gives no information about carbon fixation, cell division or grazing. However, the amount of new production does set constraints on the other systems in a water body. It may seem counter intuitive to derive the rate of the process from the standing stock but by comparing the standing stock from day-to-day we can learn about the importance of the loss terms.

We have a good understanding of the physicochemical driving forces of marine ecosystems but are still ignorant of the factors that shape species succession and the relationship between form and function in plankton. The integration of organism biology and life cycle with biogeochemistry is an important task and comparative studies of plankton ecology combined with *in situ* experiments may help us to understand the mechanisms driving pelagic ecosystems. (Smetacek *et al.*, 2002).

These studies suggested that the satisfactory retrieval of chlorophyll for coastal regions should be the focus of future work. Without it, we could be making gross underestimates of

production in these areas of great importance with respect both to the global carbon cycle and to the social and economic impact of harmful blooms. Future research to improve the resolution and understanding of data from the FRRF used as a towed instrument will also be important. Our understanding of the measurements could be improved by making FRRF measurements on vertical profiles on transects along which the FRRF is also towed. Finally, to improve our understanding of the causes of discrepancies between results from ^{14}C incubations and the FRRF, measurements from the FRRF made at fixed depths in the water column could be compared to results from ^{14}C incubations rather than comparing FRRF profiles with fixed depth ^{14}C measurements.

References

Aiken, J. 1980. The estimation of the photosynthetic activity of chlorophyll in phytoplankton, p. 125-129, Proceedings of the final ICES / JONSIS workshop on JONSDAP 76. ICES.

Aiken, J., Moore, G. F., and Holligan, P. M. 1992. Remote-sensing of oceanic biology in relation to global climate change. Journal of Phycology **28:** 579-590.

Aiken, J., Moore, G. F., Trees, C. C., Hooker, S. B., and Clark, D. K. 1995. The SeaWiFS CZCS-type pigment algorithm. NASA Goddard Space Flight Center.

Antoine, D., Andre, J.-M., and Morel, A. 1996. Oceanic primary production: 2. Estimation at global scale from satellite (coastal zone color scanner) chlorophyll. Global Biogeochemical Cycles **10:** 57-69.

Antoine, D., and Morel, A. 1996. Oceanic primary production: 1. Adaptation of a spectral light-photosynthesis model in view of application to satellite chlorophyll observations. Global Biogeochemical Cycles **10:** 43-55.

Arrigo, K. R., and Sullivan, C. W. 1992. The influence of salinity and temperature covariation on the photophysiological characteristics of Antarctic Sea ice microalgae. Journal of Phycology **28:** 746-756.

Balch, W., Evans, R., Brown, J., Feldman, G., McClain, C., and Esaias, W. 1992. The remote-sensing of ocean primary productivity - Use of a new data compilation to test satellite algorithms. Journal of Geophysical Research-Oceans **97:** 2279-2293.

Balch, W. M. 1993. The remote-sensing of ocean primary productivity - use of a new data compilation to test satellite algorithms - Reply. Journal of Geophysical Research-Oceans **98:** 16585-16587.

Balkanski, Y., Monfray, P., Battle, M., and Heimann, M. 1999. Ocean primary production derived from satellite data: An evaluation with atmospheric oxygen measurements. Global Biogeochemical Cycles **13:** 257-271.

Banse, K. 1993. On the dark bottle in the ^{14}C method for measuring marine phytoplankton production. ICES Marine Science Symposium **197:** 113-121.

Barkmann, W., and Woods, J. D. 1996. On using a Lagrangian model to calibrate primary production determined from in vitro incubation measurements. Journal of Plankton Research **18:** 767-788.

Barnes, R. A., Eplee, R. E., Schmidt, G. M., Patt, F. S., and McClain, C. R. 2001. Calibration of SeaWiFS. I. Direct techniques. Applied optics **40:** 6682-6700.

Behrenfeld, M. J., and Falkowski, P. G. 1997a. Photosynthetic rates derived from satellite-based chlorophyll concentration. Limnology and Oceanography **42:** 1-20.

---. 1997b. A consumer's guide to phytoplankton primary productivity models. Limnology and Oceanography **42:** 1479-1491.

Behrenfeld, M. J., Maranon, E., Siegel, D. A., and Hooker, S. B. 2002. Photoacclimation and nutrient-based model of light-saturated photosynthesis for quantifying oceanic primary production. Marine Ecology-Progress Series **228:** 103-117.

Bird, R. E. 1984. A simple, solar spectral model for direct-normal and diffuse horizontal irradiance. Solar Energy **32:** 461-471.

Bjorkman, O., and Demmig, B. 1987. Photon yield of oxygen evolution and chlorophyll fluorescence characteristics at 77K among vascular plants of diverse origins. Planta **170:** 489-504.

Boyd, P. W., and Abraham, E. R. 2001. Iron-mediated changes in phytoplankton photosynthetic competence during SOIREE. Deep-Sea Research Part Ii-Topical Studies in Oceanography **48:** 2529-2550.

Boyd, P. W., Aiken, J., and Kolber, Z. 1997. Comparison of radiocarbon and fluorescence based (pump and probe) measurements of phytoplankton photosynthetic

characteristics in the Northeast Atlantic Ocean. Marine Ecology-Progress Series 149: 215-226.

Brewer, P. G., and Riley, J. P. 1965. The automatic determination of nitrate in seawater. Deep-Sea Research 12: 765-772.

Collos, Y., Descolas-Gros, C., Fontugne, M., Mortain-Bertrand, A., Chretiennot-Dinet, M. J., and Frikha, M. G. 1993. Chemical, isotopic and enzymatic monitoring of free and enclosed seawater: implications for primary production estimates in incubation bottles. Marine Ecology Progress Series 93: 49-54.

Cullen, J. J., Lewis, M. R., Davis, C. O., and Barber, R. T. 1992. Photosynthetic characteristics and estimated growth-rates indicate grazing is the proximate control of primary production in the equatorial Pacific. Journal of Geophysical Research-Oceans 97: 639-654.

Di Tullio, G. R., and Laws, E. A. 1986. Diel periodicity of nitrogen and carbon assimilation in 5 species of marine phytoplankton - Accuracy of methodology for predicting N-assimilation rates and N/C composition ratios. Marine Ecology-Progress Series 32: 123-132.

Dring, M. J., and Jewson, D. H. 1982. What does C^{14} uptake by phytoplankton really measure - a theoretical modeling approach. Proceedings of the Royal Society of London Series B-Biological Sciences 214: 351-368.

Dugdale, R. C., Davis, C. O., and Wilkerson, F. P. 1997. Assessment of new production at the upwelling center at Point Conception, California, using nitrate estimated from remotely sensed sea surface temperature. Journal of Geophysical Research-Oceans C4: 8573-8585.

Dugdale, R. C., and Goering, J. J. 1967. Uptake of new and regenerated forms of nitrogen in primary productivity. Limnology and Oceanography 12: 196-206.

Dugdale, R. C., Morel, A., Bricaud, A., and Wilkerson, F. P. 1989. Modeling new production in upwelling centers - A case-study of modeling new production from remotely sensed temperature and color. Journal of Geophysical Research-Oceans 94: 18119-18132.

Dugdale, R. C., and Wilkerson, F. P. 1998. Silicate regulation of new production in the equatorial Pacific upwelling. Nature 391: 270-273.

Duysens, L. N. M., and Sweers, H. E. 1963. Mechanisms of the two photochemical reactions in algae as studied by means of fluorescence, p. 353-372. *In* J. s. o. p. physiology [ed.], Studies on mircoalgae and photosynthetic bacteria. University of Tokyo Press.

Eppley, R. W., Renger, E. H., Venrick, E. L., and Mullin, M. M. 1973. A study of plankton dynamics and nutrient cycling in the central gyre of the North Pacific Ocean. Limnology and Oceanography 18: 534-551.

Eppley, R. W., and Sharp, J. H. 1975. Photosynthetic measurements in the central North Pacific: The dark loss of carbon in 24-h incubations. Limnology and Oceanography 20: 981-987.

Eppley, R. W., Stewart, E., Abbott, M. R., and Heyman, U. 1985. Estimating ocean primary production from satellite chlorophyll - Introduction to regional differences and statistics for the Southern-California Bight. Journal of Plankton Research 7: 57-70.

Falkowski, P. 1981. Light-shade adaptation and assimilation numbers. Journal of Plankton Research 3: 203-216.

Falkowski, P. G., and Laroche, J. 1991. Molecular-biology in studies of ocean processes. International Review of Cytology-a Survey of Cell Biology 128: 261-303.

Falkowski, P. G., and Raven, J. A. 1997. Aquatic photosynthesis. Blackwell science.

Falkowski, P. G., Ziemann, D., Kolber, Z., and Bienfang, P. K. 1991. Role of eddy pumping in enhancing primary production in the ocean. Nature 352: 55-58.

Fernandez, E., and Bode, A. 1993. Seasonal patterns of dark carbon incorporation by natural phytoplankton assemblages in the central Cantabrian sea (Bay of Biscay). P.S.Z.N..I: Marine Ecology **14**: 175-183.

Field, C. B., Behrenfeld, M. J., Randerson, J. T., and Falkowski, P. 1998. Primary production of the biosphere: Integrating terrestrial and oceanic components. Science **281**: 237-240.

Fitzwater, S. E., Knauer, G. A., and Martin, J. H. 1982. Metal contamination and its effect on primary production measurements. Limnology and Oceanography **27**: 544-551.

Flameling, I. A., and Kromkamp, J. 1998. Light dependence of quantum yields for PSII charge separation and oxygen evolution in eucaryotic algae. Limnology and Oceanography **43**: 284-297.

Franks, P. J. S., and Marra, J. 1994. A simple new formulation for phytoplankton photoresponse and an application in a wind-driven mixed-layer model. Marine Ecology-Progress Series **111**: 143-153.

Frenette, J.-J., Demers, S., Legendre, L., and Dodson, J. 1993. Lack of agreement among models for estimating the photosynthetic parameters. Limnology and Oceanography **38**: 679-687.

Frenette, J. J., Vincent, W. F., Legendre, L., and Nagata, T. 1996. Size-dependent changes in phytoplankton C and N uptake in the dynamic mixed layer of Lake Biwa. Freshwater Biology **36**: 221-236.

Furnas, M. J. 1987. Effects of prescreening on productivity of size-fractionated phytoplankton. Limnology and Oceanography **32**: 483-491.

Gallegos, C. L., and Platt, T. 1985. Vertical advection of phytoplankton and productivity estimates - a dimensional analysis. Marine Ecology-Progress Series **26**: 125-134.

Geider, R. J. 1992. Respiration: taxation without representation, p. 333-360. *In* R. G. Falkowski and A. D. Woodhead [eds.], Primary Productivity and Biogeochemical Cycles in the Sea. Plenum Press.

Geider, R. J., Greene, R. M., Kolber, Z., Macintyre, H. L., and Falkowski, P. G. 1993. Fluorescence assessment of the maximum quantum efficiency of photosynthesis in the western North-Atlantic. Deep-Sea Research Part I-Oceanographic Research Papers **40**: 1205-1224.

Geider, R. J., MacIntyre, H. L., and Kana, T. M. 1997. Dynamic model of phytoplankton growth and acclimation: Responses of the balanced growth rate and the chlorophyll a:carbon ratio to light, nutrient-limitation and temperature. Marine Ecology-Progress Series **148**: 187-200.

Geiskes, W. W. C., and Kraay, G. W. 1982. Effect of enclosure in large plastic bags on diurnal change in oxygen concentration in tropical ocean water. Marine Biology **70**: 99-104.

Genty, B., Briantais, J. M., and Baker, N. R. 1989. The relationship between the quantum yield of photosynthetic electron-transport and quenching of chlorophyll fluorescence. Biochimica et Biophysica Acta **990**: 87-92.

Gordon, H. R., and McCluney, W. R. 1975. Estimation of the depth of sunlight penetration in the sea for remote sensing. Applied Optics **14**: 413-416.

Grasshoff, K. 1976. Methods of seawater analysis. Verlag Chemie.

Greene, R. M., Kolber, Z. S., Swift, D. G., Tindale, N. W., and Falkowski, P. G. 1994. Physiological limitation of phytoplankton photosynthesis in the eastern Equatorial Pacific determined from variability in the quantum yield of fluorescence. Limnology and Oceanography **39**: 1061-1074.

Gregg, W. W., and Carder, K. L. 1990. A simple spectral solar irradiance model for cloudless maritime atmospheres. Limnology and Oceanography **35**: 1657-1675.

Gregg, W. W., and Conkright, M. E. 2001. Global seasonal climatologies of ocean chlorophyll: Blending in situ and satellite data for the Coastal Zone Color Scanner era. Journal of Geophysical Research-Oceans **106**: 2499-2515.

Guillard, R. R. L., and Ryther, J. H. 1962. Studeis of marine planktonic diatoms. I. *Cyclotella nana* Hustedt and *Detonula confervaceae* (Cleve) Gran. Canadian Journal of Mircrobiology **8**: 229-239.

Han, B. P., Virtanen, M., Koponen, J., and Straskraba, M. 2000. Effect of photoinhibition on algal photosynthesis: a dynamic model. Journal of Plankton Research **22**: 865-885.

Harris, G. P. 1978. Photosynthesis, productivity and growth: the physiological ecology of phytoplankton. Arch. Hydrobiol. Geih. Ergeb. Limnol. **10**: 1-171.

---. 1980. The measurement of photosynthesis in natural populations of phytoplankton, p. 129-187. *In* T. Mouris [ed.], The physiological ecology of phytoplankton. University of California Press.

---. 1984. Phytoplankton productivity and growth measurements - Past, present and future. Journal of Plankton Research **6**: 219-237.

---. 1986. Phytoplankton ecology; Structure, function and fluctuation. Chapman and Hall.

Harris, G. P., Griffiths, F. B., and Thomas, D. P. 1989. Light and dark uptake and loss of C^{14} - methodological problems with productivity measurements in oceanic Waters. Hydrobiologia **173**: 95-105.

Harrison, W. G., Platt, T., and Lewis, M. R. 1985. The utility of light-saturation models for estimating marine primary productivity in the field - a comparison with conventional simulated *in situ* methods. Canadian Journal of Fisheries and Aquatic Sciences **42**: 864-872.

Henley, W. J. 1993. Measurement and interpretation of photosynthetic light-response curves in algae in the context of photoinhibition and diel changes. Journal of Phycology **29**: 729-739.

Hobson, L. A., Morris, W. J., and Pirquet, K. T. 1976. Theoretical and experimental analysis of the ^{14}C technique and its use in studies of primary production. Journal of the Fisheries Research Board of Canada **33**: 1715-1721.

Holligan, P. M., and Harbour, D. S. 1977. The vertical distribution and succession of phytoplankton in the western English Channel in 1975 and 1976. Journal of the Marine Biological Association of the U.K. **57**: 1075-1093.

Hooker, S. B., Esaias, W. E., Feldman, G. C., Gregg, W. W., and McClain, C. R. 1992. An overview of SeaWiFS Ocean Color. NASA Goddard Space Flight Center.

Hooker, S. B., and McClain, C. R. 2000. The calibration and validation of SeaWiFS data. Progress in Oceanography **45**: 427-465.

Ignatiades, L., Karydis, M., and Pagou, K. 1987. Patterns of dark $^{14}CO_2$ incorporation by natural marine-phytoplankton communities. Microbial Ecology **13**: 249-259.

IOC. 1994. Protocols for the Joint Global Ocean Flux Study (JGOFS) core measurements.

Jackson, G. A. 1993. The importance of the DOC pool for primary production estimates. ICES Marine Science Symposium **197**: 141-148.

Jassby, A. D., and Platt, T. 1976. Mathematical formulation of the relationship between photosynthesis and light for phytoplankton. Limnology and Oceanography **21**: 541-547.

Jeffrey, S. W., and Welschmeyer, N. A. 1997. Spectrofluorometric and fluorometric equations in common use in oceanography, p. 597-615. *In* S. W. Jeffrey, R. F. C. Mantoura and S. W. Wright [eds.], Phytoplankton pigments in oceanography: guidelines to modern methods. UNESCO.

Jitts, H. R., Morel, A., and Saijo, Y. 1976. The relation of oceanic primary production to available irradiance. Australian journal of marine and freshwater research **27**: 441-454.

Joint, I., and Groom, S. B. 2000. Estimation of phytoplankton production from space: current status and future potential of satellite remote sensing. Journal of Experimental Marine Biology and Ecology **250:** 233-255.

Joint, I., Wollast, R., Chou, L., Batten, S., Elskens, M., Edwards, E., Hirst, A., Burkill, P., Groom, S., Gibb, S., Miller, A., Hydes, D., Dehairs, F., Antia, A., Barlow, R., Rees, A., Pomroy, A., Brockmann, U., Cummings, D., Lampitt, R., Loijens, M., Mantoura, F., Miller, P., Raabe, T., Alvarez-Salgado, X., Stelfox, C., and Woolfenden, J. 2001. Pelagic production at the Celtic Sea shelf break. Deep-Sea Research Part II-Topical Studies in Oceanography **48:** 3049-3081.

Joint, I. R., Owens, N. J. P., and Pomroy, A. J. 1986. Seasonal production of photosynthetic picoplankton and nanoplankton in the Celtic Sea. Marine Ecology-Progress Series **28:** 251-258.

Joint, I. R., and Pomroy, A. J. 1986. Photosynthetic characteristics of nanoplankton and picoplankton from the surface mixed layer. Marine Biology **92:** 465-474.

Kirk. 1983. Light and photosynthesis in aquatic ecosystems, 1 ed. Cambridge University Press.

Kirkwood, D. 1989. Simultaneous determination of selected nutrients in sea water. ICES.

Kolber, Z., and Falkowski, P. G. 1993. Use of active fluorescence to estimate phytoplankton photosynthesis *in situ*. Limnology and Oceanography **38:** 1646-1665.

Kolber, Z., Wyman, K. D., and Falkowski, P. G. 1990. Natural variability in photosynthetic energy-conversion efficiency - a field-study in the Gulf of Maine. Limnology and Oceanography **35:** 72-79.

Kolber, Z. S. 1998. Fast Repetition Rate Fluorometry - A method for assessing ocean photosynthesis. Oceanology International 98. Spearhead Exhibitions Ltd. **1:** 329-340.

Kolber, Z. S., Prasil, O., and Falkowski, P. G. 1998. Measurements of variable chlorophyll fluorescence using fast reetition rate techniques: defining methodology an experimental protocols. Biochimie et Biophysica Acta **1367:** 88-106.

Krause, G. H., and Weis, E. 1991. Chlorophyll fluorescence and photosynthesis - The basics. Annual review of plant physiology **42:** 313-349.

Lande, R., and Lewis, M. R. 1989. Models of photoadaptation and photosynthesis by algal cells in a turbulent mixed layer. Deep-Sea Research Part a-Oceanographic Research Papers **36:** 1161-1175.

Langdon, C. 1993. The significance of respiration in production measurements based on oxygen. ICES Marine Science Symposium **197:** 69-78.

Lavender, S. J. 1996. Remote sensing of suspended sediment, Institute of Marine Studies. University of Plymouth and in collaboration with Plymouth Marine Laboratory.

Lavender, S. J., and Groom, S. B. 1999. The SeaWiFS Automatic Data Processing System (SeaAPS). International Journal of Remote Sensing **20:** 1051-1056.

Laws, E. A., and Bannister, T. T. 1980. Nutrient and light-limited growth of Thalassiosira fluviatilis in continuous culture with implications for phytoplankton growth in the ocean. Limnology and Oceanography **27:** 457-473.

Laws, E. A., Landry, M. R., Barber, R. T., Campbell, L., Dickson, M. L., and Marra, J. 2000. Carbon cycling in primary production bottle incubations: inferences from grazing experiments and photosynthetic studies using C^{14} and O^{18} in the Arabian Sea. Deep-Sea Research Part Ii-Topical Studies in Oceanography **47:** 1339-1352.

Lee, Z. P., Carder, K. L., Marra, J., Steward, R. G., and Perry, M. J. 1996. Estimating primary production at depth from remote sensing. Applied Optics **35:** 463-474.

Legendre, L., Demers, S., Therriault, J. C., and Boudreau, C. A. 1985. Tidal variations in the photosynthesis of estuarine phytoplankton isolated in a tank. Marine Biology **88:** 301-309.

Lewis, M. R., and Smith, J. C. 1983. A small volume, short-incubation-time method for measurement of photosynthesis as a function of incident irradiance. Marine Ecology-Progress Series **13**: 99-102.

Li, W. K. W. 1982. Estimating heterotrophic bacterial productivity by inorganic radiocarbon uptake - importance of establishing time courses of uptake. Marine Ecology-Progress Series **8**: 167-172.

Li, W. K. W., and Dickie, P. M. 1991. Light and dark C^{14} uptake in dimly-lit oligotrophic waters - relation to bacterial-activity. Journal of Plankton Research **13**: S29-S44.

Li, W. K. W., and Goldman, J. C. 1981. Problems in estimating growth rates of marine phytoplankton from short-term ^{14}C assays. Microbial Ecology **7**: 113-121.

Li, W. K. W., and Wood, A. M. 1988. Vertical-distribution of North-Atlantic ultraphytoplankton - Analysis by flow-cytometry and epifluorescence microscopy. Deep-Sea Research Part a-Oceanographic Research Papers **35**: 1615-1638.

Lizon, F., and Lagadeuc, Y. 1998. Comparisons of primary production values estimated from different incubation times in a coastal sea. Journal of Plankton Research **20**: 371-381.

Longhurst, A., Sathyendranath, S., Platt, T., and Caverhill, C. 1995. An estimate of global primary production in the ocean from satellite radiometer data. Journal of Plankton Research **17**: 1245-1271.

Lorenzen, C. J. 1972. Extinction of light in the ocean by phytoplankton. J. Cons. Perm. Int. Explor. Mer. **34**: 262-267.

MacCaull, A., and Platt, T. 1977. Diel variations in the photosynthetic parameters of coastal marine phytoplankton. Limnology and Oceanography **22**: 723-731.

Macedo, M. F., Duarte, P., and Ferreira, J. G. 2002. The influence of incubation periods on photosynthesis- irradiance curves. Journal of Experimental Marine Biology and Ecology **274**: 101-120.

Macedo, M. F., Ferreira, J. G., and Duarte, P. 1998. Dynamic behaviour of photosynthesis-irradiance curves determined from oxygen production during variable incubation periods. Marine Ecology-Progress Series **165**: 31-43.

MacIntyre, H. L., Kana, T. M., Anning, T., and Geider, R. J. 2002. Photoacclimation of photosynthesis irradiance response curves and photosynthetic pigments in microalgae and cyanobacteria. Journal of Phycology **38**: 17-38.

MacIntyre, H. L., Kana, T. M., and Geider, R. J. 2000. The effect of water motion on short-term rates of photosynthesis by marine phytoplankton. Trends in Plant Science **5**: 12-17.

Maddock, L., Boalch, G. T., and Harbour, D. S. 1981. Populations of phytoplankton in the western English Channel between 1964 and 1974. Journal of the Marine Biological Association of the U.K. **61**: 565-583.

Mantoura, R. F. C., Jeffrey, S. W., Llewellyn, C. A., Claustre, H., and Morales, C. E. 1997. Comparison between spectrophotometric, fluorometric and HPLC methods for chlorophyll analysis, p. 361-380. *In* S. W. Jeffrey, R. F. C. Mantoura and S. W. Wright [eds.], Phytoplankton pigments in oceanography: guidelines to modern methods. Monographs on oceanographic methodology. UNESCO.

Mantoura, R. F. C., and Llewellyn, C. A. 1983. The rapid-determination of algal chlorophyll and carotenoid-pigments and their breakdown products in natural-waters by reverse-phase High-Performance Liquid-Chromatography. Analytica Chimica Acta **151**: 297-314.

Mantoura, R. F. C., and Woodward, E. M. S. 1983. Optimization of the indophenol blue method for the automated- determination of ammonia in estuarine waters. Estuarine Coastal and Shelf Science **17**: 219-224.

Marra, J. 1978. Phytoplankton photosynthetic response to vertical movement in a mixed layer. Marine Biology **46**: 203-208.

---. 1980. Vertical mixing and primary production, p. 531. *In* P. G. Falkowski [ed.], Primary productivity in the sea. Plenum press.
---. 2002. Approaches to the measurement of plankton production, p. 78-108. *In* P. J. L. Williams, D. Thomas and C. S. Reynolds [eds.], Phytoplankton productivity: carbon assimilation in marine and freshwater ecosystems. Blackwell Science.
Marra, J., Haas, L. W., and Heinemann, K. R. 1988. Time course of C-assimilation and microbial food web. Journal of Experimental Marine Biology and Ecology **115**: 263-280.
McAllister, C. D., Shah, D., and Strickland, J. D. H. 1964. Marine phytoplankton photosynthesis as a function of light intensity: a comparison of methods. Journal of the Fisheries Research Board of Canada **21**: 159-189.
McClain, C. R., Barnes, R. A., Eplee, R. E., Franz, B. A., Hsu, N. C., Patt, F. S., Pietras, C. M., Robinson, W. D., Schieber, B. D., Schmidt, G. M., Wang, M., Bailey, s. W., and Werdell, P. J. 2000. SeaWiFS postlaunch calibration and validation analyses, Part 2. NASA Goddard Space Flight Center.
Mitchelson, E. G., Jacob, N. J., and Simpson, J. H. 1986. Ocean colour algorithms from the Case 2 waters of the Irish Sea in comparison to algorithms from Case 1 waters. Continental Shelf Research **5**: 403-415.
Moore, C. M. 2002. Small scale physical processes and phytoplankton growth in shelf seas, School of Ocean and Earth Sciences. University of Southampton.
Moore, G. F., Aiken, J., and Lavender, S. J. 1999. The atmospheric correction of water colour and the quantitative retrieval of suspended particulate matter in Case II waters: application to MERIS. International Journal of Remote Sensing **20**: 1713-1733.
Morel, A. 1974. Optical properties of pure water and pure seawater, p. 1-24. *In* N. G. Jerlov and E. Steeman-Neilsen [eds.], Optical aspects of oceanography. Academic.
---. 1988. Optical modeling of the upper ocean in relation to its biogenous matter content (Case-I waters). Journal of Geophysical Research-Oceans **93**: 10749-10768.
---. 1991. Light and marine photosynthesis - a spectral model with geochemical and climatological implications. Progress in Oceanography **26**: 263-306.
Morel, A., Antoine, D., Babin, M., and Dandonneau, Y. 1996. Measured and modeled primary production in the northeast Atlantic (EUMELI JGOFS program): The impact of natural variations in photosynthetic parameters on model predictive skill. Deep-Sea Research Part I-Oceanographic Research Papers **43**: 1273-1304.
Morel, A., and Berthon, J. F. 1989. Surface pigments, algal biomass profiles, and potential production in the western Mediterranean as derived and modelled from space (CZCS) observations. Limnology and Oceanography **34**: 1541-1564.
Morel, A., and Prieur, L. 1977. Analysis of variations in ocean colour. Limnology and Oceanography **22**.
Morel, A., and Smith, R. C. 1982. Terminology and units in optical oceanography. Marine Geodesy **5**: 335-349.
Morris, I., Yentsch, C. M., and Yentsch, C. S. 1971. Relationship between light carbon dioxide fixation adn dark carbon dioxide fixation by marine algae. Limnology and Oceanography **16**: 854-858.
Mueller, J. L., and Lang, R. E. 1989. Bio-optical provinces of the Northeast Pacific Ocean; A provisional analysis. Limnology and Oceanography **34**: 1572-1586.
Neale, P. J., and Marra, J. 1985. Short-term variation of Pmax under natural irradiance conditions - a model and its implications. Marine Ecology-Progress Series **26**: 113-124.
Neckel, H., and Labs, D. 1984. The solar radiation between 3300 and 12500 Angstrom. Solar physics **90**: 205-258.
Nuijs, A. M., Shuvalov, V. A., van Gorkom, H. G., Plijter, J. J., and Duysens, L. N. M. 1986. Picosecond absorbance-difference spectroscopy on the primary reactions and the

antenna-excited states in photosystem I particles. Biochimica et Biophysica Acta **850**: 310-318.

Olaizola, M., Geider, R. J., Harrison, W. G., Graziano, L. M., Ferrari, G. M., and Schlittenhardt, P. M. 1996. Synoptic study of variations in the fluorescence-based maximum quantum efficiency of photosynthesis across the North Atlantic Ocean. Limnology and Oceanography **41**: 755-765.

Olson, R. J., Sosik, H. M., Chekalyuk, A. M., and Shalapyononk, A. 2000. Effects of iron enrichment on phytoplankton in the Southern Ocean during late summer: active fluorescence and flow cytometric analyses. Deep-Sea Research Part II-Topical Studies in Oceanography **47**: 3181-3200.

O'Reilly, J. E., Maritorena, S., Mitchell, B. G., Siegel, D. A., Carder, K. L., Garver, S. A., Kahru, M., and McClain, C. 1998. Ocean color chlorophyll algorithms for SeaWiFS. Journal of Geophysical Research-Oceans **103**: 24937-24953.

Pahlow, M., and Riebesell, U. 2000. Temporal trends in deep ocean Redfield ratios. Science **287**: 831-833.

Pahl-Wostl, C., and Imboden, D. M. 1990. Dyphora - a dynamic model for the rate of photosynthesis of algae. Journal of Plankton Research **12**: 1207-1221.

Papageorgiou, G. 1975. Chlrlphyll fluorescence: an intrinsic probe of photosynthesis, p. 320-366. *In* Govindjee [ed.], Bioenergetics of photosynthesis. Academic.

Parsons, T. R., Maita, Y., and Lalli, C. M. 1984. A manual of chemical and biological methods for seawater analysis. Permangon press.

Peterson, B. 1980. Aquatic primary productivity and the ^{14}C-$C0_2$ method: A history of the productivity problem. Annu. Rev. Ecol. Syst. **11**: 359-385.

Pingree, R. D. 1975. The advance and retreat of the thermocline on the continental shelf. Journal of the Marine Biological Association of the U.K. **55**: 965-974.

Pingree, R. D., Holligan, P. M., and Mardell, G. T. 1978. The effects of vertical stability on phytoplankton distributions in the summer on the northwest European Shelf. Deep Sea Research **25**: 1101-1028.

Pingree, R. D., Holligan, P. M., Mardell, G. T., and Head, R. N. 1976. The influence of physical stability on spring, summer and autumn phytoplankton blooms in the celtic sea. Journal of the Marine Biological Association of the U.K. **56**: 845-873.

Pingree, R. D., Mardell, G. T., Holligan, P. M., Griffiths, D. K., and Smithers, J. 1982. Celtic Sea and Armorican current structure and the vertical distributions of temperature and chlorophyll. Continental Shelf Research **1**: 99-116.

Pingree, R. D., and Pennycuick, L. 1975. Transfer of heat, fresh water and nutrients through the seasonal thermocline. Journal of the Marine Biological Association of the U.K. **55**: 261-274.

Pinkerton, M. H. 2000. Validating remotely-sensed ocean colour data using a moored databuoy, School of Ocean and Earth Sciences. University of Southampton.

Platt, T. 1986. Primary production of the ocean water column as a function of surface light-intensity - algorithms for remote-sensing. Deep-Sea Research Part I-Oceanographic Research Papers **33**: 149-163.

Platt, T., Gallegos, C. L., and Harrison, W. G. 1980. Photoinhibition of photosynthesis in natural assemblages of marine-phytoplankton. Journal of Marine Research **38**: 687-701.

Platt, T., and Sathyendranath, S. 1988. Oceanic primary production : Estimation by remote sensing at local and regional scales. Science **241**: 1613-1619.

---. 1991. Biological production models as elements of coupled, atmosphere-ocean models for climate research. Journal of Geophysical Research-Oceans **96**: 2585-2592.

---. 1993. The Remote-Sensing of Ocean Primary Productivity - Use of a New Data Compilation to Test Satellite Algorithms - Comment. Journal of Geophysical Research-Oceans **98**: 16583-16584.

Platt, T., Sathyendranath, S., and Longhurst, A. 1995. Remote-sensing of primary production in the ocean - Promise and fulfillment. Philosophical Transactions of the Royal Society of London Series B-Biological Sciences **348:** 191-201.

Platt, T., Sathyendranath, S., and Ravindran, P. 1990. Primary production by phytoplankton - Analytic solutions for daily rates per unit area of water-surface. Proceedings of the Royal Society of London Series B-Biological Sciences **241:** 101-111.

Platt, T., Sathyendranath, S., White, G. N., and Ravindran, P. 1994. Attenuation of visible-light by phytoplankton in a vertically structured ocean - Solutions and applications. Journal of Plankton Research **16:** 1461-1487.

Prentice, I. C. 2001. The carbon cycle and atmospheric carbon dioxide. *In* J. T. Houghton et al. [eds.], Climate change 2001: The scientific basis: Contribution of working group I to the third assessment report of the Intergovernmental Panel on Climate Change. Cambridge University Press.

Prezelin, B. B., Tilzer, M. M., Schofield, O., and Haese, C. 1991. The Control of the Production Process of Phytoplankton by the Physical Structure of the Aquatic Environment with Special Reference to Its Optical-Properties. Aquatic Sciences **53:** 136-186.

Prieur, L., and Sathyendranath, S. 1981. An optical classification of coastal and oceanic waters based on the specific spectral absorption curves of phytoplankton pigments, dissolved organic-matter, and other particulate materials. Limnology and Oceanography **26:** 671-689.

Raven, J. 1993. Carbon: a phycocentric view, p. 123-152. *In* G. T. Evans, Fasham, M.J.R. [ed.], Towards a model of ocean biogeochemical processes. Springer.

Rees, A. P., Joint, I., and Donald, K. M. 1999. Early spring bloom phytoplankton-nutrient dynamics at the Celtic Sea Shelf Edge. Deep-Sea Research Part I-Oceanographic Research Papers **46:** 483-510.

Robinson, N. 1966. Solar radiation. Elsevier.

Rodhe, W. 1958. The primary production in lakes: some results and restrictions of the ^{14}C method. Rapp. Proc. Verb. Cons. Perm. Int. Expl. Mer: 122-128.

---. 1966. Standard correlations between pelagic photosynthesis and light, p. 367-381. *In* C. R. Goldman [ed.], Primary productivity in aquatic environments. University of California.

Rodriguez, F., Fernandez, E., Head, R. N., Harbour, D. S., Bratbak, G., Heldal, M., and Harris, R. P. 2000. Temporal variability of viruses, bacteria, phytoplankton and zooplankton in the western English Channel off Plymouth. Journal of the Marine Biological Association of the U.K. **80:** 575-586.

Ryther, J. H. 1954. The measurement of primary production. Limnol. Oceanogr. **1:** 72-84.

---. 1956. The measurement of primary production. Limnology and Oceanography **1:** 72-84.

Ryther, J. H., and Yentsch, C. M. 1957. The estimation of phytoplankton production in the ocean from chlorophyll and light data. Limnology and Oceanography **2:** 281-286.

Sakshaug, E., Bricaud, A., Dandonneau, Y., Falkowski, P. G., Kiefer, D. A., Legendre, L., Morel, A., Parslow, J., and Takahashi, M. 1997. Parameters of photosynthesis: definitions, theory and interpretation of results. Journal of Plankton Research **19:** 1637-1670.

Sathyendranath, S., and Platt, T. 1989. Computation of aquatic primary production - Extended formalism to include effect of angular and spectral distribution of light. Limnology and Oceanography **34:** 188-198.

Sathyendranath, S., Platt, T., Caverhill, C. M., Warnock, R. E., and Lewis, M. R. 1989. Remote-sensing of oceanic primary production - Computations using a spectral model. Deep-Sea Research Part I-Oceanographic Research Papers **36:** 431-453.

Sathyendranath, S., Platt, T., Horne, E. P. W., Harrison, W. G., Ulloa, O., Outerbridge, R., and Hoepffner, N. 1991. Estimation of New Production in the Ocean by Compound Remote- Sensing. Nature **353:** 129-133.

Schofield, O., Prezelin, B., and Johnsen, G. 1996. Wavelength dependency of the maximum quantum yield of carbon fixation for two red tide dinoflagellates, Heterocapsa pygmaea and Prorocentrum minimum (pyrrophyta): Implications for measuring photosynthetic rates. Journal of Phycology **32:** 574-583.

Shuter, B. 1979. A model of physiological adaptation in unicellular alga. Journal of Theoretical Biology **78:** 519-522.

Smetacek, V., Montresor, M., and Verity, P. 2002. Marine productivity: Footprints of the past and steps into the future, p. 350-369. *In* P. J. l. Williams, D. Thomas and C. S. Reynolds [eds.], Phytoplankton productivity: Carbon assimilation in marine and freshwater ecosystems. Blackwell Science.

Smith, R. C. 1981. Remote sensing and depth distribution of ocean chlorophyll. Marine Ecology Progress Series **5:** 359-361.

Smith, R. C., and Baker, K. S. 1978. The bio-optical state of ocean waters and remote sensing. Limnology and Oceanography **23:** 247-259.

Smith, R. C., Booth, C. R., and Star, J. L. 1984. Oceanographic biooptical profiling system. Applied Optics **23:** 2791-2797.

Smith, R. E. H., and Platt, T. 1984. Carbon exchange and 14C tracer methods in a nitrogen-limited diatom, Thalassiosira pseudonana. Marine Ecology Progress Series **16:** 75-87.

Sornin, J. M., Collos, Y., Delmas, D., Feuilletgirard, M., and Gouleau, D. 1990. Nitrogenous nutrient transfers in oyster ponds - Role of sediment in deferred primary production. Marine Ecology-Progress Series **68:** 15-22.

Strickland, J. D. H., and Parsons, T. R. 1968. A practical handbook of seawater analysis. Fisheries Research Board of Canada.

Strutton, P. G., Mitchell, J. G., Parslow, J. S., and Greene, R. M. 1997. Phytoplankton patchiness: quantifying the biological contribution using Fast Repetition Rate Fluorometry. Journal of Plankton Research **19:** 1265-1274.

Suggett, D., Kraay, G., Holligan, P., Davey, M., Aiken, J., and Geider, R. 2001. Assessment of photosynthesis in a spring cyanobacterial bloom by use of a fast repetition rate fluorometer. Limnology and Oceanography **46:** 802-810.

Taguchi, S. 1976. Relations between photosynthesis and cell size of marine diatoms. Journal of Phycology **12:** 185-189.

Talling, J. F. 1957. The phytoplankton population as a compound photosynthetic unit. New Phytologist **56:** 133-149.

Tassan, S., and Ferrari, G. M. 1998. Measurement of light absorption by aquatic particles retained on filters: determination of the optical pathlength amplification by the 'transmittance-reflectance' method. Journal of Plankton Research **20:** 1699-1709.

Taylor, A. H., Geider, R. J., and Gilbert, F. J. H. 1997. Seasonal and latitudinal dependencies of phytoplankton carbon- to-chlorophyll a ratios: Results of a modelling study. Marine Ecology-Progress Series **152:** 51-66.

Thomas, W. H., and Dodson, A. N. 1974. Inhibition of diatom photosynthesis by germanic acid. Separation of diatom productivity from total primary productivity. Marine Biology **27:** 11-19.

Tilzer, M. M., Hase, C., and Conrad, I. 1993. Estimation of *in situ* primary production from parameters of the photosynthesis - light curve obtained in laboratory incubators. ICES Marine Science Symposium **197:** 181-195.

Trees, C. C., Clark, D. K., Bidigare, R. R., Ondrusek, M. E., and Mueller, J. L. 2000. Accessory pigments versus chlorophyll a concentrations within the euphotic zone: A ubiquitous relationship. Limnology and Oceanography **45:** 1130-1143.

Vassiliev, I. R., Prasil, O., Wyman, K. D., Kolber, Z., Hanson, A. K., Prentice, J. E., and Falkowski, P. G. 1994. Inhibition of PS-II photochemistry by PAR and UV-radiation in natural phytoplankton communities. Photosynthesis Research **42**: 51-64.

Venrick, E. L., Beers, J. R., and Heinbokel, J. F. 1977. Possible consequences of containing microplankton for physiological measurements. Journal of Experimental Marine Biology and Ecology **26**: 55-76.

Verardo, D. J., Froelich, P. N., and McIntyre, A. 1990. Determination of organic-carbon and nitrogen in marine-sediments using the Carlo-Erba-Na-1500 analyzer. Deep-Sea Research Part a-Oceanographic Research Papers **37**: 157-165.

Verduin, J. 1960. Phytoplankton communities of western Lake Erie and the CO_2 and O_2 changes associated with them. Limnology and Oceanography **5**: 372-380.

Vollenweider, R. A. 1966. Calculation models of photosynthesis-depth curves and some implications regarding day rate estimates in primary production measurements, p. 426-457. *In* C. R. Goldman [ed.], Primary production in aquatic environments. University of California.

Watson, R. T. 2002. IPCC technical paper V: Climate change and biodiversity. *In* R. T. Watson, Gitay, H., Suarez, A. and Dokken, D.J. [ed.]. IPCC.

Welschmeyer, N. A. 1994. Fluorometric analysis of chlorophyll a in the presence of chlorophyll b and phaeopigments. Limnology and Oceanography **39**: 1985-1992.

Williams, P. J. l. 1993a. Chemical and tracer methods of measuring plankton production. ICES Marine Science Symposium **197**: 20-36.

Williams, P. J. L. 1993b. On the definition of plankton production terms. ICES Mar. Sci. Symp. **197**: 9-19.

Williams, P. J. L., Robinson, C., Sondergaard, M., Jespersen, A. M., Bentley, T. L., Lefevre, D., Richardson, K., and Riemann, B. 1996. Algal C^{14} and total carbon metabolisms .2. Experimental observations with the diatom Skeletonema costatum. Journal of Plankton Research **18**: 1961-1974.

Woodward, E. M. S. 1994. Nutrient analysis techniques, p. 26. Plymouth Marine Laboratory.

Wright, J. C. 1959. Limnology of Canyon Ferry Reservoir: Phytoplankton standing crop and primary production. Limnology and Oceanography **4**: 235-245.

Appendix I : Intercalibration of HPLC instrument and spectrofluorometer at PML

An exercise to compare chlorophyll estimates from HPLC and spectrofluorometric techniques was carried out as a result of the suspected failure of the lamp in the spectrofluorometer. A new lamp and new powerboard were fitted before the intercalibration and the comparisons carried out to ensure that similar estimates of chlorophyll were obtained from the two instruments and their respective techniques.

Water was collected from station E1, a Case I site approximately 20km south of the breakwater of Plymouth sound and not influenced by coastal run off. On return to the laboratory the water was distributed from one large carboy, in which all the water had been well mixed. For each instrument, 4 x 2l aliquots and 4 x 1l aliquot were filtered onto 25mm Whatman GF/F filters. Samples for HPLC analysis were frozen and stored in liquid nitrogen overnight prior to analysis the next morning. Extraction and analysis of pigments was carried out as described in the methods chapter. Samples for spectrofluorometric analysis were frozen and stored at –20°C immediately after filtration. The same evening, 10ml of 90% acetone was added to each sample, and the samples left overnight at -20°C before analysis the next morning.

Table A1 shows the chlorophyll concentrations measured by each technique. The estimates were very similar and results from the two instruments could not be distinguished statistically (One-way ANOVA). It was concluded that the two techniques were producing similar estimates of chlorophyll concentration.

Table A1. Chlorophyll concentration (in mg m^{-3}) measured by each technique. Spec refers to spectrofluorometric measurements.

	2l aliquots		1l aliquots	
Replicate	HPLC	Spec.	HPLC	Spec.
1	0.684	0.646	0.666	0.758
2	0.650	0.624	0.729	0.671
3	0.532	0.648	0.856	0.784
4	0.702	0.666	0.620	0.668
Average	0.642 ± 0.076	0.646 ± 0.017	0.718 ± 0.102	0.720 ± 0.060

Appendix II: IDL code to calculate error on PP_{Daily} from ^{14}C and the FRRF using Taylor series approximation.

```
;"14c_error_model.pro":a model coded in IDL, using a Taylor series
;approximation to estimate the variance associated with estimates of daily,
;depth-integrated production (PPDaily) from 14C and the FRRF.

pro l4_14c_error_model

; Create a file to write the results to and give it a name

outputfile = 'taylor_l4_14c_nonhinhib_error_out.txt'
openw,output,outputfile,/get_lun

; Print column headings on the output file

printf,output,'Date ','I_total ', 'PP_total ', 'Error_total ';

; run the non-photoinhibited model
mode = 2

;"filestems" gives dates for which calculations should be carried out
;i.e. dates for which input files are available.  These numbers are the
;prefixes used on each input file.

filestems = ['0108','0207','0309','0406','0503','0511','0805','0907',$
             '1009','1012','1211','1308','1405','1601','1709',$
            '1804','1902','1911','2008','2304','2307','2409',$
            '2611','3004','3105']

;Loop through all the dates. Call the input file for a particular date
;and carry out the error

for file_loop = 0, n_elements(filestems) - 1 do begin

  ;look for the filestem that corresponds to the current iteration of the
  ;file loop. Print the date to the screen.

   stem = filestems[file_loop]
   print, stem

  ;States that the three input files are in ASCII format.  The first
  ;(parameters) contains values for chlorophyll, the photosynthetic
  ;parameters, their variances and correlations and the value and variance
  ;of KPAR.  The second (table 1) contains the value of PAR at the surface
  ;for every hour of the day and the third (table2) contains a list of
  ;depths.

   parameters = read_ascii(stem+'_l4_frrf.txt')
   table1 = read_ascii(stem+'.txt')
   table2 = read_ascii('depth_table.txt')

   ;lists where to find the parameters in the input file

   chlorophyll = parameters.field1[0] ;Chlorophyll concnetration
   Pbnon = parameters.field1[9]           ;Value of PBm
   anon = parameters.field1[11]           ;Value of alphaB
   Pbsd_non = parameters.field1[10]    ;Error associated with Pbm
   asd_non = parameters.field1[12]     ;Error associated with alpha
   Qa_corr = parameters.field1[13]     ;Correlation Pbm and alpha
   kd = parameters.field1[3]           ;Value of KPAR
   kd_sd = parameters.field1[4]        ;Error associated with KPAR
```

```
;lists where to find PAR(IO) and depthin the relevent tables

;table 1
time = reform(table1.field1[0,*])
I0 = reform(table1.field1[1,*])

;table 2
depth = reform(table2.field1[0,*])


;limits the depth of the euphotic zone to 30m and the surface effect
; to 0.538 for overcast skies
max_depth = 30
sfce_effect = 0.538

;Create parameters to hold the cumulative totals of PAR(I), production
;(PP)and error(PPerror)as the model iterates through each hour of the
;day.

I_timetotal = 0
PP_timetotal = 0
PPerror_timetotal = 0

;carry out the calculations for every hour in the day
for time_loop = 0, n_elements(time)-1 do begin

  ;Create parameters to hold the cumulative totals as the model iterates
  ;through each depth in the water column.

  I_depthtotal = 0
  PP_depthtotal = 0
  PPerror_depthtotal = 0

  ;carry out the calculations for every depth in the water column.
  for depth_loop = 0, max_depth do begin

    ;calculate modelled PAR (Izt) and production (PPzt)

    mod_Izt = (I0[time_loop]*sfce_effect)*EXP(-(kd*depth[depth_loop]))
    mod_PPzt = (Pbnon*(1-EXP(-((anon*mod_Izt)/Pbnon))))*chlorophyll

    ;calculate error on modelled PPzt (mod_var_zt)
    ;The first stage is to adjust the parameter and error absolute
    ;values for the calculation in order to minimise rounding errors
    ;caused by working with numbers of very different sizes.

    error_Izt =
    ((I0[time_loop]/100)*sfce_effect)*EXP((kd*depth[depth_loop]))
    error_Q = Pbnon/10
    error_a = anon*10
    error_Qsd = Pbsd_non/10
    error_asd = asd_non*10

    ;define the simplified parts of the equation to make differentiation
    ;easier.

    CapA=EXP((-(error_a/error_Q))*error_Izt)
    CapC=error_Izt

    ;calculate the partial differentials of the production equation
    ;with respect to each parameter

    dpdQ= (1-CapA)-((CapA*CapC*error_a)/error_Q)    ;Pbm partial diff.
    dpda= CapA*CapC                                 ;alpha partial diff.
```

```
      dpdk= -(CapA*error_a*CapC*depth[depth_loop])    ;KPAR partial diff.

      ;define the different parts of the Taylor series equation which will
      ;need to be summed to obtain final answer. pts 1-3 are partial
      ;differentials and part 4 is the correlation coefficient.

      pt_1=(dpdQ^2)*(error_Qsd^2)
      pt_2=dpda^2*error_asd^2
      pt_3=dpdk^2*kd_sd^2
      pt_4=(2*(dpdQ*dpda))*(Qa_corr*error_Qsd*error_asd)

      ;sum the parts to calculate total variance then sqare root to get SE

      mod_var_error_zt=(pt_1+pt_2+pt_3+pt_4)
      mod_sd_error_zt = sqrt(mod_var_error_zt)

      ;Adjust the final value to account for the earlier adjustments made
      ;to the original figures to avoid rounding problems.

      mod_sd_zt = 10*mod_sd_error_zt

      ;calculate the weights required to multiply the value at each depth
      ;and time in order to be able to sum the output in an approximate
      ;integration. The constant weights each estimate as it would be
      ;during a trapezium integration. This allows all the estimates to be
      ;summed to get the final daily, depth-integrated value.  The default
      ;weight is 1.  The weight is 1/4 for all values which are calculated
      ;at the first or last depths or times but not both and 1/16 for
      ;those which are calculated at both.

      weight = 1. ; This is the default weight

      IF ((depth[depth_loop] EQ 0. OR depth[depth_loop] EQ 30.) AND $
              (time[time_loop]EQ 0. OR time[time_loop]EQ 23.)) $
        THEN weight=(1./16.)

      IF ((depth[depth_loop]EQ 0. OR depth[depth_loop] EQ 30.) AND $
              (time[time_loop] NE 0. OR time[time_loop]NE 23.)) $
        THEN weight = (1./4.)

      IF ((depth[depth_loop] NE 0. OR depth[depth_loop]NE 30.) AND $
              (time[time_loop] EQ 0. OR time[time_loop]EQ 23.)) $
           THEN weight = (1./4.)

      ;multiply calculated values of PAR, production and error by weights.

      weight_mod_Izt = weight*mod_Izt
      weight_mod_PPzt = weight*mod_PPzt
      weight_mod_sd_zt=weight*mod_sd_zt

      ;add the value for the current depth iteration to the depth total
      ;(i.e. the cumulative total for all depths at a particular time of
      ;day).

      I_depthtotal = I_depthtotal + weight_mod_Izt
      PP_depthtotal = PP_depthtotal + weight_mod_PPzt
      PPerror_depthtotal = PPerror_depthtotal + weight_mod_sd_zt

   ; end depth loop
   endfor; end depth_loop

;add the value for the current time iteration to the time total. (i.e.
;the cumulative total for all times over the day).
```

```
  I_timetotal = I_timetotal + I_depthtotal
  PP_timetotal = PP_timetotal + PP_depthtotal
  PPerror_timetotal = PPerror_timetotal + PPerror_depthtotal

  ;end time_loop
  endfor

 ;print the daily totals of PAR, production and error to the output file
 ;and format the file.

 printf,output,filestems[file_loop],I_timetotal, PP_timetotal,$
     PPerror_timetotal;
     format='(1(X,I3),3(X,F12.3))'

;end file_loop
endfor

;frees up the space temporarily allocated to the output
free_lun, output

end
```

Appendix III: IDL code to calculate error on PP_{Daily} from ^{14}C and the FRRF using Monte Carlo modelling.

```
;"intmontecarlo.pro" a Monte carlo model (coded in IDL) to calculate the
;error associted with estimates of daily, depth-integrated production
;(PPDaily) from 14C and the FRRF.

pro intmontecarlo

; Create a file to write the results to and give it a name

outputfile = '14c_montecarlo_out.txt'
openw,output,outputfile,/get_lun

; Print column headings on the output file

printf,output,'Date ','I_total ', 'PP_total ', 'Error_total ';

;"filestems" gives dates for which calculations should be carried out
;i.e. dates for which input files are available.  These numbers are the
;prefixes used on each input file.

filestems = ['0108','0207','0309','0406','0503','0511','0805','0907',$
             '1009','1012','1211','1308','1405','1601','1709',$
            '1804','1902','1911','2008','2304','2307','2409',$
            '2611','3004','3105']

;Loop through all the dates. Call the input file for a particular date
;and carry out the error

for file_loop = 0, n_elements(filestems) - 1 do begin

  ;look for the filestem that corresponds to the current iteration of the
  ;file loop.  Print the date to the screen.

  stem = filestems[file_loop]
  print, stem

  ;States that the three input files are in ASCII format.  The first
  ;(parameters) contains values for chlorophyll, the photosynthetic
  ;parameters, their variances and correlations and the value and variance
  ;of KPAR.  The second (table 1) contains the value of PAR at the surface
  ;for every hour of the day and the third (table2) contains a list of
  ;depths.

  parameters = read_ascii(stem+'_14cparams.txt')
  table1 = read_ascii(stem+'.txt')
  table2 = read_ascii('depth.txt')

  ;lists where to find the parameters in the input file

  chl = parameters.field1[0]       ; Chlorophyll concentration
  Q = parameters.field1[10]      ; Value of PBm
  a = parameters.field1[11]      ; Value of alphaB
  Q_sd = parameters.field1[12]         ; Error associated with PBm
  a_sd = parameters.field1[13]         ; Error associated with alphaB
  Qa_corr = parameters.field1[14] ; Correlation alphaB and PBm
  kd = parameters.field1[17]       ; Value of KPAR
  kd_sd = parameters.field1[18]    ; Error associated with KPAR

  ;lists where to find PAR(IO) and depthin the relevent tables

  ; table 1
```

```
time = reform(table1.field1[0,*])
I0 = reform(table1.field1[1,*])

; table 2
depth = reform(table2.field1[0,*])


;limits the depth of the euphotic zone to 30m.
max_depth = 30

;Create parameters to hold the cumulative totals of PAR(I), production
;(PP)and error(PPerror)as model iterates through each hour of the day.

I_timetotal = 0
PP_timetotal = 0
PPerror_timetotal = 0

;carry out the calculations for every hour in the day
for time_loop = 0, n_elements(time)-1 do begin

  ;Create parameters to hold the cumulative totals as the model iterates
  ;through each depth in the water column.

  I_depthtotal = 0
  PP_depthtotal = 0
  PPerror_depthtotal = 0

  ;carry out the calculations for every depth in the water column.
  for depth_loop = 0, max_depth  do begin

   ;create an array to hold the 100 repeat estimates

   PPrepeat = fltarr(100)

   ;carry out the calculations for 100 repeats
   for repeat_loop = 0, 99 do begin

     ;generate random, normally distributed numbers,mean 0 & variance 1.


     randQ = (RANDOMN(seed))       ;first stage random value for PBm
     randa = (RANDOMN(seed))  ;first stage random value for alphaB
     randkd = (RANDOMN(seed)) ;first stage random value for KPAR

     ;calculate midQ and mida- the correlated variables with
     ;normal distribution, mean 0 and variance 1.

     midQ = randQ
     mida = (Qa_corr*randQ) + (sqrt(1-(Qa_corr^2)))*randa

     ;calculate final random values which have mean mu and sd equal to
     ;that of measured values.

    finalQ = abs(Q + Q_sd*[midQ])     ;final random PBm
    finala = abs(a + a_sd*[mida])     ;final random alphaB
    finalkd = abs(kd + kd_sd*randkd) ;final random KPAR

    ; calculate PAR (Izt) and production (PP_repzt) for that iteration

    Izt = (I0[time_loop]*0.538)*EXP(-(kd*depth[depth_loop]))
    PP_repzt = (finalQ*(1-EXP(-((finala*Izt)/finalQ))))*chl

    ;put the calculated values into the previously created array
```

```
      PPrepeat[repeat_loop]= PP_repzt

      ; end the repeat loop
      endfor

    ;use an IDL function (moment) to calculate the average of the 100
    ;repeats (PPaverage), the standard deviation (PPsd) and the minimum
    ;(PPmin).

    PPzt = moment(PPrepeat)
    PPaverage = PPzt[0]
    PPmin = min(PPrepeat, max = PPmax)

    ;calculate the weights required to multiply the value at each depth and
    ;time in order to be able to sum the output in an approximate
    ;integration.The constant weights each estimate as it would be during a
    ;trapezium integration.  This allows all the estimates to be summed to
    ;get the final daily, depth-integrated value.  The default weight is 1.
    ;The weight is 1/4 for all values which are calculated at the first or
    ;last depths or times but not both and 1/16 for those which are
    ;calculated at both.

    weight = 1. ; This is the default weight

    IF ((depth[depth_loop] EQ 0. OR depth[depth_loop] EQ 30.) AND $
      (time[time_loop]EQ 0. OR time[time_loop]EQ 23.)) $
      THEN weight=(1./16.)

    IF ((depth[depth_loop]EQ 0. OR depth[depth_loop] EQ 30.) AND $
      (time[time_loop] NE 0. OR time[time_loop]NE 23.)) $
      THEN weight = (1./4.)

    IF ((depth[depth_loop] NE 0. OR depth[depth_loop]NE 30.) AND $
      (time[time_loop] EQ 0. OR time[time_loop]EQ 23.)) $
      THEN weight = (1./4.)

    ; multiply calculated values of PAR, production and error by weights.

    weight_Izt = weight*Izt
    weight_PPsd = weight*PPsd
    weight_PPave = weight*PPaverage

    ;add the value for the current depth iteration to the depth total
    ;(i.e. the cumulative total for all depths at particular time of day).

    I_depthtotal = I_depthtotal + weight_Izt
    PP_depthtotal = PP_depthtotal + weight_PPave
    PPerror_depthtotal = PPerror_depthtotal + weight_PPsd

    ; end depth loop
    endfor

  ;add the value for the current time iteration to the time total. (i.e.
  ;the cumulative total for all times over the day).

  I_timetotal = I_timetotal + I_depthtotal
  PP_timetotal = PP_timetotal + PP_depthtotal
  PPerror_timetotal = PPerror_timetotal + PPerror_depthtotal

  ;end time loop
  endfor

;print the daily totals of PAR, production and error to the output file
;and format the file.
```

```
 printf,output,filestems[file_loop],I_timetotal, PP_timetotal,$
    PPerror_timetotal;
    format='(2(X,I3),4(X,F12.3))'

 ;end file_loop
 endfor

;free up the space temporarily allocated to the output

free_lun, output

end
```

Appendix IV

SUBMITTED TO CONTINENTAL SHELF RESEARCH

The influence of water mass characteristics on phytoplankton production in the Celtic Sea

Katharine Woods, Andrew P Rees, Peter I Miller, Ian Joint*
Plymouth Marine Laboratory, Prospect Place, The Hoe, Plymouth PL1 3DH

Abstract

The influence of water mass characteristics on phytoplankton biodiversity and production has been studied in stratified, mixed and frontal water masses in the Celtic Sea. The stations were in close geographical proximity to each other and would have experienced similar solar radiation in the weeks before water column stabilisation occurred, yet very different phytoplankton assemblages were found at the stations sampled, suggesting that biodiversity is controlled largely by hydrographic conditions. Satellite remote sensing has been used to map the development of stratification and frontal development in the weeks before the cruise so that the stations sampled were placed within a strong geographical and temporal context. Stations with a well-mixed water column had high nutrient concentrations and production and the phytoplankton assemblage was dominated by diatoms. The stratified water column had nutrient depletion but primary production was still relatively high suggesting that nutrient depletion was a recent event. These stations were dominated by dinoflagellates, with few diatoms even though silicate was still present. The phytoplankton composition of the frontal stations was dominated by dinoflagellates and microflagellates. The photosynthetic characteristics of the phytoplankton assemblages were determined at the stratified stations. P^B_m values varied from 1.43 to 4.79 mg C [mg Chl]$^{-1}$ h^{-1}, while α^B ranged from 0.011 to 0.047 mg C [mg Chl]$^{-1}$ h^{-1} (μmol photons m^{-2} s^{-1})$^{-1}$.

Keywords: Tidal mixing; Fronts; Primary production; P/E parameters.

---

1. Introduction

In terrestrial ecology, it has been suggested that an overall increase in the total number of organisms present in a biotope is associated with increased community productivity (Naeem, et al., 1994); that is, there appears to be a relationship between

*Corresponding author. Tel.: + 44 1752 633100: fax: +44 1752 633101

E-mail address: i.joint@pml.ac.uk

biodiversity and productivity. Primary production in marine ecosystems is due to photosynthetic microbes which are present at low biomass but grow rapidly. As such, marine ecosystems are very different to terrestrial systems which tend to have a high biomass of slow growing primary producers. It is appropriate to investigate the factors which control marine phytoplankton biodiversity and production.

The phytoplankton species which come to dominate any water mass depend on a complex interaction of factors — nutrients, light, hydrography, grazing and infection. However, in some biogeographic provinces, a single factor may be the primary reason for the success of a phytoplankton species. For example, in oligotrophic waters, picophytoplankton dominate and much of the tropical oceans have phytoplankton assemblages composed of little more than *Prochlorococcus* and *Synechococcus*. Changes in species composition in these regions tend to be linked to perturbation events, particularly through variations of nutrient supply by events such as upwelling (Joint et al., 2001a; Donald et al., 2001) which may favour the growth of larger phytoplankton cells. An extreme example of perturbations of natural assemblages have been the recent experiments involving the addition of iron to high nitrate:low chlorophyll regions of the ocean. Iron addition resulted in enhanced growth of diatoms and other large-celled phytoplankton, rather than the picoplankton which were the major component of the ecosystem before the perturbation (Landry et al., 2001). Natural perturbations also appear to favour the development of large phytoplankton cells. In a study of an upwelling region, Joint et al. (2001a) found that the introduction of nutrient-rich water into the euphotic zone resulted in enhanced growth of large (>5μm) phytoplankton production and little stimulation of smaller phytoplankton (with cell dimensions between 2 and 5μm) or of picophytoplankton (<2μm). Factors other than nutrients are also important in determining phytoplankton biodiversity. Light is clearly critical, both in the total photon flux which is available for photosynthesis and also in spectral composition, with different phytoplankton species able to exploit conditions at the base of the euphotic zone. This paper examines the effect of hydrography on phytoplankton assemblages and investigates the effect of different degrees of vertical mixing within a small geographical area of a temperate shelf sea.

It is well established that the hydrographic conditions on the European shelf exert an effect on phytoplankton biodiversity and seasonally stratified waters are dominated by very different species than in tidally well-mixed waters (Pingree et al., 1976). Frontal regions between mixed and stratified conditions are a special case that may favour the development of high biomass, particularly of dinoflagellates. It is suggested that high biomass can develop at a tidal front because nutrient-rich water is close to the high light conditions at the sea

surface. Hence the growth conditions for dinoflagellates are optimised, which leads to the observed high phytoplankton biomass in summer (Pingree et al., 1976).

Little is known about how the transition from well-mixed winter conditions to summer conditions of mixed, stratified or frontal water columns influences the establishment of different phytoplankton populations. In this study, we have sampled a frontal region at the Celtic Sea / Irish Sea boundary during the period of thermal stratification and frontal development in the spring. The aim was to investigate primary production and understand why certain phytoplankton assemblages come to dominate in the different hydrodynamic regimes.

The boundary between the Celtic and Irish Seas is a region where high variability in hydrographic conditions occurs over short distances, with the development of a tidal front between well-mixed and seasonally stratified conditions. Variation in vertical stability of the water column is an important factor in determining the spatial and temporal variation of phytoplankton production in the region (Pingree, 1975). A large fraction of the annual production in the Celtic Sea occurs during the spring bloom (Joint and Pomroy, 1986; Joint et al., 2001b), which usually takes place in April and May and lasts for approximately two months (Rees et al., 1999). The main increase in phytoplankton biomass coincides with the formation of the seasonal thermocline, which maintains cells in the euphotic zone by limiting vertical mixing (Fasham et al., 1983). The phytoplankton spring bloom does not develop simultaneously over the whole region but starts to the south of Ireland and spreads eastwards as surface temperature increases (Pingree, 1975). The timing of the spring bloom appears to be relatively constant. In 1975, Pingree et al. (1976) reported that large changes in production and chlorophyll began after the 23 April and, twenty years later in 1994, Rees et al. (1999) found that the bloom began at the shelf edge between late April and early May.

The current study took place in late May 2000, about one month after the expected onset of the bloom. Stations were sampled in well-mixed, stratified and frontal waters of relatively close proximity to one another. All stations experienced similar weather conditions and would have had identical nutrient concentrations before the onset of stratification. Therefore the major factors influencing phytoplankton development would be hydrographic, rather than meteorological; the development of different phytoplankton assemblages would primarily be due to the scale of vertical mixing.

2. Methods

2.1 Study area

The study was carried out on *RRS Discovery* as part of a multidisciplinary cruise in the Celtic Sea from 17 – 28 May 2000 and involved a total of 11 days of sampling. The positions of the stations are shown in Fig. 1a. Initially, four stations (A, B, C and D) in St.George's Channel were each occupied for 24 h in regions where mixed or frontal conditions were expected to develop. Three stations which experience seasonal stratification (E, F and G) were sampled from 22 to 28 May 2000 to the south of the front. At station G, experiments were done over a 72h period (22 to 24 May) and at both stations E and F, sampling took place over 48 h periods (25 to 26 May and 27 to 28 May respectively).

2.2 Front detection from satellite remote sensing

We have taken advantage of recent advances in satellite remote sensing to place our field measurements within a wider geographical context. In particular, we have used AVHRR images to track the development of the front through the spring. AVHRR data are automatically calibrated by the Plymouth Marine Laboratory to give values of cloud-masked, and geo-referenced sea surface temperature (SST), using the Panorama system (Miller et al., 1997). In this region, cloud cover is a particular problem when using satellite remote sensing to determine SST and to track the development of the front. Miller (2002) has developed a novel technique which increases the value of cloud-affected sequences of SST for visualising dynamic physical and biological oceanic processes such as fronts, eddies and blooms. A composite front-map approach combines the location, strength and persistence of all fronts observed over several days into a single map, which allows intuitive interpretation of mesoscale structures (Miller, 2002). This method achieves a synoptic view without blurring dynamic features, an inherent problem with conventional time-averaging compositing methods.

The methodology requires the automated detection of all fronts on a sequence of satellite data. This stage is based upon the single-image edge detection (SIED) algorithm designed for thermal oceanic fronts (Cayula and Cornillon, 1992) and the locations of all fronts observed over 3 or 7 days are combined into a single map. The gradient magnitude at each front pixel is weighted by the probability of observing a front at that location during the sequence; this is estimated by the fraction of cloud-free views of that pixel in which a front was detected. Thus darker lines in the composite front map indicate more significant fronts either due to their gradient or persistence.

2.3 Sampling

Water samples were collected both with 30 litre Teflon-lined Niskin bottles and with 10l externally sprung Niskin bottles (X-Niskins) mounted on a rosette pylon (General Oceanics) on a large 24-way frame. Temperature and salinity were measured using a Neil Brown Mk3C conductivity-temperature-depth profiler, mounted on the rosette sampler frame. Samples were routinely taken from 10 depths within the euphotic zone just before dawn each day for the measurement of nutrient and pigment concentrations and photosynthetic activity. Additional water samples were taken at noon (± 1 h) for nutrient and pigment determination, when profiles of light (PAR – photosynthetically available radiation 400-700nm) were also obtained.

2.4 Nutrients, pigments and light analysis

Chlorophyll concentration was determined by filtering 2l seawater through 25 mm diameter Whatman GF/F filters which were frozen immediately and stored in liquid nitrogen for later analysis by HPLC (Jeffrey et al., 1997). Dissolved nutrient concentrations were analysed as soon as practicable after sampling and always completed within 4 h of sample collection; in the period between sampling and analysis, samples were stored at 4°C in the dark. Nutrient concentrations were determined by colorimetric autoanalysis using the methods of Brewer and Riley (1965) for nitrate, Grasshoff (1976) for nitrite, Kirkwood (1989) for silicate and phosphate, and ammonium by the fluorometric method described by Jones (1991). Vertical attenuation of PAR was determined with a Chelsea Technology Group 4π PAR sensor mounted above the rosette sampler. Surface PAR was measured using an ELE DRP-5 Vector Irradiance PAR sensor mounted high on the ship. Data were logged every 30 seconds and PAR was calculated as Watts m^{-2}.

2.5 Daily primary production estimates

Samples for the estimation of phytoplankton activity were taken just before dawn each day and care was taken to maintain samples in the dark to prevent light-shock to the phytoplankton cells. Water was collected from 6 depths, corresponding to 1, 5, 14, 20, 55 and 97% of irradiance just below the sea surface. Samples were decanted into acid-washed 1l polycarbonate bottles and distributed to 60ml polycarbonate bottles that had been cleaned to JGOFS standards (IOC, 1994). For each depth, three light bottles and one dark bottle were inoculated with 370 kBq (10μCi) $NaH^{14}CO_3$ and incubated in an on-deck incubator which was cooled with surface seawater. Neutral density and blue filters simulated light attenuation in the water column so that the bottles were incubated at irradiance levels approximating

those at the depths of sampling. After 24h incubation, samples were filtered through 47mm diameter, 0.2μm pore-size Nuclepore polycarbonate filters. The filters were exposed to fuming HCl to remove unfixed ^{14}C and were dried in a dessicator containing silica-gel for 12h before the addition of scintillation cocktail (Wallac OptiPhase Hi-Safe 3). The ^{14}C content of the filters was measured with a liquid scintillation counter (LKB-Wallac 1219 RackBeta LSC) and carbon fixation rates were calculated using the method of Joint and Pomroy (1986). Depth-integrated production was calculated for the euphotic water column. Attenuation coefficients were determined at mid-day and used to estimate the depths in the water column that corresponded to the percentage of surface irradiance used in the on-deck incubator.

2.6 Photosynthetic parameters

Photosynthesis-irradiance (P-E) parameters were determined at stations E, F and G on water samples collected at dawn and at midday. Two depths were sampled — <12 m (which are referred to as shallow samples) and at the base of the euphotic zone (deep samples). The samples were treated as for the 24h simulated-*in-situ* incubations and 15 bottles were incubated for 3 – 4 hours in a light gradient incubator which was cooled with surface seawater. The light source was a 12V Tungsten-Halogen lamp with a blue filter to simulate the spectrum of natural light.

At the end of the incubation period, PAR was measured at each position in the incubator using a PAR meter with a fibre optic probe and 4π light collector. The probe was placed in a bottle filled with filtered seawater and measurements taken by replacing sequentially the experimental bottle at each position in the column. After incubation, all samples were filtered, acid fumed and dried. Carbon fixation rates were normalised to chlorophyll concentration and P-E curves were fitted to the equations of Platt *et al.* (1980) using SPSS SigmaPlot version 5.0. The equation used to fit the data included photoinhibition. The parameters determined were the maximum rate of carbon fixation P^B_m (mg C [mg Chl]$^{-1}$ h^{-1}), the initial slope α^B (mg C [mg Chl]$^{-1}$ h^{-1} (μmol quanta m^{-2} s^{-1})$^{-1}$) and the derived parameter E_k (P^Bm / α^B) which is an indicator of adaptation to high or low light. Since α^B is wavelength dependent, a correction was made for the emission spectrum of the lamp using the equations of Arrigo and Sullivan (1992). The correction factor was calculated as the ratio of irradiance that would be absorbed by phytoplankton in situ to that absorbed by phytoplankton in the incubator. The parameters required for the equations were the spectrum of the lamp and that of in situ sunlight, as well as the phytoplankton absorption spectrum. The lamp spectrum was calculated from a standard halogen emission spectrum corrected for

the absorption of the blue filter. A standard irradiance spectrum of sunlight (after Neckel and Labs, 1984) was corrected for the depth of water collection and used to describe *in situ* irradiance. Phytoplankton absorption spectra were provided for each cast and each depth sampled (Richard Geider, pers. comm.). They had been calculated from the spectrophotometric analysis of 25mm diameter Whatman GF/F filters onto which 1l of water had been filtered before freezing.

3. Results

3.1 Water-column structure

Fig. 1 shows the development of the front in the Celtic Sea in the weeks prior to the cruise. In early April, sea surface temperature (SST) was uniform across the northern Celtic Sea and there was no evidence of a front in St George's Channel in AVHRR images (Fig. 1a). Composite front maps derived from satellite remotely-sensed estimates of temperature (Fig. 1 b-e) demonstrate the development of the front in the period from mid-April to mid-May, just prior to the cruise. During the week of 16-22 April, the composite map (Fig. 1b) indicates the beginning of a front that extended from the Irish coast to the middle of St George's Channel. One week later (Fig. 1c), the front extends across St George's Channel to the north Cornish coast. The feature becomes much clearer in composite maps for the first (Fig. 1d) and second (Fig. 1e) weeks of May. The front that traversed St. George's Channel had a distinct U-shape in the centre that protruded north eastwards into the channel. The frontal feature persisted throughout the spring and is evident in SST images of the region at the end of June (Fig. 1f) and throughout the summer months. It was very cloudy during the cruise and few, even partial, images were obtained. Based on the stability of the front throughout the rest of the summer, we believe that little variation occurred in front structure during the cruise — but we have no satellite images to confirm that assumption.

3.2 Chlorophyll and nutrient concentrations

The vertical structures of temperature and salinity (Fig. 2) confirm the water column structure inferred from satellite images. At station B, to the north of the front, the temperature and salinity profiles suggested a well mixed water column; however, chlorophyll concentration above 22m was slightly greater than at 27m, suggesting that the water column at the time of sampling was not strongly mixed. The highest phytoplankton biomass was found at this station, with high chlorophyll concentration throughout the water column and an average concentration of 3.1 mg m^{-3}. Station D, slightly to the north of the front, also had

temperature and salinity profiles consistent with a mixed water column. In this case, chlorophyll was homogeneous with depth but at a much lower concentration (0.95 mg m^{-3}) than at station D. Station C was also close to the front but in this case the water column was strongly stratified. Chlorophyll concentration was highest above the thermocline with values ranging from 3.3 mg m^{-3} at the surface to 0.9 mg m^{-3} at 36m depth, but within the surface mixed layer there was also a gradient with concentrations declining to 2.3 mg m^{-3} at 23m.

Stations A, E, F and G also had strong stratification but the coastal influence is apparent at station A where a strong halocline was detected. At stations A and G, chlorophyll maxima were present at the thermocline with concentrations of 1.6 mg m^{-3} at 25m and 2.5 mg m^{-3} at 30m respectively. At station F, chlorophyll concentration was homogeneous from the surface to the thermocline at 40m and had an average concentration of 0.9 mg m^{-3}. A general decrease in chlorophyll with depth was seen at station E from a concentration of 3.5mg m^{-3} at the surface to 0.6 mg m^{-3} at 50m depth.

Nutrient concentrations also reflected the physical structure of the water column (Fig. 3). The well-mixed stations, B and D, had uniform depth distribution but had different concentrations. The average nitrate concentration in the surface 30m at station B was 2.3 μmol N l^{-1} (Table 1) but was 4.3μmol N l^{-1} at station D. Concentrations of phosphate were 0.2 μmol P l^{-1} at station B and 0.3 μmol P l^{-1} at D, and for silicate were 1.1 μmol Si l^{-1} at B and 1.6 μmol Si l^{-1} at D. Ammonium concentration was also much higher at station D (2.1 μmol l^{-1} at D compared to 0.8 μmol l^{-1} at B). Station D is close to the Bristol Channel outflow which, with river inputs which drain approximately one third of the area of England and Wales, influence nutrient concentrations at station D.

Those stations with strong thermal stratification had low nutrient concentrations in the surface layer and increased concentrations below the thermocline. The highest nitrate concentrations in the surface layer under stratified conditions were found at station C (0.7μmol l^{-1}). Nitrate was close to or below the limit of detection (<0.05μmol N l^{-1}) in the surface mixed layer at stations G and E and silicate was absent (<0.1μmol l^{-1}) in the surface waters at station A and on two of the sampling days at station G. However, high silicate concentrations were found in the surface 30m at stations E and F, with maximum concentrations of 1.4.1 μmol l^{-1} and 1.1 μmol l^{-1} respectively.

3.3 Primary production

Primary production was measured by 24 h simulated-*in-situ* incubations at seven stations on ten days (Fig. 4); experiments on consecutive days at stations E and G gave some measure of day-to-day variability. Photoinhibition in the surface 5m was detected at all

stations except A and D. Below the depth at which photoinhibition occurred, vertical profiles of production were similar to those of chlorophyll (Fig. 2). At station G, which had a significant sub-surface chlorophyll maximum, the highest rate of production (81 mg C m^{-3} d^{-1}) was measured at ~20m.

Table 2 shows depth-integrated values of primary production. At station B, daily integrated production was 2388 mg C m^{-2} d^{-1} — the highest measured in this study. The water column at Station B was well-mixed, with high nutrient and chlorophyll concentrations throughout the water column. At the other mixed water column sampled (Station D) production was much lower (732 mg C m^{-2} d^{-1}), but measurements were made on a cloudy day and irradiance was low (Table 2). There was also day-to-day variability at the stations sampled on sequential dates. The production at station E on the 25 May (1020 mg C m^{-2} d^{-1}) was almost double that measured on the following day (684 mg C m^{-2} d^{-1}). Nutrient availability is an important factor in limiting primary production and surface concentrations of nitrate apparently declined over the same time period, from 0.1 μmol l^{-1} to below the limit of detection (<0.05 μmol l^{-1}). However, silicate and ammonium concentrations increased, silicate from 0.9 μmol l^{-1} to 1.4 μmol l^{-1} and ammonium from undetectable to 0.2 μmol l^{-1}. The second site that was occupied for several days, station G, showed more consistent rates over 3 days with production ranging from 1104 to 1332 mg C m^{-2} d^{-1}. Primary production was highest on the second day of sampling at this station, when nutrient concentrations were undetectable (Table 1) and irradiance was not maximal (Table 2). Between the first and second days of sampling at station G, mean nitrate concentration in the surface mixed layer decreased from 0.7 μmol l^{-1} to undetectable but increased again from the second to third days. A similar pattern was seen for the other nutrients.

3.4 P-E parameters

Eighteen photosynthesis-irradiance (P-E) experiments were done over a seven day period at stations E, F and G. Fig. 5 shows typical photosynthesis-irradiance curves obtained, in this case for water samples taken at 5 m and 40 m, that were used to derive photosynthetic parameter values (Table 3). Photosynthesis is very dependent on the spectrum of light and α^B is sensitive to the light source used in experiments, leading to errors in production estimates at low irradiances (Harrison et al., 1985). Applying the equations of Arrigo and Sullivan (1997) led to an average increase of α^B by 0.01 mg C [mg Chl]$^{-1}$ h^{-1} (μmol photons m^{-2} s^{-1})$^{-1}$ which is equivalent to a 54% of the value before correction (Table 3). E_k was reduced by a mean of 53 μmol quanta m^{-2} s^{-1}, equal to 34% of the value before correction. All subsequent discussion of P–E parameter values refers to the spectral-corrected values for α^B and E_k.

P^B_m values ranged from 1.43 to 4.79 mg C [mg Chl]$^{-1}$ h^{-1}, α^B from 0.011 to 0.047 mg C [mg Chl]$^{-1}$ h^{-1} (μmol photons m^{-2} s^{-1})$^{-1}$ and E_k from 54 to 153 μmol quanta m^{-2} s^{-1}. There was a significant covariation of P^B_m and α^B ($p<0.001$) and between E_k and α^B ($p<0.05$) but no relationship was seen between E_k and P^B_m. E_k values for samples taken at depth were lower than those for surface phytoplankton in all but one case (Station F, 27 May); in this case, the higher value of E_k resulted from a decrease in P^B_m, not an increase in α^B. In most cases, α^B values were higher for deeper samples. E_k was greater for samples taken at noon than at dawn in five out of seven cases, which again was due to an increase in P^B_m rather than a decrease in α^B. It should be noted that the water classified as the 'deep' sample at station G on 24 May was taken from 24m and was within, not below, the mixed layer. No significant relationships were found between any photosynthetic parameter and the total irradiance experienced by the phytoplankton on the day that the water samples were taken. At station G, day-to-day variability in photosynthetic parameters was low and this was consistent with the low variability in depth-integrated production. In contrast there were large changes in P-E parameter values over the two days of sampling at stations E and F.

4. Discussion

4.1 Phytoplankton assemblages

There were significant differences in the phytoplankton assemblages at the mixed, stratified and frontal stations and the species found at each station depended on the water column stability and nutrient availability. At the well mixed stations (B and D) diatoms comprised 70-93% of total phytoplankton biomass (Robin Raine, University of Galway, pers. comm.). Diatoms are good competitors under nutrient-replete conditions due to their high maximum growth rate and ability to compete under conditions of limiting light (Chisholm, 1992). At the well-mixed stations, *Thalassiosira sp.* and *Laudera sp.* were the dominant species. These phytoplankton often occur early in the growth season in temperate waters and are indicative of the onset of the spring bloom; *e.g.* Holligan et al (1984) also found these species to be abundant in the Celtic Sea spring bloom. At these well mixed stations, phytoplankton growth is limited by light rather than nutrient concentrations, which were high at the time of the cruise.

At station C, the stratified site close to the front, the assemblage was dominated by dinoflagellates and microflagellates in surface waters. However, below the thermocline diatoms were the most abundant phytoplankton. Nutrient concentrations in the surface mixed layer were not totally depleted despite strong stratification suggesting that the water column

may have stratified very recently. Station A, which was close to Ireland and may have shown coastal influences, had large numbers of dinoflagellates as well as *Pseudonitzchia*, a diatom typically abundant in late spring and early summer which does not usually dominate the spring bloom (Robin Raine, pers. comm.).

Stations G and F, in stratified waters to the south of the front, had high numbers of dinoflagellates and were nutrient depleted. Station E, in the middle of the Celtic Sea shelf, had few neritic phytoplankton species but many characteristic oceanic species. In the mixed layer at station E, nutrient concentrations were low and dinoflagellates dominated the phytoplankton. Dinoflagellates often dominate where photosynthesis is nutrient controlled and production depends on nutrient regeneration within the surface mixed layer (Joint et al., 1986; Martin-Jezequel and Videau, 1992; Weeks et al., 1993) and is consistent with their presence in the nutrient-depleted, surface mixed layer at stations G, E and F.

It is usually assumed that diatoms will dominate the phytoplankton assemblage in the spring bloom until silicate becomes depleted, when they are replaced by other non-silicate requiring phytoplankton (Trigueros and Orive, 2001). Riegman et al (1998) argues that diatoms are superior competitors for light and nutrients when silicate is available. It is interesting that silicate was present in relatively high concentrations in the surface waters at the stratified stations E and F and diatoms might have been expected to dominate. However, at station E, the assemblage contained many small athecate dinoflagellates and diatom species indicative of oceanic water (e.g. *Chaetoceros concavicornis*); station F was also dominated by dinoflagellates. Nitrate concentrations were very low at stations E and F and the major source of nitrogen would be regenerated; nevertheless, it is surprising that diatoms were not more abundant when silicate was still available.

4.2 Hydrography

All the stations were within a small geographical area and had similar nutrient concentrations before thermal stratification took place. They experienced the same weather conditions yet, a few weeks after the onset of the bloom, the phytoplankton assemblages were very different. The observed variation in biodiversity must have been due to the hydrographic conditions experienced by the phytoplankton. Vertical stability of the water column is well known to be important in determining the spatial and temporal phytoplankton production (Pingree, 1975). In this region the development of the thermocline is controlled by turbulence derived from tides (Pingree, 1975, James, 1977).

In this study, the positions and development of the front were determined using satellite remote sensing and the general pattern is consistent both with earlier model

predictions based on wind and tidal mixing (James, 1977) and with the observations of Pingree (1975) who used hydrographic data to map the development and progression of the thermocline in the Celtic Sea. However, remote sensing has allowed a better temporal description of the development of the front than had previously been possible, even at a time of significant cloud cover. The observations during the cruise can now be placed firmly within the temporal sequence of stratification and front development in 2000.

The stations can be broadly divided into two groups: those on the well mixed side of the front (B and D) and those on the stratified side (all other stations). Tidal stream amplitude is high in St. George's Channel favouring turbulent mixing, hence the lack of thermocline at stations B and D. Stations B and D are close to the regions that James (1977) expected to be well mixed throughout the year. Both these stations were close to the front and had high concentrations of nutrients. Stations A, C, F and G had varying degrees of stratification as a consequence of different hydrographic forcing. Station A was close to the Irish coast in the region where SST remote sensing suggested that stratification developed earliest (Fig. 1b and see Fig. 4 in Pingree, 1975). This early thermocline development is a result of the low tidal stream amplitudes in this area and of influence of low salinity water. Station C was the closest stratified station to the front and the thermocline was sharp at 32m, with the highest vertical diffusivity of any of the stations (John Howarth, pers. comm.). Stations F and G were both stratified stations on the continental shelf. The thermocline at station G was ca. 10m shallower than at station G (~30m compared to ~40m), it was sharper than at F and the vertical diffusivity was about twice as high. It is not clear whether the thermocline developed at both stations at similar times but remote sensing measurements of SST suggests that stratification may begin about a week earlier at station G than F. The temperature gradient in the thermocline at Station E in the outer Celtic Sea was much shallower than at the other stratified stations.

4.3 Biomass and productivity

A large range of chlorophyll concentrations and production was measured over this small geographical area in the Celtic Sea. Fronts are often assumed to be regions of high phytoplankton biomass and production (Cochlan et al., 1991) but in this study, comparable chlorophyll concentrations were measured at mixed, frontal and stratified stations. We have compared production in different hydrographic regions by using a depth-integrated P / B ratio (Table 2) obtained by dividing depth-integrated production by depth-integrated chlorophyll concentration. The rationale is that the maximum potential rate of light harvesting depends directly on the chlorophyll content of a cell. Cellular chlorophyll content is controlled by the

previous light history of the cell, the nutrients available to that cell and there is also species-dependency, with some species having higher intrinsic chlorophyll content than other species. Therefore, if it is assumed that a euphotic water column with a particular chlorophyll content has a maximum potential rate of depth-integrated primary production, then comparison of the production – biomass (P / B) ratio (mgC fixed [mg chl]$^{-1}$ d^{-1}) in different stations gives an indication of the efficiency of the phytoplankton assemblages.

Table 2 lists the P / B ratio for every station. Station B in the mixed water column had the highest primary production rate measured during the cruise (2388 mgC m^{-2} d^{-1}). The chlorophyll concentration was also high (93.9 mg m^{-2}) and the resulting P / B ratio was 25.4 mg C [mg chl]$^{-1}$ d^{-1}. Similar high P / B ratios were found at station A (close to the Irish coast), at the mixed station D mixed water and at station G in the stratified waters south of the front. High P / B ratios were found for a range of chlorophyll concentrations from high values at station B to low values at station G. We assume that the high P / B ratios indicate phytoplankton assemblages which are not significantly limited by nutrients or other factors and that the carbon fixation rate is optimal for these environmental conditions and phytoplankton species.

In contrast, low P / B ratios were determined at the frontal station (C) and at stations E and F. That is, the rate of primary production is less than would be expected for the quantity of chlorophyll which is present in the water column. At stations E and F, this may be due to nutrient limitation since the concentrations of nitrate was low. However, station G also had low nutrient concentrations but the activity of the phytoplankton was hardly affected and the P / B ratio was as high as at the stations in the well mixed regions. This station had a large sub-surface chlorophyll maximum and the maximum production in the water column was at 20m (Fig. 4) where presumably the phytoplankton could intercept any transport of nutrients across the thermocline. This mechanism of nutrient supply is also invoked to explain high biomass and production at frontal regions (Pingree et al., 1976). However, in this study, the P / B ratio was low at station C in the front. Despite the high vertical diffusivity at station C, primary production was low for the quantity of chlorophyll present in the water column.

4.4 Photosynthetic efficiency

The photosynthetic characteristics of a phytoplankton assemblage are an important factor in explaining observed differences in primary production and in this study, we have concentrated on the stratified waters south of the front. Other studies have also found that incubations in artificial light lead to low values for α^B when compared to those measured under natural light (Tilzer et al., 1993, Harrison et al.,1985). In our experiments, applying a

spectral correction increased values of α^B. The spectrum of the lamp used, even with the blue filter, had a higher proportion of red light than natural irradiance. Light harvested by the blue absorption peak of photosynthetic pigments is the dominant energy source for photosynthesis (Prézelin et al., 1991) so a relative decrease in blue photons might explain the low values of α^B obtained from the artificial light source.

There were no consistent differences in the photosynthetic parameters between different sites but a high degree of day-to-day variability was observed within each station. Such variability has previously been reported in the Celtic Sea by Joint and Pomroy (1986). The possible causes include irradiance and nutrient supply (Joint and Pomroy, 1986), storm disturbance (Côté and Platt, 1983) and diel periodicity (Putt and Prézelin, 1985; Legendre et al, 1985). However, in the present study, a possible explanationfor the variability is that different water bodies were sampled from one day to the next, albeit at the same geographical location. Pingree et al. (1976) found that horizontal advection due to tides and current introduced noise into hydrographic measurements at fixed locations in the Celtic Sea. The observed increase of α^B values with depth was expected and reflects the increased efficiency of phytoplankton adapted to low light levels. In a study of the photosynthetic characteristics of different size fractions of phytoplankton, Joint and Pomroy (1986) found higher values of α^B for picoplankton at depth but not for other size classes. They also reported that P^B_m did not always decrease with depth and that was also observed in this study (Table 3).

4.5 Nitrate flux

In a stratified water column, phytoplankton production above the thermocline is mainly dependent on the regeneration of nitrogen within the layer but there is also some transfer of nitrate from the nutrient-rich waters below the thermocline (Riegman and Noordelos, 1998, Holligan et al, 1984). This nitrate flux can be estimated from the vertical turbulent diffusion coefficient and the gradient of nutrient concentration across the thermocline. Values for the former were provided by John Howarth (pers. comm.) and the flux of nutrient across the thermocline have been calculated using the method of King and Devol, 1979). Diffusivity data were not available for 17 May (Station A). Generally, nutrient fluxes were low at all stations. The highest nitrate fluxes were 0.016 mmol N m^{-2} d^{-1} on 27 May at station F and 0.014 mmol N m^{-2} d^{-1} on 19 May at station C in the vicinity of the tidal front. All other estimates of nitrate flux were $\leq$0.003 mmol N m^{-2} d^{-1}. The high flux calculated for station F on 19 May was due to the relatively high vertical diffusivity value whilst that at the frontal station C was a consequence of a steep concentration gradient across the thermocline.

Estimates of fluxes of other nutrients across the thermocline into the surface mixed layer were low in all cases. These calculations confirm the assumption that most of the production taking place in the surface mixed layer used regenerated ammonium as the nitrogen source.

4.6 Variability within stations

The day-to-day variability in P / E parameters at stations E,F and G suggest greater heterogeneity in water masses than might be expected from the temperature and salinity data. Changes in nutrient concentrations within a water mass over a few days, when coupled with estimates of primary production can give an indication of past biological activity (Rees et al., 2002) and can also suggest if the results are consistent with sampling the same water mass. The Redfield ratio of 106C: 16N: 1P (Redfield, 1963) can be used to link nutrient assimilation with carbon uptake. If the elemental composition of a phytoplankton cell is in the Redfield ratio, the ratio of nutrients taken up by the phytoplankton will be the same, if the measurements are made over a time period consistent with the phytoplankton generation time. Although nutrient uptake experiments were not done on this cruise, changes in nutrient concentrations between successive days of sampling at the same site have been used to give an indication of how much dissolved inorganic nutrient might have been removed by phytoplankton activity. Nitrate concentration in the euphotic zone at station E decreased by 2.09 mmol N m^{-2} between 25 and 26 May. Assuming the Redfield C:N ratio of 6.625, this change corresponds to the potential assimilation of 13.85 mmol C m^{-2}. However, over the same period, the measured carbon fixation was 85 mmol C m^{-2} (1020 mgC m^{-2} d^{-1}). Therefore, if nitrate was the sole nitrogen source, it would support only 16% of the measured production. The C:N ratio has been reported to vary from <1 to >20 (Bouteiller, 1993) but this value is well outside this range. We conclude that at station E, either regenerated nitrogen sources were important or that different water masses were sampled on sequential days.

Station G was sampled from 22 to 23 May and depth-integrated nitrate concentration decreased by 11.3 mmol N m^{-2} d^{-1} — which would be equivalent to carbon fixation of 74 mmol C m^{-2} d^{-1} assuming a Redfield ratio. The measured carbon fixation was 109 mM m^{-2} d^{-1} and is well within the accepted range of C:N ratios (Bouteiller, 1993). However, between the second and third days of sampling at station G, nitrate concentration in the surface mixed layer increased by 0.19 mmol N m^{-2} d^{-1}. Measured primary production on 24 May was 111 mmol C m^{-2} d^{-1} and would have required ~17 mmol N m^{-2} d^{-1} if nitrate continued to be the major nitrogen source.

Changes in phosphate concentration also give indications of the variability at each station. Assuming the Redfield ratio, the change in phosphate concentration at station E on between 25 and 26 May would support an estimated production of 55.12 mmol C m^{-2}; this is approximately two-thirds of the measured C uptake of 85 mmol C m^{-2} d^{-1}. In contrast, the decline in phosphate at station G on 22 May would have supported a production estimate of 198 mmol C m^{-2}, almost twice the measured value of 109 mmol C m^{-2} d^{-1}.

The large day-to-day variability in nutrient concentrations and their incompatibility with the day-to-day variation in production suggests that this study was not Lagrangian and that different water masses and different phytoplankton assemblages were encountered at the same geographical positions. Therefore, it is difficult to relate properties sampled on sequential days or to attempt to construct mass balance budgets for nutrients.

5. Summary

The development of the front seen in the satellite images was in agreement with the sequence of stratification described by Pingree (1975) and James (1977). The variability in tidal stream amplitude controls the development of the thermocline, which in turn determines the succession of phytoplankton populations. At the time of the cruise (late May), the front in St. George's Channel was fully developed. Fully stratified stations south of the frontal regions (stations E, F and G) were depleted of nutrients in the surface mixed layer and dominated by dinoflagellates. The frontal and coastal stratified stations (C and A respectively) still contained low levels of nutrients in the surface mixed layer. At station A, this was due to partial stratification and the phytoplankton community was typical of the late bloom. At station C, dinoflagellates rather than diatoms dominated, despite the presence of silicate. Stations B and D in the well-mixed waters north of the front contained species typically found during the spring bloom. In the stratified waters, the flux of nutrients from below the thermocline to the surface mixed layer was low and most production is thought to use nutrients regenerated within the surface waters. The highest primary production was found at station B in the well-mixed waters. Production on the well-mixed side of the front was light controlled in contrast to that on the stratified side that was nutrient controlled. The studies at sites E, F and G were not Lagrangian and the high day to day variability in photosynthetic parameters is probably as much a result of horizontal advection as of changes in biological activity.

Acknowledgements

We thank Robin Raine (University of Galway), John Howarth (Proudman Oceanographic Laboratory), John Stephens (Plymouth Marine Laboratory) and Richard Geider (University of Essex) for the use of their data. This study was partly funded by the UK Natural Environment Research Council through the Plymouth Marine Laboratory core strategic research programme Microbially Driven Biogeochemical Cycles (MDB) and by the EU Commission project PROOF (CEC contract number EVK3-CT-1999-00019).

References

Arrigo, K. R., Sullivan, C.W. 1992. The influence of salinity and temperature covariation on the photophysiological characteristics of Antarctic sea ice microalgae. Journal of Phycology 28, 746-756.

Bouteiller, A.L. 1993. Comparison of in-bottle measurements using ^{15}N and ^{14}C. ICES Marine Science Symposium 197, 121-131.

Bricaud, A., Babin, M., Morel, A., Claustre, H. 1995. Variability in the chlorophyll-specific absorption coefficients of natural phytoplankton: Analysis and parameterization. Journal of Geophysical Research 100 (C7), 13321-13332.

Brewer, P.G., Riley, J.P. 1965. The automatic determination of nitrate in seawater. Deep-Sea Research 12, 765-772.

Cayula, J. F., and Cornillon, P. 1992. Edge-detection algorithm for SST images. Journal of Atmospheric and Oceanic Technology 9, 67-80.

Chisholm, S. W. 1992. Phytoplankton size. *In* P. Falkowski and A. D. Woodhead [eds.], Primary productivity and Biogeochemical Cycles in the Sea. Plenum Press

Cochlan, W.P., Price, N.M., Harrison, P.J. 1991. Effects of irradiance on nitrogen uptake by phytoplankton – Comparison of frontal and stratified communities. Marine Ecology Progress Series 69, 103-116.

Côté, B., and Platt, T. 1983. Day-to-Day variations in the spring-summer photosynthetic parameters of coastal marine-phytoplankton. Limnology and Oceanography 28, 320-344.

Donald, K.M., Joint, I., Rees, A.P., Woodward, E.M.S., Savidge, G. 2001. Uptake of carbon, nitrogen and phosphorus by phytoplankton along the 20° W meridian in the NE Atlantic between 57.5°N and 37°N. Deep Sea Research II 48, 873-897.

Fasham, M. J. R., Holligan, P. M., and Pugh, P. R. 1983. The spatial and temporal development of the spring phytoplankton bloom in the Celtic Sea, April 1979. Progress in Oceanography 12, 87-145.

Grasshoff, K. 1976. Methods of seawater analysis. Verlag Chemie Weinheim, 317pp.

Harrison, W.G., Platt, T., Lewis, M.R. 1985. The utility of light-saturation models for estimating marine primary productivity in the field: a comparison with conventional "simulated" in situ methods. Canadian Journal of Fisheries and Aquatic Science 42, 864-872.

Holligan, P. M., Williams, P. J. L., Purdie, D., and Harris, R. P. 1984. Photosynthesis, Respiration and Nitrogen Supply of Plankton Populations in Stratified, Frontal and Tidally Mixed Shelf Waters. Marine Ecology-Progress Series 17, 201-213.

IOC 1994. Protocols for the Joint Global Ocean Flux Study (JGOFS) core measurements. Manuals, Guides IOC 29: 126pp.

Jeffrey, S.W., Mantoura, R.F.C., Wright, S.W. 1997. Phytoplankton pigments in oceanography. UNESCO.

James, I. D. 1977. A model of the annual cycle of temperature in a frontal region of the Celtic Sea. Estuarine and Coastal Marine Science 5, 339-353.

Joint, I.R., Pomroy, A.J. 1986. Photosynthetic characteristics of nanoplankton and picoplankton from the surface mixed layer. Marine Biology 92, 465-474.

Joint, I., Rees, A., Woodward, M. 2001a. Primary production and nutrient assimilation in the Iberian Upwelling in August 1998. Progress in Oceanography 51, 303-320.

Joint I., Wollast, R., Chou, L., Batten, S., Elskens, M., Edwards, E., Hirst, A., Burkill, P., Groom, S., Gibb, S., Miller, A., Hydes, D., Dehairs, F., Antia, A., Barlow, R., Rees, A., Pomroy, A., Brockmann, U., Cummings, D., Lampitt, R., Loijens, M., Mantoura, F., Miller, P., Raabe, T., Salgado, X., Stelfox, X., Woolfenden, J. 2001b. Pelagic production at the Celtic Sea Shelf Break - the OMEX I project. Deep-Sea Research II 48, 3049-3081.

Jones, R.D. 1991. An improved fluorescence method for the determination of nanomolar concentrations of ammonium in natural waters. Limnology and Oceanography 36, 814-819.

King, F.D., Devol, A.H. 1979. Estimates of vertical eddy diffusion through the thermocline from phytoplankton nitrate uptake rates in the mixed layer of the eastern tropical Pacific. Limnology and Oceanography, 24, 645-651.

Kirkwood, D.S. 1989. Simultaneous determination of selected nutrients in seawater. ICES CM:C:29.

Landry, M.R., Ondrusek, M.E., Tanner, S.J., Brown, S.L., Constantinou, J., Bidigare, R.R., Coale, K.H., Fitzwater, S. 2000. Biological response to iron fertilization in the eastern equatoral Pacific (IronEx II). I. Microplankton community abundances and biomass. Marine Ecology Progress Series 201, 27-42.

Legendre, L., Demers, S., Therriault, J. C., and Boudreau, C. A. 1985. Tidal variations in the photosynthesis of estuarine phytoplankton isolated in a tank. Marine Biology 88, 301-309.

Martin-Jezequel, V., and Videau, C. 1992. Phytoplankton and bacteria over the transient area of the continental slope of the Celtic Sea in spring. I. Vertical distribution and productivity. Marine Ecology Progress Series 85, 289-301.

Miller, P., Groom, S. B., McManus, A., Selley, J., and Mironnet, N. 1997. Panorama: a semi-automated AVHRR and CZCS system for observation of coastal and ocean processes, p. 539-544, RSS97: Observations and Interactions, Proceedings of the Remote Sensing Society. Reading, England.

Miller, P., Jégou, A. M., and Froidefond, J. M. 2002. Composite front maps from improved visualisation of retention structures in Bay of Biscay, p. 7, 8th International Symposium on Oceanography of the Bay of Biscay. Gijón, Spain.

Naeem, S., Thompson, L.J., Lawler, S.P., Lawton, J.H., Woodfin, R.M. 1994. Declining biodiversity can alter the performance of ecosystems. Nature 368, 734-737.

Neckel, H., and Labs, D. 1984. The solar radiation between 3300 and 12500 Angstrom. Solar physics 90, 205-258.

Pingree, R. D. 1975. The advance and retreat of the thermocline on the continental shelf. Journal of the Marine Biological Association of the U.K. 55, 965-974.

Pingree, R.D., Holligan, P.M., Mardell, G.T., Head, R.N. 1976. The influence of physical stability on spring, summer and autumn phytoplankton blooms in the Celtic sea. Journal of the Marine Biological Association U.K. 56, 845-873.

Platt, T., Gallegos, C.L., Harrison, W.G. 1980. Photoinhibition in natural assembalges of marine phytoplankton. Journal of Marine Research 34, 687-701.

Prézelin, B.B., Tilzer, M.M., Schofield, O., Häse, C. 1991. The control of the production process of phytoplankton by the physical structure of the aquatic environment with special reference to its optical properties. Aquatic Science 53, 136-186.

Putt, M., and Prezelin, B. B. 1985. Observations of diel patterns of photosynthesis in cyanobacteria and nanoplankton in the Santa-Barbara Channel During El-Nino. Journal of Plankton Research 7, 779-790.

Redfield, A.C., Kechum, B.H., Richards, F.A. 1963. The influence of organisms on the composition of sea water. In: Hill, M.N. (Ed.), The Sea, Vol.2. Wiley, New York, pp.26-77.

Riegman, R., Flameling, I. A., and Noordeloos, A. A. M. 1998. Size-fractionated uptake of ammonium, nitrate and urea and phytoplankton growth in the North Sea during spring 1994. Marine Ecology-Progress Series 173, 85-94.

Riegman, R., and Noordeloos, A. A. M. 1998. Size-fractionated uptake of nitrogenous nutrients and carbon by phytoplankton in the North Sea during summer 1994. Marine Ecology-Progress Series 173, 95-106

Rees, A.P., Joint, I., Donald, K.M. 1999. Early spring bloom phytoplankton-nutrient dynamics at the Celtic Sea Shelf Edge. Deep Sea Research II 46, 483-510.

Rees, A.P., Woodward, E. M., Robinson, C., Cummings, D.G., Tarran, G.A., Joint, I. 2002. Size-fractionated nitrogen uptake and carbon fixation during a developing coccolithophore bloom in the North Sea during June 1999. Deep Sea Research II. 49, 2905-2927.

Tilzer, M.M., Häse, C., Conrad, I. 1993. Estimation of in situ primary production from parameters of the photosynthesis-light curve obtained in laboratory incubators. ICES Marine Science Symposium 197, 181-195.

Trigueros, J.M., Orive, E. 2001. Seasonal variations of diatoms and dinoflagellates in a shallow, temperate estuary, with emphasis on neritic assemblages. Hydrobiologia, 444, 119-133.

Weeks, A., Conte, M.H., Harris, R.P., Bedo, A., Bellan, I., Burkhill, P.H., Edwards, E.S., Harbour, D.S., Kennedy, H., Llewellyn, C., Mantoura, R.F.C., Morales, C.E., Pomroy, A.J., Turley, C.M. 1993. The physical and chemical environment and changes in community structure associated with bloom evolution – the Joint Global Flux Study North-Atlantic Bloom experiment. Deep Sea Research II 40, 347-368

Figures Captions

Fig. 1. a) AVHRR image of the Celtic Sea showing sea surface temperature (SST) on 8 April, b) composite front map derived from satellite remotely-sensed estimates of temperature for 16 – 22 April 2000, c) composite map for 23 - 29 April, d) composite map for 30 April – 8 May 2000, e) composite map for 7-13 May 2002, f) SST images of the region on 26 June 2000.

Fig. 2. Representative profiles of temperature (---), salinity (—) and chlorophyll (●): a) station A on 17 May 2000, b) station B on 18 May 2000, c) station C on 19 May 2000, d) station D on 20 May 2000, e) station E on 25 May 2000, f) station F on 27 May 2000 and g) station G on 22 May 2000.

Figure 3. Representative profiles of concentrations of nitrate (●), phosphate (□), silicate (▲) and ammonium (◇) : a) station A on 17 May 2000, b) station B on 18 May 2000, c) station C on 19 May 2000, d) station D on 20 May 2000, e) station E on 25 May 2000, f) station F on 27 May 2000 and g) station G on 22 May 2000.

Figure 4. Representative profiles of primary production from 24h simulated-*in-situ* incubations: a) station A on 17 May 2000, b) station B on 18 May 2000, c) station C on 19 May 2000, d) station D on 20 May 2000, e) station E on 25 May 2000, f) station F on 27 May 2000 and g) station G on 22 May 2000. Values are the mean of three light bottle measurements with standard deviation.

Figure 5. Photosynthesis-irradiance curves from the afternoon casts on 28 May using water sampled from a) 5m and b) 40m.

Table 1.
Average nutrient concentration in the surface 30m of the water column.

Station	Date	Nitrate µmol N l^{-1}	Ammonium µmol N l^{-1}	Total nitrogen µmol N l^{-1}	Phosphate µmol P l^{-1}	Silicate µmol Si l^{-1}	N:P ratio
A	17 May	0.34	0.24	0.60	<0.05	nd	>30
B	18 May	2.27	0.76	3.03	0.23	1.13	13.2
C	19 May	0.67	0.22	0.89	0.07	0.67	12.7
D	20 May	4.31	2.05	6.37	0.33	1.61	19.3
E	25 May	0.11	<0.05	0.13	0.10	0.94	1.3
E	26 May	<0.05	0.17	0.17	0.09	1.42	1.9
F	27 May	<0.05	0.07	0.07	0.05	1.06	1.4
G	22 May	0.65	0.29	0.94	0.11	0.17	8.5
G	23 May	<0.05	<0.05	<0.05	<0.05	<0.05	—
G	24 May	<0.05	0.10	0.13	0.10	0.13	1.3

The limit of detection was 0.05µmol l^{-1}.

Table 2.
Primary production, chlorophyll concentration and daily irradiance at each station. Primary production and chlorophyll concentration values are integrated to the depth at which irradiance is 1% of that just below the sea surface.

Station	Date	Euphotic depth (m)	Chlorophyll concentration mg m^{-2}	Primary production mg C m^{-2} d^{-1}	Depth-averaged production:chlorophyll (P / B) ratio mgC [mg Chl]$^{-1}$ d^{-1}	Daily PAR mol quanta m^{-2} d^{-1}
A	17 May	36	35.1	924	26.3	1.89
B	18 May	30	93.9	2388	25.4	2.88
C	19 May	25	71.1	948	13.3	3.60
D	20 May	30	28.3	732	25.9	1.54
E	25 May	30	104.4	1020	9.8	2.98
E	26 May	30	54.7	684	12.5	3.20
F	27 May	35	43.5	708	16.3	3.04
G	22 May	25	46.6	1308	28.1	3.61
G	23 May	35	63.8	1332	20.9	2.47
G	24 May	28	43.9	1104	25.1	3.16

Table 3.

Photosynthetic parameters (P^B_m, α^B and E_k) determined on samples taken at dawn (AM) and early afternoon (PM) from near surface and deeper in the water column. Values are listed for parameters obtained with and without the application of a spectral correction to account for the spectrum of the lamp used to determine P / E characteristics. Ek (µmol quanta m^{-2} s^{-1}), α^B mg C [mg Chl]$^{-1}$ h^{-1} (µmol quanta m^{-2} s^{-1})$^{-1}$, $P^B m$ mg C [mg Chl]$^{-1}$ h^{-1}

				Photosynthetic parameters				
				No spectral correction			Spectral corrected	
Station	Date	Time	Depth (m)	$P^B m$	α^B	E_k	α^B	E_k
E	25 May	AM	5	1.63	0.022	75	0.030	54
		PM	35	2.96	0.025	120	0.047	63
E	26 May	AM	4	1.91	0.011	177	0.015	126
		PM	5	1.85	0.009	218	0.012	153
		PM	30	2.77	0.020	139	0.035	79
F	27 May	AM	5	1.43	0.008	178	0.011	126
		PM	40	3.79	0.016	243	0.027	142
F	28 May	AM	12	1.86	0.011	164	0.018	101
		PM	5	1.95	0.012	168	0.018	106
		PM	40	3.61	0.023	156	0.036	100
G	22 May	AM	5	2.26	0.016	140	0.023	97
		PM	6	3.61	0.021	170	0.029	125
G	23 May	AM	5	2.69	0.016	174	0.022	123
		PM	7	2.80	0.018	155	0.027	102
		PM	36	1.61	0.014	115	0.025	64
G	24 May	AM	5	3.34	0.024	138	0.035	97
		PM	5	2.24	0.015	148	0.022	104
		PM	24	3.59	0.028	127	0.051	70

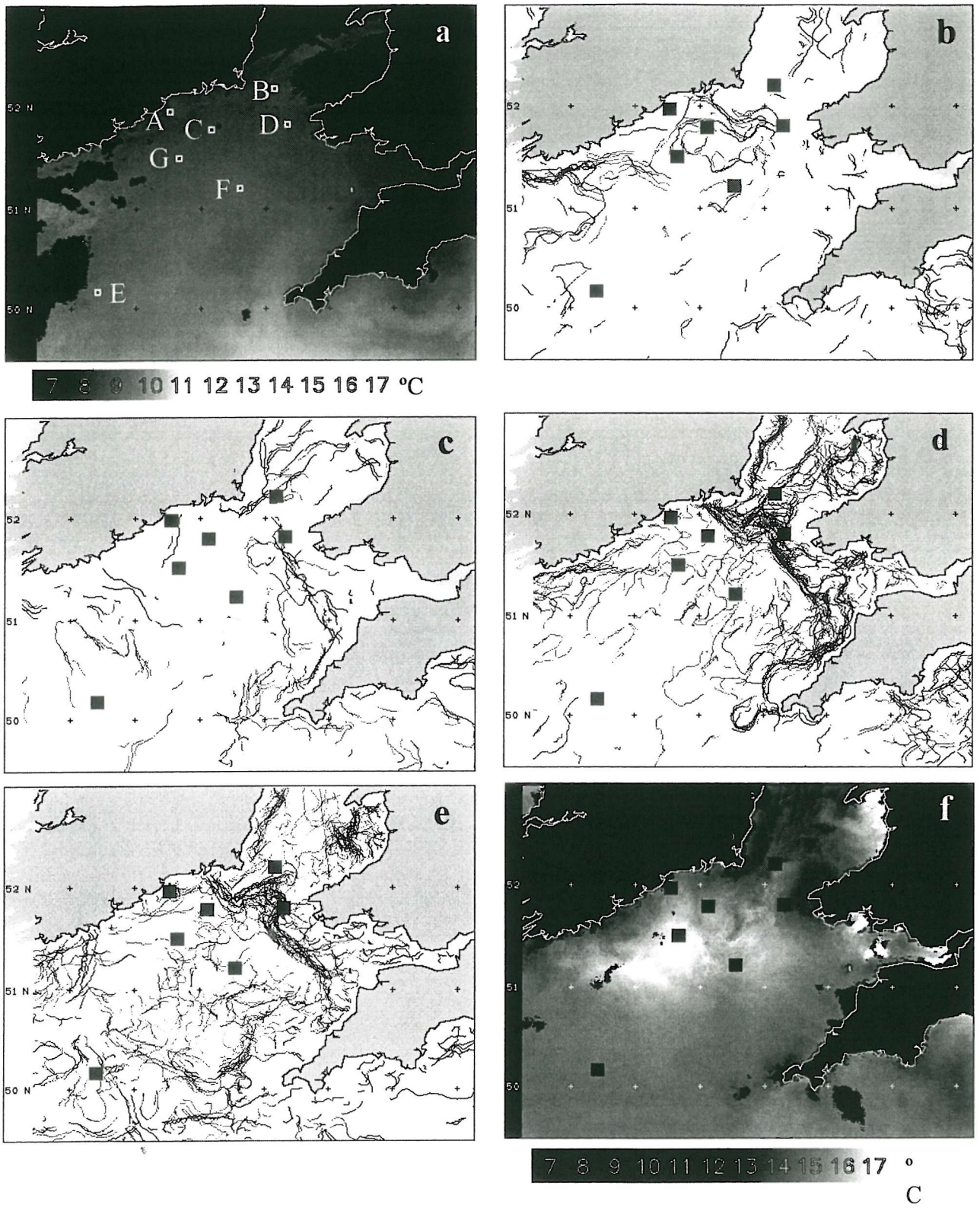
a
A
B
C
D
E
F
G
52 N
51 N
50 N
7 8 9 10 11 12 13 14 15 16 17 °C
b
52
51
50
c
52
51
50
d
52 N
51 N
50 N
e
52 N
51 N
50 N
f
52
51
50
7 8 9 10 11 12 13 14 15 16 17 °C

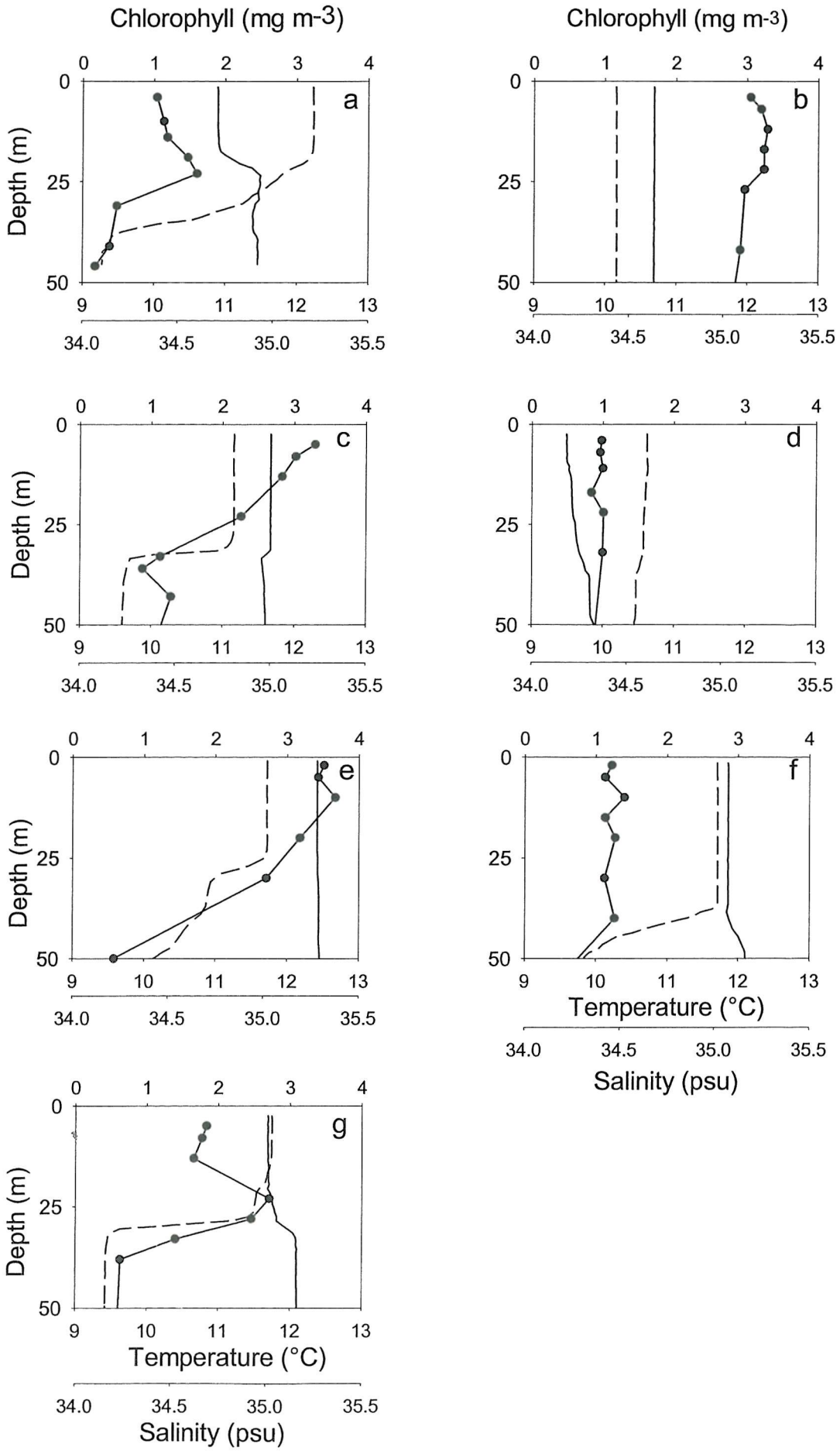
Chlorophyll (mg m-3)
Chlorophyll (mg m-3)
Depth (m)
a
b
c
d
e
f
g
Temperature (°C)
Salinity (psu)

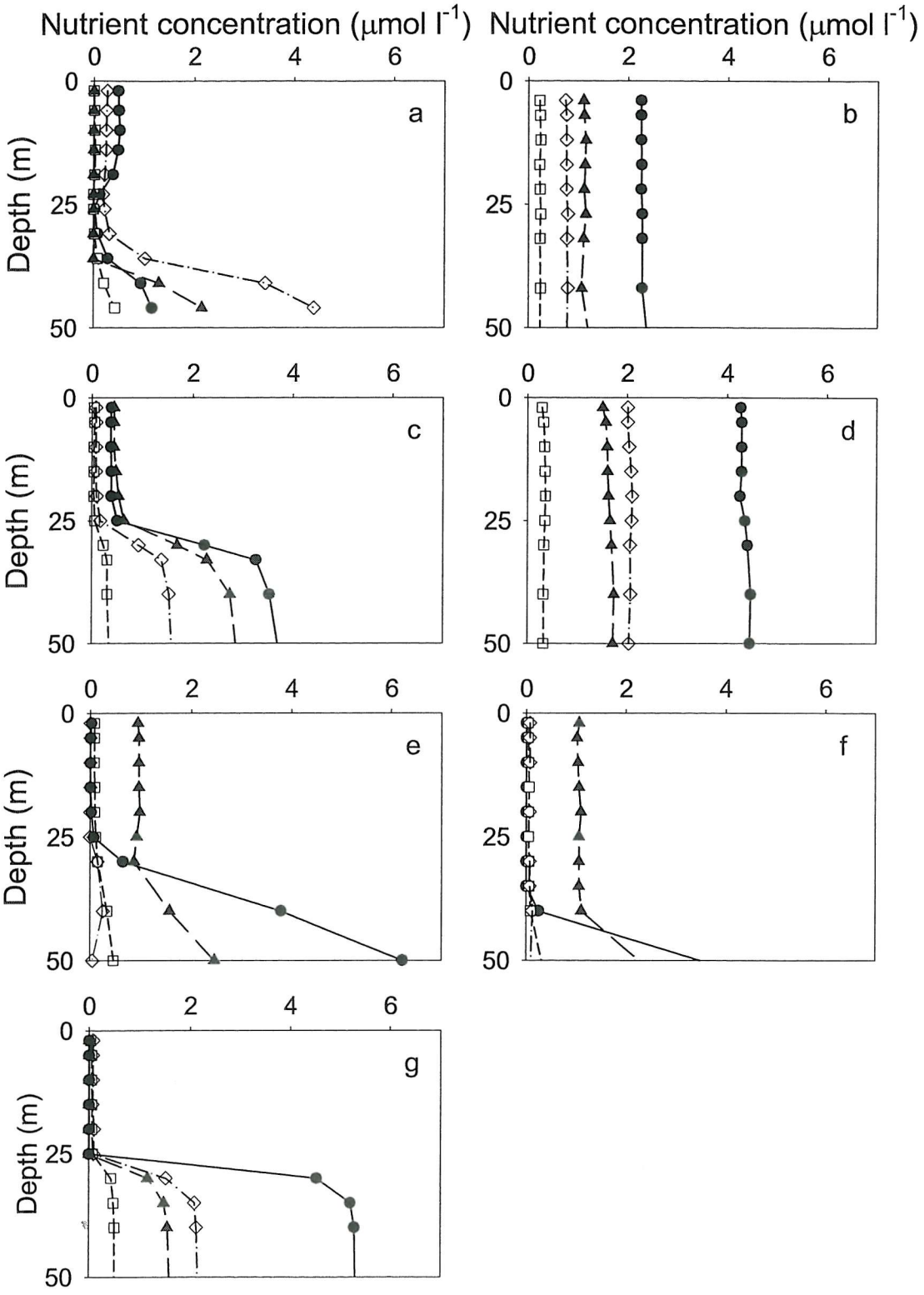
Nutrient concentration (μmol l-1)
Nutrient concentration (μmol l-1)
Depth (m)
0
2
4
6
25
50
a
b
c
d
e
f
g

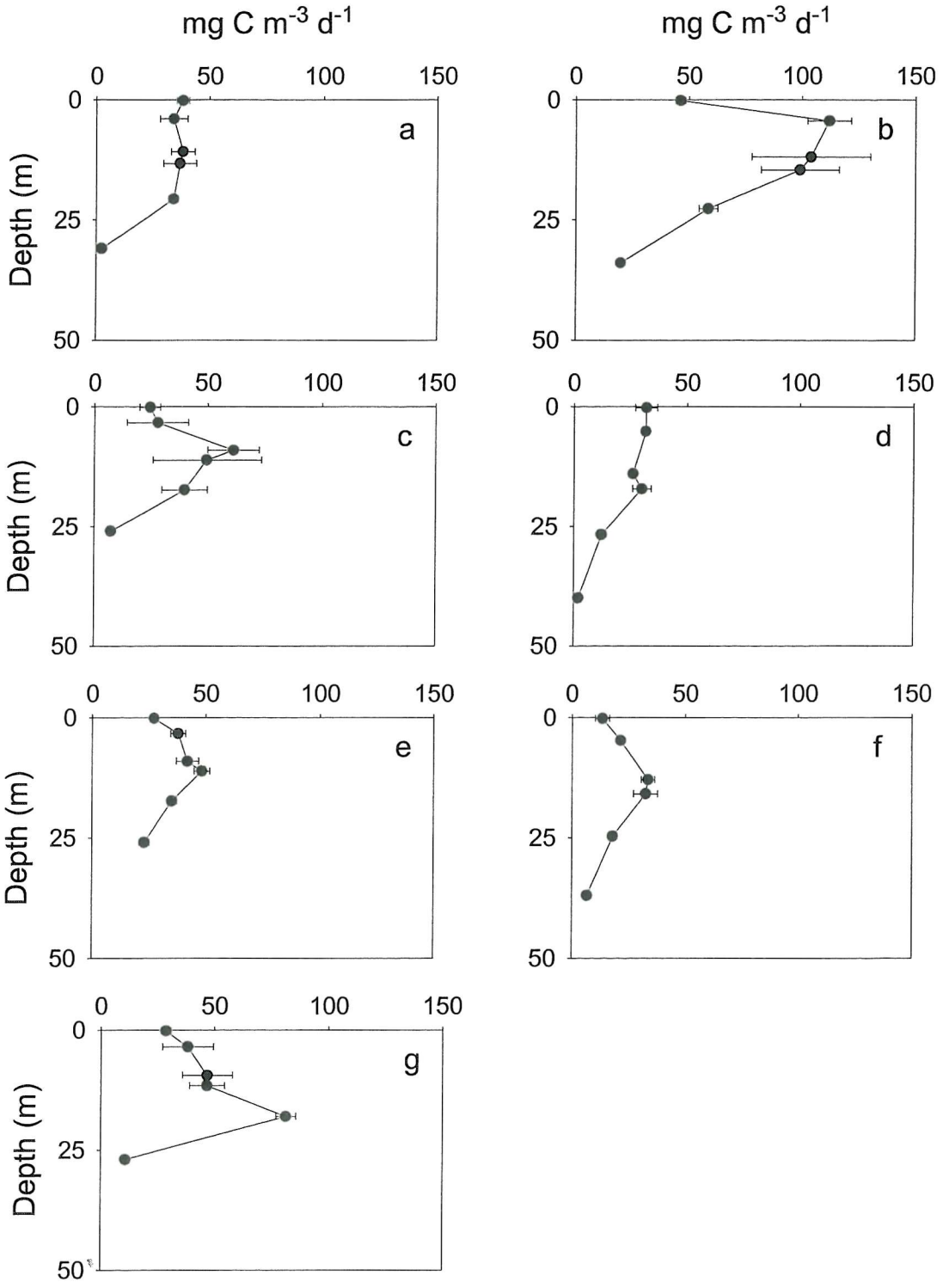
mg C m-3 d-1
mg C m-3 d-1
Depth (m)
0
50
100
150
0
25
50
a
b
c
d
e
f
g

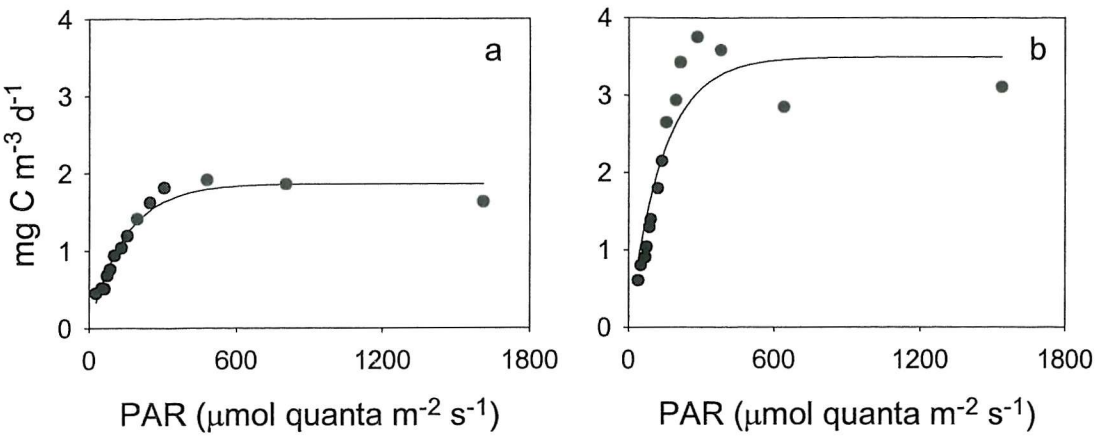
a
b
mg C m-3 d-1
0
1
2
3
4
0
600
1200
1800
PAR (µmol quanta m-2 s-1)